

# Sheffield Hallam University

*Chromogenic detection of dipeptidyl peptidase IV (DPP-IV) activity using peptide-functionalized gold nanoparticles*

ALDEWACHI, Hasan

Available from the Sheffield Hallam University Research Archive (SHURA) at:

<http://shura.shu.ac.uk/18152/>

## A Sheffield Hallam University thesis

This thesis is protected by copyright which belongs to the author.

The content must not be changed in any way or sold commercially in any format or medium without the formal permission of the author.

When referring to this work, full bibliographic details including the author, title, awarding institution and date of the thesis must be given.

Please visit <http://shura.shu.ac.uk/18152/> and <http://shura.shu.ac.uk/information.html> for further details about copyright and re-use permissions.

Chromogenic Detection of Dipeptidyl Peptidase IV (DPP-IV) Activity  
using Peptide-Functionalized Gold Nanoparticles

Hasan Saad Aldewachi



A thesis submitted in partial fulfilment of the requirements of

Sheffield Hallam University

for the degree of Doctor of Philosophy

November 2017

Sheffield, UK

# Abstract

---

Metal nanoparticles offer a useful platform for a wide range of biological applications especially for biosensing, bioimaging and drug delivery. This thesis presents a body of original research describing the synthesis, characterisation and development of a novel and convenient biosensing assay for detection of dipeptidyl peptidase IV (DPP-IV) enzyme activity using peptide functionalized gold nanoparticles.

The distinctive optical and physical properties of gold nanoparticles (Au NP) were harnessed for the development of a colorimetric assay for rapid sensing of DPP-IV activities and screening DPP-IV inhibitors. The citrate reduction method for Au NPs synthesis was optimised and several potential peptide substrates (GPDC, VP-EN-DC, C/G dipeptide, GPG-EN-PEG4-LA, GPDCALNNC) were designed to provide substrates that mimic the DPP-IV natural substrates. The performances of the substrate functionalized Au NPs were assessed for their appropriateness for the detection of the enzyme activity.

Addition of DPP-IV to the solutions containing the functionalized Au NPs resulted in cleavage of the substrate and thus causing the aggregation of the Au NPs which in turn led to a shift of the surface plasmon peak toward longer wavelengths, and a change of the colour of the colloidal suspension from red to blue. Overall, real-time detection of DPP-IV activity over a broader range (0-40 U/L) with high selectivity and stability was obtained, thus providing a method that can be used to determine the levels of DPP-IV/CD26 in biological fluids such as serum and plasma.

Further assay developments were conducted to overcome limitations encountered with the original Au NP assay, especially the narrow dynamic linear range and stability in high ionic strength solutions. Validation and comparison of the Au NP assay developed has revealed that this method is highly correlated to the gold standard chromogenic Gly-Pro-pNA method for detection of enzyme activity in biological samples. Very good recoveries (in the range 83.6 –114.9%) were obtained in spiked serum samples, which indicate that this assay could provide a suitable alternative for enzyme activity detection with the naked eye and without the need for sophisticated instruments.

Investigations into the effects of incorporating different stabilizers in order to improve the stability of the peptide functionalized Au NP in high ionic strength solutions were also investigated. Gold nanoparticles have different shapes and structures and an alternative approach for detection of DPP-IV activity using gold nanorods due to their higher refractive index sensitivities was explored.

As a conclusion, three out of five approaches, all utilising Au NP-ligand conjugates were demonstrated useful for the detection of the DPP-IV activity. The system developed here is portable and would permit on-site analysis of samples, which offers a real alternative approach from traditional assays and reduces the need for laboratory testing. The logical next step in this research would be the continuation of experiments to transform this test into a point of care testing device that could offer an early detection tool for disease management.

# Acknowledgements

---

First and foremost, I would like to thank almighty God for all of his blessings on me that I can't count it.

I would like to express my utmost gratitude to my mentor and advisor Dr Philip Gardiner, for his continued guidance which helped me accomplish the goals of my research. Dr Gardiner has been a great source of inspiration, for his patience and perseverance has helped embed confidence in myself to explore new opportunities.

My thanks also to my second supervisor, *Prof.* Nicola Woodroffe, for her generous help at all stages of the project. I would also like to thank Mootaz Salman, Mohammed Tawfiq, Tamim Chalati, Peter Kanegoni and Abdu Rahman Eswayh for all their help and cooperation as well as their friendship and advice. I would never forget to thank Marguerite Lyons for being more than an administrator but a real help hand for all what we needed and asked for.

I would like to thank Dr Zabaeda Islam at Leeds EPSRC Nanoscience and Nanotechnology Research Equipment Facility (LENNF) for the TEM analysis of gold nanoparticles. I would also like to thank Dr Abdullatif Alfutaimie at Manchester University for allowing us to use their zetasizer instruments for the zeta potential and hydrodynamic radius measurements of gold nanoparticles.

My thanks to Sheffield Hallam University for making this dream achievable and Mosul University (my mother University) for giving me this opportunity to develop my career. I am also very grateful to the Royal Society of Chemistry, for their financial support towards attending the scientific meeting and national and International conferences. My thanks also go to the Ministry of Higher Education and Scientific Research for supporting me with the scholarship.

To conclude, I would like to dedicate this Doctoral Thesis to my family, who I will never be able to give back all the support they have given to me as it is immeasurable. Thanks to my mum, dad, my mother-in-law, father-in-law and my lovely sister, Aya and my brothers Hussein and Ahmed. To my beloved wife, Sana, who stands by me and always comforts and cares for me. I am so blessed to have you. To my beautiful daughters Hala and Lena who made me forget the stress and fears when I see them playing and laughing around me.

# Publications List during PhD

---

1- **Hasan Saad Aldewachi**, Nicola Woodroffe, Simon Turega, Philip H.E. Gardiner, (2017) Optimization of gold nanoparticle-based real-time colorimetric assay of dipeptidyl peptidase IV activity. *Talanta* 169, 13–19.

2- **Hasan Saad Aldewachi**, Tamim Chalati, Nicola Woodroffe, Neil Bricklebank, Basil Sharraq, Philip H.E. Gardiner, Gold Nanoparticle-Based Colorimetric Biosensor for Enzyme Detection and Quantification. *Nanoscale* (In press).

3- Vladimir Bochenkov, Jeremy Baumberg, Mikhail Noginov, Felix Benz, **Hasan Aldewachi**, *et al.* (2015) Applications of plasmonics: general discussion. *Faraday Discussion*, 178, 435.

4- Peer Reviewer in *Talanta Journal*.

# International Conferences and grants

---

1. **H. Aldewachi**, N. Woodroofe, P. Gardiner. Peptide Ligand Containing a Spacer Functionalized Gold Nanoparticle for Colorimetric Dipeptidyl Peptidase IV Activity Measurement and Inhibition. 5<sup>th</sup> International Conference on Bio-Sensing Technology. 7 - 10 May 2017 | Riva del Garda, Italy. Poster Presentation (£400 travel grant from RSC)
2. **H. Aldewachi**, N. Woodroofe, P. Gardiner. Gold nanoparticle modified with peptide ligands containing spacer system for colorimetric detection of Dipeptidyl Peptidase IV activity. XIII International Conference on Nanostructured Materials, August 7 to 12, 2016 Quebec, Canada. (Oral Presentation) (£250 travel grant from RSC)
3. **H. Aldewachi**, N. Woodroofe, P. Gardiner, Simple Colorimetric Assay for DPP-IV Activity Using Peptide / Self- Spacer Functionalized Gold Nanoparticles. "Europt(r)ode XIII - Conference on Optical Chemical Sensors and Biosensors - Austria, March 20 - 23, 2016 (Poster).
4. **H. Aldewachi**, N. Woodroofe, P. Gardiner. Simple and Real-Time Colorimetric Assay for DPP-IV Activity Using Peptide Functionalized Gold Nanoparticles. 4th International Conference and Exhibition on Biosensors and Bioelectronics, 28-30 September 2015 Atlanta, USA (Oral Presentation) (£750 travel grant from RSC)
5. **H. Aldewachi**, M. Hines, Z. Islam, N. Woodroofe, P. Gardiner. Facile Colorimetric Measurement of Dipeptidyl Peptidase IV (DPP-IV) Activity Via Peptide Capped Gold Nanoparticles Nanoplasmonics: Faraday Discussion 178 16 - 18 February 2015, London, United Kingdom (£200 travel grant from RSC)
6. **H. Aldewachi**, M. Hines, M. McCulloch, N. Woodroofe, P. Gardiner. Colorimetric Measurement of Dipeptidyl Peptidase IV (DPP-IV) Activity Via Peptide Capped Gold Nanoparticles 5th EU Chemistry Congress in Istanbul, 31 August- 4<sup>th</sup> of September 2014 Istanbul, Turkey (Poster) (£500 travel grant from RSC)

# Declaration

---

I hereby declare that except where due acknowledgment has been made; the work is that of my own; and the work has not been submitted previously, in whole or in part, to qualify for any other academic award. The content of the thesis is the result of work which has been carried out since the official commencement date of the approved research program; and, any editorial work, paid or unpaid, carried out by a third party is acknowledged.

Hasan Saad Aldewachi

August 2017

## Copyright

The copyright of this thesis rests with the author. No quotation from it should be published without prior consent and information derived from it should be acknowledged.

“Where Nature finishes producing its own species, man  
begins, using natural things and with the help of this  
nature, to create an infinity of species”  
Leonardo da Vinci, XV-XVI

# Table of Contents

Abstract .....	ii
Acknowledgements .....	iv
Publications List during PhD .....	v
International Conferences and grants .....	vi
Declaration .....	vii
List of Figures .....	xii
List of Tables.....	xvi
List of Abbreviations.....	xvii
<b>1 General Introduction and Literature Review .....</b>	<b>1</b>
1 Introduction.....	2
1.1 History of Gold Nanoparticles .....	3
1.2 Synthesis and Functionalization of Gold Nanoparticles .....	5
1.2.1 Citrate Reduction .....	6
1.2.2 Brust - Schiffrin Method .....	11
1.2.3 Seed-Mediated Growth Procedure .....	14
1.3 Colloidal Au NP Functionalization and Stabilization.....	15
1.3.1 DLVO and non-DLVO forces.....	16
1.3.2 Stabilization Strategies.....	17
1.4 Synthesis of Peptide Functionalized Au NPs .....	20
1.4.1 Ligand Exchange.....	20
1.4.2 Direct Synthesis .....	21
1.4.3 Chemical Coupling .....	21
1.5 Properties of Metallic Nanoparticles .....	22
1.5.1 Localized Surface Plasmon Resonance (LSPR) .....	22
1.5.2 Quantum Size Effects.....	25
1.5.3 Tuneable Surface Chemistry .....	26
1.6 Biomedical Applications of Au NPs.....	26
1.6.1 Biosensing Applications.....	28
1.6.2 Targeted Drug and Gene Delivery .....	31
1.6.3 Gold Nanoparticles for Visualization and Labelling .....	32
1.6.4 Photothermal Therapy .....	33
1.6.5 Gold Nanoparticles for Enzyme Activity Detection .....	34
1.7 Dipeptidyl peptidase IV .....	37

1.7.1 Classification.....	38
1.7.2 Sequence and Three-Dimensional Structure.....	39
1.7.3 Mechanism of Hydrolysis by DPP-IV/CD26.....	40
1.7.4 Enzyme Localisation and availability.....	40
1.8 Functions of DPP-IV/CD26.....	41
1.8.1 Proteolytic Function.....	42
1.8.2 Co-stimulatory, Receptor, Immunological Functions.....	43
1.8.3 Other Miscellaneous Functions.....	44
1.9 DPP-IV/CD26 Protein Levels and Activity.....	45
1.9.1 DPP-IV/CD26 Activity in Pathological Conditions.....	45
1.9.1 Assay of DPP-IV Activity.....	47
1.10 Research Aims.....	50
<b>2 Experimental Techniques.....</b>	<b>52</b>
2 Experimental Techniques.....	53
2.1 UV-Visible Spectroscopy.....	53
2.2 Transmission Electron Microscopy (TEM).....	54
2.3 Zeta-Potential.....	57
2.4 Dynamic Light Scattering (DLS).....	59
2.5 X- Ray Photoelectron Spectroscopy XPS.....	61
2.6 Fourier Transform Infrared Spectroscopy (FTIR).....	63
2.7 Electrospray Ionization Mass Spectrometry (ESI-MS).....	65
2.8 Nuclear Magnetic Resonance (NMR) Spectroscopy.....	66
2.9 Gel Electrophoresis.....	68
3 Chapter.....	70
<b>Development of Gold Nanoparticle-Based Real Time Colorimetric Assay of Dipeptidyl Peptidase IV activity.....</b>	<b>70</b>
3.1 Introduction.....	71
3.2 Materials and Methods.....	74
3.2.1 Reagents and Materials.....	74
3.2.2 Preparation of Citrate-Capped Gold Nanoparticles and GPDC-Capped Gold Nanoparticles Bioconjugate (P-Au NPs).....	75
3.2.3 Instrumentation for Gold Nanoparticle Characterization.....	76
3.2.4 Colorimetric Assay of DPP-IV/CD26 Activity.....	78
3.3 Results and Discussion.....	79
3.3.1 Design of the Peptide Substrate.....	79

3.3.2 Synthesis of GPDC-Functionalized Gold Nanoparticles .....	79
3.3.3 Examination of Peptide Coupling by XPS.....	81
3.3.4 Analysis of Gold Nanoparticle Size and Charge Before and After Functionalization by DLS and Zeta Potential Measurement .....	86
3.3.5 Sensitivity of GPDC-Capped Gold Nanoparticle to DPP-IV/CD26 activity.....	87
3.3.6 Investigation of the Assay Dynamic Range .....	90
3.3.7 Selectivity Study .....	91
3.3.8 Control Studies.....	92
3.3.9 Study of the Reaction Time Course .....	93
3.3.10 Quantifying Thiol Ligand Density .....	95
3.3.11 DPP-IV Directed Cleavage of Peptide Substrate .....	96
3.4 Conclusion .....	99
4 Chapter.....	101
<b>Assay Development: Incorporation of Spacer for generation of Peptide Functionalized Gold Nanoparticle for use in Colorimetric Measurement of Dipeptidyl Peptidase IV Activity .....</b>	<b>101</b>
4.1 Introduction.....	102
4.2 Experimental.....	104
4.2.1 Reagents and Materials .....	104
4.2.2 Preparation of Citrate-Capped Gold Nanoparticle and Peptide Coupled Gold Nanoparticle Bioconjugate (P-Au NP) .....	104
4.2.3 Instrumentation for Gold Nanoparticle Characterization.....	104
4.2.4 Colorimetric Assay of DPP-IV/ CD26 Activity.....	105
4.3 Results and Discussion .....	106
4.3.1 Design of the Peptide Substrate .....	106
4.3.2 Investigation of Peptide Coupling to Gold Nanoparticle Surface by DLS and Zeta potential Measurements .....	107
4.3.3 Sensitivity of VP-EN-DC Capped Au NPs to DPP-IV activity.....	108
4.3.4 Selectivity Study .....	112
4.3.5 Investigation of the Assay Dynamic Range .....	112
4.3.6 Stability of the Modified Au NP Formulation .....	113
4.3.7 Determination of the optimal pH of the Assay .....	115
4.3.8 Application of the Colorimetric Assay Using Modified Au NPs for Detection of DPP-IV Activity in Biological Samples .....	116
4.3.9 Method Comparison.....	118
4.3.10 Inhibition of the DPP-IV Enzyme.....	119

4.4	Conclusions.....	121
5	Chapter.....	123
	<b>Enhancing Gold Nanoparticle Stability for Colorimetric Detection of DPP-IV/CD26 .....</b>	<b>123</b>
5.1	Introduction.....	124
5.2	Experimental.....	128
5.2.1	Materials and Methods.....	128
5.2.2	Au NPs modified with capping ligands were prepared as follows: .....	128
5.2.3	Instrumental Techniques .....	129
5.2.4	Assay of DPP-IV activity.....	130
5.3	Results and Discussion .....	131
5.3.1	Investigation of coupling by UV-Visible Spectroscopy .....	131
5.3.2	Evaluation of Ligand Coupling by Gel Electrophoresis .....	132
5.3.3	Evaluation of Other Ligands Coupling to Gold Nanoparticle Surface by FTIR..	133
5.3.4	Stability of Modified Au NP in High Ionic Strength Solutions.....	135
5.3.5	Investigation of Zeta potential and Hydrodynamic Radius.....	137
5.3.6	Detection of DPP-IV/CD26 Activity .....	138
5.3.7	Quantitative Determination of DPP-IV/CD26 Activity.....	139
5.4	Conclusion .....	140
6	Chapter.....	143
	<b>Gold Nanorods as Potential Alternatives for the Development of DPP-IV Colorimetric Sensors.....</b>	<b>143</b>
6.1	Introduction.....	144
6.1.1	Au NRs Synthesis .....	145
6.1.2	Biomedical Applications of Au NRs.....	145
6.2	Experimental.....	147
6.2.1	Materials and Methods.....	147
6.2.2	Preparation of NRs.....	147
6.2.3	Functionalization of Au NRs with Peptide Ligands .....	147
6.2.4	Instrumental technique .....	147
6.3	Results and Discussion .....	148
6.4	Conclusion .....	151
7	Chapter.....	153
	<b>Conclusions and Future Work.....</b>	<b>153</b>
	References .....	161

## List of Figures

Figure 1-1 Schematic representation of the preparation of citrate stabilized Au NP in an aqueous medium.....	6
Figure 1-2 The LaMer mechanism of nucleation.....	8
Figure 1-3 The one and two-phase Brust–Schiffrin method for Formation of thiol-capped Au NPs.....	13
Figure 1-4 Schematic representation of Au NPs conjugated with various functional probes both through the gold–thiolate bond and by passive adsorption.....	15
Figure 1-5 Stabilization of Au NPs by various repulsion forces. ....	19
Figure 1-6 Schematic Representation of Localized Surface Plasmon Resonance (LSPR) excitation of Au NPs. ....	23
Figure 1-7 Versatile properties of Au NPs employed for biomedical applications. ....	27
Figure 1-8 The operational principle of the lateral flow test strip. ....	31
Figure 1-9 Protein or enzyme detection by reversible crosslinking mechanism (CL)....	36
Figure 1-10 Non-Crosslinking aggregation of peptide modified Au NPs .....	37
Figure 1-11 Schematic representation of substrates cleaved by DPP-IV/CD26.....	39
Figure 1-12 Principle of luminescent DPP-IV/CD26 assay.....	48
Figure 1-13 Schematic illustration of the combined colorimetric/electrochemical method for DPP-IV activity assay.....	49
Figure 1-14 Experimental flow chart for the design of a peptide modified Au NPs colorimetric assay.....	51
Figure 2-1 A diagram of the components of a typical spectrometer.....	54
Figure 2-2 Schematic diagram of a Transmission Electron Microscope.. ....	56
Figure 2-3 Schematic representation of the electrical double layer that surrounds a particle in an aqueous medium.....	58
Figure 2-4 Schematics of the operation of particle size analyser and zeta potential instrument. ....	61

Figure 2-5 (A) The photoemission process involved for XPS surface analysis. (B) XPS survey spectrum from citrate stabilized Au NPs showing various gold, sodium, oxygen peaks and a silicon peak.....	63
Figure 2-6 True color photograph of gold nanostructures in agarose gel .....	69
Figure 3-1 Illustration of the changes induced by target interaction with substrate modified Au NPs represented by UV-visible spectrophotometry and TEM imaging. ...	72
Figure 3-2 Schematic representation of the working principle of the GPDC peptide modified Au NP system for the determination of DPP-IV/CD26 activity.....	74
Figure 3-3 Particle size histogram of citrate-capped Au NPs. ....	76
Figure 3-4 UV-Vis absorption spectra of dispersed citrate-Au NPs and GPDC capped Au NPs .....	80
Figure 3-5 XPS survey scan of GPDC capped Au NPs.....	85
Figure 3-6 S 2p narrow scan XPS spectra for GPDC capped Au NPs. ....	85
Figure 3-7 S 2p narrow scan XPS spectra for GPDC capped Au NPs. ....	85
Figure 3-8 Au 4f narrow scan XPS spectra for GPDC capped Au NPs. ....	86
Figure 3-9 Zeta potential measurements of bare Au NPs and GPDC-capped Au NPs .	87
Figure 3-10 Effect of DPP-IV/CD26 activity on colour and absorption spectra of GPDC capped Au NPs.....	89
Figure 3-11 TEM micrograph of GPDC functionalized gold nanoparticles before (left) and after (right) interaction with DPP-IV/CD26 enzyme.. ....	89
Figure 3-12 Calibration curve of $Abs_{642}/Abs_{522}$ versus the concentration of DPP-IV/CD26. (Inset): Expanded linear region. ....	90
Figure 3-13 Response of functionalized Au NP incubated with 20 U/L of DPP-IV compared to the effect produced by other enzymes and proteins. ....	91
Figure 3-14 Response of the GPDC functionalized Au NP solution to the addition of DPP-IV/CD26 20 U/L in control experiment. ....	92
Figure 3-15 Plot of ratio of absorbance of GPDC-Au NPs at 642/522 nm versus reaction time at various enzymatic activities of DPP-IV/CD26. ....	94
Figure 3-16 Changes in the hydrodynamic size with time in the presence of 20 U/L of DPP-IV measured by DLS. ....	95

Figure 3-17 Mass spectrum of GPDC capped Au NPs after hydrolysis with DPP-IV/CD26.....	97
Figure 3-18 400 MHz <sup>1</sup> H NMR spectra of: (A) GPDC and (B) GPDC + DPP-IV.....	98
Figure 4-1 Schematic representation of the working principle for measurement of DPP-IV/CD26 activity.....	106
Figure 4-2 Zeta potential measurements of citrate stabilized Au NPs , VP-EN-DC modified Au NPs .....	107
Figure 4-3 UV–vis Absorption spectra of VP-EN-DC capped Au NPs after incubation with different activities of DPP-IV. ....	111
Figure 4-4 Hydrodynamic size distribution for modified Au NPs. before (left) and after (right) incubation with DPP-IV/ CD26.....	110
Figure 4-5 TEM micrograph of GPDC functionalized gold nanoparticles before (left) and after (right) interaction with DPP-IV/CD26 enzyme with various magnifications. ....	111
Figure 4-6 Response of the VP-EN-DC functionalized Au NPs solution incubated with 20 U/L of DPP-IV compared to effect produced by other enzymes, proteins .....	112
Figure 4-7 Calibration curve of $A_{700}/A_{525}$ versus the different activities DPP-IV incubated with VP-EN-DC functionalized Au NPs.....	113
Figure 4-8 The stability of the functionalized Au NP during storage. UV-vis absorption spectra of the colorimetric assay in absence of DPP-IV/CD26 . ....	114
Figure 4-9 Effect of pH changes on the VP-EN-DC capped Au NP assay for detection of DPP-IV enzyme activity.....	115
Figure 4-10 UV-vis absorption spectra of the colorimetric assay using spiked DPP-IV standards (0, 5, 10, 15, 20 and 25 U/L DPP-IV /CD26) with human serum samples...	117
Figure 4-11 Ratio plots of $A_{750}/A_{525}$ versus DPP-IV/CD26 activity.....	119
Figure 4-12 Comparison of the assay results toward DPP-IV in human serum specimens using the developed colorimetric assay and the Gly-Pro-pNA based commercial method .....	118
Figure 4-13 Inhibitory ratio of different concentrations of Vildagliptin on DPP-IV (20 U/L) activity.....	120
Figure 5-1 UV-Vis absorption spectrum of modified Au NPs .....	131

Figure 5-2 Agarose gel electrophoresis of citrate and peptide capped Au NPs.....	132
Figure 5-3 Infrared spectra of stabilized ligands.....	134
Figure 5-4 Effect of introducing different stabilizing groups on the stability of Au NPs. .....	135
Figure 5-5 UV-Vis study of C/G capped Au NP stability as a function of NaCl concentration.....	136
Figure 5-6 UV–Visible absorption spectra of C/G capped Au NPs after incubation with different activities of DPP-IV..	139
Figure 5-7 Calibration curve of $A_{700}/A_{525}$ versus the different activities of DPP-IV incubated with C/G capped Au NPs.....	140
Figure 5-8 Schematic depicting the design of the stealth peptide sequence inspired by the analysis of human protein surface... ..	145
Figure 6-1 Gold nanorods peak absorption and scattering.....	146
Figure 6-2 Comparison of the UV-visible spectra of Au NPs and Au NR .....	147
Figure 6-3 UV–visible absorption spectrum of Au NRs.....	150
Figure 6-4 UV-Vis absorption spectra of GPDC capped Au NRs.....	149
Figure 6-5 UV-Vis absorption spectra of dispersed citrate-Au NRs and VP-EN-DC capped Au NPs .....	150
Figure 6-6 DPP-IV/CD26 activity detection using a peptide modified Au NR assay. .	151

## List of Tables

Table 1-1 Chronological development of nanotechnology and nanoscience.....	5
Table 1-2 Physiological Peptides/Hormones Identified as Substrates of DPP-IV/CD26 and Subject to Modulation by DPP-IV/CD26.....	43
Table 1-3 Activity levels of human dipeptidyl peptidase IV in plasma and serum in men and women.....	45
Table 1-4 DPP-IV/CD26 as a marker of diseases.....	46
Table 2-1 Classification of colloid stability according to zeta potential values .....	58
Table 3-1 Comparison of the assay sensitivity as defined by the limit of detection (LOD) and limit of quantification (LOQ) of colorimetric, fluorometric and luminescent DPP-IV assays.....	72
Table 3-2 Surface composition in atomic % as determined by quantitative XPS survey scans .....	83
Table 4-1 Recoveries of DPP-IV/CD26 activity in spiked human serum samples using the P-Au NPs.....	116
Table 4-2 Categories of screening assay quality by the value of the Z-factor.....	120
Table 5-1 Peptide sequences trialled to enhance Au NP stability.....	126
Table 5-2 Summary of ligand, functionalized gold nanoparticle properties.....	127
Table 5-3 Average zeta potential and hydrodynamic radius of different peptide stabilized Au NPs.....	137
Table 7-1 Summary of the performance of developed assays.....	154

# List of Abbreviations

---

AA: Amino acid

ADA: adenosine deaminase

APC: antigen-presenting cells

Au NP: Gold nanoparticle

Au NR: Gold nanorod

CALNN: Cys-Ala-Leu-Asn-Asn

CCL5: Chemokine (C-C motif) ligand 5

CD26: Cluster of differentiation 26

cDNA: Complementary DNA

CL: Cross-linking

CSF: Cerebrospinal fluid

CTAB: Cetyl trimethyl ammonium bromide

CXCL: Chemokine ligand

DLS: Dynamic light scattering

DLVO: Derjaguin-Landau-Verwey-Overbeck

DMSO: Dimethyl sulphoxide

DPP-IV: Dipeptidyl peptidase IV

DPP-IVi: Dipeptidyl peptidase IV inhibitors

dsDNA : Double-stranded DNA

ECM: extracellular matrix

EDC: [1-ethyl-3-(3-dimethylaminopropyl) carbodiimide hydrochloride]

ESI-MS: Electrospray Ionization Mass Spectrometry

(FAP- $\alpha$ ): Fibroblast activation protein-alpha

Fc: Ferrocene

FDA: Food and drug administration

FEG: Field emission gun

FTIR: Fourier transform infrared

Gly-Pro pNA: Glycylproline *para*-nitroanilide

HSA: Human serum albumin

HTS: High throughput screening

LC/MS: Liquid chromatography/ mass spectrometry

LOD: Limit of detection

LSPR: Localized Surface Plasmon Resonance

NCL: Non-crosslinking

NHS: N-hydroxy sulfosuccinimide

NIR: Near-infrared region

NK cells: Natural killer cells

nm: Nanometre

NMR: Nuclear Magnetic Resonance

OD: Optical density

PEG: Polyethylene glycol

pNIPAAm: Poly- (N-isopropyl acrylamide)

POC: Point of care

ssDNA : Single-stranded DNA

sDPP-IV: Soluble form of DPP-IV enzyme

Sulfo-NHS: N-hydroxy sulfosuccinimide

TAE: Tris base, acetic acid and EDTA

TCR: T cell receptor

TEM: Transmission Electron Microscopy

TOAB: Tetra octyl ammonium bromide

Tris: Tris (hydroxy methyl) aminomethane

UHV: Ultra-high vacuum

UV-Vis: Ultraviolet-Visible

VP-EN-DC: Val-Pro-NH-(CH<sub>2</sub>)<sub>2</sub>-NH-Asp-Cys

XPS: X-ray Photoelectron Spectroscopy

Standard amino acid abbreviations:

Ala: Alanine (A)

Arg: Arginine (R)

Asn: Asparagine (N)

Asp: Aspartic acid (D)

Cys: Cysteine (C)

Gly: Glycine (G)

His: Histidine (H)

Leu: Leucine (L)

Pro: Proline (P)

Ser: Serine (S)

Val: Valine (V)

# Chapter 1

---

## General Introduction and Literature Review

---

# 1. Introduction

Nanoparticles (NPs) (derived from the Greek word nanos, meaning dwarf) are defined in a variety of ways, but the most widely accepted definition refers to stable colloid solutions of clusters of atoms in which 50% or more of the particles (small clusters or large molecules) are in the size range 1 – 100 nm, and have properties that are not in common with non-nanoscale particles of the same chemical composition (Royal Academy of Engineering & Royal Society 2004; Ahlbom et al. 2009). Although most definitions focus on the dimensions as the critical property that defines NPs, some scientists argue that the unique electrical, optical, magnetic and catalytic properties found at nanoscale dimensions are more relevant for their classification (Weller 1993; Alivisatos 1996; Storhoff & Mirkin 1999; Niemeyer 2001; Oliveira et al. 2015).

Metallic NPs have distinctive optical, electronic, chemical and magnetic properties that are remarkably unlike those of the individual atoms or their bulk counterparts. The main factors that account for these characteristics are high surface to volume ratio (Schmid 2011), quantum size effect (Kubo 1962; Lemire et al. 2004) and electrodynamic interactions (Pinchuk et al. 2007).

The possibility of controlling and tuning these unique optical and electronic properties make these materials prime candidates for a wide range of technological and biomedical applications. These attractive and unique properties make nanomaterials physicochemically altered and often superior to both the atomic and bulk materials of the same element (Hadjipanayis & Siegel 2012). For instance, aluminum which is stable at macro scale turns combustible at the nanoscale (Shafirovich *et al.* 2007); gold (Au), which is practically insoluble in water at the macro scale becomes more soluble at the nanoscale (Pengo *et al.* 2003). Platinum, which is chemically inert at macro scales, can serve as a potent chemical catalyst at the nanoscale (Cheong *et al.* 2010). While a

known insulator, silicon turns into a conductor of electrical current at the nanoscale (Hu et al. 2003; Szczech & Jin 2011).

## 1.1 History of Gold Nanoparticles

The first reference to the use of soluble Au compounds is found in Egyptian manuscripts from the Greco-Roman era in the 5th or 4th century B.C when “soluble” gold emerged in Egypt and China (Daniel & Astruc 2004). One of the most remarkable aspects of the behaviour of gold was the unusual optical effects displayed by glass containing colloidal gold, which was observed in the Lycurgus Cup (Freestone *et al.* 2007). The cup is made of a dichroic glass, which changes colour when exposed to light; ruby red in transmitted light and green in reflected light. Colloidal Au was also employed in the manufacture of ruby glass, in a process described by the German alchemist, Andreas Libavius, in his textbook, *Alchemia*, in 1597, in which he described how to make red crystals out of Au dissolved in liquid or oil (Hunt 1976). Gold has been used extensively for cosmetic, decorative, and for medicinal purposes. In the 17<sup>th</sup> century, a formula for mixing tin oxide with gold particles in a crude form of aqua regia was recorded in the Bologna manuscript, to yield "a beautiful purple" pigment. The above process was used to impart glass with a red coloration, as well as to determine the presence of gold when used as a chemical test (Habashi 2016).

Colloidal Au was used in the last century in one of the laboratory methods for the study of the cerebrospinal fluid (CSF) by using the reaction of Lange (Green 1925; Dykman & Khlebtsov 2012). A chance discovery made by Zsigmondy whilst looking for a method to prevent colloidal gold nanoparticles (Au NPs) from precipitation; he fortuitously found that only healthy CSF kept homogeneous Au NPs in solution, while precipitation occurred in pathological CSF samples (Green 1925). The value of the colloidal gold reaction in detecting and differentiating an infected from a non-infected condition of the central nervous system was a useful diagnostic tool, not only for early

diagnosis but also for the prognosis of obscure neurological conditions. Briefly, a series of diluted spinal fluid samples in aqueous saline solution were treated with a colloidal gold solution and the reaction was allowed to stand for 24 hours to get a final reading. Depending on the pathological conditions investigated, a certain pattern of colour change of the colloidal auric solution occurs. This application may have been the first recorded practical application of extremely small gold particles for biosensing.

Modern scientific evaluation of colloidal Au began with Michael Faraday's work in the 1850s, which recognized that the colour observed was due to the size of the Au particles (Faraday 1857). Faraday's rationale in investigating colloidal phenomena followed his interests in the interaction between light and matter. A few years later, the term "colloid" (from the French word, colle which means glue or gum) was linked to the use of Au particles in aqueous suspensions (Daniel & Astruc 2004).

In the 20th century, Ostwald and Zsigmondy's research on colloids (Svedberg 1909; Ostwald 1927; Hauser 1955) and Gustav Mie's theoretical explanation for the optical effects associated with nanosized metal particles by solving Maxwell's equation for the absorption and scattering of electromagnetic radiation by spherical particles laid the theoretical foundations for the use of NPs. Technological advances in the development of molecular beam techniques such as Transmission Electron Microscopy (TEM) and UV-visible Spectroscopy have made it possible to study and determine the morphological, physical and chemical properties of Au NPs (Mulvaney 1996; Link & El-Sayed 2000). The chronology of the historical events that led to the development of nanotechnology is listed in Table 1-1.

**Table 1-1** Chronological development of nanotechnology and nanoscience

Period	Authors	Achievement	Reference
4 <sup>th</sup> A. D	Romans	Lycurgus Cup	(Freestone <i>et al.</i> 2007)
17 <sup>th</sup> Century	Andreas Cassius	"Purple of Cassius" for glass staining	(Habashi 2016)
1857	Faraday	Scientific evaluation of Au NPs colour change	(Faraday 1857)
1902	Zsigmondy	Invention of ultramicroscope	(Champness 2001)
1951-1973	Frens-Turkevich	Synthesis of Au NP preparations	(Frens 1973)
1960	Feynman	Mention of nanoparticles in a famous lecture in which he stated that "there's plenty of room at the bottom" meaning developments at the nanoscale are possible.	(Feynman 1960)
1971	Faulk and Taylor	First biomedical use of Au in immunochemical staining	(Faulk and Taylor 1971)

## 1.2 Synthesis and Functionalization of Gold Nanoparticles

Since the first experiments on the production of Au NPs by the reduction of gold trichloride by phosphorus were developed by Faraday in 1857, a variety of approaches have been used for the synthesis of Au NPs but these mainly involve reduction of Au salts such as potassium or sodium tetra chloroaurate in the presence of a stabilizing agent (Frens 1973; Dykman *et al.* 1998; Chen *et al.* 2010b; Duan *et al.* 2015). Over the years, modifications to the synthesis of Au NPs have been tailored to make them suitable for further use (Schmid 1992; Grabar *et al.* 1995; Manea *et al.* 2008; Chen *et al.* 2010b; Hayat 2012; Hong 2013; Ren *et al.* 2015). The three commonly used synthesis

methods are (i) citrate reduction, (ii) Brust-Schiffrin and (iii) seed-mediated growth method.

### 1.2.1 Citrate Reduction

Citrate reduction, which was introduced by Turkevich and co-workers (Turkevich et al. 1951; Enustun & Turkevich 1963) is the most popular method, which involves the reduction of hot chloroauric acid (HAuCl<sub>4</sub>) solution with trisodium citrate leading to the formation of Au NPs (Figure 1-1). Frens reported the synthesis of Au NPs of sizes between 16 and 147 nm by varying the ratio of the reducing/stabilizing agent (in this case trisodium citrate) to Au salt to control their formation (Frens 1973). The resultant colloidal Au particles are nearly spherical or spheroid and have an overall negative surface charge due to the carboxylate ion coverage.

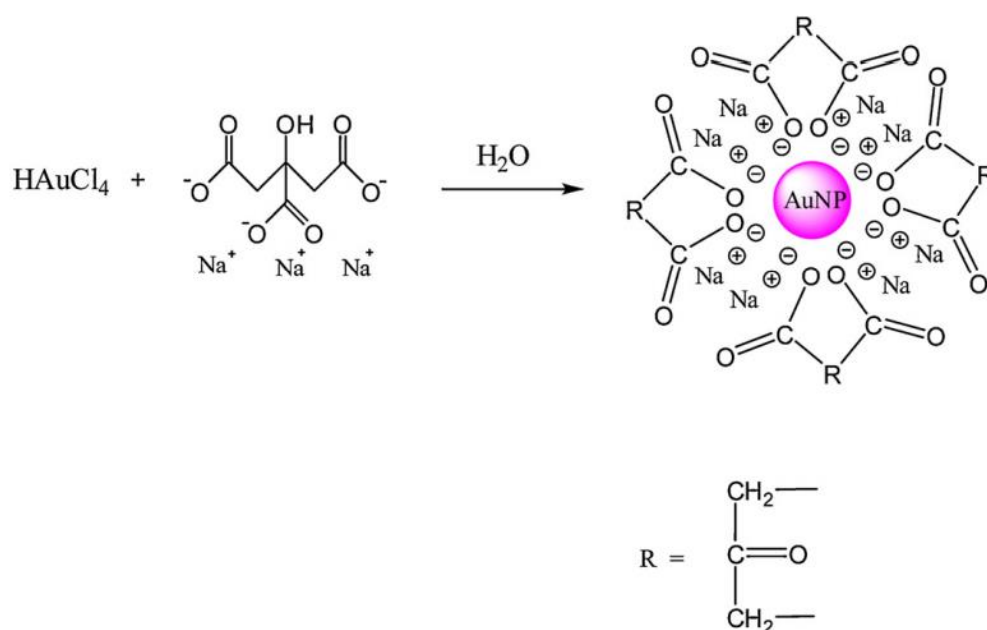


**Figure 1-1** Schematic representation of the preparation of citrate stabilized Au NP in an aqueous medium.

The HAuCl<sub>4</sub> solution is boiled, and the trisodium citrate dihydrate is then quickly added under vigorous stirring. Reprinted with permission (Zhao *et al.* 2013). The interaction involves coordination of one or multiple carboxylate groups to the surface Au atoms (Al-johani *et al.* 2017).

Numerous efforts have been made in an attempt to elucidate the mechanism of Au NP formation. A number of models have been proposed, many of which involve the formation of an aggregation phase, at the initial stages of the synthesis (Kumar *et al.* 2007; Mikhlin *et al.* 2011). These mechanisms misinterpreted the cause of the gray-bluish colour during the initial phase of the synthesis and attributed it to formation of aggregate intermediates, contrary to this explanation; further studies demonstrated that large Au aggregates are not formed at any time of the synthesis (Wuithschick *et al.* 2015).

The classical nucleation theory (developed by Becker and Döring more than 80 years ago) (Becker & Döring 1935), is considered as the basic model to describe the underlying mechanism for NP growth, which goes through the LaMer burst nucleation, followed by simultaneous growth of all the particles (LaMer & Dinegar 1950). According to this theory, nuclei (seeds) function as templates for crystal growth. Nuclei growth is governed by two mechanisms: (i) the monomer's diffusion (a "monomer" in the case of AuX clusters studied here is defined as a single AuX unit, where X = Cl<sub>4</sub>), in a thermodynamically unstable state, onto the surface of a nucleus and (ii) the rate of the reaction of the diffusing species on the surface (Finney & Finke 2008; Thanh *et al.* 2014).

According to the LaMer theory, the process of NP formation can be divided into two separate phases, which can be identified as spontaneous nucleation and isotropic growth. The essence of the mechanism, as illustrated in Fig. 1-2, goes through three sequential steps (LaMer & Dinegar 1950): (I) a slow increase in the monomer concentration in solution until it reaches some critical concentration (C), or more specifically a critical supersaturation point,  $C/C_{eq}$  where  $C_{eq}$  is the solubility of monomer in the solution, phase I in Fig. 1-2, (II) a "burst nucleation" which substantially lowers the free monomer concentration in solution, after this point

nucleation stops due to decrease in the free monomer concentration; (III) subsequent nucleation growth happens under the control of the diffusion of the monomers through the solution (Finney & Finke 2008; Thanh et al. 2014).

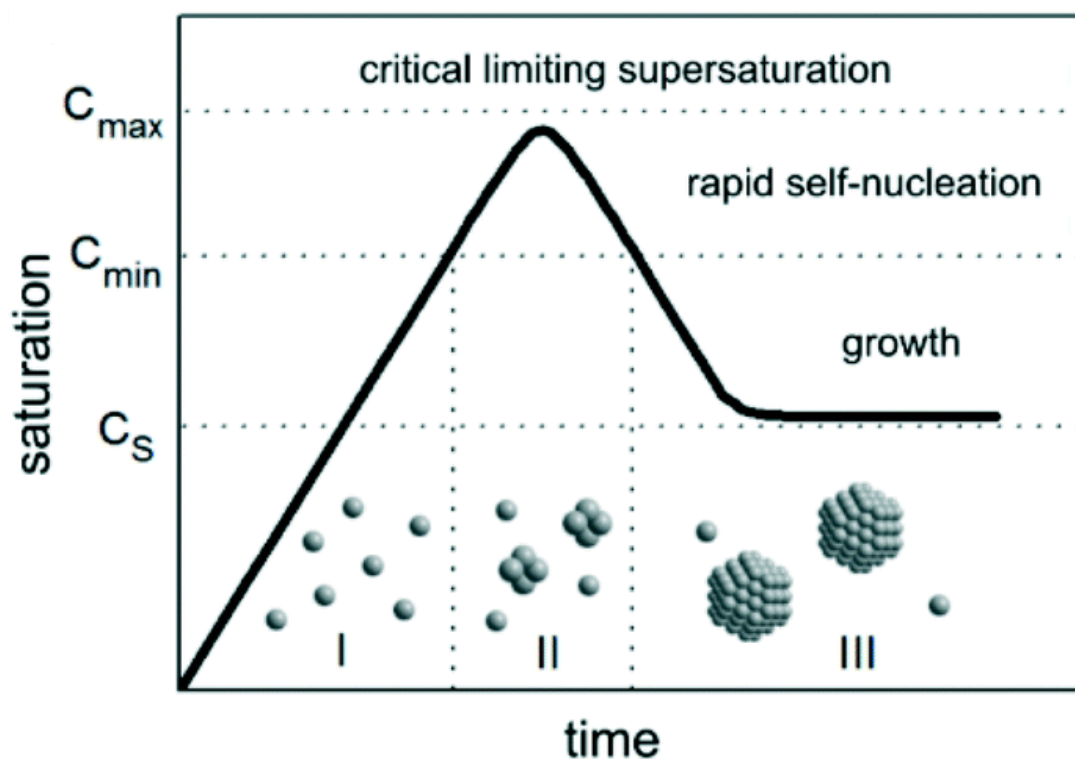


**Figure 1-2** The LaMer mechanism of (sulphur) nucleation. The (theoretical) curve shows monomer concentration as a function of time.

As a result of the consumption of the monomeric species by growth of a number of the preformed nuclei, the concentration of the monomeric species decrease until supersaturation is reached. At this stage the nucleation is stopped (the end of the nucleation stage) and the remaining stable nuclei continue to grow with a supersaturation below the critical level for nucleation (Stage III). Reprinted with permission (Polte 2015).

A further step towards a more relevant explanation for the formation of transition-metal nanoclusters, was introduced by Turkevich and his colleagues (1953) based on the "organizer model" (the "organizer" in this case was proposed to be the citrate ion). In this theory, it is proposed that dicarboxy acetone formed as a result of oxidation of sodium citrate is responsible for inducing nucleation events and aids in the formation of large macromolecules of gold ions and reducing agent (Wuithschick *et al.* 2015).

Shortly after LaMer suggested his mechanism, a growth model was proposed by Reiss (1951) which was known as "growth by diffusion" in which the growth rate of the NPs

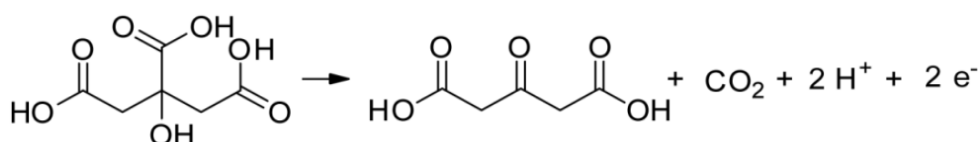
depends exclusively on the monomer diffusion into the particles, leading to faster growth of smaller particles in the presence of large particles and slower growth of larger particles, which in turn leads to more uniform size distribution known as size focusing. Reiss's model was extended later to take dissolution effects into account. The dissolution effect is known as - Ostwald ripening - in which larger nuclei grow more favourably at the expense of smaller ones (Sugimoto 1987). The LaMer model has been verified experimentally and the application of the nucleation theory has been extended to the formation of metal nanoclusters such as the formation of AgCl and AgBr clusters (Sugimoto *et al.* 2000).

The LaMer theory has since undergone modifications; a two-step mechanism was proposed whereby the process of nucleation and growth happen simultaneously (Watzky & Finke 1997). Chow and Zukoski undertook a re-evaluation of the formation mechanism for Au NPs by studying the kinetics of the Turkevich process (Chow & Zukoski 1994). They proposed that Au NP generation happens through a mechanism involving the formation of large particles that diminish in size over the course of the reaction. It should be noted that this mechanism agrees with the LaMer classical growth model, but allows primary particles to reversibly aggregate.

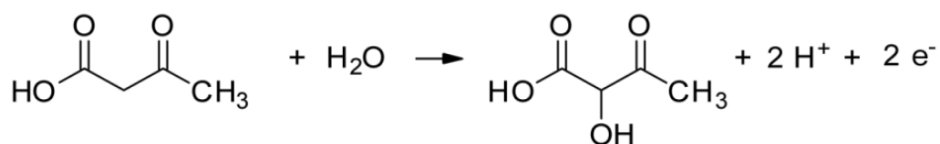
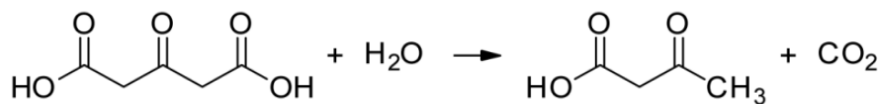
Nevertheless, several studies have revealed that the nucleation theory for the growth of NPs has failed to explain or accurately predict the particle size or the size distribution, (Finney & Finke 2008; Polte 2015). Pong and colleagues proposed a fundamentally distinct “necklace-breaking” mechanism by indicating that the small Au nuclei (ca. 5 nm diameter), formed by citrate-assisted reduction of H<sub>2</sub>AuCl<sub>4</sub>, primarily self-assemble into a network of joined chains. When Au accumulation increases, these chains lengthen in size, which in turn causes the spherical particles to be released from these structures, establishing the nanosphere product usually detected from this synthesis (Pong *et al.* 2007).

The use of the organic matrix during the initial stages of synthesis ensures dispersion of the Au NPs when nucleation occurs (Danks *et al.* 2016). The initial step of this process, with reactions occurring in series and parallel, is the oxidation of citrate that yields dicarboxy acetone, which is thought to take part in the reduction process of aurate ( $\text{Au}^{3+}$ ) and followed by further oxidation to yield acetic acid and formic acid (Scheme 1-1) which leads to the presence of a variety of species in solution, all of which play a role in the formation mechanism of Au NPs (Doyen *et al.* 2013). Then, the  $\text{Au}^{3+}$  ions are reduced to  $\text{Au}^{1+}$  and  $\text{Au}^0$ , and the  $\text{Au}^{1+}$  is assembled on the  $\text{Au}^0$  atoms to produce the Au NP (Zhao *et al.* 2013).

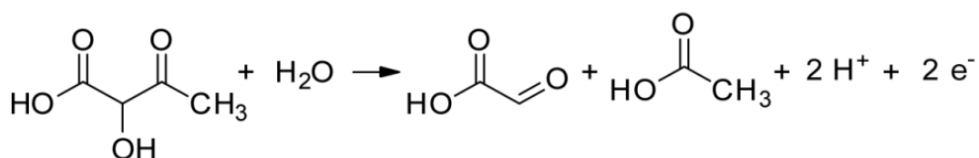
Oxidation of citrate to dicarboxyacetone



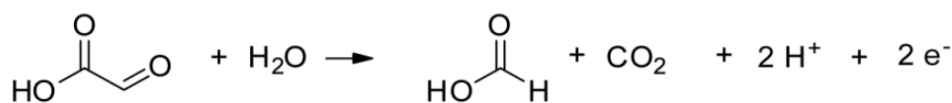
Decarboxylation of dicarboxyacetone to acetoacetic which is oxidized to hydroxyacetoacetic acid



Oxidation of hydroxyacetoacetic acid to acetic acid and glyoxylic acid



Oxidation of glyoxylic acid to formic acid



**Scheme 1-1** The Pathway of citrate oxidation/ decarboxylation during Au NP formation process. All species are represented in their fully protonated form (Doyen *et al.* 2013).

The citrate anion acts not only as a reducing and capping agent, to control the growth of the NPs and inhibiting their aggregation, but also serves to control the pH of the solution, as citrate has 3 protonation equilibrium states with respective pKa values of 3.1, 4.8, and 6.4 (Ji *et al.* 2007; Polte *et al.* 2010). Between the pH of 4.5-7, nearly monodispersed Au NPs with sizes ranging from 20 to 40 nm were synthesized (Patungwasa & Hodak 2008; Li *et al.* 2011; Liang *et al.* 2011). It has been reported that citrate could also serve as a “molecular linker” which participates in the formation of Au NPs (Doyen *et al.* 2013) when Au<sup>3+</sup> ions are reduced to Au<sup>1+</sup> by citrate, which in turn is oxidized to dicarboxy acetone forming a multimolecular complex between the products of redox reaction (Kumar *et al.* 2007).

Other parameters have been shown to control the size and size distribution of Au NPs prepared by the citrate reduction process. These include the effects of temperature (Li *et al.* 2011), ionic strength (Zabetakis *et al.* 2012) and the introduction of high-power ultrasound (Su *et al.* 2003). It has been also found that smaller and narrower Au NP size distribution can be obtained by reversing the sequence of the addition of citrate and chloroauric acid (Sivaraman *et al.* 2011; Ojea-Jiménez *et al.* 2011).

### **1.2.2 Brust - Schiffrin Method**

The synthesis of smaller Au NPs (2 - 5 nm) has been demonstrated in the organic phase utilizing the Brust and Schiffrin method (Brust *et al.* 1994). Briefly, the gold salt is dissolved in water and then transferred to the organic phase using an appropriate phase-transfer agent, such as tetra octyl ammonium bromide (TOAB). The addition of dodecanethiol to the organic phase AuCl<sub>4</sub><sup>-</sup> (1:1 molar ratio), followed by reduction with aqueous sodium borohydride (BH<sub>4</sub><sup>-</sup>) in the biphasic system, leads to the formation of dodecane thiolate-capped Au NPs and change of the organic phase colour from the characteristic orange to red or brown, depending on the Au NP size (Toma *et al.* 2010).

The role of the alkanethiol is to stabilize the colloidal Au NPs (Figure 1-3). The Brust-Schiffrin method was improved to a more facile and efficient procedure in which  $\beta$ -mercaptophenol-modified Au NPs were synthesized in a methanol solution, without the phase transfer agent TOAB, thereby avoiding the introduction of TOAB impurities (Brust *et al.* 1995). Indeed, these Au NPs can be frequently extracted and redissolved in organic solvents such as toluene, chloroform and hexane, without irreversible aggregation or dissociation (Martin *et al.* 2010). Furthermore, the NPs can be easily handled and functionalized as stable organic and molecular compounds, because they form monolayer protected clusters.

Au NPs are stabilized by relatively robust thiolate bonds, forming cuboctahedral and icosahedral shapes (Zhao *et al.* 2013). The sulphur-containing substances inhibit the growth process because of the nucleation-growth-passivation kinetics model, by which higher S/Au molar ratios provide smaller core sizes (Templeton *et al.* 2000). Highly monodispersed and smaller Au NPs can also be produced by increasing the rate of  $\text{NaBH}_4$  addition and reducing the solution temperature. Cheng *et al.* (2003) made Au clusters modified with cetyl trimethyl ammonium bromide (CTAB) that could be dispersed in aqueous solutions because of the polar nature of the capping ligands. Methods that can be used to transfer the NPs from the organic to aqueous phase have been reported, making it possible to produce platforms that can be used for biological applications (Gittins & Caruso 2001).

The critical parameter that limits Au NP size using the Brust method, compared with that obtained by using the Turkevich method, is essentially the use of the more powerful reducing agent  $\text{NaBH}_4$  in the former resulting in a faster reduction reaction (Zhao *et al.* 2013).

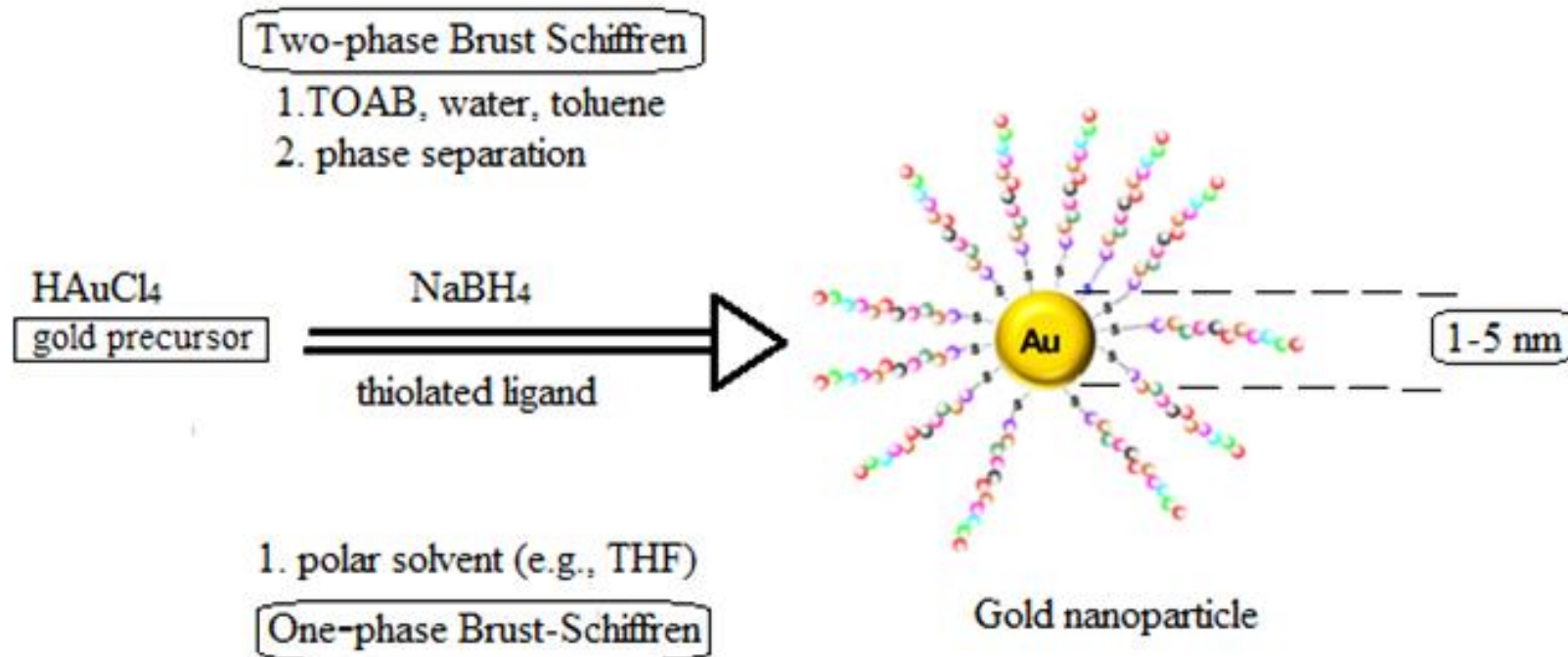


**Figure 1-3** The one and two-phase Brust–Schiffrin method for the formation of thiol-capped Au NPs. TOAB: tetra octyl ammonium bromide, THF: tetrahydrofuran. The coloured beads represent the thiolated ligands

### 1.2.3 Seed-Mediated Growth Procedure

The seed-mediated growth method is the most commonly used approach to produce other shapes of NPs (rods, stars, wires, cubes, etc.). In this method, spherical “seed” particles 3.5 - 4 nm are initially produced in the presence of a strong reducing agent such as  $\text{NaBH}_4$  and are then added to a growth solution containing more of the metal ions that will be deposited onto the seeds. A weak reducing agent, usually ascorbic acid (vitamin C), is used in the growth solution. Surfactants can be added to induce anisotropic growth (Murphy *et al.* 2005).

Jana *et al.* (2001) investigated the production of citrate modified Au NPs by the seed-mediated method using a wide range of reducing agents and conditions. They found that even in the presence of seeds, further nucleation occurs. There was therefore a need to control the conditions in order to avoid undesirable nucleation. The rate of addition of the reducing agent to the metal seed and the chemical reduction potential of the reducing agent were all factors that they needed to be carefully controlled.

Numerous physical techniques, such as vacuum deposition, electrical circuitry dispersion and laser ablation methods, have been used to split bulk gold into NPs (Rajput 2015). The shapes of the Au NPs can be modified and various Au NP forms can be fabricated by physical processes. However, the physical methods essentially rely on the use of expensive instrumentation with complicated sample preparation steps, with potential drawbacks, such as poor reproducibility, and they are time-consuming.

### 1.3 Colloidal Au NP Functionalization and Stabilization

Attaching stabilizer /functional groups with molecular recognition motifs are of critical importance for the use of NPs in various biomedical applications. For this purpose, a variety of biological probes have been used for the stabilization and/or functionalization of colloidal Au NPs, which include nucleic acids, enzymes, receptors, lectins, antibodies, aptamers and superantigens (Figure 1-4) (Sato *et al.* 2003; Aili *et al.* 2009; Wang *et al.* 2009; Piao & Chung 2012; Liu *et al.* 2015a). By selecting the appropriate functional group at the distal end of the molecule, it is possible to design and generate a distinct interface to interact with biomolecules and/or cells in certain ways.

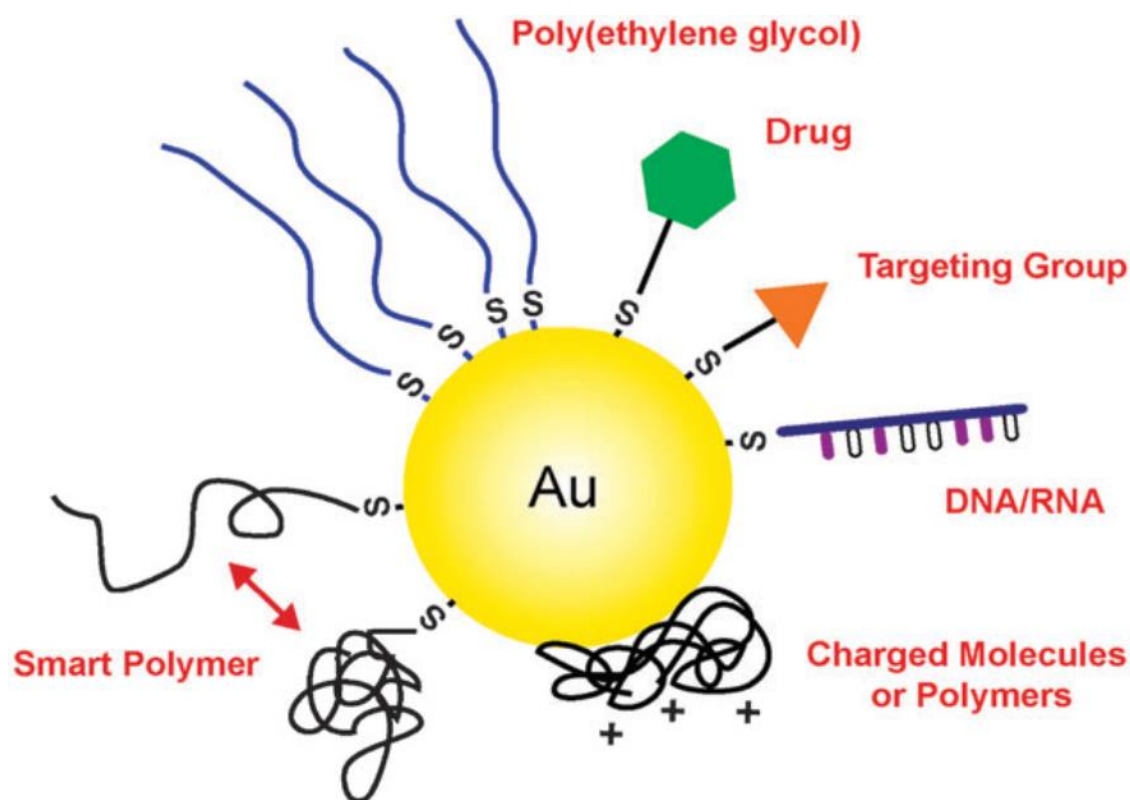


**Figure 1-4** Schematic representation of gold nanoparticles conjugated with various functional probes both through the gold–thiolate bond and by passive adsorption. Reprinted with permission from Cobley *et al.* (2011).

### 1.3.1 DLVO and non-DLVO forces

Since the dispersion and aggregation states of colloidal NPs influence their optical, electronic and catalytic behaviours (Snoswell *et al.* 2005), the forces that regulates the colloid stability and how to control these are essential considerations. The stabilization phenomenon of Au particles in a well-defined and controlled assembly has been generally explained by the Derjaguin-Landau-Verwey-Overbeck (DLVO) theory, usually expressed in terms of the balance between attractive van der Waals forces and the repulsive electrostatic interactions (Lyklema 2000; Kim *et al.* 2008). The DLVO theory accounts for the potential energy variations that occur when two particles approach each other with the resultant net attraction and repulsion forces as a function of interparticle distance (Glomm 2005). The van der Waals forces arise from interaction of particle-particle pair and can be expressed by the equation:

$$\omega(r) = -A/\pi^2 \rho_1 \rho_2 r^6 \dots\dots\dots (1)$$

Where  $r$  is the distance between 2 particles,  $\rho_1$  and  $\rho_2$  are the number of atoms per unit volume of the two interacting particles,  $A$  is the so-called Hamaker constant (Israelachvili 2011). As the effective Hamaker constant is a positive value, van der Waals forces between like particles would become attractive. On the other hand, electrostatic forces are repulsive for identical charged particles, due to the overlapping of electrical double layers. These two forces typically interact to create an energy barrier. The strength of the energy barrier controls the colloid stability in the solvent medium. The strength of the energy barrier and hence the colloid stability is governed by several factors such as the Hamaker constant, surface potential and electrolyte concentration (Zhou *et al.* 2009).

$$G = G_{vdW} + G_{elec} \dots\dots\dots (2)$$

Where  $G_{vdW}$  stands for attractive Van der Waals forces and  $G_{elec}$  stands for repulsive electrostatic forces.

Although there is considerable support for the DLVO model, it has long been accepted that the classical DLVO theory does not completely explain the results in several experimental settings, where forces acting between surfaces did not seem to obey, if not contradict the predictions of the theory, especially when two particles approach closer than a few nanometres (Lyklema 2005; Boinovich 2010). When two particles or surfaces come into close proximity, different hydrophobic, steric and solvation forces come into play, contributions from these are known as the ‘non-DLVO’ forces. These forces have been shown to be repulsive, attractive or oscillatory, and they can be much stronger than either of the two DLVO forces (Israelachvili 2011). Efforts to reconcile the theory and experiment have resulted in the inclusion of a variety mechanisms to account for the effects of long-range surface non-DLVO forces. One of the most commonly studied non-DLVO<sup>2</sup>-forces is called the Casimir force, which is a small attractive force that acts between two close parallel uncharged conducting metals. The effect is due to quantum vacuum fluctuations of the electromagnetic field. As a result of the presence of these forces the traditional DLVO theory has been extended and the interactions were described as follows (Hertlein *et al.* 2008):

$$G = G_{\text{vdW attraction}} + G_{\text{elec repulsion}} + G_{\text{non-DLVO forces}} \dots\dots\dots (3)$$

### 1.3.2 Stabilization Strategies

The key to the Au NP-based colorimetric sensing platform is the control of the colloidal Au NP dispersion and aggregation stages with a biological process (or analyte) of interest. Stabilization of colloidal Au is achieved either electrostatically or sterically or by a combination of both electrostatic and steric repulsion forces (Fig 1-5). Preparation of Au NPs by citrate reduction methods produce metal NPs stabilized electrostatically against aggregation induced by van der Waals attraction (De Vasconcelos *et al.* 2005). With respect to electrostatic stabilization, the surface charges, such as the negatively

charged citrate, attract positively charged counter ions in the surrounding solution forming an electric double layer with Coulombic repulsion that stabilizes the colloid particles, provided that the electric potential of the double layer is sufficiently high (Fig 1-5A) (Fendler 1996; Zhao *et al.* 2008). However, the double layer is very sensitive to variations in the ionic strength of the solution. The electrostatic repulsion decreases significantly at high salt concentrations, resulting in the compression of the double layer and displacement of the adsorbed citrate anions, leading to aggregation of the NPs (Chow & Zukoski 1994; Dougan *et al.* 2007; Hunter 2013; McDonagh *et al.* 2015).

In the case of steric stabilization (Figure 1-5B), ligands adsorbed onto the colloid surfaces form barriers which prevent colloidal aggregation. For effective steric stabilization, the adsorbed ligand molecules should be dense and thick in order to entirely protect the particles (De Gennes 1987). The strength of this stabilization effect is much less sensitive to salt concentrations, but is determined by the molecular size and the capping density of the ligands (Smitham *et al.* 1975; Napper 1977; Lourenco *et al.* 1996; Schiffelers *et al.* 2004). Common colloidal stabilizers include charged small molecules, polymers, and polyelectrolytes (De Vasconcelos *et al.* 2005; McDonagh *et al.* 2015). Highly charged ligands provide dual stabilization of the NPs (i.e., electrostatic and steric). This effect termed electrosteric effect, involves charges that are distributed along the ligand chains, and this is the most effective stabilization strategy (Figure 1-5C). Highly charged polymeric substances (e.g. polyethylene glycol, thiol- or thioether-functionalized polymers) are effective stabilizers of metal NPs (Schiffelers *et al.* 2004; Yu *et al.* 2013).

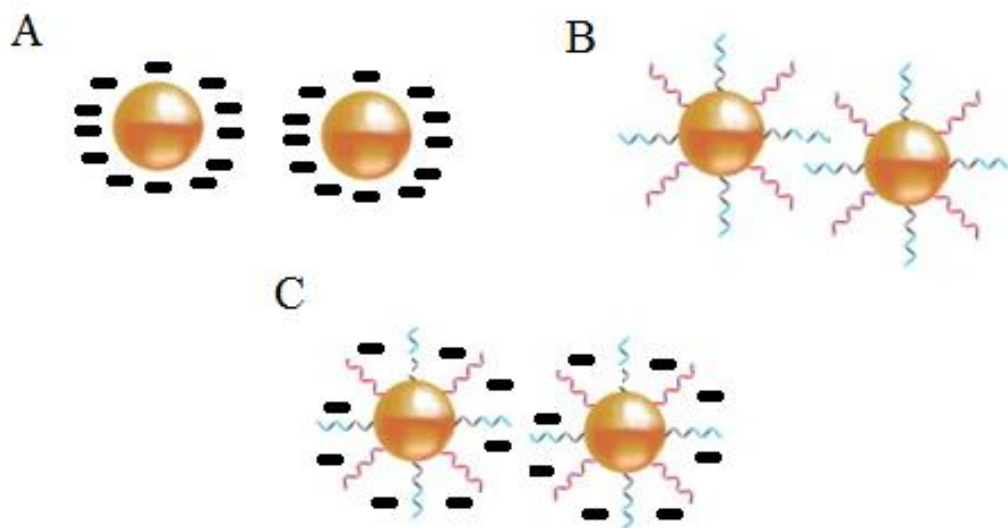
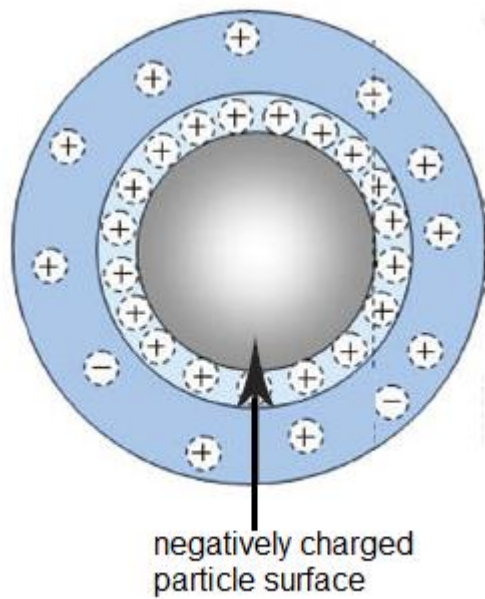


**Figure 1-5** Stabilization of Au NPs by different forces (each of these nanoparticles are surrounded by double electric layer as in the image above).

A- Electrostatic, where charges are the main property in maintaining stability

B- Steric, where the structure of the ligands attached to the NP surface control stability

C- Electrosteric, combines both steric and electrostatic forces to maintain the colloidal stability

## 1.4 Synthesis of Peptide Functionalized Au NPs

Citrate Au NPs lack the stability and functionality required in order to be used as an effective sensing system, especially in a biological environment, where ionic strength and the presence of biological molecules can affect the stability of the colloidal solution. Peptides are one of the most frequently used biological molecules for functionalization of Au NP surfaces because they can be used as biorecognition probes for various enzymes. In most cases, the peptides are coupled through thiol bond that can remain adsorbed for up to 5 weeks, under physiological conditions (Dreaden *et al.* 2012). The main methods for the preparation of peptide-functionalized Au NPs are: (1) ligand exchange; (2) direct synthesis; and (3) chemical coupling (Zong *et al.* 2017).

### 1.4.1 Ligand Exchange

The ligand exchange process is the most frequently used approach to prepare peptide functionalized Au NPs. This usually involves replacing one ligand that stabilizes the NP during or after synthesis, with a functional ligand or other coatings capable of providing colloidal stability (Hostetler *et al.* 1999; Templeton *et al.* 2000). The ligand exchange method has been utilized effectively to prepare a variety of Au NPs capped with cysteine-capped peptides. Treating citrate Au NPs with a cysteine-containing peptide results in a ligand exchange, which as a consequence produces peptide capped Au NPs (Dinkel *et al.* 2016). In this way, the particles can be made biocompatible, and the surface can be loaded with molecules for biomedical applications (Zhu *et al.* 2012; Yang *et al.* 2014; Plissonneau *et al.* 2016). As the interaction of thiol tagged peptides with Au NPs is much stronger than that of the citrate ions, this reaction proceeds preferentially. The thiolate–gold (RS–Au) bond strength is approximately  $210 \text{ kJ mol}^{-1}$  (Häkkinen 2012).

### 1.4.2 Direct Synthesis of functionalized Au NPs

This approach involves the direct synthesis of peptide functionalized Au NPs rather than a stepwise synthesis approach used in ligand exchange. This chemical strategy proceeds by reacting the gold salt ( $\text{HAuCl}_4$ ) with a reducing molecule that acts as an electron transfer agent (Pujols-Ayala *et al.* 2003). When preparing, peptide functionalized Au NPs using this strategy, tyrosine functions as the reducing agent of  $\text{AuCl}_4^-$  to  $\text{Au}^0$ , and the free amine at the N-terminus of the peptide is coupled to the gold surface, resulting in a colloidal suspension (Bhattacharjee *et al.* 2005). This strategy is of limited use because of the difficulty in controlling the size of the Au NPs produced, especially when using excess peptides that lead to Au NP aggregation, due to H-bonding between the terminal amine group and the side chains of the amino acid residues. Another method for the direct synthesis of functionalized Au NPs uses reduction with heparan sulphate I (Ban *et al.* 2008). The gold precursor ( $\text{HAuCl}_4$ ) is first mixed with the heparan sulphate in water followed by the addition of a trisodium citrate solution ( $\text{Na}_3\text{C}_6\text{H}_5\text{O}_7$ ). By using this approach, it was possible to use a mild conditions for ligand coupling thus limiting degradation of the polysaccharide as well as a method that would not only depend on reductive amination chemistry with the reducing end of the polysaccharide.

### 1.4.3 Chemical Coupling

This strategy entails the use of Au NPs functionalized with molecules that can act as sites for subsequent coupling, such as thiolated derivatives of poly ethylene glycol (PEG), glutathione or mercaptosuccinic acid. There are numerous procedures for cross-linking peptides to functionalized Au NPs. Amongst the most frequently employed strategies is so-called click chemistry (Boisselier *et al.* 2008) and [1-ethyl-3-(3-dimethylaminopropyl) carbodiimide hydrochloride]/ N-hydroxy sulfosuccinimide (EDC/sulfo-NHS) coupling (Bartczak & Kanaras 2011). Synthesis of peptide capped

Au NPs by this strategy resulted in inefficient binding between the biomolecules and the capped NPs or the particle biomolecule conjugates are unstable (Pease *et al.* 2007).

## 1.5 Properties of Metallic Nanoparticles

### 1.5.1 Localized Surface Plasmon Resonance (LSPR)

Au, Ag and Cu colloids have occupied 5d, 4d or 3d shells, respectively, but only half filled in the corresponding 6s, 5s or 4s levels and display strong absorption bands in the visible region, due to the energy levels of their  $d-d$  transitions. The plasmon frequency is driven into the visible part of the spectrum and these colloids are therefore intensely coloured. This intense colouration, associated with metal colloids, is a result of the absorption and scattering of light, as described theoretically by Gustav Mie (Link & El-Sayed 1999). It is anticipated that the unusual effects associated with metallic NPs fundamentally arise from their nanometre dimensions, especially in the range of 10-100 nm, which relates to the mean free path (the distance the electron travels between scattering collisions with the lattice centres) of an electron in a metal at room temperature. In noble metals, the decrease in size below the electron mean free path gives rise to intense absorption in the visible-near-UV. This result from the coherent oscillation of the free electrons from one surface of the particle to the other and is called the surface plasmon absorption (El-Sayed 2001).

The interactions of the oscillating electric field of an incident light beam results in transfer of surface electrons to vacant orbitals, giving rise to a collective oscillation of the electrons within the conduction band, which induces the formation of a dipole in the NP. The boundary and surface effects of a particle become more dominant when dimensions of the particles approach the nanoscale. The optical properties of small metal NPs are dominated by collective oscillation of conduction electrons (Moskovits 1985; Smith 2008). When the incident photon frequency is resonant with the collective oscillation of the conduction band electrons, the radiation is absorbed to give an

absorption band forms. This phenomenon is known as the surface plasmon resonance (SPR). The interaction between light and the conduction electrons is shown in Fig. 1-6.

This process can be separated into two forms of interactions: scattering, in which the incident light changes its direction at the same wavelength after interacting with the medium, and absorption, in which the energy is converted into vibrations of the lattice, naturally noticed as heat. Together, these processes are referred to as extinction. Moreover, a strong electric close field is produced near the surface of the particle by the LSPR effect (Cobley *et al.* 2011).

The position of the SPR band depends on numerous factors such as: particle size, shape, interparticle interactions, dielectric properties of the solution, stabilizing ligand shells as well as the nature of the surrounding medium (Mulvaney 1996; Link & El-Sayed 1999; Amendola *et al.* 2017).

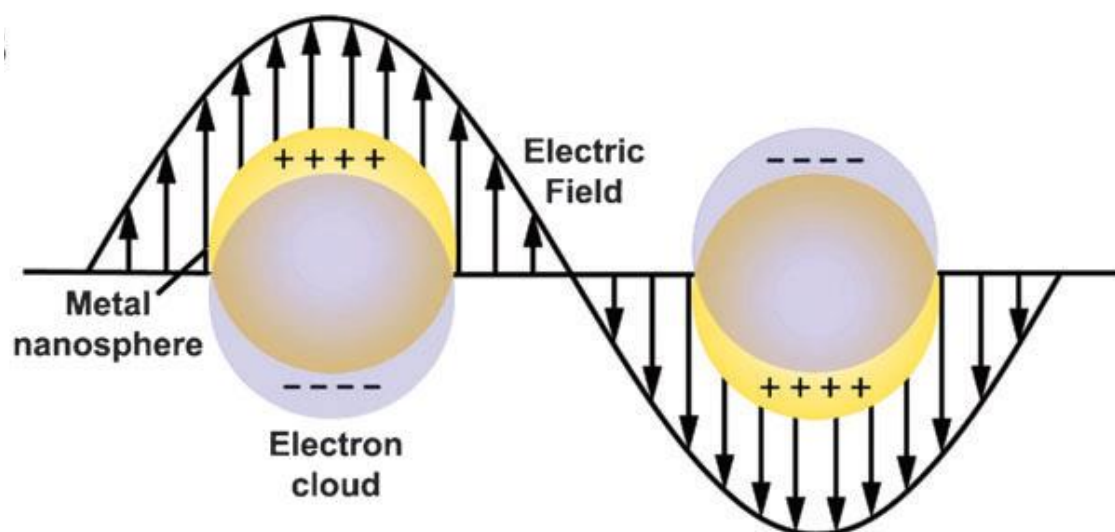


**Figure 1-6** Schematic Representation of Localized Surface Plasmon Resonance excitation of Au NPs.

Interaction of the electromagnetic radiation with the metal NP surface electrons induces dipole oscillation and hence produces surface plasmon resonance. Reprinted with permission from (Chou *et al.* 2014)

The refractive index of the solvent has been shown to influence the position of the surface plasmon band, as predicted by the Mie theory (Mulvaney, 1994). For instance, colours of colloidal Au NP suspensions prepared in water and in mixtures of butyl

acetate and carbon disulphide displayed colour variation from pale red through to purple in solution. Impurities in the system can be observed since the refractive index of Au NPs greatly differs from that of Au oxide or Au chloride. It has been demonstrated that an alteration in the refractive index of the Au NP suspension leads to a corresponding shift in the surface plasmon band (Underwood & Mulvaney 1994).

The surface plasmon oscillation is affected when NPs aggregate (i.e. to  $\leq 2.5$  times the particle diameter), allowing the single particles to electronically interact with each other (Sardar *et al.* 2009). It has been found that the electromagnetic coupling of NPs becomes effective when the interparticle distances are less than  $1/5$  times their individual diameters. Aggregation can induce the coupling of the Au NP plasmon modes, producing a redshift and broadening of the SPR band, associated with the longitudinal resonance in the optical spectrum. As a result, aggregation usually changes the original red colour of the Au NP dispersion into purple or blue (Link & El-Sayed 1999). It has been demonstrated that such spectral changes, which are induced by the aggregation of NPs, can be employed to detect biomolecular recognition events, such as detection of DNA and protein biomarkers for cancer and other disease diagnosis (Elghanian *et al.* 1997).

Changes in the shape of the particles also contribute towards observed changes in the absorption spectrum. For instance, the SPR band is shifted to a higher wavelength in elliptical particles, owing to the reduced spacing between the particles and the extent of the shift is an exponential function of the distance between two particles (Blatchford *et al.* 1982).

When the radius of the particle is less than the mean free path of the conduction electrons, the photon scatter at the particle boundaries results in broadening and fading of the surface plasmons. As a result, SPR is absent for Au NPs with core diameter less than 2 nm, as well as for bulk Au. There is only a minor temperature effect on the

plasmon absorption in Au NPs, as the Fermi distribution of the electrons changes only gradually with temperature, and the scattering rate depends mainly on the availability of vacant states just above or below the Fermi level (Link & El-Sayed 1999).

The majority of other metal colloids that are usually brown or grey in colour, do not have absorption bands in the visible region, and the absorption spectra emerge flat and featureless (Creighton & Eadon 1991).

### **1.5.2 Quantum Size Effects**

It is well known that the reduction of the particle size to values comparable to the wavelength of an electron at the Fermi energy (~about 1 nm for a metal) leads to extreme confinement of electron mobility and a size quantization of its momentum (Kubo 1962). Reduction in particle size to a few tenths of nanometres leads to unique physical and optical properties (Papavassiliou 1979; Kreibig & Genzel 1985; Bohren & Huffman 2008; Kerker 2013). Bulk gold has a standard yellow colour, imparted by a decrease in reflectivity of light at the end of the spectrum. Whenever Au is partitioned into smaller and smaller particles, the ratio of the surface atoms to interior atoms increases, leading to pronounced changes in the physical and chemical properties of the NP (Link & El-Sayed 2000). Confinement of the system arises from size reduction of the particles, which has an effect on the energy level spacing. The spacing between neighbouring conduction energy states increases inversely with the size of the particle (Perenboom *et al.* 1981; Halperin 1986). In order to observe noticeable spacing of the energy levels within the conduction band, the metal particles should be reduced to a few nanometres size (Link & El-Sayed 2000). The free mobile electrons are trapped in the quantum box (the particle) and show the collective oscillation frequency of the plasmon resonance, giving rise to the well-known absorption between 520 - 530 nm for 5-20 nm

spherical Au NPs with a deep-red colour, which can be used in a variety of optical applications.

### **1.5.3 Tuneable Surface Chemistry of Au NPs**

The surface of Au NPs can be tailored by ligand functionalization to impart stabilization against van der Waals attraction forces and to bind molecules of interest selectively (Grandbois *et al.* 1999; Dougan *et al.* 2007). The common approaches for functionalization of Au NPs are either through chemical modification of the Au NPs for specific protein/antibody covalent bonding or by adsorption via electrostatic forces. Since thiol moieties bind strongly to Au surfaces by forming dative bonds (Hermanson 2013), the most frequently used ligands are thiol containing or thiol-modified molecules, such as thiolated DNA strands (Liu *et al.* 2009), thiolated glucose or galactose (Zeng *et al.* 2012), cysteine-containing peptides (Wang *et al.* 2006; Huang *et al.* 2012) which bind to the surface of the Au particles by formation of thiolate-Au bonds. Alternatively, biological ligands can also be coupled to the surface of Au particles by bioconjugate chemistry, through the coupling of amino groups on the biological molecules with carboxy groups at the free ends of stabilizer molecules by using carbodiimides, such as EDC (Hermanson 2013).

Under certain conditions, noncovalent bonding is another strategy by which macromolecules can be attached to the colloidal gold surface, with a minimum change in the specific activity of the bound ligands. With numerous strategies that can be implemented for Au NP surface modification, almost all biological molecules can be non-covalently attached to the particle surface (Sperling *et al.* 2008).

## **1.6 Biomedical Applications of Au NPs**

Au NPs are currently used in a variety of biomedical applications, due to their favourable properties that make them attractive candidates for biomedical use and these

include but are not limited to the dimensions of the metal NPs, which are comparable to those of biomolecules such as proteins (enzymes, antigens, antibodies) or DNA, whose dimensions are in the range of 2-20 nm offering great advantages for integration of nanotechnology to biotechnology, in addition to their biocompatibility and facile surface chemistry (Niemeyer 2001; Whitesides 2003; Katz & Willner 2004; Rosi & Mirkin 2005). In early applications, Au NPs were employed as immunocytochemical probes in transmission electron microscopy (Faulk & Taylor 1971). Here antibodies were labelled with colloidal Au in order to enable direct visualization of Salmonella surface antigens using an electron microscope. This was the first demonstration that a colloidal Au conjugate can function as an immunostaining agent. Mirkin and colleagues reported on the optical and melting features for an aggregate of Au NPs and their use for detection of oligonucleotides (Elghanian *et al.* 1997). They observed a colour change caused by assembly of 13 nm Au NPs due to a specific interaction between oligonucleotides attached to the Au NPs surface. Figure 1-7 depicts some aspects of the multidisciplinary applications of Au NP in the biological and medical fields.

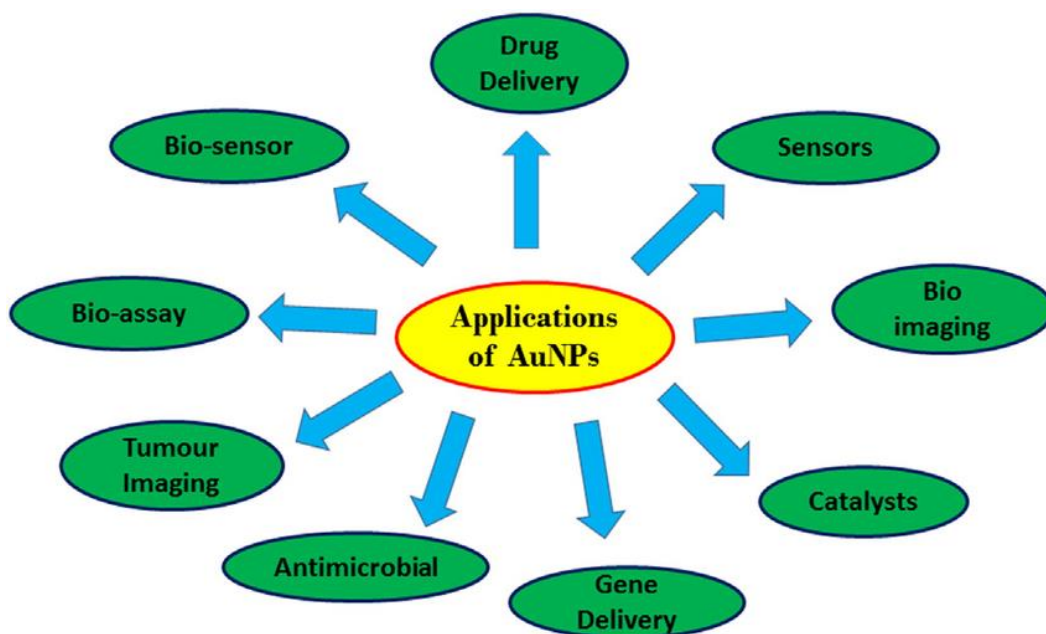


**Figure 1-7** The versatile applications of Au NPs employed for biomedical applications Reprinted with permission from (Ahmed & Ikram 2016)

### 1.6.1 Biosensing Applications of Au NPs

Au NPs present a remarkable platform for the development of biosensing analytical methods. The probe-analyte interaction can cause electronic or optical changes that can be detected (Penn *et al.* 2003; West & Halas 2003; Alivisatos 2004). The properties of these NPs, can be tuned for particular applications such as molecular recognition, chemical sensing and imaging.

Au NP – based sensing techniques generally involve colorimetry, fluorescence, electrochemistry, surface enhanced Raman scattering (SERS) and systems in which quartz crystal microbalance and bio-barcodes are used (Cheng *et al.* 2015). Among these sensing approaches, colorimetric assays based on target recognition induced aggregation or redispersion of Au NPs have been used widely, due to the ease with which the measurement strategy can be designed. When the particles aggregate in an organized fashion, colour changes can be systematically varied, from pink through violet to blue (Creighton & Eadon 1991; Basu *et al.* 2007; Bergamini *et al.* 2015). This phenomenon has been used for testing specific genetic sequences (Alivisatos 2004) and as a colorimetric indicator in home pregnancy tests (e.g. First Response®, marketed in the 1990s) (Rojanathanes *et al.* 2008). The latter test is based on the specific recognition of human chorionic gonadotropin (hCG), a hormone produced during pregnancy, by Au NPs conjugated with an anti-hCG antibody.

It is the anticipated colour change during Au NP aggregation (or dispersion of an aggregate) that provides the basis for absorption-based colorimetric detection. Besides the detection of analytes, such colour changes can also be utilized to measure changes in the lengths of molecules. The concept of such “rulers on the nanometre scale” is based on colour changes of Au NPs dependent on distance between NPs. Different sites of a macromolecule can be coupled to Au NPs, by monitoring the colour of the Au NPs, the distance between these sites can be measured and in this way, for example,

conformational changes in molecules can be determined (Sönnichsen *et al.* 2005). Conjugation with pH-sensitive molecules can also transform gold nanostructures into all-optical pH sensors (Bishnoi *et al.* 2006).

At present, there are two fundamental strategies for metal NP use in colorimetric assays: the use of Au NPs conjugated with thiol-modified molecules (Liu *et al.* 2009; Huang *et al.* 2012; Wang *et al.* 2014a) or aptamers (Pavlov *et al.* 2004; Wei *et al.* 2007; Hu *et al.* 2015) and the use of unmodified Au NPs (Xia *et al.* 2010; Pan *et al.* 2012; Liu *et al.* 2015b; He *et al.* 2017). The first approach relies on immobilization of a ligand or a biological substrate, specific to the target analyte of interest, onto the NP surface. Upon the addition of the target analyte, the analyte activity induces changes in the NP stability; these stimuli can cause the Au NPs to either aggregate or disperse, accompanied by a shift in the absorption spectrum of the aggregated/dispersed Au NPs, resulting in a visible colour change at nanomolar concentrations (Dykman & Khlebtsov 2012).

The second sensing approach, which employs unmodified Au NPs takes advantage of the observation that at high ionic strength (300 mM NaCl), single-stranded DNA (ssDNA) prevents bare Au NPs from aggregation, whereas double-stranded DNA (dsDNA) does not (Li & Rothberg 2004). It has also been shown that aptamers undergo ligand-induced conformational changes that can be sensed by Au NPs. This method can be used as a simple and promising colorimetric probe for aptamer-based sensors (Xia *et al.* 2010); in fact, the colour change of Au NPs through addition of salt can be used to detect the presence or absence of analytes that cause conformational changes in aptamers (Yarbakht & Nikkhah 2016). Many other target analytes have already been detected using this strategy such as enzymes, proteins, ions and other small molecules (Chen *et al.* 2010a; Chandrawati & Stevens 2014; Cheng *et al.* 2015).

The extent of aggregation/dispersion is proportional to the absorption peak shift, so the change in the SPR band position offers a direct measure of quantity or activity of the inducing agent (e.g., an active enzyme). For Au NPs, progressively increased aggregation is characterized by a gradual decrease in the absorbance of the plasmon peak at 520 nm and the appearance of a new peak at between 600-700 nm. These changes are associated with solution colour change from red to purple or blue depending on the degree of aggregation. In some instances, the LSPR spectrum may end up featureless and the solution turns colourless, an indication of extreme aggregation, where the SPR band shifts into the infra-red (IR) region and most visible light is reflected (Lim 2016).

As a result of their specificity, sensitivity, and ease of visualisation, several Au NP assay platforms have been developed by incorporating them into test systems for hand-held diagnostics (Figure 1-8). These test strips have found application in the detection of toxins, infectious agents and inflammatory diseases (Koo *et al.* 2005; Rasooly & Herold 2009; Zhang & Ying 2015). Another important advantage offered by the use of Au NPs is multiplex detection of several analytes simultaneously (Nash *et al.* 2012; Rawat *et al.* 2015; Quintela *et al.* 2015). For instance, Nash and colleagues reported a hybrid Au NP and iron oxide reagent system for multiplexed biomarker detection, as demonstrated with the pan-aldolase and *Plasmodium Falciparum* histidine-rich protein 2 (PfHRP2) in spiked pooled plasma samples.

### Lateral Flow Assay Architecture

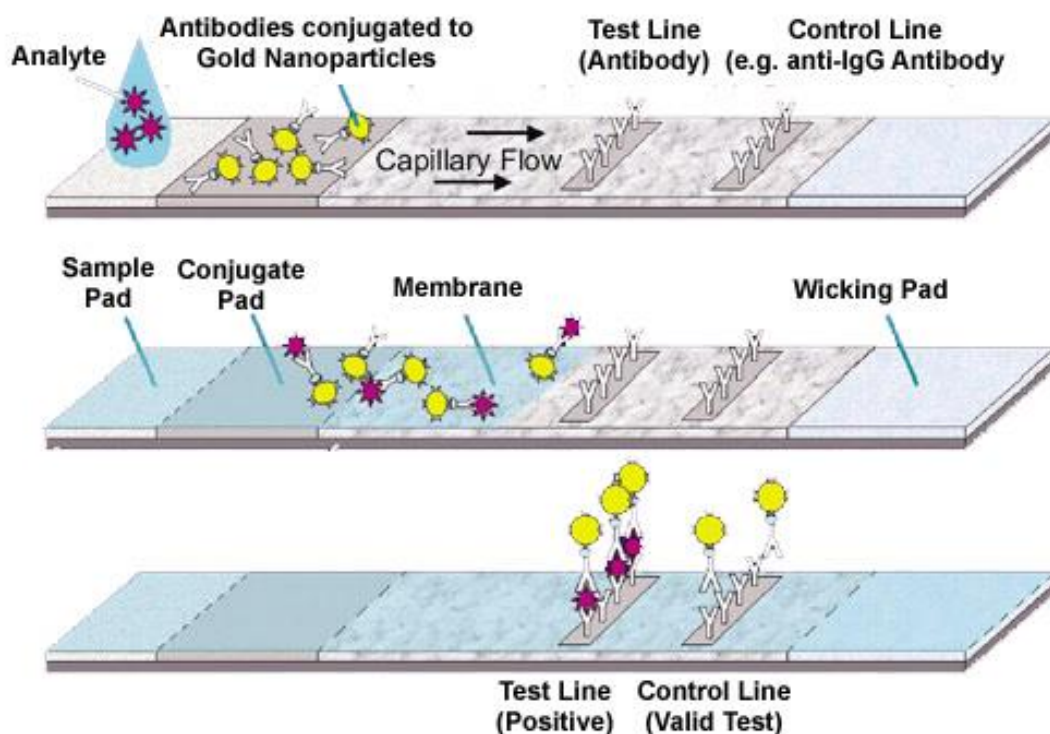


**Figure 1-8** The operational principle of the lateral flow test strip. It can be simply described as follows: the sample solution is pipetted onto the sample pad and gold-labelled antibody is added to the gold conjugate pad. The antibody migrates upward due to the action of capillary forces. When colloidal Au NP-antibody conjugate reaches the test line, the coated antigens would compete with the analyte antigens in the sample for binding to specific sites on the gold-labelled antibody. Results on the Au NP assisted immunoassay would display as positive, negative, and invalid determination because of the absent coloration in the control zone ([www.cytodiagnosics.com](http://www.cytodiagnosics.com)).

#### 1.6.2 Targeted Drug and Gene Delivery Using Au NPs Nanostructures

Drug delivery is one example of how Au nanostructures can be applied for therapy in addition to diagnosis in what is known as “theranostic applications” (Daniel & Astruc 2004; Yavuz *et al.* 2009). Most work in this area has focused on cancer therapy, as functionalized Au NPs can be designed to target specific cell types and organelles such as the nucleus or mitochondria. Through targeting the drug to the desired site, the dose of the drug can be increased at the tumour site, while at the same time limiting the exposure of (and consequent toxicity to) healthy tissue (Peer *et al.* 2007).

Another innovative application of Au nanostructures involves the use of Au nanocages that are modified with polymers such as poly- (N-isopropyl acrylamide) (pNIPAAm) that combine the photothermal properties of Au nanocages with delivering their cargo to a specific site. When the Au nanocages are illuminated with a laser, the actively absorbed light is transformed into heat through the photothermal effect. When the temperature increases beyond a certain threshold, the pNIPAAm coating undergoes a conformational change, which in turn exposes the nanocage pores, allowing the pre-loaded drug to be released (Yavuz *et al.* 2009).

### **1.6.3 Gold Nanoparticles for Visualization and Labelling of Biological Molecules**

Au NPs have been employed extensively in diverse visualization and bioimaging techniques to detect chemical and biological agents (Agasti *et al.* 2010; Hahn *et al.* 2011). The particles are directed and concentrated at the targeted site to deliver contrast for visualization. Au NPs are excellent contrast agents as they can be visualized with a variety of imaging techniques. Images are obtained via the interaction of light with Au NPs (Jain 2007). Au particles can also be utilized for labeling because they display different colours due to their ability to scatter light depending on their sizes and shapes (Sonnichsen, 2002; Mirkin 2001).

Fields in which NP-based contrast has proven to be beneficial include: tumour imaging for directed surgery, imaging of gene expression *in vivo* to identify disease development and to assess the efficacy of anti-cancer drugs. Specifically, the two-photon luminescence of Au NPs allows visualization of cancer markers on or inside cells (Durr *et al.* 2007; Park *et al.* 2008; Maiorano *et al.* 2010).

With the help of dark-field electron microscopy, Au NPs have superior ability to uncover specific bio-interactions compared with fluorescent labels, as the particle scattering cross section is 3 to 5 times greater than that of fluorescence molecules (Hu *et al.* 2008). This principle was employed by El-Sayed's group for development of a novel

diagnostic tool for cancer, with the aid of Au NPs coupled to tumour-antigen-specific antibodies against the membrane of cancerous cells, as compared with binding to healthy cells (El-Sayed *et al.* 2005).

#### **1.6.4 Photothermal Therapy Using Au NPs**

The efficient transfer of light into heat by Au NPs allows the highly specific thermal treatment of diseased or infected tissues. The basic concept of using Au NPs for thermal therapy depends on exposing cells to higher than normal temperatures, which lead to cell death via apoptosis. The sensitivity of cells to temperature offers the possibility of the use of photodynamic therapy in the treatment of certain forms of cancer. Malignant cells in tumour tissue exhibit a disorganized and packed vascular structure, and as a result, heat dissipation is delayed in contrast to healthy tissues (Song 1984). In practice, Au NPs can be functionalized with ligands that are specific to receptors overexpressed on cancer cells. The particles are then locally concentrated in the cancerous tissue illuminated with the external light source to make Au NPs a heat source for the surrounding cancerous tissues, without exposing healthy tissue to high temperatures (Sperling *et al.* 2008).

Gold nanorods (Au NRs) or hollow structures are preferred when light penetration is required as they absorb light in the IR region (Chen *et al.* 2007; Huang *et al.* 2008). Heating with magnetic particles is preferred for tissues that are deep inside the body. Upon irradiating magnetic particles with radiofrequency (RF) fields, heat is produced by the repetitive cycling of the magnetic hysteresis loop (Tran & Webster 2010). Since chemo- and radiotherapy are still the cornerstone therapy for cancer, NPs that display dual functions of heat mediator foci with the capability to transport and to discharge medicines may extend their scope for biomedical applications (Yoo *et al.* 2013).

### 1.6.5 Gold Nanoparticles for Enzyme Activity Detection

In traditional enzyme detection and quantification assays, the activity is usually detected either by recording absorbance or fluorescence emitted from labelled substrates, modified with either chromogenic or fluorogenic reporter molecules, fluorescence resonance energy transfer (FRET) substrates or by indirect sensor systems that depend on sensing the reactions of unmodified substrates, to produce a detectable spectroscopic signal (Gul *et al.* 1998; Eisenthal & Danson 2002; Goddard & Reymond 2004). Although these approaches, in general, are adequate for many applications (some are commercially available), they are less sensitive and in some cases, are limited only to *in vitro* use (Corrie *et al.* 2015).

In the last two decades, Au NP-based colorimetric biosensing assays have attracted great attention in diagnostic applications, due to their simplicity versatility and biological compatibility. A variety of NP-based sensing systems have been developed, with varying degrees of success and sensitivity. These nanoparticulate systems are valuable tools for the detection and measurement of enzyme activity in real time and may offer a useful high-throughput screening (HTS) tool for enzyme activity and drug discovery (Anker *et al.* 2008). The most common method of measuring the rate of catalytic enzyme activity is the use of spectrophotometric assays. Although these assays are easy to use and interpret, a major limiting factor is the requirement for a fluoro-/chromo-genic reporter. However, in most cases, this means that the activity of the enzyme is detected indirectly or that improved enzyme activities may be selected based on the use of an idealised substrate, which may not translate to the real one (Westley *et al.* 2017).

The use of Au NPs in colorimetric assays involves two mechanisms: interparticle bond formation or cross-linking (CL) aggregation which represents the prototype approach through which Au NPs are brought together. This occurs either by using crosslinker

molecules that have two binding tags linking two Au NPs to each other (e.g peptides with thiol and/or guanidine anchors) (Figure 1-9A) or by direct interaction (without crosslinkers) such as antigen - antibody interactions and DNA hybridization (Figure 1-9B). Mirkin and co-workers (1997) pioneering work on the development of polynucleotide sensor is a model example, in which Au NPs functionalized with a thiolated DNA strand are fabricated and incubated with target DNA molecules to trigger Au NP aggregation, by hybridizing two complementary DNA strands on Au NPs giving rise to colorimetric detection of oligonucleotides. This platform has also been utilized by many others for the detection of a wide variety of biological and chemical molecules (Tiwari *et al.* 2010; Xia *et al.* 2010; Pan *et al.* 2012; Wang *et al.* 2015; Liu *et al.* 2015a).

The other approach for enzyme (protein) biosensing occurs through the removal of colloidal stabilization effects, which are known as non-crosslinking (NCL) aggregation. In such systems, Au NP aggregation is induced by the stronger interaction between ligands and target analyte, accompanied with the complete or partial release of the ligand from the surface of the NPs, without the formation of interparticle bonds (Figure 1-10), which provides real-time measurement of enzyme activity in contrast to the relatively slow process induced by inter-particle crosslinking (Zhao *et al.* 2007). This strategy was first used for the detection of polynucleotide polymorphisms (Sato *et al.* 2003). When a target polynucleotide is complementary to the ligand in sequence and chain length, it will hybridize to the DNA on Au NPs, this, in turn, alters the NP resistance to salt-induced aggregation.

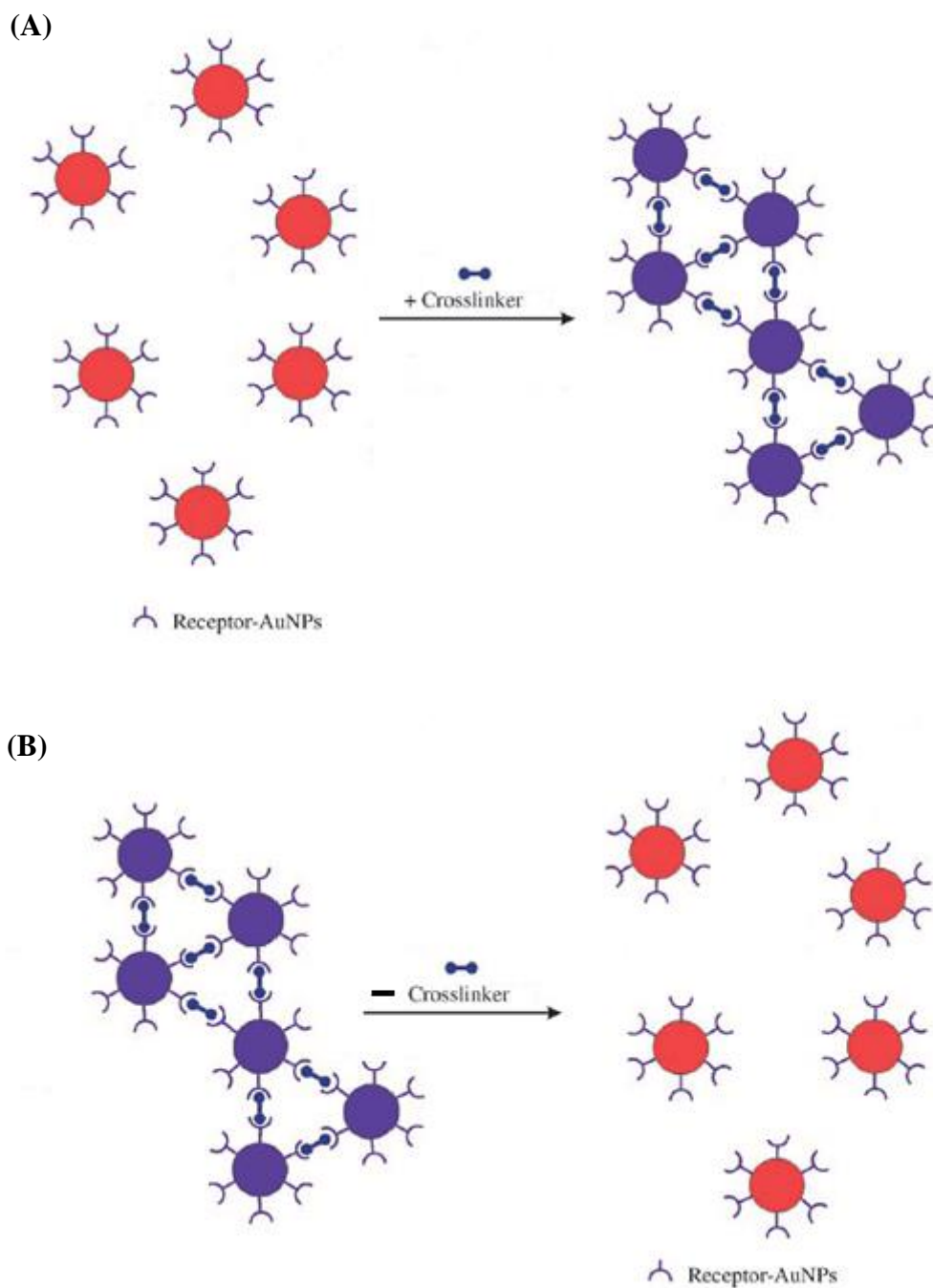


**Figure 1-9** Protein or enzyme detection by reversible crosslinking mechanism (CL). (A) Addition of crosslinker results in aggregation. (B) Removal of crosslinker results in the dispersion of the Au NP aggregates and the reaction is reversed.

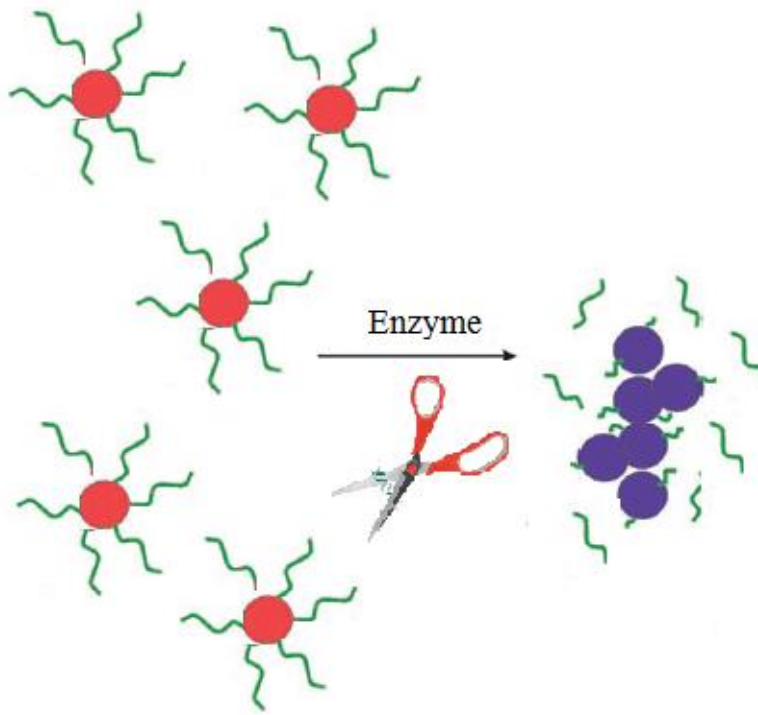


**Figure 1-10** Non-Crosslinking aggregation of peptide (green) modified Au NPs. The presence of enzyme can cause colloidal aggregation of the Au NPs, without cross linkers due to a change in stability. Such a change may occur if the dispersed particles are linked to cleavable molecules. Cleavage of the substrate can be initiated by a change in the biological environment or caused by an exogenous stimulus.

### 1.7 Dipeptidyl peptidase IV

Dipeptidyl peptidase IV (DPP-IV/CD26 EC 3.4.14.5) is a serine exopeptidase that was discovered and purified from pig kidney cortex by Hopsue-Havu and Glenner (1966). Using a synthesized chromogenic substrate, it has been shown to cleave N-terminal X-prolyl residues from various peptides. DPP-IV/CD26 was also known as glycyl prolyl  $\beta$ -naphthylamidase because of its ability to specifically cleave the amide bond between the N-terminal glycyl proline and  $\beta$ -naphthylamine (Hopsu-Havu & Glenner 1966; Öya *et al.* 1972; Hino *et al.* 1975). Subsequent studies revealed that DPP-IV is a cell surface antigen, also known as CD26 (Hegen *et al.* 1990). Moreover, DPP-IV/CD26 is also known as adenosine deaminase complexing protein 2 (ADCP2) (Richard *et al.* 2000). DPP-IV/CD26 is a multifunctional protein, which is involved in proteolysis, signal transduction and modulation of the immune and inflammatory responses (Wagner *et al.*

2016). Because of this multiplicity of actions and biological functions, there is a great deal of pharmaceutical, biomedical and industrial communities interest in the biochemical behaviour of this protein (Boonacker & Van Noorden 2003).

DPP-IV/CD26 is responsible for the truncation of many bioactive peptides by splitting dipeptides from proteins and peptides containing proline or alanine in the penultimate N-terminus amino acid position. The use of DPP-IV/CD26 inhibitors for the management of type II diabetes has been approved by Food and Drug Administration (FDA) because of their ability to reduce the inactivation of incretins, resulting in enhancing insulinotropic actions. It has been demonstrated that serum DPP-IV/CD26 activity increases in prostate cancers, type 2 diabetes mellitus, hepatitis and hepatobiliary diseases (Wilson *et al.* 2000; Firneisz *et al.* 2001; Ahmed *et al.* 2015). In contrast, its activity decreases in patient's sera with renal cancer, pancreatic cancer, systemic lupus erythematosus, rheumatoid arthritis, anorexia and bulimia nervosa (van West *et al.* 2000; de la Haba-Rodriguez *et al.* 2002; Pro & Dang 2004; Varona *et al.* 2010).

### **1.7.1 Classification**

DPP-IV/CD26 is a member of the S9 prolyl oligopeptidase family along with prolyl endopeptidase (PEP), acylaminoacyl peptidase and glutamyl endopeptidase (Buckley *et al.* 2004). The DPP family includes other members that display DPP-IV/CD26-like activity, such as quiescent cell proline dipeptidase (QPP), fibroblast activation protein-alpha (FAP- $\alpha$ ), dipeptidyl peptidase 8 (DPP8) and dipeptidyl peptidase 9 (DPP9) (Scanlan *et al.* 1994; Abbott *et al.* 2000). They all belong to the DASH "DPP-IV/CD26 Activity and Structure Homologues" group of peptidases that preferentially cleave X-proline and X-alanine at the penultimate position (scissile residue, P1-position) (Fig.1-11) of the polypeptide substrates, which include: chemokines, neuropeptides, peptide hormones and incretins in weakly basic medium (pH 8) (Bušek *et al.* 2004). These

substrates play important roles in immune regulation, neurodegenerative diseases, heart failure, ischemic injuries, nutritional control, inflammatory and infectious diseases, oncological processes and nociception (Hildebrandt *et al.* 2001; Lambeir *et al.* 2008; Deacon 2011).

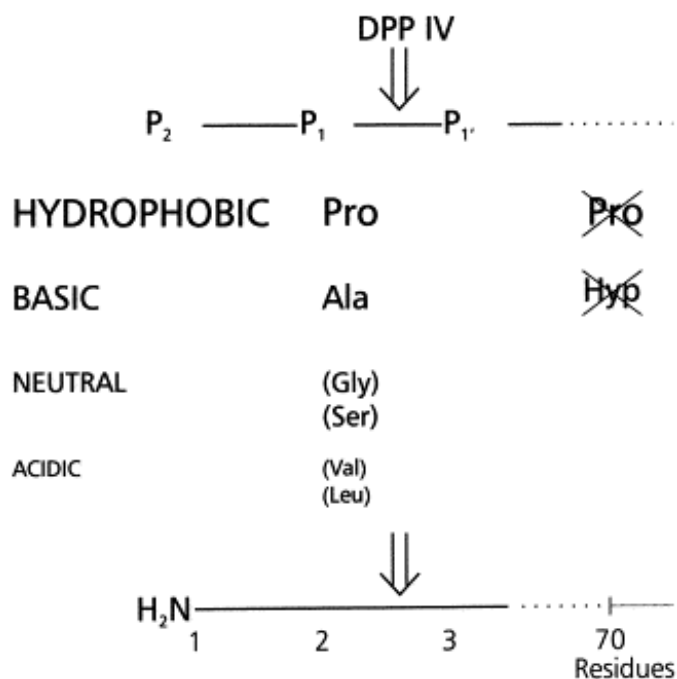


**Figure 1-11** Schematic representation of substrates cleaved by DPP-IV/CD26. Dipeptides are released from the N-terminus of peptides with Pro or Ala in the P1-position. Certain peptides with other small amino acids in P1 position are cleaved at slower rates. In the P2 position, bulky, hydrophobic or basic amino acids with an obligate free amino group are preferred. Reprinted with permission from (Mentlein 1999).

### 1.7.2 Sequence and Three-Dimensional Structure of DPP-IV/CD26

Human DPP-IV/CD26 is a 766-amino acid (AA) protein whose primary structure was determined by cloning and sequencing of cDNA of rat DPP-IV/CD26 (Ogata *et al.* 1989). The protein is anchored to the lipid bilayer by a hydrophobic transmembrane segment composed of 22 AA residues (AA7-29) that are attached to the N-terminus six AA in the cytoplasmic region, which has been shown to be involved in the enzymatic activity and quaternary structure by dimerization (Chung *et al.* 2010).

The opposite end of the segment is linked to the large extracellular part by a flexible stalk (AA, 29-48). The extracellular region is composed of a heavily glycosylated region (AA 49-289), a cysteine-rich region containing 9 of 12 cysteines (AA 290-510), and the catalytic domain (Lambeir *et al.* 2003). A soluble form of the protein (sDPP-IV/CD26), lacking the intracellular part and the transmembrane region, is found in body fluids (Durinx *et al.* 2000).

### **1.7.3 Mechanism of Hydrolysis by DPP-IV/CD26**

The catalytic active site is composed of three AAs Ser630, Asp708 and His740 and has dual function, binding the substrate and catalysing the reaction. Nucleophilic serine 630 attacks the scissile bond of the substrate in the opposite position, compared to classical serine proteases. Substrate-assisted catalysis and a pH-dependent conformational enzyme isomerization are implicated in the catalytic mechanism of DPP-IV/CD26 (Demuth & Heins 1995; Kim *et al.* 2006).

DPP-IV/CD26 accepts all amino acid residues at the N-terminus, provided they are in the protonated form, but with more affinity for hydrophobic aliphatic residues (Kaspari *et al.* 1996). Substrate recognition by DPP-IV/CD26 is defined not only by the AA sequence of the substrate but also by its size. It has been demonstrated that the rate of substrate cleavage by DPP-IV/CD26 is inversely proportional to substrate AA chain length (Hoffmann *et al.* 1993). Peptide bonds involving the cyclic AA proline are not subject to proteolysis by most proteases, even those with broad selectivity (Mentlein 1988; Yaron *et al.* 1993).

### **1.7.4 Enzyme Localisation and availability**

The enzyme is a type 2 transmembrane glycoprotein expressed on the surface of many cell types in almost all organs and tissues of the body, with the highest concentration in the proximal tubule of the kidney and luminal membrane of epithelial cells of the small

intestine, as well as in liver hepatocytes, prostate tissue and activated leukocytes. It has been demonstrated that DPP-IV/CD26 is also expressed in the endocrine cells of the pancreatic islets (Omar *et al.* 2014). As mentioned earlier, the enzyme is also present in blood in the soluble form (sDPP-IV/CD26), which is thought to be produced as a result of proteolytic cleavage of the membrane-bound form or as specially encoded soluble variant (Iwaki-Egawa *et al.* 1998; Mentlein 1999). In other biological fluids, such as synovial fluid, cerebrospinal, seminal fluid, saliva and bile have been found to contain the soluble form of the enzyme (Durinx *et al.* 2000). Some studies argue that the soluble forms may originate from shedding from endothelial or epithelial cells and from circulating leucocytes (Lambeir *et al.* 2003; Cordero *et al.* 2009). Recently, bone marrow cells have been determined as one of the sources of soluble serum DPP-IV/CD26 by transplantation studies in DPP-IV deficient rats (Wang *et al.* 2014c).

## 1.8 Functions of DPP-IV/CD26

DPP-IV/CD26 is considered as a moonlighting protein due to its multifunctional roles and its widespread expression (Boonacker & Van Noorden 2003). The functions of DPP-IV/CD26 include protease activity, in addition to acting as a co-stimulatory protein for both CD3 and CD2 dependent T-lymphocyte activation, tyrosine phosphorylation of T-cell receptor (TCR/CD3) signal transduction pathway proteins, adhesion molecules for collagen and fibronectin, receptor molecules for adenosine deaminase (ADA) on lymphocytes, regulation of glucose homeostasis and apoptosis (Kim *et al.* 2014). DPP-IV/CD26 accomplishes some of its physiological functions through interactions with other proteins, such as caveolin-1 and the mannose-6-phosphate/insulin-like growth factor II receptor (M6P/IGFIIR) (Havre *et al.* 2008).

It has been reported that DPP-IV/CD26 plays a role in inflammation-mediated diseases such as atherosclerosis and multiple sclerosis (Zhong *et al.* 2013). DPP-IV/CD26 is involved in endocrine function by cleaving growth-hormone-releasing factor (GHRF)

(Bercu & Walker 2012). In addition, DPP-IV/CD26 plays a role in nervous system function by acting as a regulatory molecule for a variety of neuropeptides such as neuropeptide Y (Hildebrandt *et al.* 2003). DPP-IV/CD26 is also relevant in diseases such as rheumatoid arthritis (Cordero *et al.* 2015) and asthma (Ohnuma *et al.* 2005; Schmiedl *et al.* 2010). DPP-IV/CD26 has a significant role in the allergic response of skin (e.g. atopic dermatitis and contact dermatitis) (Tasic *et al.* 2011, Komiya *et al.* 2017).

It has been proposed that DPP-IV/CD26 could be involved in the link between adipose tissue and obesity and metabolic syndrome, which is a cluster of conditions involving increased blood pressure, high blood sugar, excess body fat around the waist and abnormal cholesterol or triglyceride levels, that occur together (Lamers *et al.* 2011). Faster wound healing as well as faster scar formation has been reported in conditions of DPP-IV/CD26 deficient mice, which was attributed to rapid macrophage recruitment at the site of skin damage as a consequence of DPP-IV/CD26 deficiency (Baticic Pucar *et al.* 2017). Involvement in these roles makes the enzyme a valuable potential diagnostic and prognostic tool for various health conditions.

### **1.8.1 Proteolytic Function of DPP-IV/CD26**

DPP-IV/CD26 has a remarkable capacity to cleave the peptide bond following a penultimate proline, thereby releasing proline-containing dipeptides from the N-terminus of polypeptide chains. Thus it is one of the few enzymes able to facilitate the digestion of proline-rich proteins and polypeptides. As DPP-IV/CD26 is highly expressed in the epithelial cells of the small intestine it has a crucial role in the hydrolysis of proline-containing dietary proteins such as gluten, gliadin and casein (Table 1-2). These allergenic proteins are highly resistant to breakdown by other proteolytic enzymes and can cause several serious adverse food reactions including the enteropathic manifestations of coeliac disease (Detel *et al.* 2007).

**Table 1-2** Physiological peptides/hormones identified as substrates of DPP-IV/CD26 and subject to modulation by the enzyme (Gupta *et al.* 2009).

Physiological Process	Peptide/Hormone
Nutrient metabolism and glucose homeostasis	GLP-1 (7-37*) & GLP-1 (7-36*) amide
	GIP (1-42) & Glucagon
Growth and development	Insulin-like growth factor-1 (IGF-1)
	Growth hormone releasing factor (GHRF)
	Growth hormone-releasing hormone (GRH (1-29)
	GRH (1-44)
Digestive & Vascular system	GLP-2 (1-33)
	Trypsinogen & Trypsinogen pro-peptide
	Gastrin releasing peptide (GRP)
	Pro-colipase & Enterostatin
	$\beta$ -Casomorphin, Aprotinin & Bradykinin
Reproductive system	Human chorionic gonadotropin $\alpha$ (hCG $\alpha$ )
	Leutinising hormone $\alpha$ chain (LH $\alpha$ )
	Prolactin
Neuroendocrine & Endocrine system	PACAP (1-27) & PACAP (1-38)
	Thyrotropin $\alpha$ & Vasostatin-1
Nervous system	Substance P & Peptide YY (1-36)
	Neuropeptide Y & Enkephalins
Immune system	Interleukin-2 & Interleukin-1 $\beta$
	$\alpha_1$ -Microglobulin (GCP-2) & RANTES
	Stromal cell-derived factor-1 $\alpha$ (SDF-1 $\alpha$ ) & SDF-1 $\beta$
	Macrophage-derived chemokine (MDC)
	Interferon- $\gamma$ -inducible protein-10 (IP-10)
	Monocyte chemotactic protein-1 (MCP-1&2)

\* Circulating GLP-1 peptide forms in the plasma.

GLP: Glucagon Like Peptide, GIP: Gastric Inhibitory Peptide, PACAP: Pituitary Adenylate Cyclic Activating Peptide.

### 1.8.2 Co-stimulatory, Receptor, Immunological Functions of DPP-IV/CD26

The exact role of DPP-IV/CD26 as a co-stimulatory molecule is not yet fully understood. However, it has been reported that with DPP-IV/CD26-mediated co-stimulation, interleukin 2 (IL-2) production is higher in cells expressing wild-type DPP-IV/CD26, suggesting that the DPP-IV/CD26 enzymatic activity might contribute to, but is not crucial for, signal transduction in T-lymphocytes (Morimoto & Schlossman 1998; Wesley *et al.* 2005).

CD26 was identified as the binding protein for adenosine deaminase (ADA) that is responsible for irreversible deamination of adenosine and 2'-deoxyadenosine to inosine

and 2'-deoxyinosine respectively, thereby functioning as a receptor (Oravec *et al.* 1997; Gonzalez-Gronow *et al.* 2005). Complex formation between CD26 and ADA preserves the individual enzymatic activities of both molecules and this observation has triggered research into the functional implications of this in immune regulation (Franco *et al.* 1998; Kim *et al.* 2015).

The DPP-IV /CD26 protein plays a major role in the immune response as it is expressed on the surface of B lymphocytes, natural killer (NK) cells, and macrophages as well as T cells, further supporting a role for the enzyme in the immune response (Tanaka *et al.* 1994; Stankovic *et al.* 2008). Further evidence of the crucial role of DPP-IV/CD26 activity in T cell proliferation was found in studies involving soluble CD26 molecules. Studies have pointed to the association of DPP-IV/CD26 in the physiological control of several peptides that function as biochemical mediators between and within the cells of the immune and neuroendocrine system (Dang & Morimoto 2002; Ansorge & Langner 2013). Within the immune system, DPP-IV/CD26 plays a significant role in the regulation of chemokine activity. This role is thought to be the result of a combination of its exopeptidase activity and its non-enzymatic interactions with different molecules such as HIV envelope glycoprotein gp120 and streptokinase (Goodwin *et al.* 2013).

### **1.8.3 Other Miscellaneous Functions of DPP-IV/CD26**

The DPP-IV/CD26 gene family contains 4 peptidases, all involved in cell-extracellular matrix (ECM) interactions, apoptosis and tissue remodelling, but with different functions and substrates (Yu *et al.* 2006). The interaction of DPP-IV/CD26 with proteins of the ECM may support cell migration and DPP-IV/CD26 could perform as a functional collagen receptor for CD4<sup>+</sup> T cell activation (Wilson *et al.* 2000). These interactions were found to include collagen and fibronectin. Furthermore, since chemokine-chemokine receptor interactions are important in haematopoiesis and

immune function, CD26 could be exploited to enhance the haematopoietic efficacy of stem cell and progenitor cell transplantation (Broxmeyer 2008).

### 1.9 DPP-IV/CD26 Protein Levels and Activity

Reference DPP-IV/CD26 protein levels may not accurately reflect the levels of active DPP-IV/CD26 enzyme; thus, it is useful to determine DPP-IV/CD26 activity rather than DPP-IV/CD26 level using an antibody-based assay. Standard levels of DPP-IV/CD26 activity in serum and CSF for healthy children and adults have been assessed by various research groups (Durinx *et al.* 2001; Lambeir *et al.* 2003; Cordero *et al.* 2009; Delezuch *et al.* 2012). Overall, these studies showed that the activity of DPP-IV/CD26 in healthy individuals' plasma is in the range of 12.5 - 42 U /L, and is generally higher in men than women (Table 1-3) and it tends to decrease significantly with age (Durinx *et al.* 2001; Lambeir *et al.* 2003).

**Table 1-3:** Activity levels (U/L) of human dipeptidyl peptidase IV in plasma and serum in men and women (Lambeir *et al.* 2003).

	Activity in serum (U/L) *			Activity in citrated plasma (U/L) *		
	Mean	SD	range	Mean	SD	range
women	27.5	6.1	17.0-50.8	23.2	4.4	14.0-39.7
men	32.3	6.4	17.7-52.6	25.9	5.1	12.5-42.0

\*One unit of enzyme activity is defined as the amount of enzyme that will hydrolyze 1.0  $\mu$ mole 7-(Gly-Pro-)-amino-4-methylcoumarinamide substrate per min at 37 °C, pH 8.3.

#### 1.9.1 DPP-IV/CD26 Activity in Pathological Conditions

The alterations of human DPP-IV/CD26 activity in serum and DPP-IV/CD26 protein levels have been demonstrated in various diseases. Table 1-4 presents a summary of recent articles that have reported changes in DPP-IV/CD26 activity in a variety of health conditions

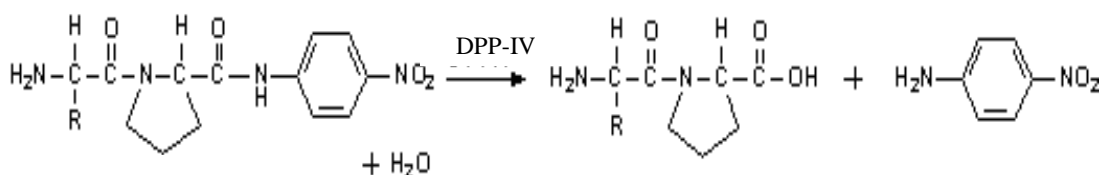
**Table 1-4: DPP-IV/CD26 as a marker of diseases.** \*Some authors reported the activity in ng/L where average activity is around 619 ng/L. \*\*Not statistically different.

Disease type	DPP-IV/CD26 (U/L)	Citation
Cancers		
- Melanoma	lower activity 21.81±6.79	Matić <i>et al.</i> 2012
- Lung cancer	n/a	Blanco-Prieto <i>et al.</i> 2015
- Gastric cancer	lower activity 511±84.8*	Boccardi <i>et al.</i> 2015
- Prostate cancer	lower activity	Nazarian <i>et al.</i> 2014
- Renal cancer	lower activity	Varona <i>et al.</i> 2010
- Colorectal carcinoma	higher activity (> 850*)	De Chiara <i>et al.</i> 2014;
- Thyroid carcinoma	overexpression	Aratake <i>et al.</i> 2002;
Rheumatoid arthritis	lower activity	Cordero <i>et al.</i> 2015
Chronic obstruction pulmonary disease	lower activity	Somborac-Bačura <i>et al.</i> 2012
Diabetic nephropathy	slightly higher activity**	(Sun <i>et al.</i> 2012)
Psychological		
- depression	lower activity 34.2±7.6	(Maes <i>et al.</i> 1996)
- schizophrenia	higher activity 46.9±11.4	(Maes <i>et al.</i> 1996)
Hepatitis C virus	higher activity 20.9±9.6	(Firneisz <i>et al.</i> 2001)
Cholestasis	higher activity 50.2±12.2	(Perner <i>et al.</i> 1999)
Miscellaneous		
- anorexia and bulimia	lower activity 22.7& 27.3	(Van West <i>et al.</i> 2000)
- alcohol abstinence	lower activity 27.7±6.3	(Maes <i>et al.</i> 1999)
- mucopolysaccharidoses I, II	activity 3.5 times higher	(Hetmańczyk <i>et al.</i> 2016)

### 1.9.1 Assay of DPP-IV Activity

A number of methods have been developed for the measurement of DPP-IV/CD26 activity in a variety of biological samples. Chromogenic and fluorogenic enzyme substrates have formed the cornerstone for the assay of DPP-IV/CD26 activity (Nagatsu *et al.* 1976; Kato *et al.* 1978). Glycylproline *para*-nitroanilide (Gly-Pro pNA) has been used as a routine substrate for the chromogenic assay. In the standard assay, DPP-IV/CD26 in glycine-NaOH buffer (pH 8.7) or in Tris-maleate buffer (pH 7) is incubated with Gly-Pro pNA at 37 °C for 15 minutes. The rates of *para* nitro aniline release from the substrate were expressed as the change in absorbance at 405 nm in the reaction solution (Equation. 1-2). The activity of DPP-IV/CD26 is expressed in term of unit/Litre (U/L) in which the activity is defined as the quantity of the enzyme that hydrolyzes 1 micromole of substrate per min at 37 °C (Lambeir *et al.* 2003). Gly-Pro pNA is a useful chromogenic substrate for the assay of the enzyme in serum and various tissues (Ogawa & Nagatsu 1979). Nevertheless, the sensitivity of the assay is inadequate for the determination of low enzyme activity, especially in samples collected from patients on drugs which inhibit the activity of the enzyme.

**Equation 1-2** Equation showing the cleavage of Gly-Pro-pNA by DPP-IV to form *p*-nitroaniline the absorbance of which is measured at 405 nm as indication of enzyme activity.



A very sensitive DPP-IV/CD26 activity assay, using the same concept of linking the substrate to a fluorogenic substrate (aminomethyl coumarin) is available and can be used to determine the enzyme activity in human CSF (Kato *et al.* 1978). Although sensitive, most fluorogenic probes suffer from poor aqueous solubility and therefore,

require the use of organic co-solvents, which have been reported to reduce enzyme activity and thus limit their application to cell-free assays (Lai *et al.* 2007).

Promega® have developed a bioluminescent assay for DPP-IV/CD26 that can detect Gly-Pro cleaving activity in human serum at very low detection limit (0.035 U/L) (O'Brien 2006). Using the pro luminescent DPP-IV substrate, Gly-Pro-amino luciferin, DPP-IV/CD26 results in cleavage of the substrate and generation of a luminescent signal produced by the luciferase reaction (Fig. 1-12).

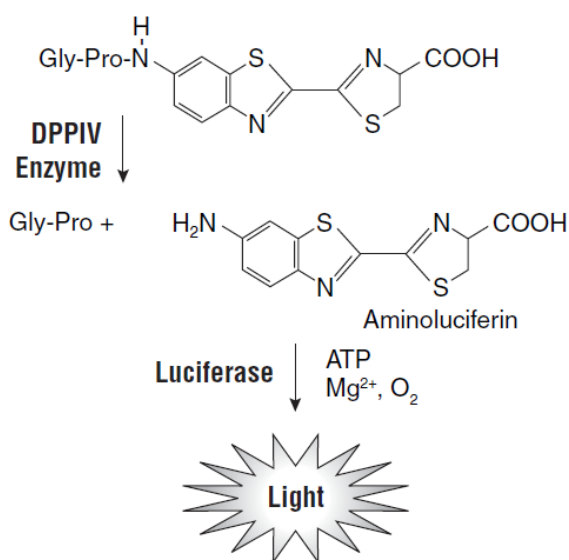


**Figure 1-12** Principle of Luminescent DPP-IV/CD26 assay.

H-Gly-Pro-amino luciferin is cleaved by DPP-IV to release amino luciferins. Aminoluciferin in turn functions as a substrate for a coupled luciferase reaction to emit luminescence that can be measured by a luminometer. Reprinted with permission from (O'Brien 2006).

Recently, an electrochemical biosensor has been developed for electrochemical analysis of DPP-IV activity using redox-labelled ferrocene (Fc) peptide substrates, immobilized on gold electrodes (Zhang *et al.* 2015). The addition of DPP-IV to Fc labelled peptide substrate induces a site-specific cleavage leading to a reduction in a number of redox species as the substrate cleaved, which in turn leads to a change in the Faradaic current, which can be measured by voltammetry. Labelling of the peptide substrates Fc offers improved sensitivity. However, the redox-labelled electrochemical biosensors have been found to encounter considerable signal loss after long-term storage due to the

decomposition of redox tags (Kang *et al.* 2009). Moreover, labelling of peptides increases the experimental complexity, affecting the behaviour of the protease at the cleavage site and increasing the cost of the analysis (Cao *et al.* 2013).

Xia *et al.* (2016) incorporated the Au NP colorimetric technique on a solid-liquid interface (electrode/electrolyte), which thus transformed a liquid-phase DPP-IV colorimetric assay into an electrochemical analysis with enhanced sensitivity for the determination of the DPP-IV activity and screening for its inhibitor (Figure 1-13).

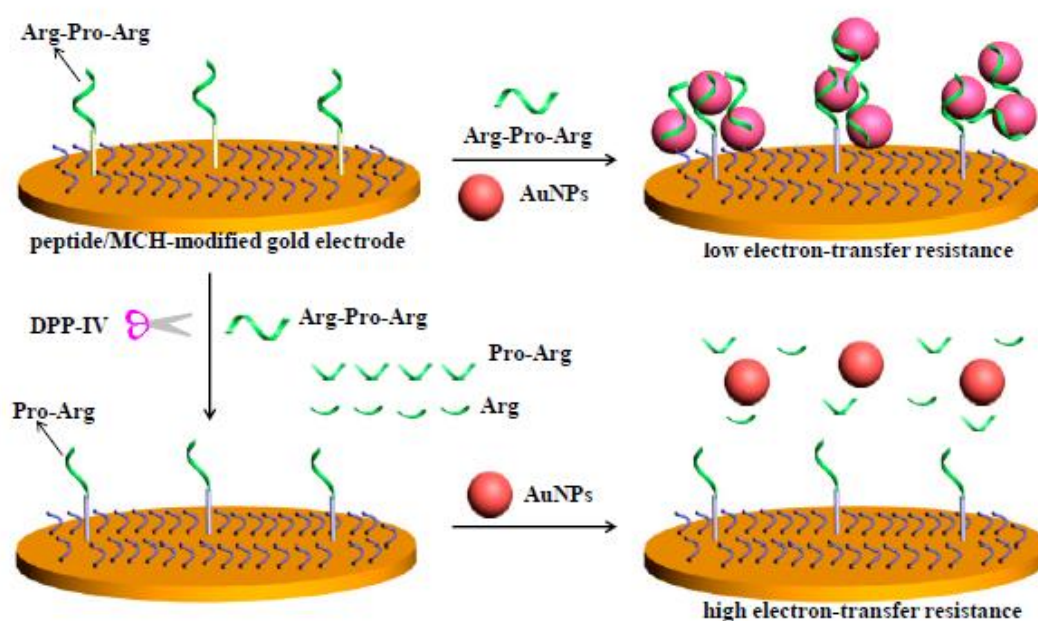


**Figure 1-13** Schematic illustration of the combined colorimetric/electrochemical method for DPP-IV activity assay.

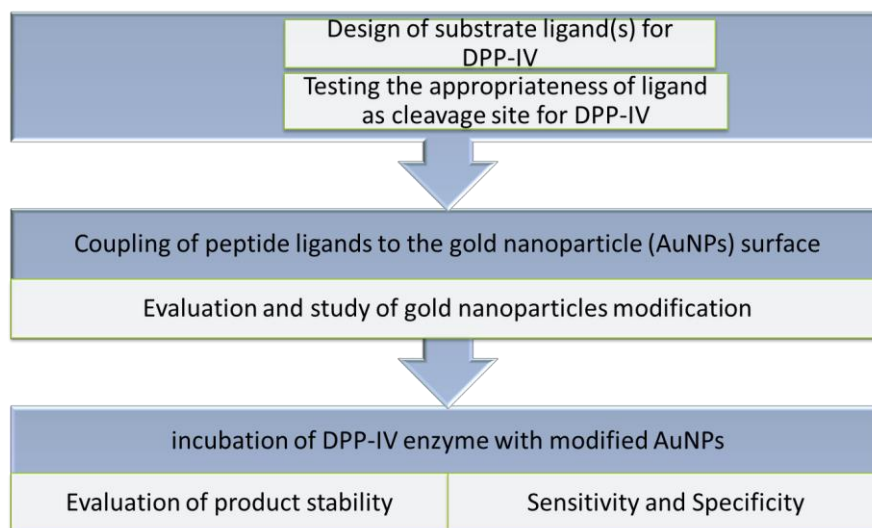
Modification of a gold electrode with the peptide substrate (Arg-Pro-Arg) allowed for the deposition of higher amounts of Au NPs on the electrode surface through the tripeptide-induced assembly of Au NPs due to low electron transfer resistance. Reprinted with permission from (Xia *et al.* 2016).

This method was based on the design of the peptide sequence (Arg-Pro-Arg) with two binding tags to crosslink unmodified Au NPs (Xia *et al.* 2016). In this method, the Au NPs were not functionalized with the peptide substrate making their method prone to possible interferences from the sample matrix. In addition, their two-stage method is not amenable to real-time monitoring of enzyme activity (Laromaine *et al.* 2007).

## 1.10 Research Aims

The primary aim of this thesis was to design and develop a rapid, selective and highly sensitive diagnostic assay for detection and quantitative determination of DPP-IV/CD26 activity in biological samples, using the superior chromogenic properties of Au NPs together with a novel DPP-IV/CD26 targeted peptide with the objective of developing point of care (POC) (*i.e.* near-patient) sensor. Monitoring the expression of specific protease enzymes that are implicated in disease processes could offer a rapid diagnosis so treatment can be initiated as early as possible. In a recovering patient, abnormal enzyme expression may also give warnings of a recurrence of disease (Hetmańczyk *et al.* 2016). As the DPP-IV enzyme has been identified as a target for drug therapy, the test could be utilized for HTS of inhibitory drug compounds.

Scheme 1-2 shows the basic design and optimization stages for the development of the colorimetric peptide modified Au NP sensor. In the following chapters, details on the design of different peptide sequences and functionalization of Au NP preparations, including various instrumental techniques used to study and validate the coupling process are described. Methods were optimised for the successful conjugation of ligands to the Au NP surface. Validation of the developed methods was investigated through correlating results obtained with traditional assays already in use and by application to real biological samples.



**Scheme 1-2** Experimental flow chart for the design of a peptide modified Au NPs colorimetric assay.

The use of Au NPs for biosensor applications, the biochemical role of DPP-IV in health and disease and methods for the measurement of DPP-IV activity have been reviewed in Chapter 1. Chapter 2 presents the laboratory techniques used in this work. Chapter 3 outlines the development of a peptide-functionalised assay for the detection of DPP-IV, a protease biomarker for many diseases. A DPP-IV substrate was designed for the enzyme and to subsequently change the interparticle distance, followed by a distinct colour change in the Au NP upon enzyme addition. Chapter 4 introduces a modified peptide substrate ligand with a spacer in an attempt to enhance sensitivity and the linear range of the assay. The modified sensor and the novel approach have promising applications in assay of serum samples and for HTS of DPP-IV inhibitors *in vitro*. Chapter 5 summarises the use of 3 different approaches to enhance the stability of Au NP systems for more reliable and reproducible results in complex biological samples. Chapter 6 introduces the results of preliminary trials of a developed Au NR biosensing method for the detection of DPP-IV/CD26 activity.

## Chapter 2

---

### **Experimental Techniques**

---

# Experimental Techniques

A variety of spectroscopic and imaging techniques were used to characterize the functionalized Au NPs synthesized in this project. These are detailed below.

## 2.1 UV-Visible Spectroscopy

Ultraviolet-Visible (UV-Vis) spectroscopy is a technique applied to measure the light that is absorbed and transmitted by a material (known as the extinction, which is expressed as the total of absorbed and transmitted light). The technique relies on the interaction of electromagnetic radiation with matter (Mulvaney 1996; Aryal *et al.* 2006b). The interaction of light with colloidal Au NPs induces a distinct optical feature known as LSPR, which results in a strong absorbance band in the visible region (500 - 600 nm), which can be measured by UV-Vis spectroscopy (Fig. 2.1) (Mulvaney 1996; Klar *et al.* 1998; Petryayeva & Krull 2011) .

The maximum absorbance wavelength increases (red shift) with an increase in particle size. The peak optical density (OD), or absorbance of the sample, is directly proportional to the concentration of NPs in solution (Pesika *et al.* 2003; Myers *et al.* 2013). UV-Vis measurements can also be applied to assess the functionalization of Au NPs. Upon attachment of ligands to the Au NP surface, the LSPR spectrum red shifts and broadens. This shift is the result of a change in the local refractive index at the Au NP surface and forms the basis for the study of changes to Au NP size.

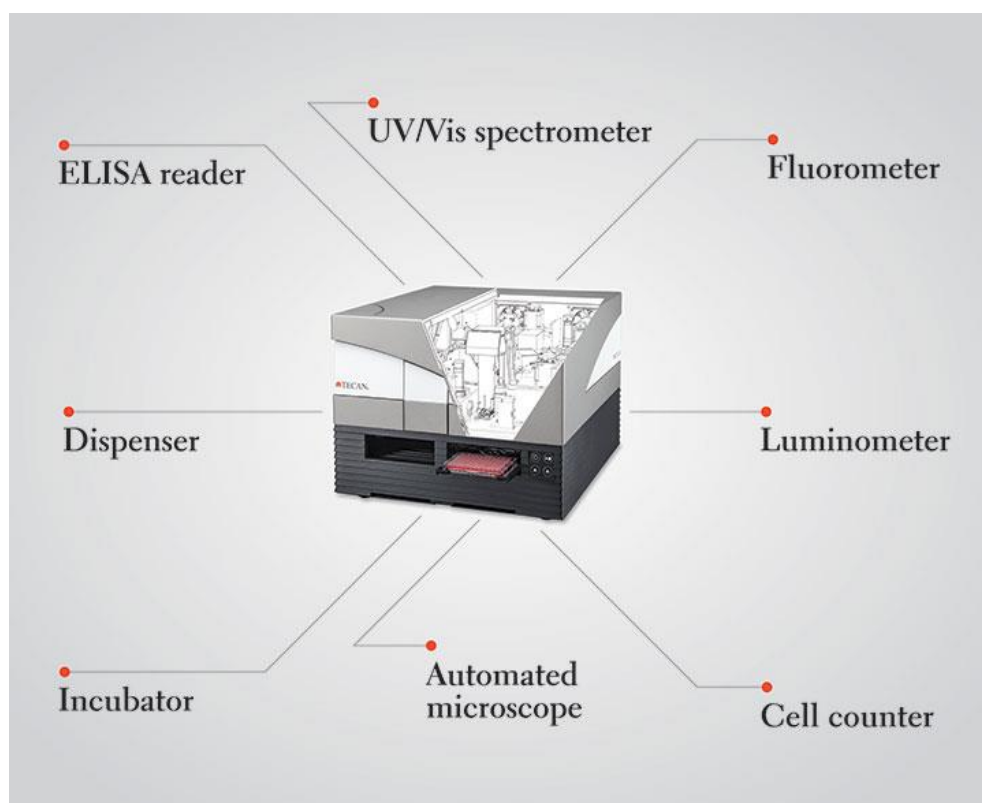


**Figure 2-1** A diagram of the components of a typical spectrometer.

## 2.2 Transmission Electron Microscopy (TEM)

The most common technique for characterisation of Au NPs is high resolution TEM, which can be used to study Au NPs, providing the size distribution and dispersity of the sample. The mean number of gold atoms can also be calculated from the mean diameter,  $d$ , of the cores.

TEM utilizes a beam of electrons directed at an ultra-thin specimen which illuminates the sample and yield a highly-magnified image. The image is formed by the transmission of electrons through the specimen, magnified and focused by a magnetic lens and captured by a fluorescent screen or to be detected by a sensor such as a charge-coupled device. TEM is capable of imaging at a significantly higher resolution than light microscopes, owing to the fact that the De Broglie wavelength of electrons is many orders of magnitude smaller than that of photons (2.5 pm at 200 kV) (Williams & Carter 2009).

By making use of electrons to magnify objects, it is possible to view objects much smaller than can be viewed by light microscopy, typically it is possible to achieve a resolution of 0.2nm and magnifications of up to 2,000,000x, whereas most light microscopes are limited by diffraction to about 200 nm resolution and useful magnifications below 2000x can be obtained. This enables the instrument user to observe minute detail, which is thousands of times smaller than the smallest resolvable object in a light microscope. Louis de Broglie demonstrated that every particle or matter propagates like a wave (Broglie 1924), and the concept is known as particle-wave duality. The wavelength of a particle or a matter can be calculated as follows.

$$\lambda = \frac{h}{p} \dots\dots\dots(4)$$

Where  $\lambda$  is the wavelength of a particle,  $h$  is Planck's constant ( $6.626 \times 10^{34}$  joule per second), and  $p$  is the momentum of a particle. Since the momentum is the product of the mass and the velocity of a particle,

$$\lambda = \frac{h}{mv} \dots\dots\dots(5)$$

The velocity of electrons can be calculated by:

$$v = \sqrt{\frac{2eV}{m}} \dots\dots\dots(6)$$

For the electron beam to move uninterrupted through the TEM it must be operated at low pressures to avoid electrons colliding with air particles or forming an electrical arc. The electrons are produced by a thermal source such as tungsten filament, lanthanum hexaboride (LaB<sub>6</sub>) filament or a field emission source, such as an electron gun, capable of generating a stream of monochromatic electrons (Lafferty 1951). The electrons are accelerated using voltages between 100 kV and 300 kV to guarantee that the electrons pass through the sample. Operating the TEM at high voltage offers better resolution because the electrons travel at a shorter wavelength; however, the electrons will have

extra energy and could damage the sample. At too low a voltage, the electrons will not be transmitted through the sample and will not produce an image.

A TEM is composed of several components, which incorporate a vacuum system in which the electrons move, an electron emission source for generation of the electron stream, a series of electromagnetic lenses to focus the electron beam (see Fig 2-2).

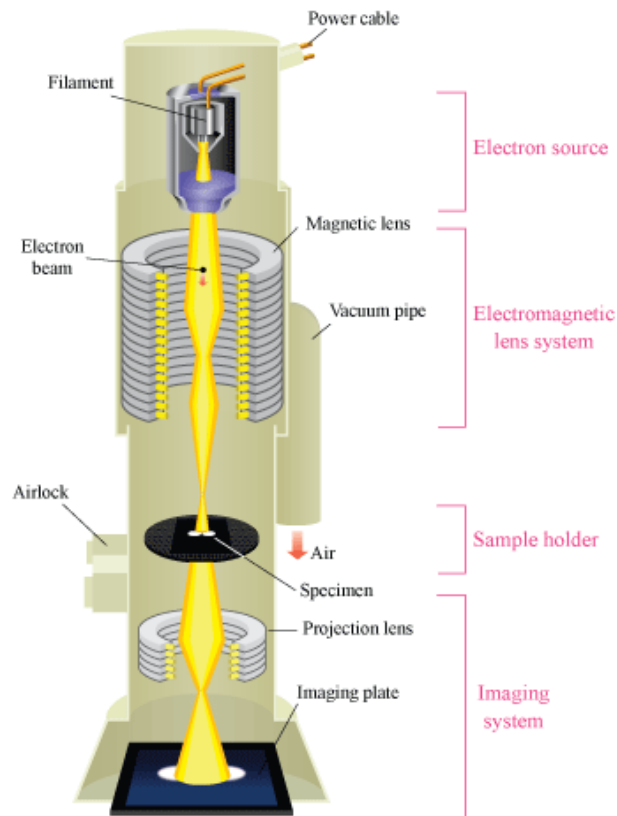


**Figure 2-2** Schematic diagram of a Transmission Electron Microscope.

A TEM contains four parts: electron source, an electromagnetic lens system, sample holder, and imaging system. Adapted from <http://www.edn.com>.

TEM is the most direct method for the determination of the size, distribution and the dispersity of NPs (Howie *et al.* 1982; Fisker *et al.* 2000). However, the main limitation is with sample representation, because only limited areas are selected from the grid, which might result in a non-representative image of the sample. In addition sample destruction, due to the high energy of the electron beam utilized is restrictive (Bovin & Malm 1991).

### 2.3 Zeta-Potential Measurements

Zeta potential analysis is a technique for determining the surface charge of NPs in colloidal solution by measuring the effective electrical charge associated with the surface of particle/molecules in the medium. Owing to the characteristic nature of the NP surface electrical double layer, an electrical potential develops on the NP surface boundary, known as the zeta potential of the particles, with values that typically range from +100 mV to -100 mV (Fig. 2-3) (Hunter 2013).

The magnitude of the zeta potential provides valuable data about the relative stability of a formulation of the suspensions of particles in aqueous or non-aqueous media, i.e. the tendency of the solid particles to aggregate (flocculate) is a function of the zeta potential, depending on the degree of electrostatic repulsion between adjacent, similarly charged particles in a dispersion. In addition to understanding the state of the NP surface, it provides a good indication of the stability of the NPs in the suspension media; particles with higher magnitude zeta potential exhibit increased stability due to a larger electrostatic repulsion between particles as shown in (Table 2-1). If all the particles in suspension have a large negative or positive zeta potential ( $> 30$  mV) then they will tend to repel each other and there will be no tendency for the particles to come together. However, if the particles have low zeta potential values then there will be no sufficient force to prevent the aggregation.

It is important to investigate zeta potential parameters during development of nanoparticulate biosensing systems, especially given the fact that biological matrices are known to alter the stability features of NPs with different mechanisms (e.g., protein adsorption) (Ritz *et al.* 2015).

**Table 2-1** Classification of colloid stability according to zeta potential values. Data were obtained from (O'Brien *et al.* 1990; Hanaor *et al.* 2012)

Zeta potential [mV]	Stability behaviour of the colloid
from 0 to $\pm 10$	Rapid coagulation or flocculation
from $\pm 10$ to $\pm 20$	Incipient instability
from $\pm 20$ to $\pm 30$	Moderate stability
more than $\pm 30$	High stability

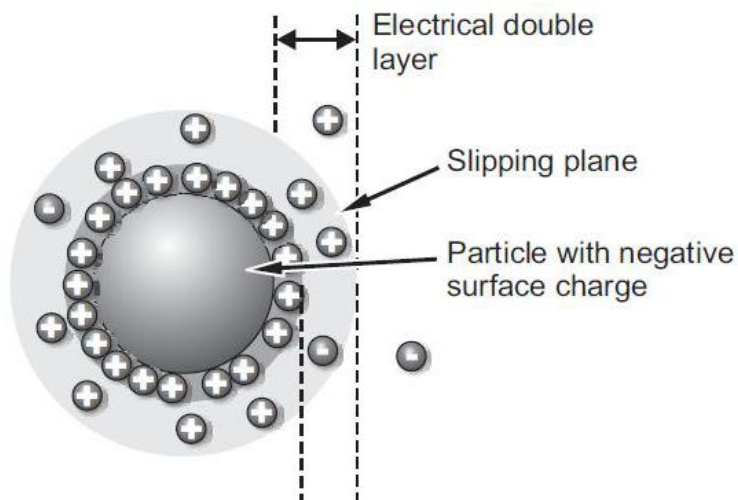


**Figure 2-3** Schematic representation of the electrical double layer that surrounds a particle in an aqueous medium. The potential that exists at the slipping plane is known as the zeta potential. Adapted from (Malvern 2007).

## 2.4 Dynamic Light Scattering (DLS)

Dynamic light scattering (DLS) is an analytical technique applied for determining the hydrodynamic size and size distribution of NPs and colloids in a liquid media, by measurement and interpretation of the fluctuations in the intensity of scattered light data on a microsecond time scale, also known as photon correlation spectroscopy. Analysis of these intensity fluctuations permits the evaluation of the diffusion coefficients, which in turn provides the particle size through the Stokes-Einstein equation (Miller 1924; Jans *et al.* 2009). Stokes radius is reported interchangeably with effectively hydrated radius ( $R_H$ ) in solution (Atkins *et al.* 2010), it is highly related to solute mobility, which is determined by the nature of the solvent. A small ion with a large hydrated shell, for example, may have a greater Stokes radius than a larger ion with a small shell. This is because the smaller ion drags a greater number of water molecules with it as it moves through the solution (Chu 2008). In 1905, Albert Einstein found that the diffusion coefficient of an ion to be proportional to its mobility constant.

$$D = \frac{k_B T}{6\pi\eta r} \dots\dots\dots(7)$$

Where

$D$  is the diffusion constant;

$k_B$  is Boltzmann's constant;

$T$  is the absolute temperature;

$\mu_q$ , the electrical mobility of the charged particle;

$\eta$  is the dynamic viscosity;

$r$  is the radius of the spherical particle.

This can be rearranged to solve for  $r$ , the radius:

$$R_H = r = \frac{k_B T}{6\pi\eta D} \dots\dots\dots(8)$$

Particles in liquid media undergo random Brownian motion due to bombardment from the solvent molecules (Tscharnuter 2006), observed in the resultant Doppler effects on the wavelength of the incident light and the scattered light from the particles (Angus *et al.* 1969). The modulation of the scattered light intensity as a function of time is analyzed, and the hydrodynamic size of the particles can be determined. Information on the size, shape, and interactions of colloidal particles in liquid systems, as well as their structure and internal dynamics can also be determined (Figure 2-4) (Berne & Pecora 2013).

A significant advantage of the DLS method is that it is a non-invasive technique in that it does not require sample handling and does not affect the NP dispersion state, and the data is obtained over a large number of particles (usually  $10^8$ – $10^9$ ) enclosed in a known volume (Khlebtsov & Khlebtsov 2011). DLS is a highly sensitive method for the determination of particle aggregation, which makes it a more reliable test, than absorption spectroscopy, for detection of biospecific interactions using Au NPs. This technique can be utilized for measurements of particle size distributions, particularly in the range 2–500 nm. DLS results can be distorted when the sample is not monodisperse because large particles existing in the sample can screen smaller ones and cause measurement interference (Tomaszewska *et al.* 2013).

Uncritical application of the DLS method, without confirmation from other measurements, may result in misleading interpretation of the measurements due to the contribution from the rotational diffusion to the correlation function of the scattered intensities of aspherical Au NPs with diameters  $> 40$  nm (Khlebtsov & Khlebtsov 2011). Therefore the measurements from other techniques such as TEM, is required. There is not always agreement between DLS and the TEM measurements, but the results from both measurements are comparable.

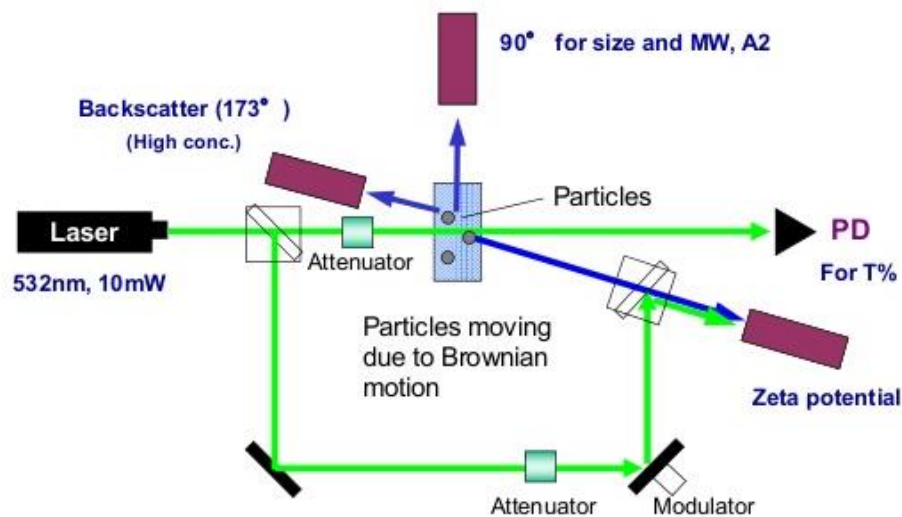


**Figure 2-4** A schematic diagram showing the operation of particle size analyser and zeta potential instrument.

A light source is introduced into the cell, and the scattered light is collected at either 90° or 173° as shown in the diagram above. The system automatically selects the optimum scattering angle and cell position depending on the sample concentration and intensity. The signal obtained from the scattered light is fed into a multi-channel correlator that generates a function used to determine the translational diffusion coefficient of the particles analyzed. Adapted from (www.Horiba.com).

## 2.5 X- Ray Photoelectron Spectroscopy XPS

X-ray photoelectron spectroscopy (XPS) also known as electron spectroscopy for chemical analysis (ESCA) is the most commonly applied surface analysis technique, as it can be used for the analysis of a broad range of materials and provides important chemical state and quantitative data from the surface of the material being investigated. In addition, it can be used to determine the chemisorptive properties of ligands adsorbed onto the Au NP surface and the oxidation states of metallic NPs.

XPS is performed by irradiating the surface of a sample with a beam of mono-energetic X-rays causing photoelectrons to be emitted from the sample surface (Fig 2-5A). An electron energy analyser is used to measure the energy of the emitted photoelectrons. A photoelectron spectrum is recorded by counting ejected electrons over a range of electron kinetic energies.

The average depth of analysis for an XPS measurement is approximately 5-10 nm. Electrons excited further down in the material will be reabsorbed or trapped, meaning that XPS is generally only used to analyse the surface of materials, or approximately the depth of one NP. XPS requires high vacuum ( $P \sim 10^{-8}$  millibar) or ultra-high vacuum (UHV;  $P < 10^{-9}$  millibar) conditions, although a current area of development is ambient pressure XPS, in which samples are analysed at pressures of a few tens of millibars (Ali-Löytty *et al.* 2016).

Peaks appear in the spectrum from atoms emitting electrons of a specific energy (Figure 2-5B). From the binding energy (i.e the energy required to detach the electron from the surface) and intensity of a photoelectron peak, the elemental identity, chemical state and quantity of a detected element can be determined. The binding energy depends on several factors, including the following:

- The element from which the electron is ejected,
- The orbital from which the electron is released,
- The chemical environment of the atom from which the electron was emitted.

XPS can be employed to study the surface chemistry of a material in its as-collected state, or after treatment, for example: cracking, slicing or grinding in air or UHV to expose deeper layers of the sample. XPS is routinely used to analyse inorganic compounds, metal alloys, semiconductors, polymers, elements, teeth, bones, medical implants, biomaterials and many others (Chusuei & Goodman 2002).

XPS has been employed to investigate the surface chemistry of gold substrates before and after functionalization with biological molecules, as it provides valuable information about specific interactions between functional groups of organic molecules and metals, to obtain a clear picture of assembling processes allowing the characterization of molecule-molecule and molecule-surface interactions and the oxidation states of metallic NPs. Moreover, from the XPS high-resolution spectra,

information about the bonds formed between the different species involved in the functionalization, can also be determined (Gonella *et al.* 2005; Spampinato *et al.* 2016). Spampinato and co-workers (2016) characterized the surface chemistry of gold substrates before and after functionalization with thiol-modified glucose self-assembled monolayers and subsequent biochemical specific recognition of maltose binding protein by using XPS. The technique was proved to be very useful means for examining all the functionalization steps, including the study of the biological behaviour of the glucose-modified particles in the presence of the maltose binding protein.

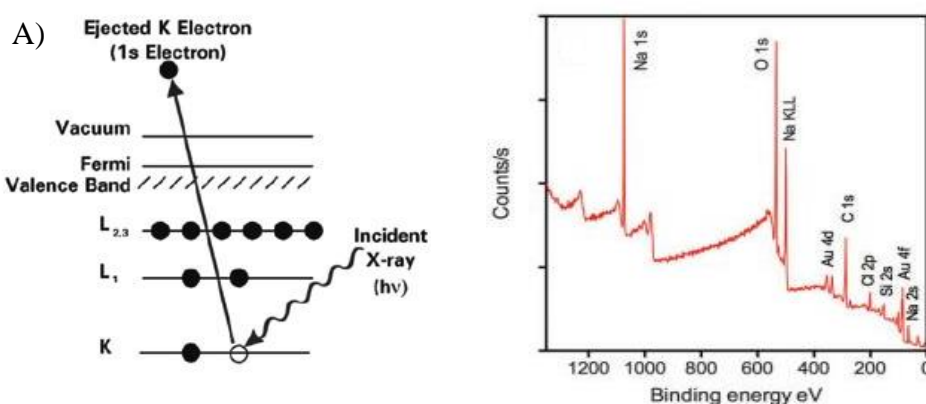


**Figure 2-5** (A) The photoemission process in XPS surface analysis. The discs represent electrons and the bars represent energy levels within the material being analysed. The equation governing the process is  $KE = h\nu - BE$ , where KE is the photoelectron kinetic energy,  $h\nu$  is the exciting photon energy, and BE is the electron binding energy. Adapted from [www.xpssimplified.com](http://www.xpssimplified.com) (B) XPS survey spectrum from citrate stabilized Au NPs showing various gold, sodium, oxygen peaks and a silicon peak. Reprinted with permission from (Sierra *et al.* 2016).

## 2.6 Fourier Transform Infrared Spectroscopy (FTIR)

Fourier transform infrared (FTIR) spectroscopy has emerged as a useful tool for the qualitative analysis of the functional groups present in compounds/molecules. The basic concept for recording the infrared spectrum of a sample is by shining a beam of IR light through the sample. When the frequency of the IR light matches the vibrational frequency of a bond, absorption occurs. Analysis of the transmitted light indicates how much energy was absorbed at each wavelength.

FTIR can be employed to obtain a direct characterization of molecular conjugation on the surface of Au NPs (Wulandari *et al.* 2008). Moreover, vibrational spectra of adsorbed thiolates on Au NP surfaces provide valuable data on interactions between molecules and on the orientation of molecules with respect to the surface (Bürigi 2015). IR spectra result from transitions between quantized vibrational energy states. When atoms/molecules in a sample irradiated by a source of IR beam, they display a number of vibrational modes. Each mode represents a harmonic displacement of the atoms from their equilibrium positions. The frequency of each vibrational mode is characteristic of a functional group, because for many vibrational modes only a few atoms have a large displacement and the rest of the molecule is stationary. Thus, the observation of a spectral feature in a certain area of the spectrum is generally indicative of a particular chemical functional group in the sample (Griffiths & De Haseth 2007). With the development of extensive spectra/structure correlation tables, it has become easier to assign IR absorption spectra in a given IR spectrum to the vibrational modes related to the specific functional group.

As mentioned earlier, the surface-to-volume ratio is very high in the case of NPs, when compared to the bulk form of the material. The number of atoms that constitute the surface can influence the vibrational spectra of NPs. FTIR spectroscopy is used to characterize the nature of surface molecules in NPs (Baraton 2002). Since the NPs have a large surface area, the functionalization of the surface using organic or biological molecules can alter the NP surface properties. Aryal *et al.* (2002) studied the interaction of thiol with Au NPs in aqueous medium by employing FT-IR spectroscopy together with other spectroscopic identification techniques such as UV-vis, Raman, and NMR. The disappearance of S-H stretching in the IR of the protons in close proximity to the metal centre verified the existence of the S-Au interaction in cysteine capped Au NPs.

The FTIR spectra of the modified NPs have extra peaks in comparison with the FTIR pattern of an unmodified NP. The property change with diverse molecules can simply be identified with FTIR spectroscopy (Shankar *et al.* 2004; Correa *et al.* 2016). The main benefits of the FTIR characterization method include speed of analysis (e.g. minutes per measurement), high spatial resolution, availability of miniaturized instrumentation (Pease *et al.* 2007; Tsai *et al.* 2011).

## 2.7 Electrospray Ionization Mass Spectrometry (ESI-MS)

ESI-MS is a 'soft ionization' technique used in mass spectrometry to produce ions with very little fragmentation, using an electrospray in which a high voltage is applied to a liquid to create an aerosol. It can be used to determine the molecular weight of unknown compounds such as proteins and peptides (Li *et al.* 2009). After a sample is loaded onto the instrument it is vaporised then charged (by exposure to a stream of electrons). The charged species are accelerated through magnetic fields that separate the ions by mass to charge ( $m/z$ ). A detector determines the mass to charge ratio of those ions and the results are presented in a mass spectrum (see Fig 2-6).

ESI utilizes electrical energy to assist the transfer of ions from solution into the gaseous state, before they are analysed by MS. Ionic species in solution can thus be analysed by ESI-MS with improved sensitivity. Neutral compounds can be converted to ionic form in solution or in the gaseous phase by protonation or cationisation (e.g. metal cationisation) and hence can be investigated by ESI-MS (Helfrich & Bettmer 2011).

ESI-MS is convenient for the analysis of functionalized Au NPs, which typically are covered by ligands because it is a soft ionization technique and can provide information the ligand composition (Tracy *et al.* 2007). Ionic signals are displayed in MS spectrum according to their  $m/z$  against relative abundance with the highest signal expressed as 100% abundance and referred to as the base peak.

A molecule (M) is usually ionised by the addition of a charged species such as  $H^+$  or  $Na^+$  to produce the ions  $[M + H]^+$  or  $[M + Na]^+$ . The  $m/z$  of these species would be given by the molecular weight of  $M + 1$  in the former case, or the molecular weight of  $M + 23$  in the latter. This way, the molecular components in the mixture can be identified.

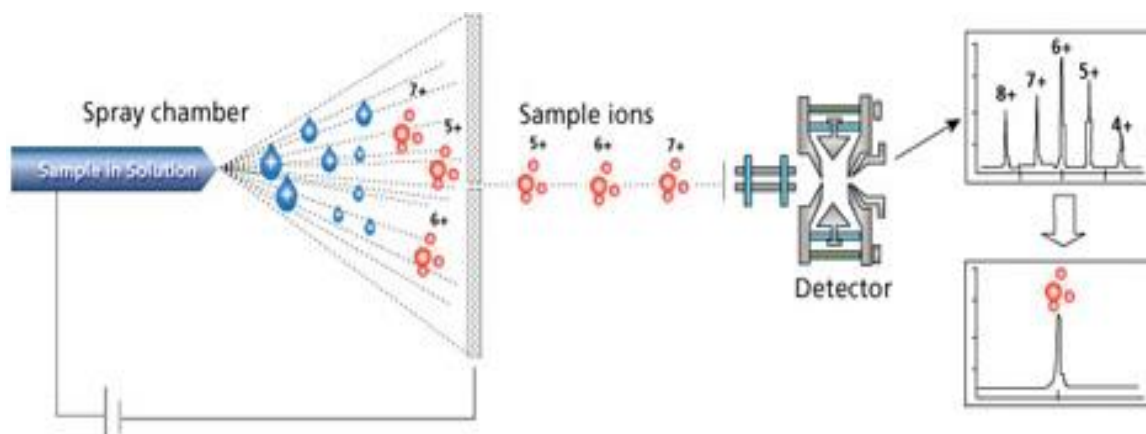


**Figure 2-6** A schematic diagram of the working principle of an ESI-MS. A high voltage is applied to a liquid sample to create an aerosol using an electrospray. The moderating influence of the solvent clusters on the reagent ions, and of the high gas pressure, reduces fragmentation during ionization and results in primarily intact quasi-molecular ions. Adapted from (Sigma-Aldrich).

## 2.8 Nuclear Magnetic Resonance (NMR) Spectroscopy

NMR spectroscopy is a powerful and theoretically complex analytical tool that exploits the magnetic properties of certain atomic nuclei. This type of spectroscopy is used in quality control and research for determining the content and purity of a sample, as well as providing a way for the elucidation of the entire structure of a molecule using one set of analytical measurements. NMR is based on the fact that when a population of magnetic nuclei is placed in an external magnetic field, NMR active nuclei (such as  $^1H$  or  $^{13}C$ ) have magnetic properties that can be utilized to yield chemical information by absorbing electromagnetic radiation at a frequency characteristic of the isotope, it can give access to the features of the electronic structure of a molecule and its individual functional groups (Shah *et al.* 2006).

NMR has proven to be a useful tool to study Au NP surface modifications to obtain essential knowledge in interfacial chemical and physical phenomena that occur on the surface of NPs. Moreover, NMR can be applied to the investigation of changes to the functional groups coupled to the Au NP surface. Several studies have demonstrated the sensitivity of solution NMR spectroscopy to the electronic environment and structure of the functional groups on nanomaterial surfaces (Tataurova 2014; Coelho et al. 2015; Zhou et al. 2016).

The effectiveness of the NMR technique in structural studies of functionalized Au NPs has been exemplified in many reports to provide insights into: Au NP formation mechanisms (Doyen *et al.* 2013), structural characterization of peptide immobilization to the Au NP surface (Bower *et al.* 2005) and investigation of a specific biomedical application for modified Au NPs (Coelho *et al.* 2015). Coelho and colleagues (2015) investigated the structure and physicochemical properties of Au NPs, modified with PEG, designed for the drug delivery of the proteasome inhibitor, Bortezomib (BTZ), in cancer therapy. NMR have provided valuable information on BTZ – PEG Au NPs interactions and the mechanism of drug incorporation and location inside the PEG Au NPs.

Recently, NMR has been used as a means to: quantify the degree of ligand exchange between various types of thiolated molecules on the surface of Au NPs by determination of ligand density values for single-moiety ligand shells; to recognize trends in Au NP functionalization efficiency depending on ligand type, concentration, and reaction time, as well as for characterization of different functionalization trends, where the new ligand may either substitute the existing ligand shell or add to it (backfilling) (Smith *et al.* 2015).

Although the sensitivity of NMR spectroscopy has been enhanced significantly and steady progress continue to be made in the application of the technique. However it is

still the weak link when compared with other spectroscopy techniques such as MS, and this limits its application in Au NP research, especially as a few milligrams of substance is required in order to obtain satisfactory results (Emwas 2015).

## 2.9 Gel Electrophoresis

Gel electrophoresis is a method used for separation of macromolecules (DNA, RNA and proteins) and their fragments, based on their size and charge. Gel electrophoresis has also been used to differentiate miscellaneous Au NPs varying in size and shape, based on the mobility of the NPs in acetate buffer (Pellegrino *et al.* 2007; Zheng *et al.* 2015).

The bright red colour of Au NPs allows direct visual or spectroscopic analysis of gel bands, which appear as coloured lines in a gel. Compared to other separation techniques, such as high performance liquid chromatography (HPLC), capillary electrophoresis, diafiltration, or size-exclusion chromatography, gel electrophoresis offers much more facile identification of functionalized Au NPs from citrate-capped Au NPs, because the mobility of particles in a gel is dependent on the surface charge density and the size/molecular weight of the particles.

Agarose gel concentration is a critical factor in the separation of NPs in order to ensure optimum pore size that eliminates undesirable NP-gel matrix interactions and for this reason the agarose gel concentration needs to be in the range of (0.5- 1.0 %) to provide pore diameters in the gel of  $\varnothing = 200-400$  nm. The use of gel electrophoresis for the study of metal nanostructures, in addition to identification of functionalized NPs from bare NPs, allows for separation of different shapes of NPs and this application has been used for the visual separation and identification of a mixture of Au NPs in solution containing both nanospheres and nanorods. The gel showed clear separation of gold spheres (red) mixed with gold rods (green). The concept has also been successfully

applied to the separation of silver nanorods from other silver nanostructures as shown in Figure 2-7 (Hanauer *et al.* 2007).

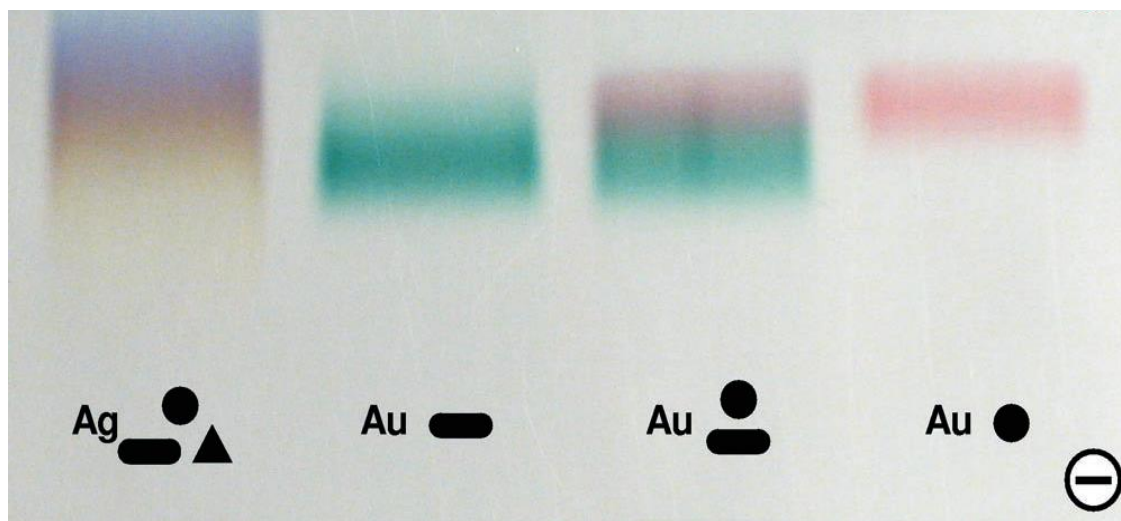


**Figure 2-7** True colour photograph of a 0.2% agarose gel run for 30 min at 150 V (15 cm electrode spacing) at  $\text{pH} \approx 9$ .

The dashed line at the bottom indicates the position of the gel wells. The four lanes contain, from left to right, Ag NPs, Au NRs ( $\approx 40 \times 20$  nm), gold rods and spheres mixed just before electrophoresis, and spherical Au NPs ( $\text{Ø} \approx 15$  nm) as indicated symbolically. Reprinted with permission from (Hanauer *et al.* 2007). Copyright American Chemical Society.

## Chapter 3

---

### **Development of a Gold Nanoparticle-Based Real Time Colorimetric Assay of Dipeptidyl Peptidase IV activity**

---

### 3.1 Introduction

It has been suggested that the measurement of DPP-IV/CD-26 activity can be potentially used as a diagnostic and prognostic marker for various inflammatory disorders, tumours and hematological malignancies (Jones *et al.* 2001; Ni *et al.* 2003; Sun *et al.* 2012). Therefore, there is a demand for a simple, selective and sensitive assay that can be used to measure the activity of DPP-IV/CD26 in health and disease.

To date, the most commonly used methods for the determination of DPP-IV enzymatic activity are based on the use of chromogenic, fluorogenic, bioluminescent and electrochemical sensors (Nagatsu *et al.* 1976; Kato *et al.* 1978; O'Brien *et al.* 2006; Xia *et al.* 2016). A list of the methods developed for the detection and determination of DPP-IV enzyme activity and a comparison of their sensitivities is given in Table 3-1. It can be seen that electrochemical methods currently provide the best sensitivity with at least 2 orders of magnitude lower detection limits than those obtained by other methods. However, these methods required the use of complex instrumentation. A further drawback associated with the use of the current chromogenic substrates is that they contain over reactive leaving groups, which render them easily susceptible to non-enzymatic cleavage by interfering proteins in biological samples as found in the case *p*-nitro anilide substrates (Goddard & Reymond 2004).

Au NPs with the size range of 1–100 nm, have highly sensitive distance-dependent optical properties, originating from the interaction between incident electromagnetic radiation and metal conduction electrons. Such interactions generate a substantial shift of absorption bands in the visible region of the electromagnetic spectrum, as a result of the alteration in the dielectric field of the particles in close proximity to each other (Figure 3-1), thus making it possible to monitor molecular events visually, without the need for complex instrumentation (Klajn *et al.* 2010; Paterson & De La Rica 2015).

**Table 3-1** Comparison of the assay sensitivity as defined by the limit of detection (LOD) and limit of quantification (LOQ) of colorimetric, fluorometric and luminescent DPP-IV assays.

Substrate	LOD (U/L)	LOQ (U/L)	Type of Assay	Reference
Gly-Pro-p-nitroanilide	1.56	2.92	Colorimetric	(Matheussin <i>et al.</i> 2010 )*
Gly-Pro-4-Me-β-NA)	0.10	0.26	Fluorometric	
Gly-Pro-AMC	0.18	0.27	Fluorometric	
DPPIV-Glo™ Protease*	0.035	0.040	Luminescent	
Fc-Tyr-Pro-Phe-Phe-NH <sub>2</sub>	3.9 x 10 <sup>-5</sup>	0.5 x 10 <sup>-3</sup>	Electrochemical	(Zhang <i>et al.</i> 2015)
Arg-Pro-Arg Au NP	0.07 5.5 x 10 <sup>-4</sup>	0.1 -	Colorimetric & electrochemical	(Xia <i>et al.</i> 2016)

\* The first 4 assay data were all obtained from one reference.

(GP: glycyl proline; Me: methoxy; NA: naphthylamide; AMC: aminomethyl coumarin; Fc: Ferrocene)

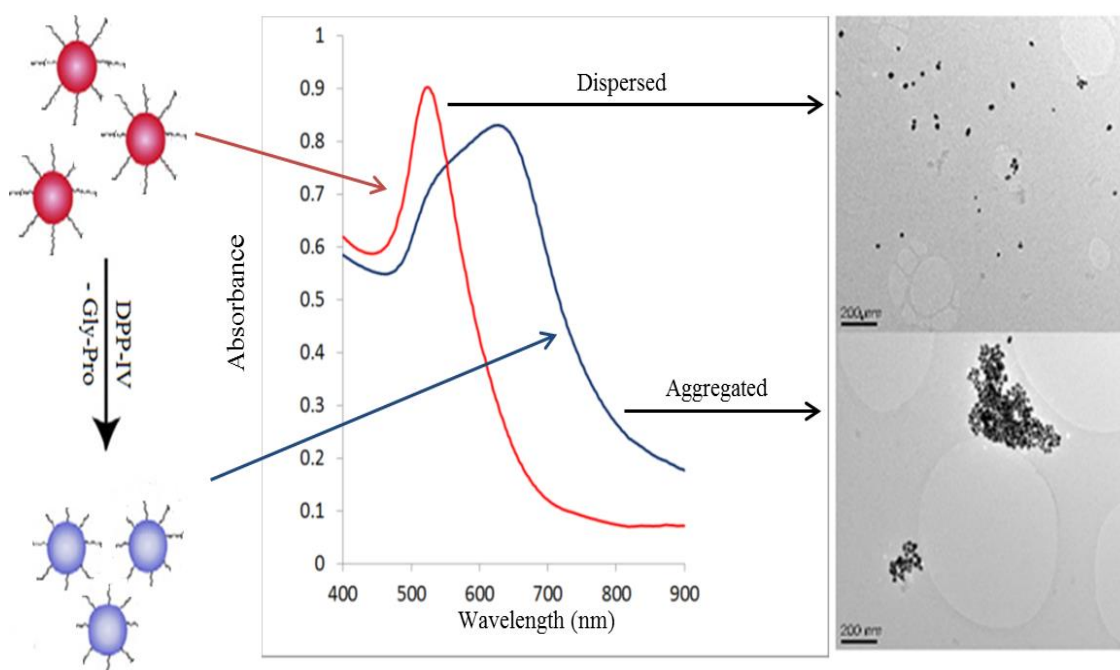


**Figure 3-1** Illustration of the changes induced by target interaction with substrate modified Au NPs represented by UV-visible spectrophotometry and TEM imaging. Reprinted with permission from (Aldewachi *et al.* 2017)

Nanoplasmonic colorimetric assays offer high sensitivity because of the high extinction coefficients of Au NPs,  $10^2$ - $10^3$  times higher than those of conventional coloured dyes (Ding *et al.* 2014). Using thiol chemistry, recognition substrates, e.g. peptides with cysteine residues, alkane thiolate or tiopronin (Sellers *et al.* 1993; Templeton *et al.* 1999; Mocanu *et al.* 2009; Krpetic *et al.* 2009) can be used to functionalize the Au NP surface in a colloidal solution. When the enzyme is added, the stability will be affected due to the cleavage of immobilized peptide substrate resulting in the aggregation of the Au NPs with an accompanying colour change. Detection of enzymatic activity by using metal (typically gold) nanoparticle based colorimetric assays is an attractive alternative to traditional enzymatic assays because colour changes are visible to the naked eye. Such colour changes, caused by presence of the analyte, induce Au NP aggregation and forms the basis for colorimetric detection. A variety of enzymes (lipases, proteases, kinases and nucleases) have been detected using this approach (Zhang *et al.* 2014; Chen *et al.* 2014; Cheng *et al.* 2014; Wang *et al.* 2015). Label-free colorimetric assays in which the substrate reporter molecule is not covalently attached to the Au NPs, but through electrostatic and hydrophobic interactions for the detection of various biological targets and molecules such as thrombin, alkaline phosphatase, adenosine deaminase and cancer biomarkers have also been reported (Chen *et al.* 2010a; Li *et al.* 2013; Liu *et al.* 2014; Cheng *et al.* 2015).

In this chapter, the development of a rapid and simple colorimetric assay is described for the measurement of DPP-IV/CD26 activity, using Au NPs functionalized with a synthetic peptide Gly-Pro-Asp-Cys (GPDC). The substrate is hydrolysed by DPP-IV/CD26 resulting in non-crosslinking aggregation of the Au NPs with an associated colour change see Fig. 3-2. This design has been chosen in order to avoid the limitations encountered with a colorimetric Au NP assay recently developed by Xia and his colleagues in which a two-step crosslinking Au NP assay for detection of DPP-IV



pure, were purchased from Sigma-Aldrich Co. Ltd (UK) and used without further purification. Thrombin from bovine plasma was purchased from GE HealthCare (UK). Deuterated water NMR solvent was purchased from Sigma-Aldrich (UK). The DPP-IV/CD-26 enzyme was reconstituted in 50 mM Tris buffer, pH 8.3, at an activity of 250 U/L, aliquoted and stored at -80°C. A 10 mM citrate buffer solution at pH 6 was used to solubilize the peptide. All solutions (except NMR solution which was prepared in deuterated water) were prepared using deionized water with a resistivity of 18.2 MΩ cm prepared with Milli-Q Academic Purification equipment, Millipore (UK).

### **3.2.2 Preparation of Citrate-Capped Gold Nanoparticles and GPDC-Capped Gold Nanoparticles Bioconjugate (P-Au NPs)**

All glassware was washed in aqua regia (HCl: HNO<sub>3</sub> 3:1) and then washed with deionized water and placed in the oven to dry.

Citrate Au NPs (~15 nm) diameter were prepared by citrate reduction of HAuCl<sub>4</sub> (Grabar *et al.* 1995). Briefly, 10 ml of 38.8 mM sodium citrate dihydrate at 50-60°C was added to 100 ml of 1 mM HAuCl<sub>4</sub> under vigorous stirring at boiling point to form a ruby red coloured solution after a series of colour changes. The colour change manifested is caused by SPR of the forming Au NPs. The solution was brought to room temperature; the pH was adjusted to 7.4 using 0.5 M NaOH and the solution was filtered through a 0.22 μm pore diameter Millipore syringe filter to remove unreacted salts. The filtrate was stored at 4°C until required. The peptide conjugated Au NPs (P-Au NPs) were prepared by addition of an aqueous solution of 2 mM peptide in citrate buffer pH 6, to the solution of 8 nM citrate Au NPs (based on an extinction coefficient of  $\sim 1.61 \times 10^8 \text{ M}^{-1} \text{ cm}^{-1}$  at 520 nm for Au NPs) in a 1 to 10 (v/v). After overnight reaction at room temperature, excess peptides were removed by centrifugation of the Au NPs (13000 rpm, 30 min at 4°C) using an Eppendorf centrifuge (Eppendorf, Germany). The

pelleted Au NPs were resuspended in deionized water and stored at 4 °C. The UV-visible absorption spectrum was obtained to determine the concentration of Au NPs.

It was found that the average diameter of synthesized Au NP was 14.5 nm after the analysis of 689 NPs by TEM (Fig. 3-3), the elongation of the particles was typically between 1.01 and 1.21. The particles can, therefore, be described as spherical or spheroid to a good approximation.

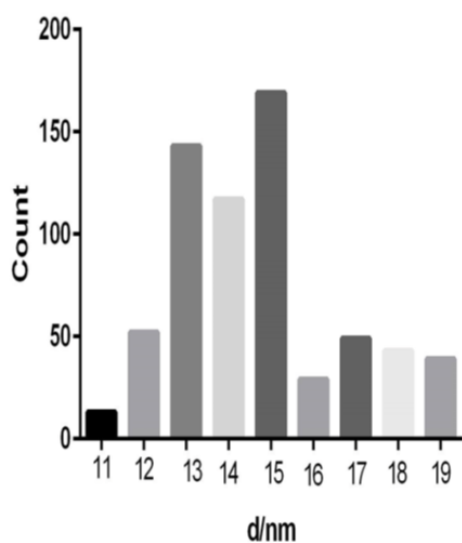


**Figure 3-3** Particle diameter histogram of citrate-capped Au NPs. The average diameter of Au NPs was calculated from a group of representative TEM micrographs using ImageJ software.

### 3.2.3 Instrumentation for Gold Nanoparticle Characterization

The ultraviolet-visible (UV-vis) absorption spectrum of the samples was recorded with a microplate reader (Tecan 2000, San Francisco, USA) in transparent 96 well microplate (Nunclon, Thermo Scientific, UK). ESI-Mass spectrometry of peptides was performed on an API-150EX MS single quadrupole LC/MS system (Applied Biosystems, UK).

The XPS spectra were obtained on a Kratos Axis Ultra DLD XPS spectrometer, UK. The X-ray source was a monochromated aluminum radiation (1486.6eV), operated with an X-ray emission current of 20 mA and an anode high tension (acceleration voltage) of 12 kV. The purified samples were lyophilized and the powdered solid was submitted for

XPS. XPS sample analysis was carried out at the Sheffield Surface Analysis Centre, Sheffield University by Deborah Hammond. The powdered sample was placed on a standard sample stud employing double-sided adhesive tape and the take-off angle was fixed at 90° relative to the sample plane. Wide scans were collected between 1200 to 0 eV at 0.5 eV resolution and 160 eV band pass energy, as shown in (Fig. 3-3A). In addition, high resolution scans were collected for C 1s, O 1s, N 1s, S 2p, and Au 4f peaks at 0.05 eV resolution and 20 eV band pass energy for varying lengths of time between 5 and 20 minutes per scan. The data were analysed using Vision2 software (Kratos Analytical, UK) and the analysis of the XPS peaks was performed using a commercial software package (Casa XPS v2.3.16PR1, Casa Software Ltd., UK). The atomic weight percentages (wt%) were determined from the experimentally calculated peak intensities and normalized by atomic sensitivity factors provided by Kratos Analytical, UK. Peak fitting was performed with no preliminary smoothing.

Dynamic light scattering (DLS), (Malvern Zetasizer Nano-ZS, UK) for sizing measurements were carried out using a 10mm disposable sizing cuvette and the particle size measurements were performed in triplicate.

Transmission electron microscope (TEM) Samples were sent to Leeds EPSRC Nanoscience and Nanotechnology Research Equipment Facility (LENRF) and were analysed by Zabeada Islam. TEM images were taken on a CM200 Tecnai TF20. Field emission gun TEM (FEGTEM) operated at an accelerating voltage of 200 kV and equipped with a Gatan Orius SC600A CCD camera to capture images. Samples were prepared by placing a drop of citrate-Au NPs solution (or P- Au NPs) on a copper grid. The films on the TEM grids were allowed to dry for 5 minutes under a heat bulb before analysis. Final statistical size distributions were arrived at by TEM-based size analysis of the purified particles (n ~ 700 particles). The size analysis of the particles was performed using Image J analysis software.

Mass spectrometric measurements were carried on an electrospray ionization mass spectrometry (ESI-MS) (Thermo Scientific, Sanjose, California, USA) in the BMRC labs in positive ion mode to analyse peptide cleavage products of DPP-IV substrate. Samples were introduced by direct infusion using the syringe pump on the instrument at a flow rate of 5  $\mu\text{L}/\text{min}$  with an acquisition time of five minutes.

$^1\text{H}$  nuclear magnetic resonance (NMR) spectra were obtained in deuterated water ( $\text{D}_2\text{O}$ ) on a Bruker AVANCE III (400 MHz) NMR spectrometer (Bruker, Coventry, West Midlands, UK) in the BMRC labs.

### **3.2.4 Colorimetric Assay of DPP-IV/CD26 Activity**

For assaying DPP-IV/CD26 activity, varying activities of DPP-IV (2, 4, 6, 8, 10, 15, 20, 25 and 30 U/L) in 50 mM Tris buffer pH 8.3 were added to 100  $\mu\text{L}$  of GPDC-modified Au NP solution and the mixture was incubated at 37  $^\circ\text{C}$  for 10 minutes, in the wells of a transparent 96 well microtiter plate. The UV-vis absorption spectrum of the solution was recorded using an absorbance scan from 400-900 nm. The experiments were conducted in triplicate (3 different sample preparations) for the assays of detection and quantitative determination of DPP-IV/CD26 activity. DPP-IV/CD26 activity was determined kinetically during 10 min at 37  $^\circ\text{C}$  by measuring the absorbance ratios at 642 and 522 nm ( $A_{642}/A_{522}$ ). A linear fit was used for quantitative determination of enzyme activity because it provides the simplest way for calculation of activity or concentration. Method detection limit was used to evaluate assay sensitivity. The values of the Michaelis constant ( $K_M$ ) were determined by non-linear regression analysis using DynaFit software (Biokin Ltd.).

### 3.3 Results and Discussion

#### 3.3.1 Design of the Peptide Substrate

The peptide substrate, Gly-Pro-Asp-Cys (NH<sub>2</sub>-GPDC-OH) was designed to mimic the structure of the chromogenic substrate Gly-Pro-*p*-nitroanilide, which is one of the most frequently used substrates for DPP-IV/CD26 detection. The main difference between the two is that the peptide substrate mimics natural substrates of the enzyme instead of linking the dipeptide to a chemical moiety. The rationale for the choice of this sequence included the presence of the following: (i) the enzyme cleavage site in the dipeptide (NH<sub>2</sub>-Gly-Pro) for DPP-IV/CD26, as the enzyme functions selectively on a dipeptide sequence that contains a protonated amino group (Lambeir *et al.* 2003) (ii) cysteine (C) as anchor to facilitate the immobilization of the peptide onto the Au NP surface and (iii) inclusion of aspartic acid (D) in order to enhance the negative charge on the NP surface and provide further distance between the substrate ligand attached to the NP surface which in turn enhances the stability of the colloidal solution by means of electrosteric stabilization.

#### 3.3.2 Synthesis of GPDC-Functionalized Gold Nanoparticles

Evidence for the successful formation of citrate-capped Au NPs was supported by UV-vis spectroscopy (Fig 3-4). In the inset on Fig 3-4, the peak has shifted from 520 (blue curve) to 522 nm (red curve) after Au NP modification with GPDC peptide. The extinction of GPDC capped Au NPs was slightly higher than that of the unmodified Au NPs (blue curve), mainly because of changes in refractive index on the Au NP surface resulting from the coupling of a peptide layer to the surface of the NPs.

Independent modification of the Au NP surface provides a way to alter their optical behaviour. The incorporation of ligands changes the level of the electromagnetic interaction and as a result the optical function due to the asymmetric environment (Ghosh and pal 2007).

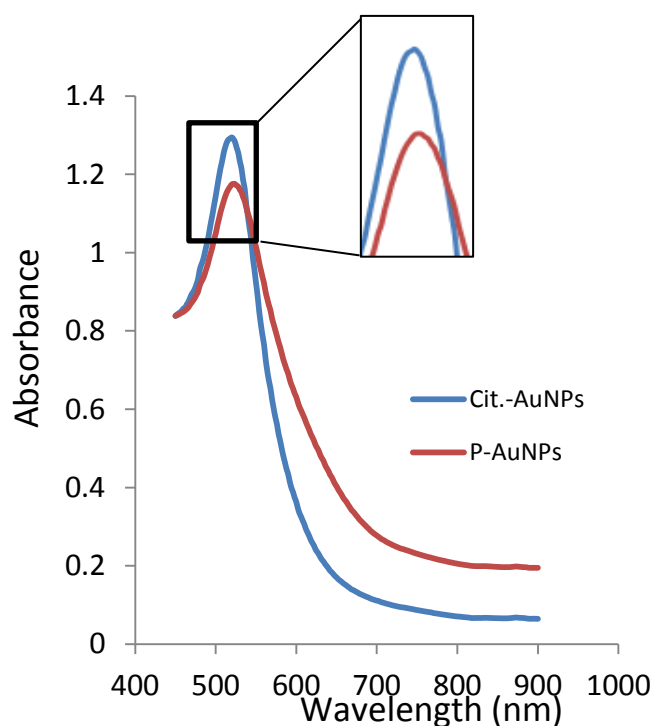


**Figure 3-4** UV-Vis absorption spectra of dispersed citrate-Au NPs (blue) and GPDC capped Au NPs (red).

Inset: enlarged section showing the shift of the absorption spectra after peptide immobilization.

A number of published papers have examined the effect of functionalization of Au NPs on its optical properties. For example; Ghosh and Pal (2007) observed that the LSPR of gold colloids changes variably when binding different cationic and anionic surfactants of variable chain length, which they attributed to different dielectric environments imposed by these ligands at the gold/surfactant interface. In contrast to this observation, Underwood and Mulvaney (1994) observed that spectra of polymer stabilized metal particles displayed distinct surface plasmon bands that are not influenced by the adsorption of epoxy groups to the metal surface.

The effect of ligand coupling to the LSPR of gold colloids can be accounted for by assuming the contribution of the dielectric of the organic shell. When a metallic NP is coated with a ligand shell whose refractive index is different from that of the ambient (i.e., the Au nanocore), the field that acts on the particle becomes unhomogeneous. The

density of the binding ligands coating offers a dielectric covering on the particle surface, leading to a change in the dielectric constant of the medium and causing a red shift of the  $\lambda_{\text{max}}$  of the LSPR (Mulvaney 1996).

It was necessary to determine the optimum pH for successful conjugation of peptides to Au NPs (Peng, Chen *et al.* 2007). The optimum pH for GPDC conjugation was determined by performing a preliminary titration at two different pH values namely, pH 4.5 and 6 and examining the extent of conjugation by Bradford assay. Although the theoretical isoelectric point for GPDC was predicted to be 3.8 (ExpASy). A pH of 6 was found to be more effective for successful conjugation. Whilst the optimal pH for coating usually lies around the isoelectric point of the protein, there are no general rules and adsorption interaction isotherms should be conducted in each case (Keating *et al.* 1998).

### **3.3.3 Examination of Peptide Coupling by XPS**

Both citrate and peptide modified Au NP solution were analysed by XPS to determine the elemental composition of the GPDC-Au NPs and more importantly to elucidate the nature of the Au-S linkage. In XPS, the nature of sulphur atoms determines their position in the spectrum, with the species with the lowest binding energy (162.5 eV) being the most reduced of the sulphur atom types, the species at ~164 eV being slightly more oxidized, and the species between 167-169 eV being a strongly oxidized sulphur species (Table 3-2).

**Table 3-2** Sulphur binding energies (eV) in XPS spectrum referenced to adventitious C1s peak at 284.8eV. Adapted from www.xpssimplified.com

Chemical state	Binding energy S2p <sub>3/2</sub> / eV
Metal sulfide	~161.5
Thiol bound to gold, Au-S	162.5
Thiol, R-SH	~164
Na <sub>2</sub> (SO <sub>3</sub> ) <sub>2</sub>	166.5
Metal sulfate	~169

Wide scan spectra of Au NPs modified with peptide ligand (GPDC) (Figure 3-5) was showing signals due to Au and S. Although the sulphur concentration was low, as shown in Table (3-3) due to its low availability in the peptide ligand, it was possible to detect the S2p peak at approximately 162.2 eV, consistent with the formation of a thiolate linkage between the ligand and the gold core (Fig. 3-6). Although the high-resolution spectrum for another area suggests there may also be some untreated thiol with a binding energy of 164 eV (Fig. 3-7). There was no evidence for oxidised sulphur, which appears at ~167 eV on gold clusters (Lee *et al.*, 1998; Schoenfish and Pemberton, 1998).

Binding energy values reported for sulphur in GPDC-Au NPs are consistent with a system in which the sulphur species is bound to the surface of gold as a thiolate, which usually occur in the range between 162.0 to 162.9 eV (Bourg *et al.*, 2000; Bain *et al.* 1989).

The high-resolution Au (4f) spectra for both samples contain a doublet for Au (4f<sub>7/2</sub>) and Au (4f<sub>5/2</sub>) with binding energies *c.a.* 84 and 87.7 eV, respectively (Fig 3-8). These values are similar to those reported by Brust (83.8 eV and 87.5 eV) (Brust *et al.* 1994) and Yee and colleagues (84.2 eV and 87.85 eV) (Yee *et al.* 2003) for Au NPs capped with dodecanethiol. The binding energy of Au(I) in a gold thiolate is 86.3 eV and Au NPs that are reported to contain a fraction of their surface atoms in the Au(I) oxidation

state show an Au 4f<sub>7/2</sub> peak with a binding energy of 84.9 eV (McNeillie *et al.* , 1980). The Au (4f<sub>7/2</sub>) observed at 84.0 eV in the GPDC-Au NPs suggested that the bulk of the gold atoms are in the Au (0) oxidation state.

The main gold peak was fixed at 84 eV and was chosen as the binding energy reference. A smaller peak at lower binding energy was regularly seen (Fig. 3-8). A search of the literature suggests whilst XPS of Au NPs has often seen small peaks at higher binding energies, suggesting Au(I) or Au(III) complexes, a peak at lower binding energy is less easily explained. This lower binding energy peak was typically 2 eV lower than the main Au peak and approximately 20% of the total area.

Overall XPS data have provided valuable information regarding the ligands coating the surface of Au NPs. A wide scan spectrum confirmed the presence of sulphur and gold in the sample of peptide modified Au NP. The high resolution of Au (4f) spectrum showed a doublet for Au at Au (4f<sub>7/2</sub>) and Au (4f<sub>5/2</sub>) in the region of 84 and 87.7 eV respectively, which are similar to the values of gold thiolates reported in the literature (Brust *et al.* 1994; Yee *et al.* 2003). Furthermore, the presence of the peak for Au (4f<sub>7/2</sub>) shows that the bulk of the gold atoms are in the Au (0) oxidation state, confirming the successful synthesis of Au NPs.

The XPS spectra for C, O and N remained unaffected during the process of Au NPs modification with the peptide ligands, which gives an indication that these elements were not implicated in any form of bonding with Au NP surface.

**Table 3-3** Surface composition in atomic % of GPDC capped Au NPs as determined by quantitative XPS survey scan. (Area 1 & 2 represent 2 different spots for the same sample). Apart from indium that appeared due to sample pressing by indium foil the atom % is highly representative.

Sample	Na	F	O	In	N	Au	C	Cl	S
Area 1	3.2	0.6	24.2	0.9	6.3	13.4	49.2	1.9	0.4
Area 2	2.8	0.5	24.6	3.5	5.9	11.6	48.6	2.0	0.7

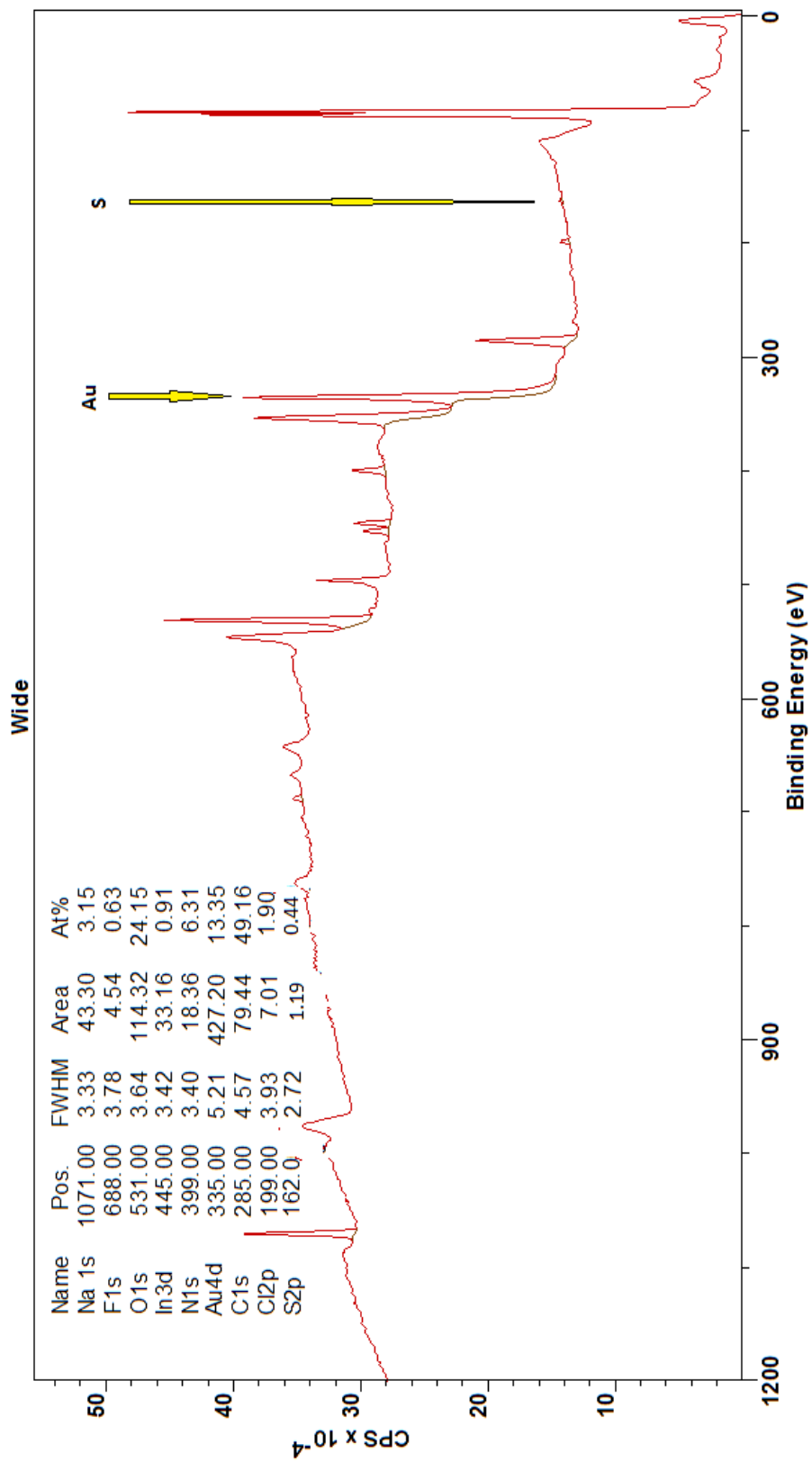


**Figure3-5** XPS survey scan of GPDC capped Au NPs

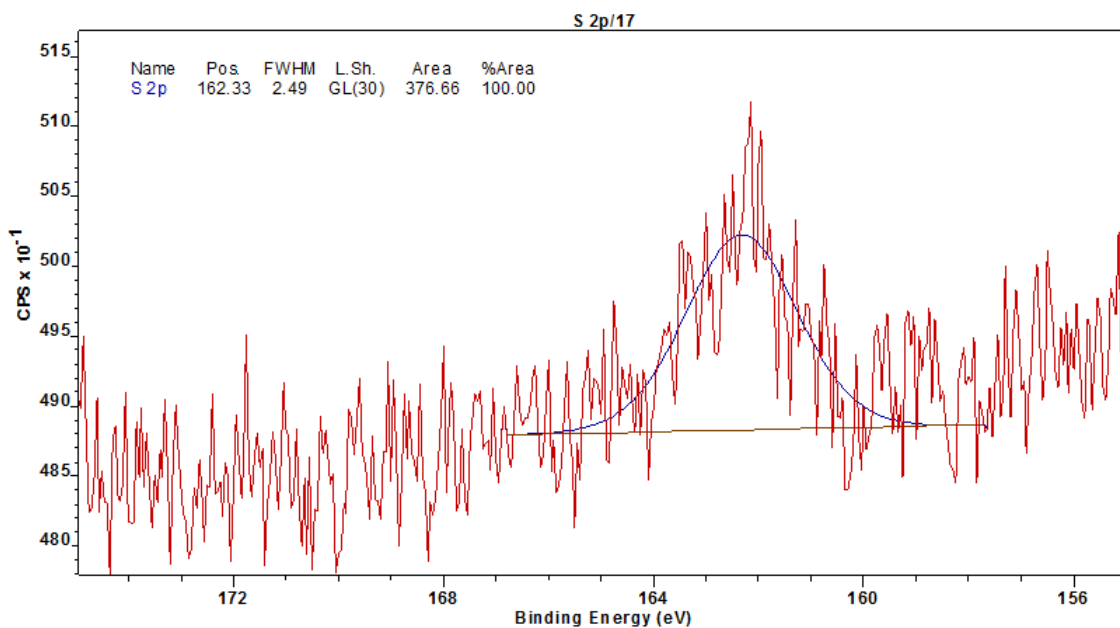


**Figure 3-6** S 2p narrow scan XPS spectra for GPDC capped Au NPs. The XPS spectra from certain area showed that all sulphur has transformed into thiolate.

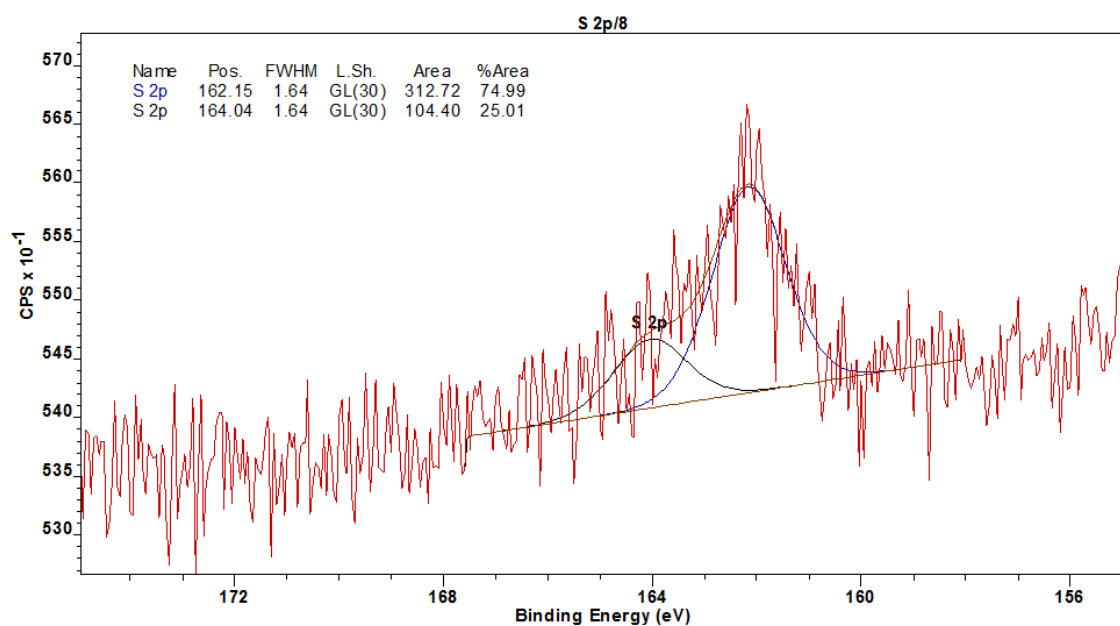


**Figure 3-7** S 2p narrow scan XPS spectra for GPDC capped Au NPs. In addition to the presence of main S peak at 162 eV, a small peak at 164 eV suggests that not all S might have converted into thiolate.

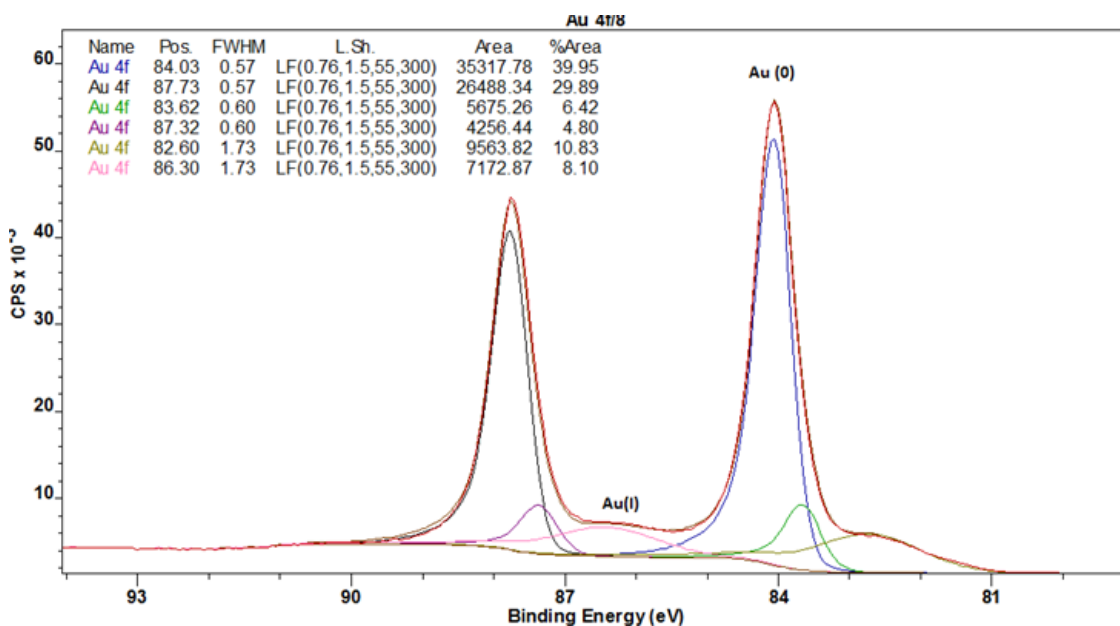


**Figure 3-8** Au 4f narrow scan XPS spectra of GPDC capped Au NPs.

### 3.3.4 Analysis of Gold Nanoparticle Size and Charge Before and After Functionalization Using DLS and Zeta Potential Measurement

DLS measurements show that the peptide capped Au NPs has an average hydrodynamic diameter of 36.5 nm in comparison to 21.9 nm for the unmodified NPs. This difference in diameter is indicative of the surface functionalization of the Au NPs with the GPDC peptide. The surface modification of the Au NPs with the peptide was further verified by zeta potential measurements. Upon adsorption of GPDC, the zeta potential shifted from  $-9.4 \pm 0.5$  mV for citrate stabilized Au NPs to  $-23.5 \pm 2.5$  mV for GPDC-capped Au NPs (Fig 3-9). The observed alteration in the zeta potential value can be attributed to the increased net negative charge of the peptide immobilized to the NPs surface. The changes in the zeta potential of the Au NPs demonstrated the successful surface functionalization of the particles and resulted in functionalized Au NP formulation with higher stability than unmodified Au NPs which serves as a good fit for incubating the NPs in ionic solution.

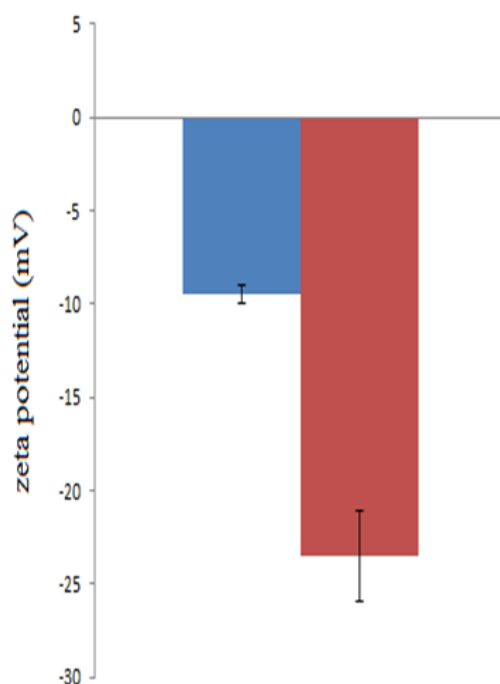


**Figure 3-9** Zeta potential measurements of bare Au NPs (blue) and GPDC-capped Au NPs (red) verified the surface functionalization of the particles. Error bars represent the standard deviation ( $n = 3$ ) of 3 Au NP preparations.

### 3.3.5 Sensitivity of GPDC-Capped Gold Nanoparticle to DPP-IV/CD26 activity

The addition of DPP-IV/CD26 to GPDC functionalized Au NPs solution resulted in a colour change from red to pale blue and the UV-Vis spectra displayed a clear red-shift with accompanying band broadening. A new band appeared at about 642 nm and there was a gradual increase in the band intensity and decrease in the absorbance of the band at 522 nm with an increase in DPP-IV/CD26 activity. The colour intensity increases with higher DPP-IV/CD26 activity, as more of the peptide substrate was cleaved by DPP-IV/CD26 causing further Au NP aggregation (Fig 3-10). The shift of absorbance to a higher wavelength correlated well with increasing DPP-IV/CD26 activity, whilst TEM images demonstrated that Au NP aggregates were formed in the presence of DPP-IV/CD26 (Fig. 3-11).

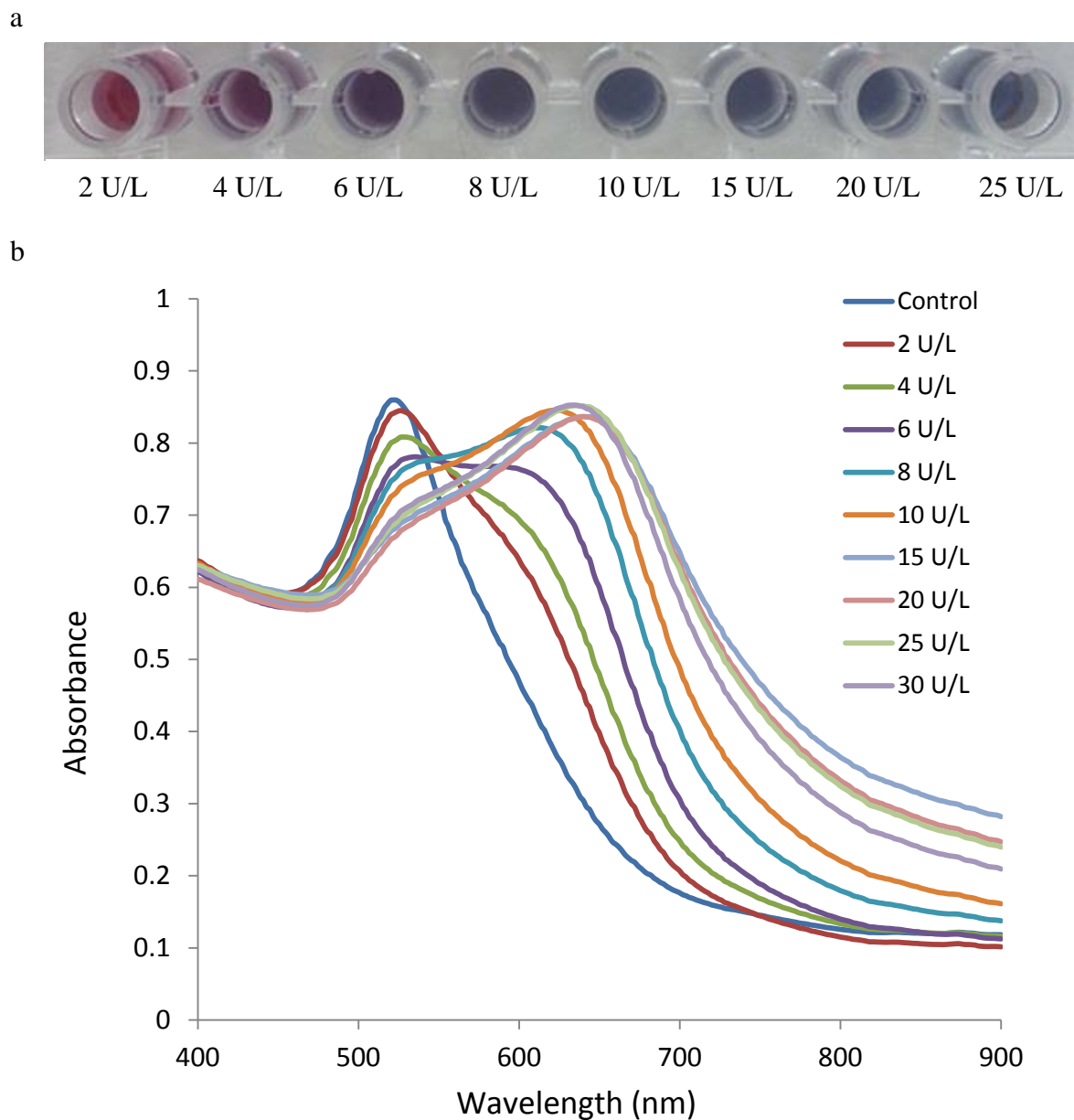


**Figure 3-10** Effect of DPP-IV/CD26 activity on colour and absorption spectra of GPDC capped Au NPs.

a) Solution colour changes after the addition of DPP-IV/CD26 (left to right) 0, 2, 4, 6, 8, 10, 15, 20, 25 and 30 U/L (b) Absorption spectra of GPDC capped-Au NPs after incubation with different activities of DPP-IV/CD26.

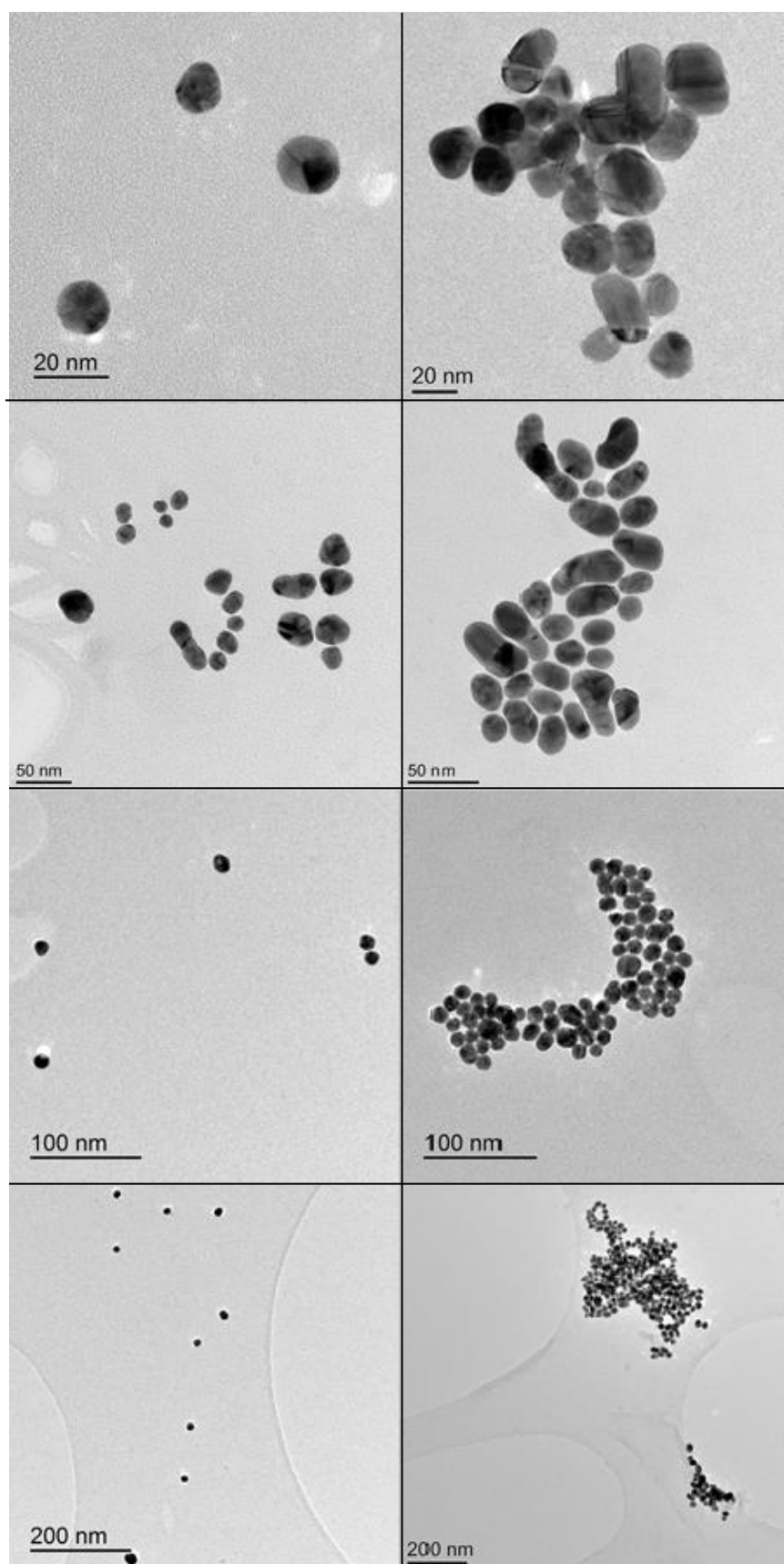


**Figure 3-11** TEM photo micrograph of GPDC functionalized gold nanoparticles before (left) and after (right) interaction with DPP-IV/CD26 enzyme. Various magnifications have been used to show the nature of aggregate formed after treating the modified Au NPs with DPP-IV/CD26 enzyme.

### 3.3.6 Investigation of the Assay Dynamic Range

The linearity of the calibration graph for the assay was investigated for DPP-IV/CD26 activity ranging from 0–30 U/L. As the activity of DPP-IV/CD26 increases, the Au NP biosensor system displayed gradual colour change from red to pale blue, while the absorption peak at 522 nm decreased and the absorption peak at 642 nm increased. These two wavelengths were selected to represent the relative extent of aggregation and dispersion of the GPDC capped Au NPs, respectively (Zhu *et al.* 2012; Nossier *et al.* 2016; Wu *et al.* 2017). A linear relationship between enzyme activity and absorbance ratio ( $Abs_{642}/Abs_{522}$ ),  $R^2 = 0.9924$  was observed in the range 2–12 U/L, with the signal levelling out at higher activities (Fig. 3-12). The DPP-IV/CD26 activity in serum of healthy humans range between 17.0 - 52.6 U/L, with lower levels in hypertensive and immunocompromised patients (Bella *et al.* 1982; Lambeir *et al.* 2003). The limit of detection (based on  $3\sigma_b/slope$ , where  $\sigma_b$  was the standard deviation of blank samples) was determined to be 1 U/L for the developed assay.

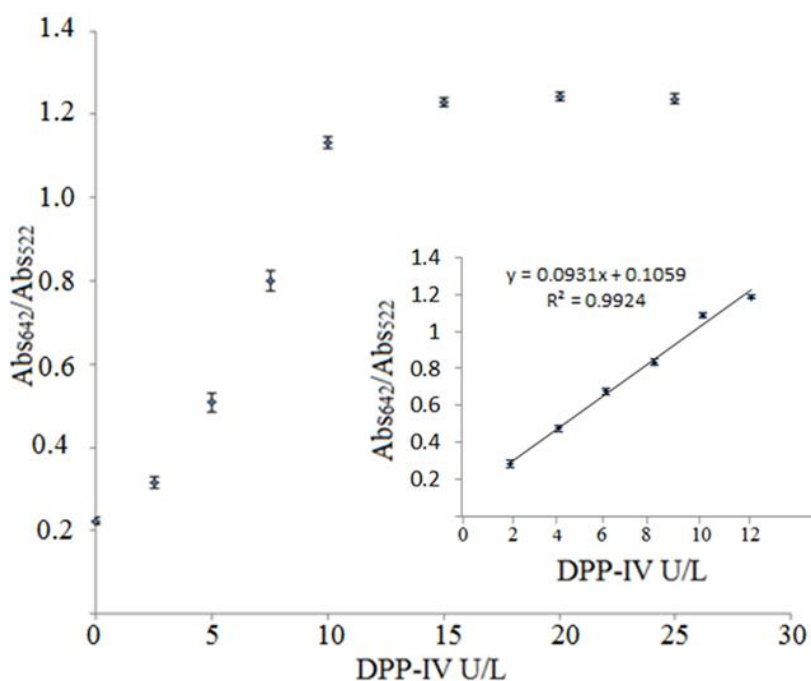


**Figure 3-12** Calibration curve of  $Abs_{642}/Abs_{522}$  versus the activity of DPP-IV/CD26. (Inset): Expanded linear region (2- 12 U/L). Error bar represents the standard deviation ( $n = 3$ ). DPP-IV/CD26 assay was performed under the optimal conditions (room temperature, incubation for 15 minutes).

### 3.3.7 DPP-IV/CD26 Selectivity Study

In order to confirm that Au NP aggregation and interaction of the GPDC functionalized Au NPs is selective to DPP-IV/CD26 activity; experiments were performed with potential interfering proteins and enzymes including trypsin, thrombin, albumin and lysozyme. As shown in Figure 3-13, the signal intensities from the peptide modified Au NP solutions incubated with thrombin, trypsin, albumin or lysozyme were negligible, demonstrating the selectivity of the assay. The GPDC modified Au NPs particles did not produce a noticeable colour change when incubated with the denatured DPP-IV/CD26 (heating at 80 °C for 15 minutes) demonstrating the specificity of the enzyme activity.

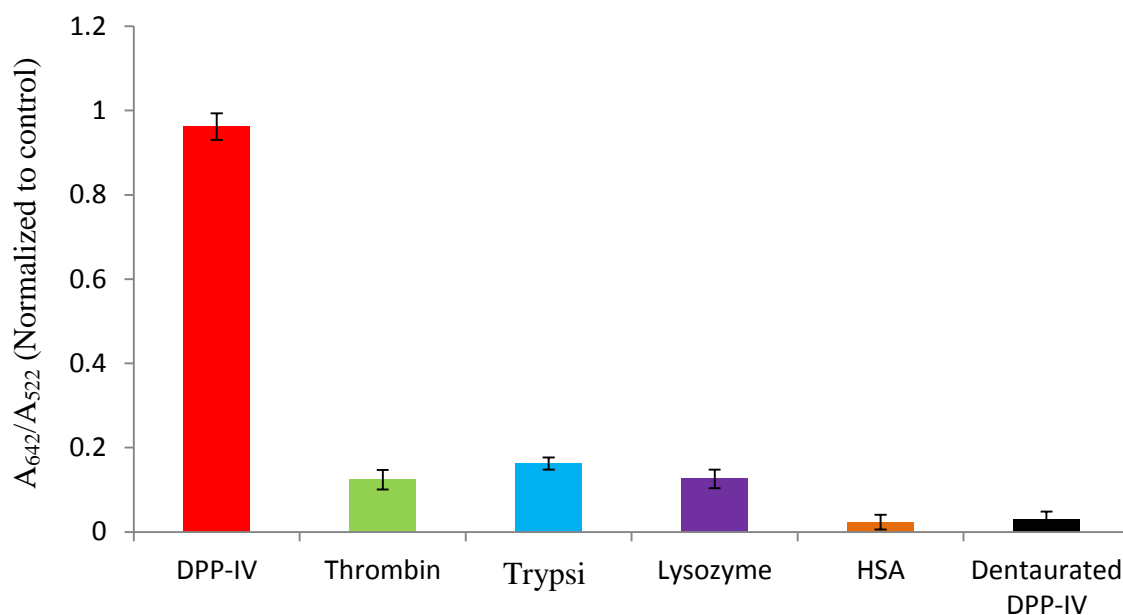


**Figure 3-13** Response of the functionalized Au NP incubated to the addition of 20 U/L of DPP-IV/CD26 compared to effect produced by other enzymes and proteins such as lysozyme (1  $\mu\text{g}/\text{mL}$ ), thrombin (20 U/mL), trypsin (20  $\mu\text{g}/\text{L}$ ), human serum albumin (HSA) (2 mg/mL) and denatured DPP-IV (heating at 80 °C 15 minutes) under the same conditions. Error bars represent the standard deviation ( $n = 3$ ).

### 3.3.8 Control Studies

Control experiments were conducted to ensure that the colour change after DPP-IV enzyme addition was due to enzymatic hydrolysis of the GPDC capped Au NPs rather than any nonspecific effect. Different sample mixtures were tested as shown in (Figure 3-14).

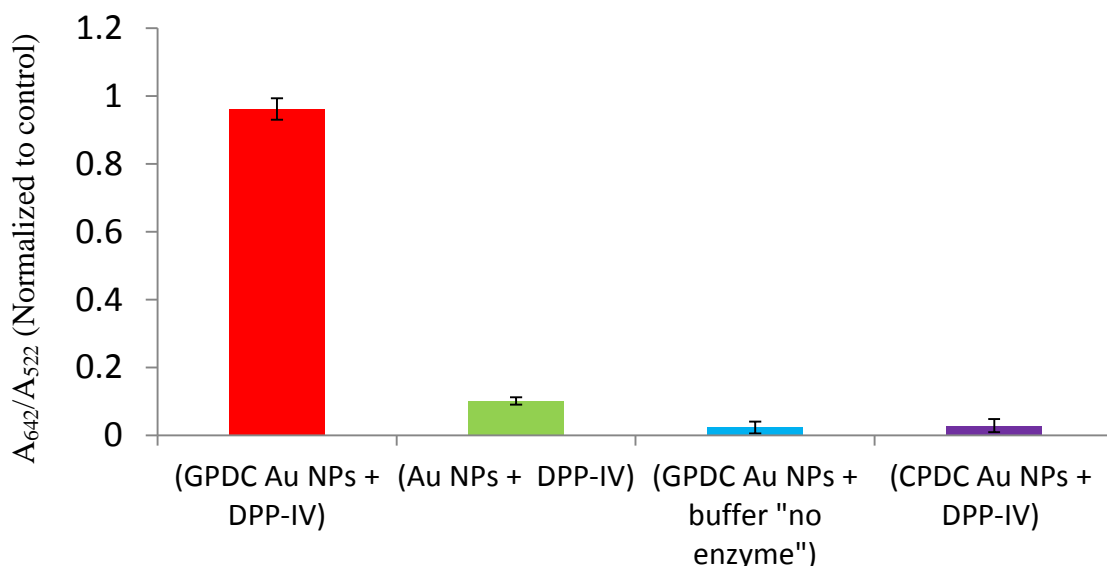


**Figure 3-14** Response of the GPDC functionalized Au NP solution to the addition of 20 U/L in control experiment.

Response to the addition of DPP-IV enzyme to a GPDC functionalized Au NP (red), non-functionalized Au NP (green), Au NP mixture with a peptide substrate not cleavable by DPP-IV/CD26 enzyme (purple) and response to the addition of Tris buffer (pH 8.3) to a GPDC functionalized Au NP (blue). Error bars represent standard deviation (n=3).

In all of the control experiments none resulted in a shift in  $\lambda$  max that was comparable to that caused by the addition of DPP-IV/CD26 enzyme. The first control experiment carried out by adding Tris buffer to GPDC-Au NPs without the enzyme (negative control) to ensure that the addition of the buffer did not cause spectral change. This observation indicates that the NPs aggregate as a result of the activity of DPP-IV/CD26 and not due to other components in the solution. The second control experiment was the addition of 20 U/L of DPP-IV/CD26 to unmodified citrate Au NP suspensions, to test whether a similar response is obtained in the absence of modification of the Au NPs

(positive control). The final control used Au NP labelled peptide substrate that did not meet the requirement for proper hydrolysis by the DPP-IV/CD26. For this purpose, a CPDC peptide was used which bridges the ligand from both sides which make the substrate not amenable to hydrolysis by DPP-IV/CD26, due to loss of free amine end. Again, no aggregation was seen demonstrating that the colour change after DPP-IV/CD26 addition was due to hydrolysis of the peptide and not due to dissociation of the peptide from the NP surface.

The stability of the colloidal system is governed by steric hindrance and electrostatic repulsion forces between the charged peptide capping ligands. The DPP-IV/CD26 induced cleavage of GPDC reduces the length of the peptide arm and thus the distance between particles decreases, which in turn affects the plasmon resonance of the functionalized NPs due to the removal of steric barriers between the particles resulting in irreversible aggregation.

### **3.3.9 Study of the Reaction Time Course**

The reaction dynamics of peptide functionalized Au NP aggregation was studied to establish the optimum time for enzymatic hydrolysis of the modified Au NPs. The aggregation of the peptide functionalized Au NPs led to a reduction in absorption at 522 nm (SPR band), and an increase in absorption at longer wavelengths in the UV-vis absorption spectrum, the ratio between 642 nm and the 522 band ( $A_{642}/A_{522}$ ) were plotted at different time points to monitor the aggregation of peptide functionalized Au NPs as shown in Fig.3-15. As can be seen by incubating the peptide functionalized Au NPs with DPP-IV/CD26 at different enzyme activities, the  $A_{642}/A_{522}$  increases gradually and then reaches a limit. The higher the DPP-IV/CD26 activity, the faster the  $A_{642}/A_{522}$  ratio reaches a plateau. Indeed, the  $A_{642}/A_{522}$  with the least DPP-IV/CD26 activity reaches a plateau within 10 min, an indication that this method is rapid and stable

signals can be obtained after 10 min incubation. High DPP-IV/CD26 activity was associated with increased rate of substrate hydrolysis.

DLS measurements were used to follow the changes in the size of Au NPs over time, following enzyme addition. The DLS data clearly shows that the hydrodynamic size of the Au NPs gradually increased after the addition of the enzyme and plateaued after about 10 minutes (Fig.3-16). The  $K_M$  value for DPP-IV/CD26 of the GPDC substrate coupled to Au NPs was determined using the same purified DPP-IV/CD26 dilution by plotting end point versus enzyme activity yielding a sigmoidal curve and the  $K_M$  value was determined to be  $83.4 \pm 2.2 \mu\text{M}$ .

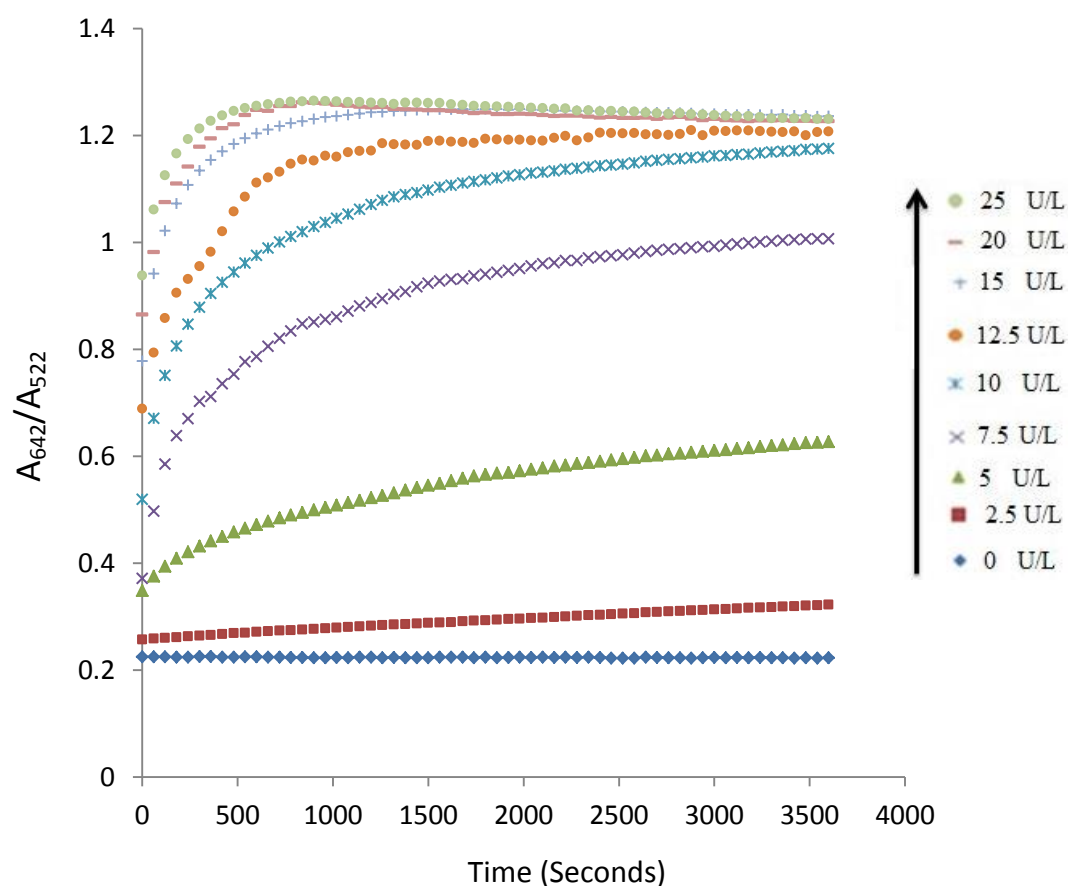


**Figure 3-15** Effect of incubation time and DPP-IV/CD26 activity on absorbance change in GPDC capped Au NPs.

Plot of ratio of absorbance of GPDC-Au NPs at 642/522 nm versus reaction time at various enzymatic activities of DPP-IV/CD26 (0, 2.5, 5, 7.5, 10, 12.5, 15, 20 and 25 U/L) for 60 minutes.

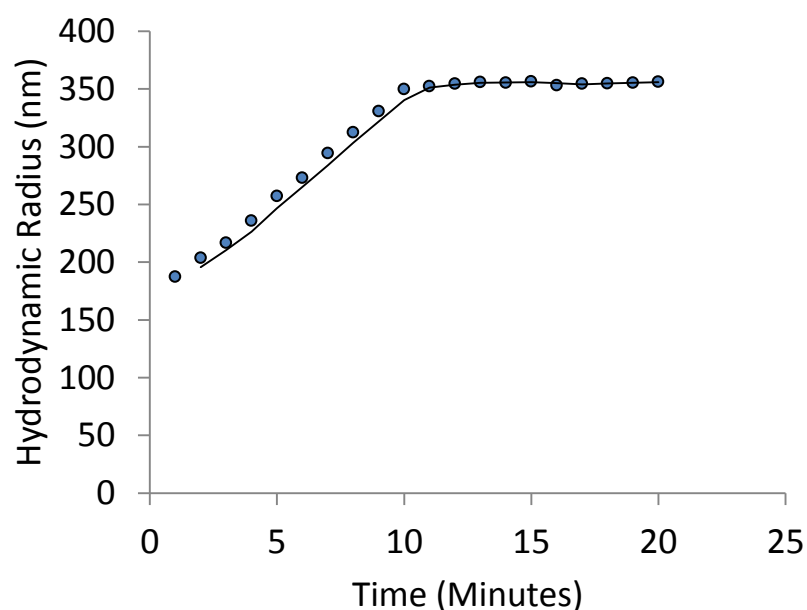


**Figure 3-16** Changes in the hydrodynamic size measured by DLS with time in the presence of 20 U/L of DPP-IV/CD26 measured by DLS.

### 3.3.10 Quantifying Thiol Ligand Density

The average number of gold atoms per NP ( $N_{\text{Au/Au NP}}$ ) can be calculated theoretically. Assuming a spherical shape and a uniform structure, the average number of gold atoms (N) can be calculated using Equation 9, where  $\rho$  is the density for gold ( $19.3 \text{ g/cm}^3$ ) (Lu *et al.* 2012) and M stands for atomic mass of gold (197 atomic mass unit). With an increase in diameter, the average number of gold atoms per gold nanoparticle ( $N_{\text{Au/Au NP}}$ ) will increase with cube (Liu *et al.*, 2007).

$$N_{\text{Au/Au NP}} = \frac{\pi \rho D^3}{6M} = 30.896 D^3 \dots\dots\dots (9)$$

Based on the TEM results reported previously in chapter 3.2.2 and substituting in Equation 9, the average number of gold atoms per NP is calculated to be 94,190.

The ligand coverage via the gold-to-sulphur ratio can be calculated based on the fact that the gold atoms constitute the particle core with each ligand on the NP surface carrying a single sulphur atom only, the number of sulphur atoms per Au NP ( $N_{\text{S/Au NP}}$ )

will increase to the square of the Au NP diameter and is proportional to the maximal coverage factor  $\kappa_{\max}$  and can be calculated using Equation 10.

$$N_{s/GNP} = \kappa \pi D^2. \dots\dots\dots (10)$$

Combining the two equations (Equation 11), it assumes that spherical NPs monodispersed with complete saturation with a monolayer of thiol ligands on the particle surface (Hinterwirth *et al.* 2013).

$$= \frac{\pi \rho D^3}{\kappa_{\max} \pi D^2} = \kappa_{\max}^{-1} \times 9.83 \times D. \dots\dots\dots (11)$$

Using equation 3, the calculated theoretical maximum number of GPDC ligands on the surface of Au NPs is  $5.39 \times 10^6$ .

### 3.3.11 DPP-IV/CD26 Directed Cleavage of Peptide Substrate

Supernatant from the DPP-IV treated Au NP suspension were examined by mass spectrometry to detect the expected peptide cleavage products (Figure 3-17). A peak at  $m/z$  of 173 was seen that corresponds to the  $[M+H]^+$  cleavage product, Gly-Pro, which indicates the cleavage of the GPDC capped Au NPs by DPP-IV/CD26 activity.

Solution state  $^1H$  NMR spectroscopy was used to study the changes to the structure of peptide substrate after incubation with DPP-IV. The study focused on analysis of the induced alterations of a number of NMR parameters, such as chemical shifts and whether new signals appear as a result of peptide substrate hydrolysis.

The NMR study was first carried out on GPDC capped Au NP samples to fully characterize the structure and thereafter on GPDC Au NPs + DPP-IV, allowing the analysis of changes induced by the enzyme addition to GPDC Au NPs, on characteristic NMR parameters of the species present in the sample. Representative  $^1H$  NMR spectra of GPDC Au NPs and GPDC Au NPs + DPP-IV in water with 50%  $D_2O$  with the assignment of the characteristic proton resonances in the molecules presented in Fig.3-

18. Although clear changes can be noticed after incubating the peptide substrate with DPP-IV/CD26 such as (peak signal at 4.4 ppm) position but obtained results were not conclusive.

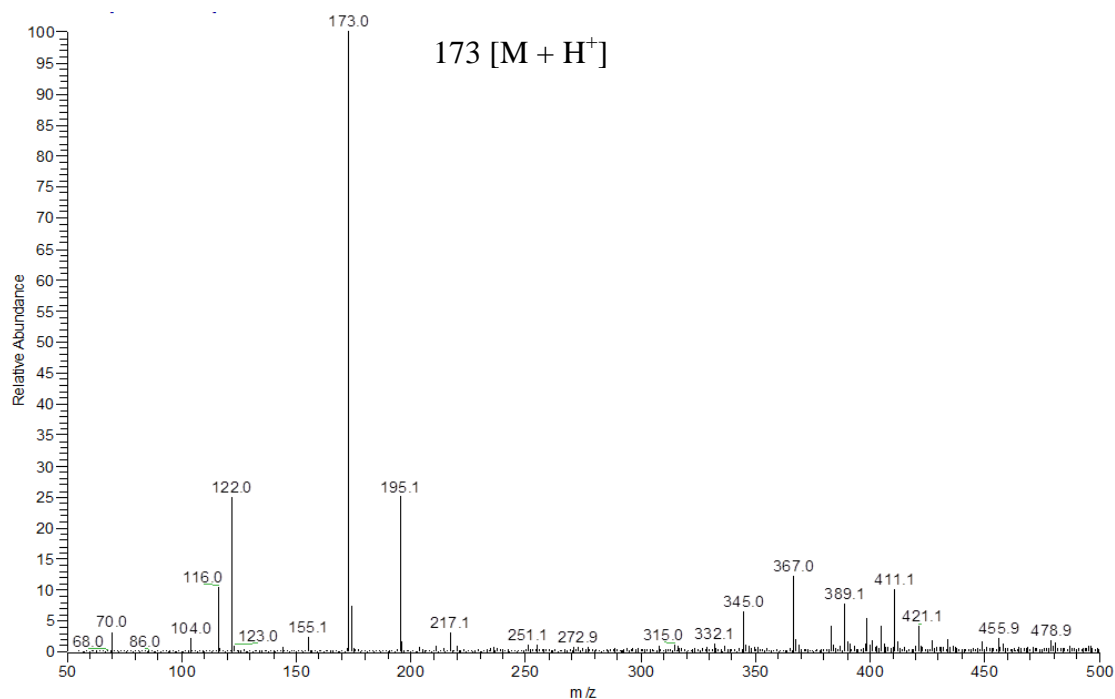


**Figure 3-17** MS spectrum of GPDC capped Au NPs after hydrolysis with DPP-IV/CD26.

The peak appeared at the m/z value 173 corresponding to the desired peptide sequence, Gly-Pro. Gly-Pro standard was used as a reference peak, which produced a signal at 173 m/z.

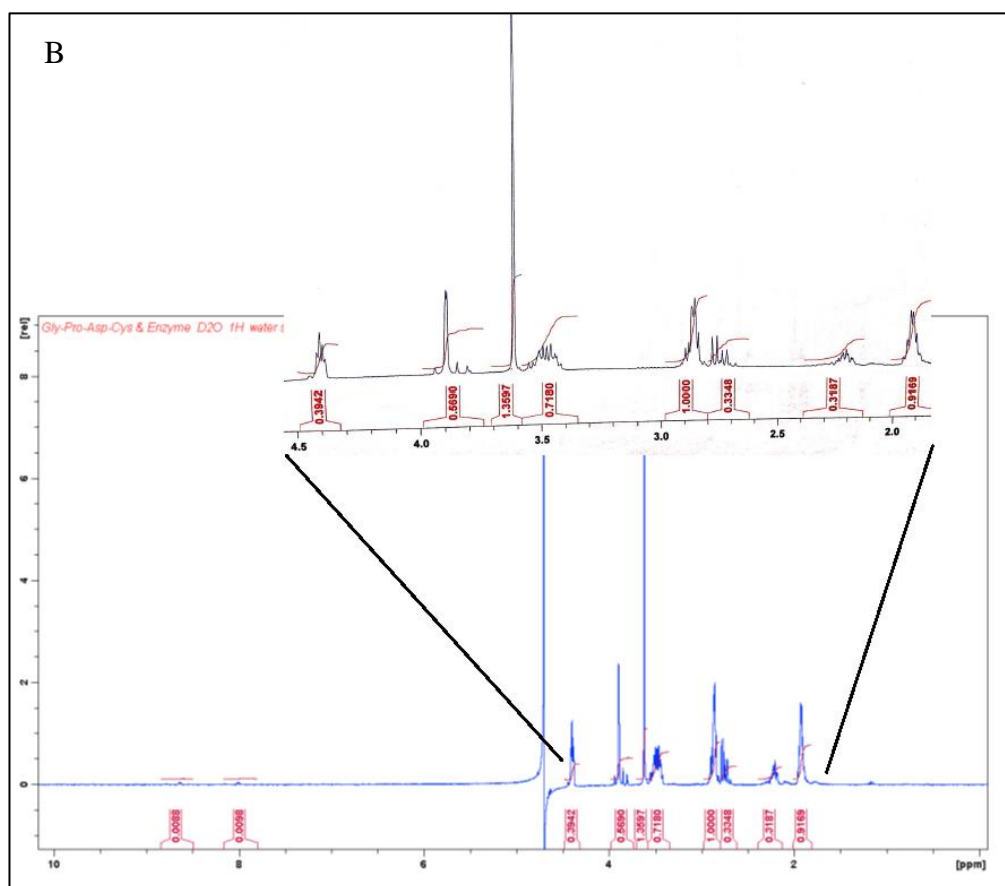
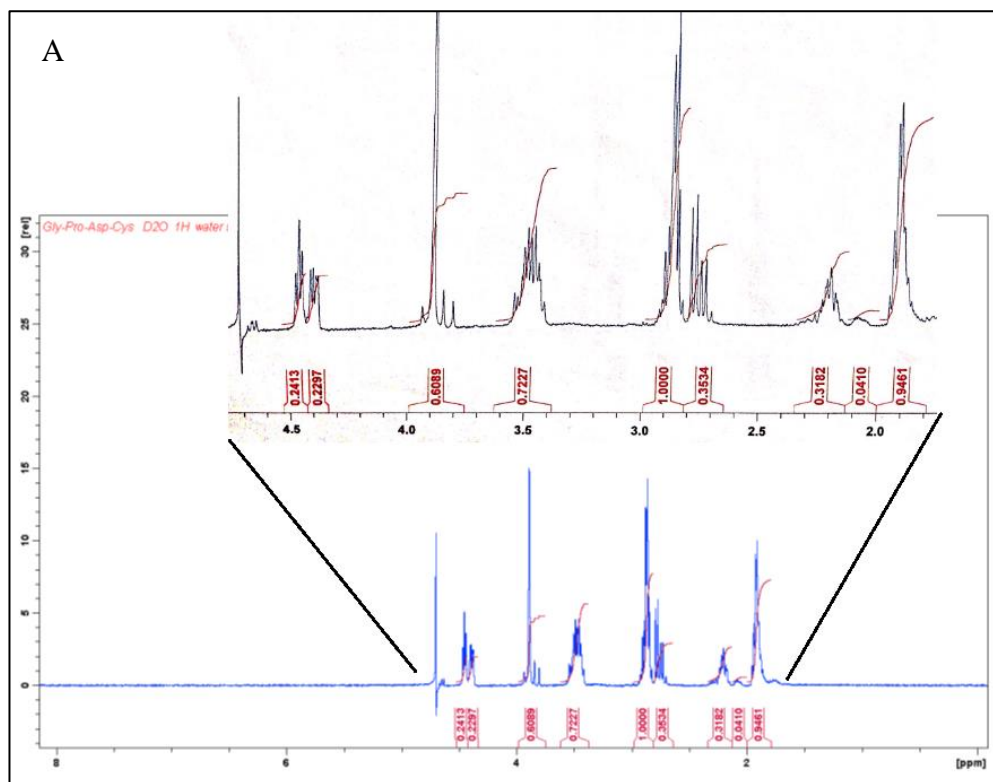


**Figure 3-18** 400 MHz  $^1\text{H}$  NMR spectra of: (A) GPDC and (B) GPDC + DPP-IV.

### 3.4 Conclusion

A solution-based DPP-IV/CD26 detection assay, utilising peptide substrate conjugated to Au NPs, was developed and its usefulness demonstrated. The peptide substrate was designed to mimic the natural enzyme substrates. Several techniques have been used to investigate and study the coupling of the peptide to the Au NP surface including XPS, UV-Visible spectroscopy, zeta potential and hydrodynamic radius measurements.

The first indication for the successful synthesis of P-Au NPs was obtained from UV-visible spectroscopy. A slight shift in the SPR band from ~520 nm to 522 indicated a change in the surrounding environment of the Au NP surface. Zeta potential and hydrodynamic size changes further confirmed successful attachment of peptide to Au NP, was evidenced noticed by an increase in Au NP formulation stability and the radius of the modified NPs.

XPS data provided valuable information about the ligands coupling to the surface of Au NPs; wide scan spectrum confirmed the presence of sulphur and gold in the sample, which agreed with the chemical structure. High resolution of Au (4f) spectrum showed a double for Au at Au (4f<sub>7/2</sub>) and Au (4f<sub>5/2</sub>) for all samples analysed in the region of 84 and 88 eV respectively, which are similar to the values of gold thiolates reported in the literature (Brust *et al.*, 1994, Yee *et al.*, 2003). The presence of the peak for Au (4f<sub>7/2</sub>) shows that the bulk of the gold atoms are in the Au (0) oxidation state.

The cleavage of the peptide substrate was demonstrated by mass spectrometry by comparing the m/z of the hydrolysis product Gly-Pro with a mass spectrum for a standard Gly-Pro dipeptide. These data verify that DPP-IV can hydrolyse GPDC when immobilized on Au NPs surface. This method displayed selectivity for DPP-IV over other serum enzymes. In the absence of DPP-IV/CD26 activity (negative control), GPDC- modified AuNPs are stably suspended in solution (red colour). Peptide capping hinders attraction of the Au NPs. While in the presence of DPP-IV/CD26 activity

(positive sample), after enzymatic digestion, the peptide capping is reduced, this allows the attraction force among Au NPs leading to aggregation (blue colour). Data obtained from TEM photo micrographs and DLS calculations confirmed this proposal.

The developed assay allowed quantitative estimation of DPP-IV/CD26 activity, with a linear response range from 2 U/L to 12 U/L for DPP-IV/CD26 determination was obtained. Mass spectrometry was utilized to confirm that the cleavage site of the immobilized peptide could be recognized by DPP-IV.

The relevance of this NP-based assay resides in the fact that visual detection or simple instrumentation can be used for the detection and determination of the enzyme activity. Accordingly, it could be used for the preliminary analysis of DPP-IV containing samples without the need for specialized instruments. Nevertheless, it provides sensitivity comparable or even better than that provided by the current chromogenic Gly-Pro-pNA method. However, it is less sensitive than luminescent Promega<sup>®</sup> assay and much less than those based on the fluorescent or the NP-based recently reported by Xia and co-workers (Xia *et al.* 2016) or that based on electrochemical sensing which depend on immobilizing ferrocene peptide to the surface of a gold electrode reported by Zhang (Zhang *et al.* 2015). Also, none of the above mentioned techniques can be used by untrained personnel.

There are a few areas where this work could be improved upon; such as enhancing the stability of peptide functionalized Au NP especially for use in high ionic strength solutions. A possible solution would be the incorporation of a short stabilizer ligand to enhance colloidal stability. In spite of these limitations, the development of an Au NP based colorimetric assay for DPP-IV/CD26 detection was successfully used in the studies conducted later in this thesis. This work led to the development of an assay with improved parameters in terms of practicality, range of enzyme activity detection and linearity as described in Chapters 4 and 5.

## Chapter 4

---

### **Assay Development: Incorporation of Spacer for generation of Peptide Functionalized Gold Nanoparticle for use in Colorimetric Measurement of Dipeptidyl Peptidase IV Activity**

---

## 4.1 Introduction

DPP-IV inhibitors (DPP-IVi) as therapeutic agents appear to have a potential in the management of type 2 diabetes, either singly or in combination with existing medication, such as metformin. DPP-IVi have their hypoglycaemic effect by blocking the action of DPP-IV, which is responsible for the inactivation of incretin hormones, thereby prolonging the half-life of glucagon-like peptide-1 and glucose-dependent insulinotropic polypeptide leading to increases in insulin and C-peptide, with subsequent decrease in glucagon and improvements in oral glucose tolerance.

Research efforts have been directed toward further potential pharmacological applications of DPP-IV/CD26 inhibitors in the management of ischaemic heart injury, atherosclerosis and osteoporosis (Jungraithmayr *et al.* 2012). Therefore, there is the need to develop a simple quantitative and sensitive HTS method for the potential DPP-IVi candidates.

Currently, Au NP-based colorimetric enzyme assays rely on the design of short peptide substrates to discriminate between different proteases, depending on the reactivity of the enzyme (Sato *et al.* 2003). Colour changes resulting from the aggregation or dispersion of the Au NPs, induced by the presence of the enzyme, can be used to measure enzyme activity. Stevens and colleagues, for example, reported a protease detection method based on the re-dispersion of Au NP assemblies induced by the enzymes (Laromaine *et al.* 2007). However, the use of Au NP aggregates as probes can result in poor access of the enzyme to the peptide substrates, affecting both the detection time and assay sensitivity. Recently, Sun and co-workers have devised a new approach for protease detection based on Au NP aggregation induced by enzyme-hydrolyzed peptides, through the introduction of multiple charged residues, in order to improve the stability of the colloidal Au NP solutions (Chen *et al.* 2014).

Kim and colleagues (2017) have recently introduced a new approach to enhance Au NP platform sensitivity based on centrifugation and silver enhancement. These modifications have resulted in a threefold improvement in detection limit, but the additional steps are time consuming and add to cost (Kim *et al.* 2017b). Their strategy for improving enzyme activity assays relied on a method that combines centrifugation and silver staining for the self-assembly of Au NPs. The idea is based on the principle that self-assembled aggregated Au NPs settle quickly after centrifugation, resulting in weak silver staining of the supernatant. Alternatively, dispersed Au NPs are strongly stained with silver enhancement in the supernatant after centrifugation.

The stability of Au NP solutions can be controlled by functionalizing the NP surface with diverse thiol-containing peptides. Most of the Au NP-based assays for the measurement of enzyme activity are largely dependent on enzyme reactions to initiate Au NP aggregation (Wang *et al.* 2006; Zhang *et al.* 2014). There are a number of considerations in the design of the enzyme activity measurement platforms. The length of the peptide substrate is one of the essential parameters in the design of enzyme activity measurements using Au NP platforms. Besides conferring steric stabilization on the Au NP colloidal solutions, it is essential to maintain optimum distances between the Au NP and the substrate to ensure effective enzyme- substrate interaction (Ramezani *et al.* 2015). NP curvature sometimes interferes with peptide cleavage or hydrolysis due to steric hindrance imposed on large enzymes. To overcome this problem, the use of spacers in order to increase the distance of the hydrolysable moiety from the NP surface is considered in order to reduce steric hindrance and thus result in improved and faster aggregation of the Au NPs. In this chapter, a highly sensitive assay for DPP-IV/CD26 using Au NPs functionalized with designed peptide probe Val-Pro-NH-(CH<sub>2</sub>)<sub>2</sub>-NH-Asp-Cys (VP-EN-DC) was developed and used for the measurement of DPP-IV/CD26 activity levels.

## **4.2 Experimental**

### **4.2.1 Reagents and Materials**

The enzyme, gold and citrate salts were all supplied and used as described in Chapter 3. The peptide (VP-EN-DC) ~ 95% pure was purchased from Cambridge Research Biochemicals (UK). The peptide was dissolved in 50 mM glycine buffer solution (pH 10.3). Vildagliptin was purchased from Cayman Chemicals (USA). DPP-IV/CD26 assay kit for biological samples was purchased from Enzo Life Sciences (USA). Normal human serum control was purchased from Thermo Scientific (UK). All solutions were prepared using deionized water with a resistivity of  $18.2 \text{ M}\Omega \text{ cm}^{-1}$  purified on Milli-Q Academic purification system (Millipore, UK).

### **4.2.2 Preparation of Citrate-Capped Gold Nanoparticle and Peptide Coupled Gold Nanoparticle Bioconjugate (P-Au NP)**

Citrate Au NPs (~15 nm) diameter was prepared as described previously in Chapter 3 (section 3.2.2). The peptide modified Au NPs (P-Au NPs) were prepared by addition of an aqueous solution of 2 mM (VP-EN-DC) peptide in 50 mM glycine buffer pH 10, to the solution of citrate Au NPs in a volume ratio of 1 to 10. After overnight reaction at room temperature, excess peptides were removed by centrifugation (14500 rpm, 20 min at  $4^{\circ}\text{C}$ ) using an Eppendorf centrifuge (Eppendorf, Germany), the pellets containing the modified Au NPs were resuspended in Tris buffer pH 8.3 and stored at  $4^{\circ}\text{C}$ .

### **4.2.3 Instrumentation for Gold Nanoparticle Characterization**

The same UV-visible spectroscopy and TEM instrumentation methods were used as described in Chapter 3 (section 3.2.3).

#### 4.2.4 Colorimetric Assay of DPP-IV/ CD26 Activity

To perform the colorimetric assays for DPP-IV/ CD26, 100  $\mu$ L aliquots of P-Au NPs were mixed with 100  $\mu$ L of the enzyme at varying activities in 50mM Tris buffer at pH 8.3 in the wells of a transparent 96-well microtiter plate. The contents were gently mixed using a plate shaker at 300-400 rpm for 60 seconds and then incubated at 37°C for 15 minutes. The UV-vis absorption spectrum of the solution was recorded using an absorbance scan from 400-900 nm. To study the reaction dynamics, P-Au NPs were exposed to a range of activities of DPP-IV/ CD26 (0, 2.5, 5, 7.5, 10, 15, 20, 25, 30, 35 and 40 U/L) and the aggregation of the P-Au NPs was monitored by UV/Vis spectrophotometry.

To evaluate the inhibition ability of the potential inhibitor, DPP-IV was first mixed with the tested inhibitor for 15 min at 37 °C. Then, VP-EN-DC capped Au NPs were added into the mixture to react for 30 minutes. The detection procedures are the same as those for DPP-IV (see section 3.2.4). The inhibitory ratio (%) of the potential inhibitors on enzymatic activity was expressed as follows: inhibitory ratio (%) =  $(R3 - R2)/(R1 - R2) \times 100\%$ , where R1 is the  $A_{700}/A_{525}$  ratio (the absorbance ratios at 700 and 525 nm) of P-Au NPs in the absence of DPP-IV, R2 is the  $A_{700}/A_{525}$  ratio of P-Au NPs in the presence of DPP-IV, R3 is the  $A_{700}/A_{525}$  ratio of P- Au NPs in the presence of DPP-IV and inhibitor.

#### 4.2.5 Monitoring of DPP-IV Activity using Gly-Pro-pNA Based Assay Protocol.

Initially, 20  $\mu$ L of DPP-IV standards with various activities in 50 mM Tris buffer (pH 8.3) or blank serum sample was added into a mixture containing 70  $\mu$ L of 50 mM Glycine buffer (pH 8.7) and 10  $\mu$ L of 100mM of Gly-Pro-pNA in DMSO as the substrate. Then, the resulting mixture was incubated 10 min at 37 °C. After that, UV-absorbance of the mixture was measured at 405 nm.

## 4.3 Results and Discussion

### 4.3.1 Design of the Peptide Substrate

The peptide substrate, [Val-Pro-NH-(CH<sub>2</sub>)<sub>2</sub>-NH -Asp-Cys] was designed with the following considerations: (i) the cysteine (C) residue is to enable the attachment via thiol-gold chemistry of the peptide substrate to the surface of the Au NPs; and (ii) the valine (Val) and proline (Pro) dipeptide residues constitute the cleavage point for DPP-IV/ CD26 and (iii) ethylene diamine was incorporated into the structure in order to act as a spacer, so that possible steric hindrance, caused by the curvature of the Au NPs is reduced. A schematic diagram of the enzyme reaction followed by Au NP aggregation is shown in Fig.4-1.

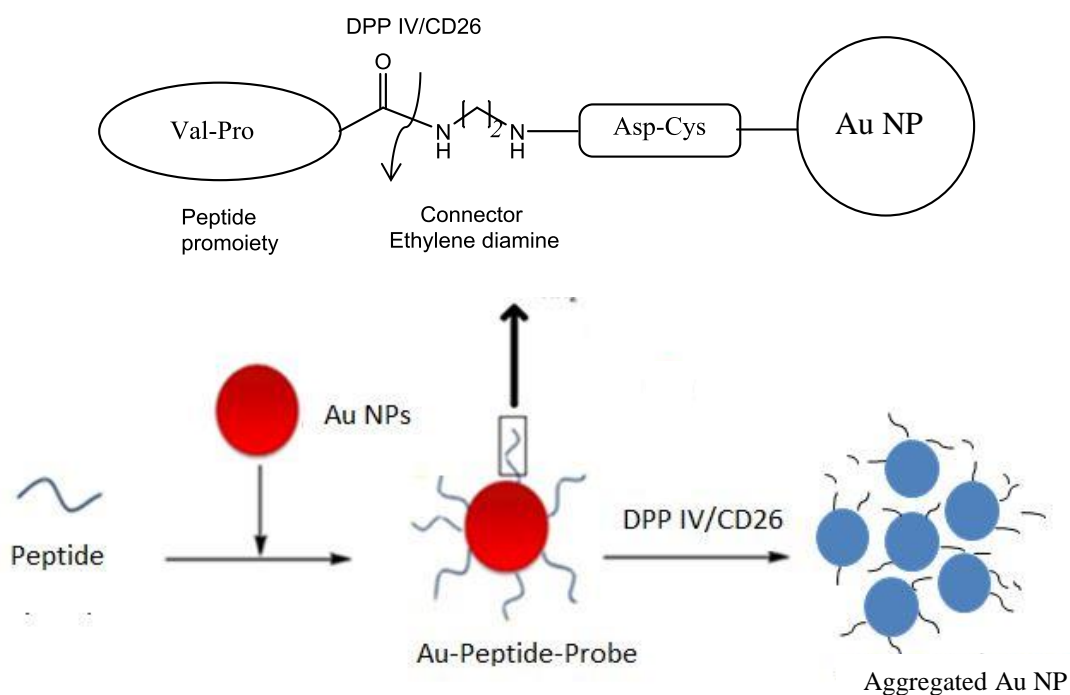


**Figure 4-1** Schematic representation of the working principle for the measurement of DPP-IV/CD26 activity with peptide-conjugated Au NPs.

DPP-IV/CD26 hydrolyses the amide bond between Val-Pro and ethylene diamine (ED) leading to a reduction in the Au NP colloid stabilization and hence resulting in their aggregation accompanied by a colour change from red to blue.

#### 4.3.2 Investigation of Peptide Coupling to Gold Nanoparticle Surface Using DLS and Zeta Potential Measurements

The absorption peak was shifted slightly from 522 nm for the unmodified Au NPs to 525 nm after Au NP modification with the VP-EN-DC peptide. DLS measurements showed that the peptide modified Au NPs have an average hydrodynamic diameter of 45.1 nm in comparison to 21.9 nm for the unmodified NPs. This difference in diameter is indicative of the surface functionalization of the Au NPs with the peptide. The extent of the Au NP surface modification was assessed by zeta potential measurements, which changed upon the addition of the substrate. The zeta potential shifted from  $-9\pm 1.5$  mV for citrate stabilized Au NPs (blue) to  $-28\pm 4$  mV for VP-EN-DC capped (red), respectively as shown in Fig. 4-2. The observed alteration in the zeta potential value indicates displacement of negatively charged citric acid by the VP-EN-DC peptide. The enhancement of negative charges is most likely due to negatively charged aspartic acid residue on the surface after ligand exchange. Another explanation of the increase in zeta potential in the presence of the modified peptide arises from the possibility of a change in the medium dielectric constant and/or viscosity, which is known to affect the zeta potential measurements (Alkilany *et al.* 2014).

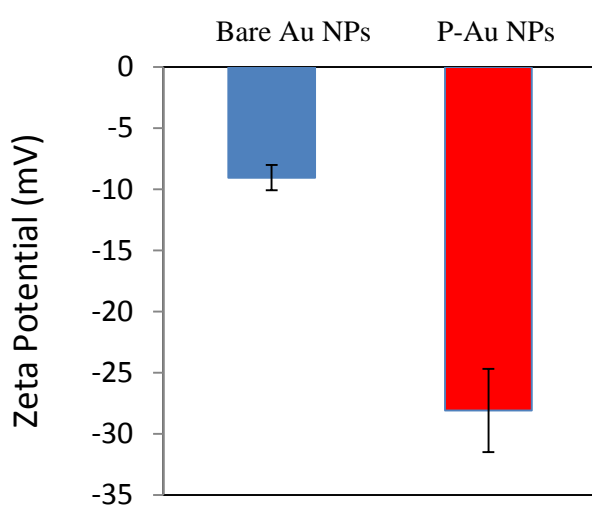


**Figure 4-2** Zeta potential measurements of citrate stabilized Au NPs (blue), VP-EN-DC modified Au NPs (red). Error bar represents the standard deviation of the measurement ( $n = 3$ )

### 4.3.3 Sensitivity of VP-EN-DC Capped Au NPs to DPP-IV activity

The addition of DPP-IV/CD 26 to the VP-EN-DC functionalized Au NPs resulted in colour change from red to pale blue. The absorbance of the surface plasmon resonance band (SPR) at 525nm decreased with accompanying band broadening beyond 650nm (Fig.4-3) indicative of the formation of aggregates. Greater band broadening was obtained in the case of VP-EN-DC Au NPs when compared with that observed with GPDC Au NPs aggregation. The reason for this can be attributed to the formation of Au NP aggregates with a higher than 400 nm size aggregates, which result in both transversal and longitudinal surface plasmon resonance effects (Suresh *et al.* 2015). Furthermore, increased DPP-IV activity was associated with the gradual increase in the absorbance at higher wavelength (700 nm) and decrease at lower absorbance wavelength (525 nm) with a resultant colour change and band broadening. Results from the DLS technique show that the dispersed VP-EN-DC functionalized Au NP aggregates in the presence of DPP-IV/CD26, have a tenfold increase in the average hydrodynamic diameter from 45.1 nm to 413 nm (Figure 4-4). DLS data were in good agreement with band broadening observed with UV-visible spectroscopy showing that the size of formed aggregates was larger than that obtained with GPDC Au NP aggregates. The possible explanation for large aggregate formation might be due to neutral charge of spacer (ethylene diamine) remaining on the surface of Au NPs. TEM results data are consistent with the DLS results, with the addition of DPP-IV; Au NPs tend to aggregate (Figure 4-5).

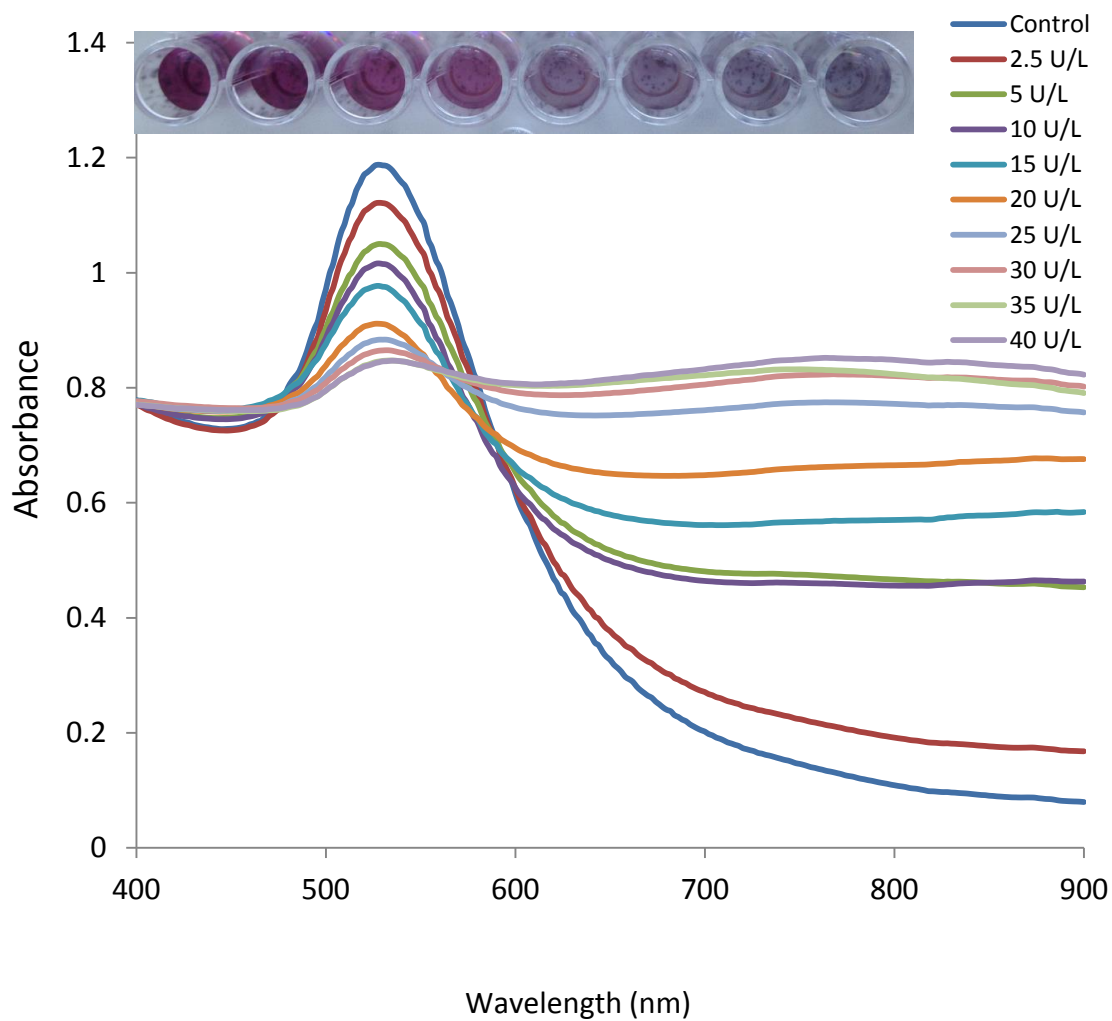


Figure 4-3 UV-vis Absorption spectra of VP-EN-DC Au NPs after incubation with different activities of DPP-IV ranged from 0 to 40 U/L. (Inset: Colour changes with increasing DPP-IV/CD26 activity (left to right) to the VP-EN-DC Au NPs assay.

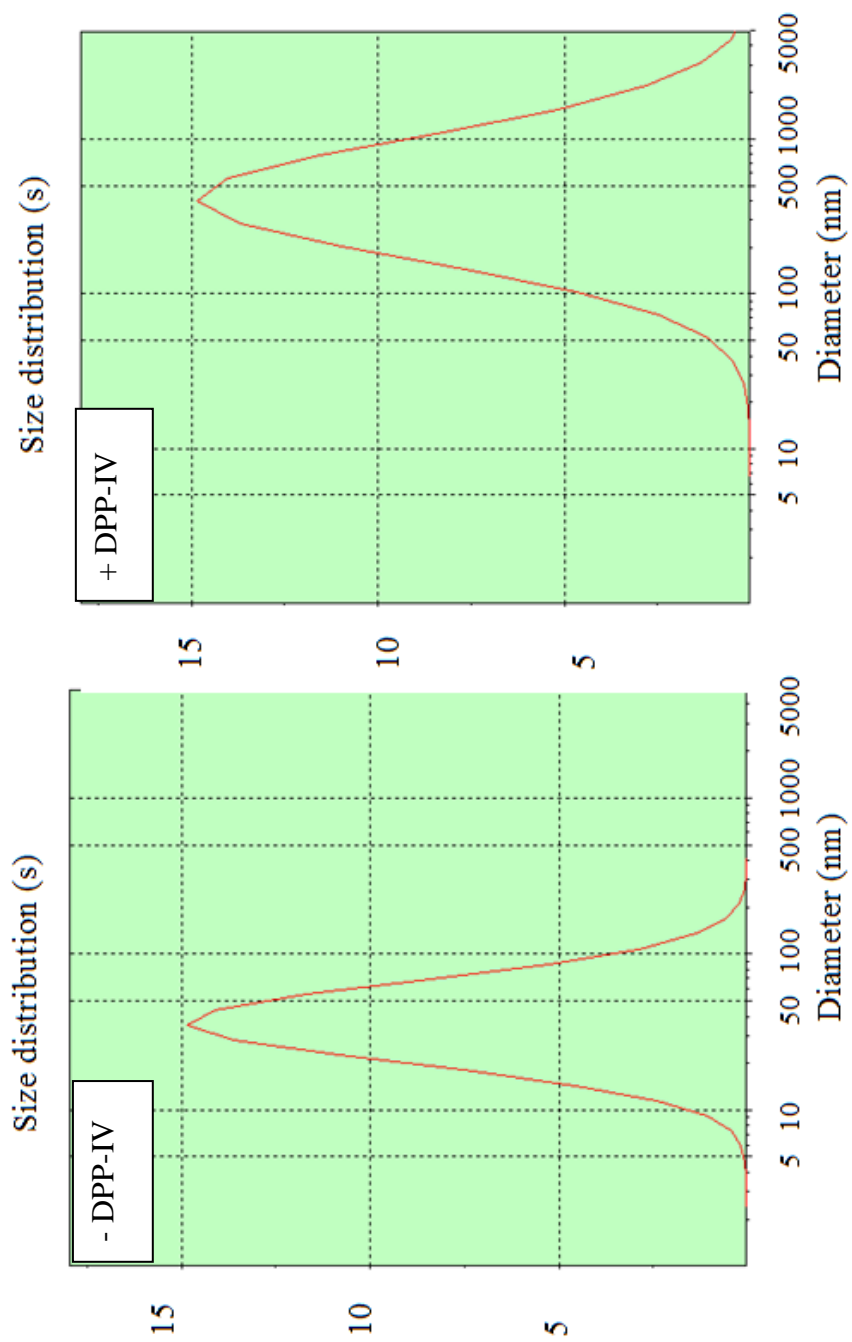
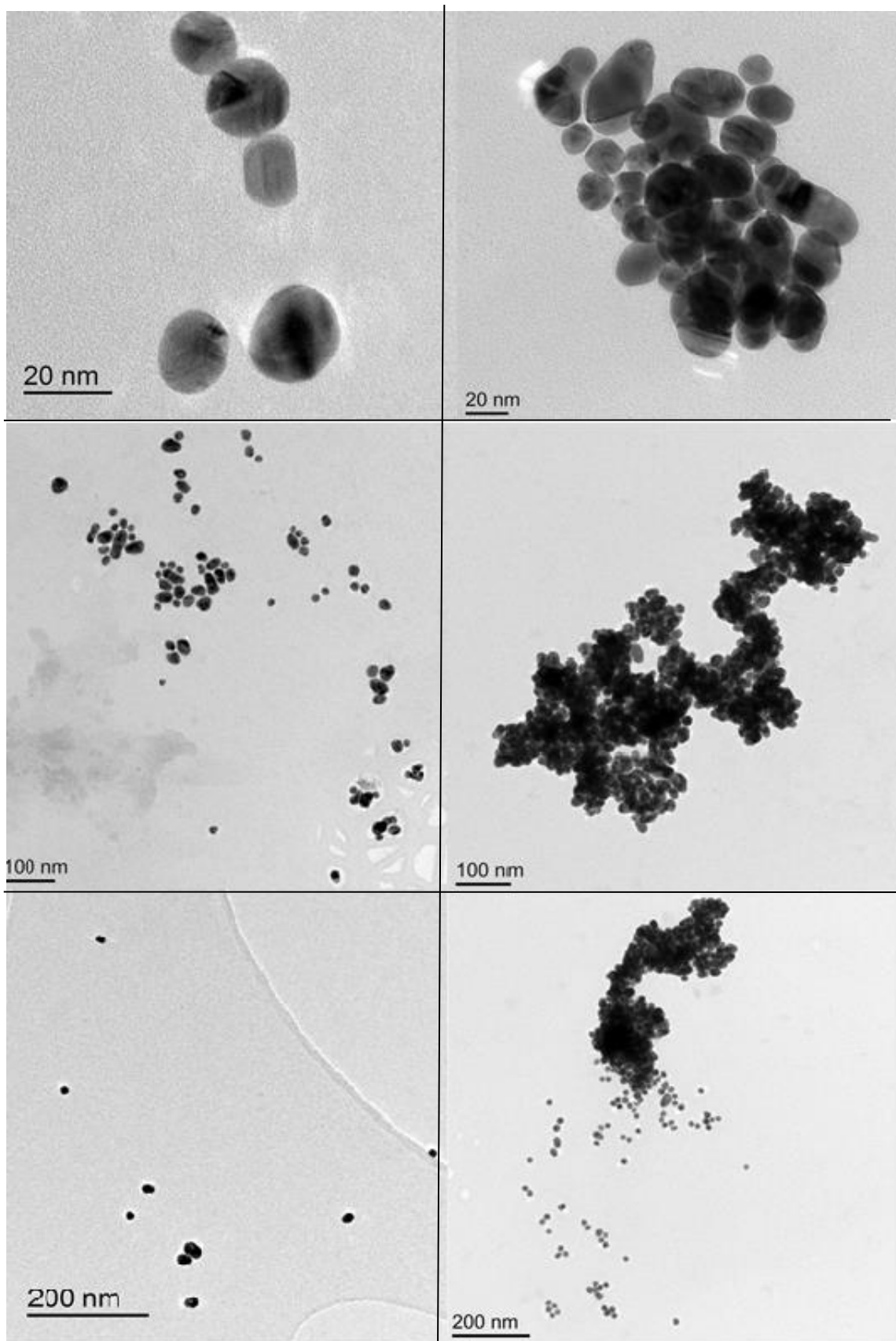


Figure 4-4 Hydrodynamic size distribution for modified Au NPs. before (left) and after (right) incubation with DPP-IV/ CD26.



**Figure 4-5** TEM photo micrograph of VP-EN-DC functionalized gold nanoparticles before (left) and after (right) interaction with DPP-IV/CD26 enzyme with various magnifications.

#### 4.3.4 Selectivity Study

To further assess the selectivity of the method, experiments were performed with potential interfering proteins and enzymes such as trypsin, thrombin, lysozyme, HSA and denatured DPP-IV/CD26, to examine whether this treatment with any of these compounds could trigger Au NP aggregation. As shown in Fig. 4-6, the proteases thrombin and trypsin and the non-protease HSA and lysozyme produced signals that were commensurate with the background, revealing that the assay is selective and DPP-IV/CD26 enzyme activity-dependent.

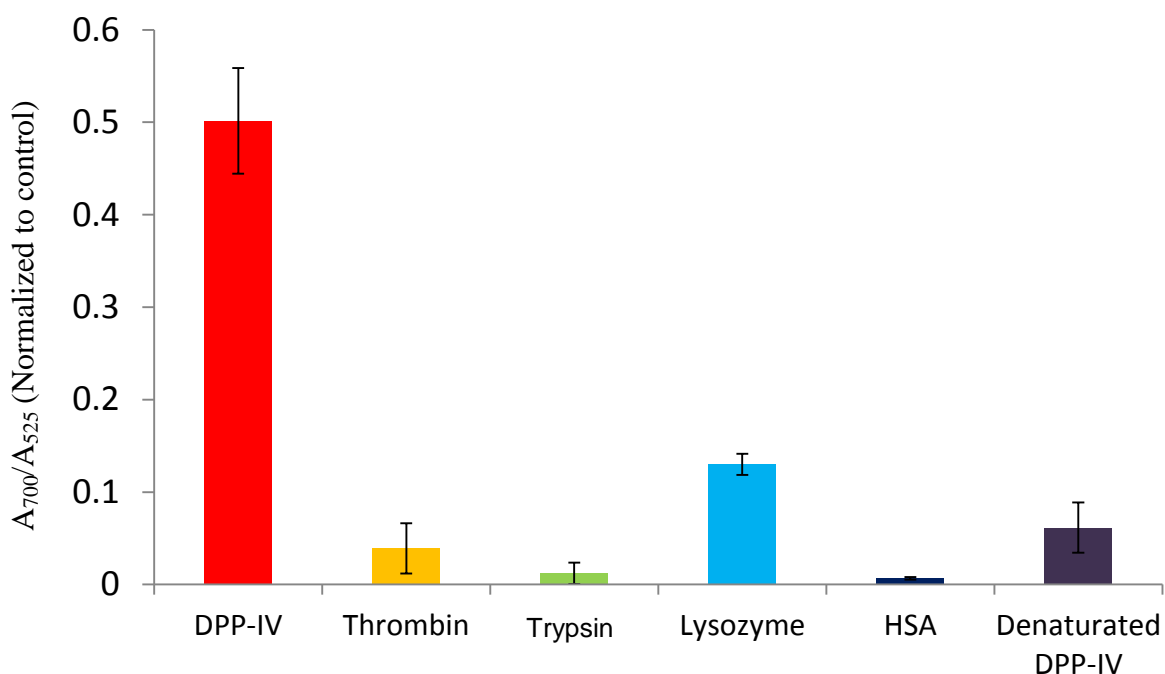


**Figure 4-6** Response of the VP-EN-DC functionalized Au NPs solution incubated with 20 U/L of DPP-IV/CD26 compared to effect produced by other enzymes, including lysozyme (1 $\mu$ g/mL), thrombin (20 U/mL), trypsin (20  $\mu$ g/mL), HSA (2mg/mL) and denatured DPP-IV/CD26 (heating at 80 $^{\circ}$ C, 15 minutes) under the same conditions, demonstrating the specificity of the Au NP-based assay solely mediated by DPP-IV/CD26 activity. Error bar represents the standard deviation (n = 3). For proteins, concentration units and for enzyme, activity units were used.

#### 4.3.5 Investigation of the DPP-IV/CD26 Assay Linear Dynamic Range

Linear regression analysis was performed by plotting a calibration graph of the ratio of the absorbance readings at 525 nm and 700 nm for each standard (were chosen to

represent both dispersed and aggregated Au NPs respectively) against DPP-IV/ CD26 activity after incubation at 37°C for 15 minutes. The calibration plots displayed a good linear relationship between the red shifts of the LSPR peak ( $\Delta\lambda$  max) and DPP-IV/ CD26 activities in the range from 0 to 40 U/L, with a detection limit (LOD) of 1.5 U/L based on  $3\sigma_b/\text{slope}$ , where  $\sigma_b$  was the standard deviation of blank samples. The straight-line equation between the points was ( $y = 0.0198x + 0.2232$ ,  $R^2 = 0.9761$ ) as shown in Fig.4-7.

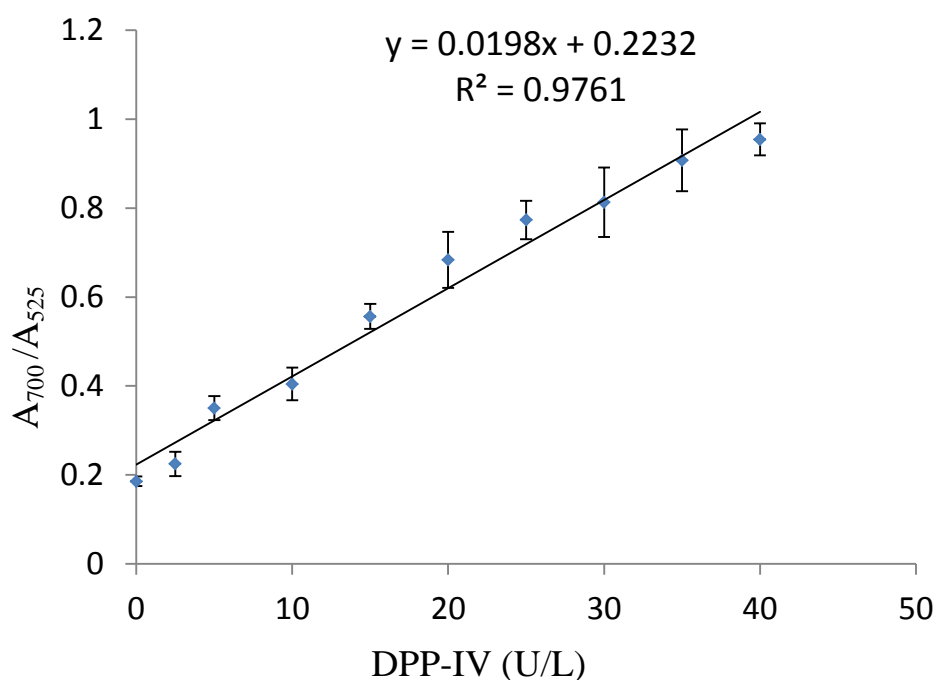


**Figure 4-7** Calibration curve of  $A_{700}/A_{525}$  versus the different activities DPP-IV incubated with VP-EN-DC functionalized Au NPs. Error bars represent the standard deviation ( $n=3$ ).

#### 4.3.6 Stability of the Modified Au NP Formulation

The stability of the peptide modified Au NP platform after prolonged storage is another important concern to provide an acceptable shelf life for a diagnostic assay. The stability of the peptide modified Au NPs over time was investigated. When not in use, the modified Au NP was stored at (4°C) and tested monthly with a 20 U/L DPP-IV/CD26. No significant change in UV-visible absorption spectra were observed after storage for 3 months (Fig.4-8), demonstrating the modified Au NP long-term stability.

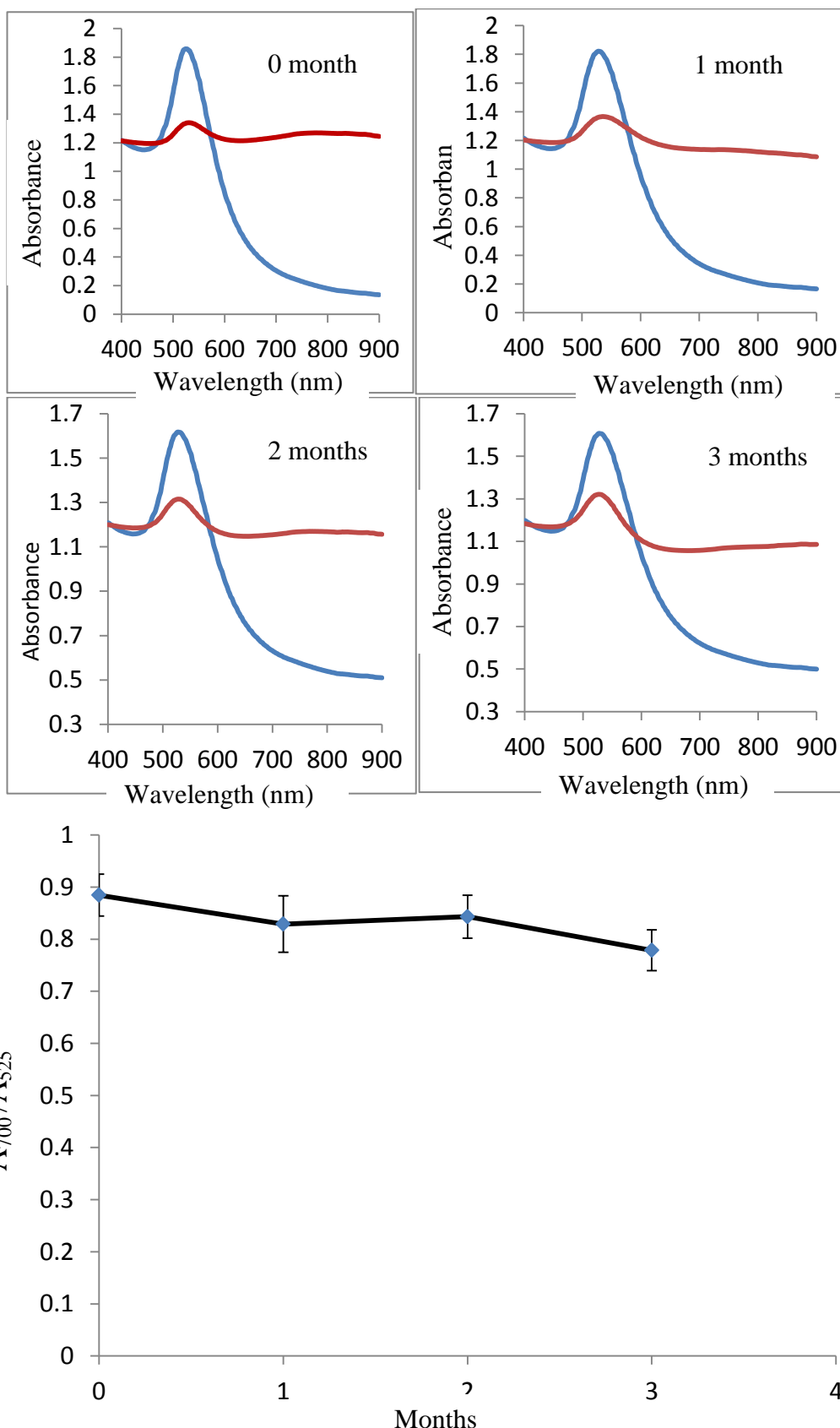


**Figure 4-8** The stability of the functionalized Au NP during storage for 3 months. UV-vis absorption spectra of the colorimetric assay toward 0 U/L DPP-IV/CD 26 (blue curve) and 20 U/L DPP-IV/CD 26 (red curve) after the Au NP was stored for 0, 1, 2, 3 months, respectively). Error bars represent the standard deviation of the measurement ( $n = 3$ ).

#### 4.3.7 Determination of the Optimum pH of the Assay

pH is an important factor that has to be considered in the evaluation of enzyme activity and Au NP stability. Numerous studies have been conducted to evaluate the effect of pH modification on altering the aggregation state of Au NP formulations (Li *et al.* 2003; Shim & Gupta 2007). A standard DPP-IV/CD26 enzyme activity (25 U/L) was used in a series of 50 mM Tris buffer solution with pH values ranging from 6.7 to 10.3, which were added to VP-EN-DC capped Au NP solution to study the optimal environment for the colorimetric assay (Fig 4-9). The underlying goal of these studies was to evaluate the effect of pH alteration on the formation or disruption of stabilizing forces such as hydrogen bonds and electrostatic interactions between modified Au NPs.

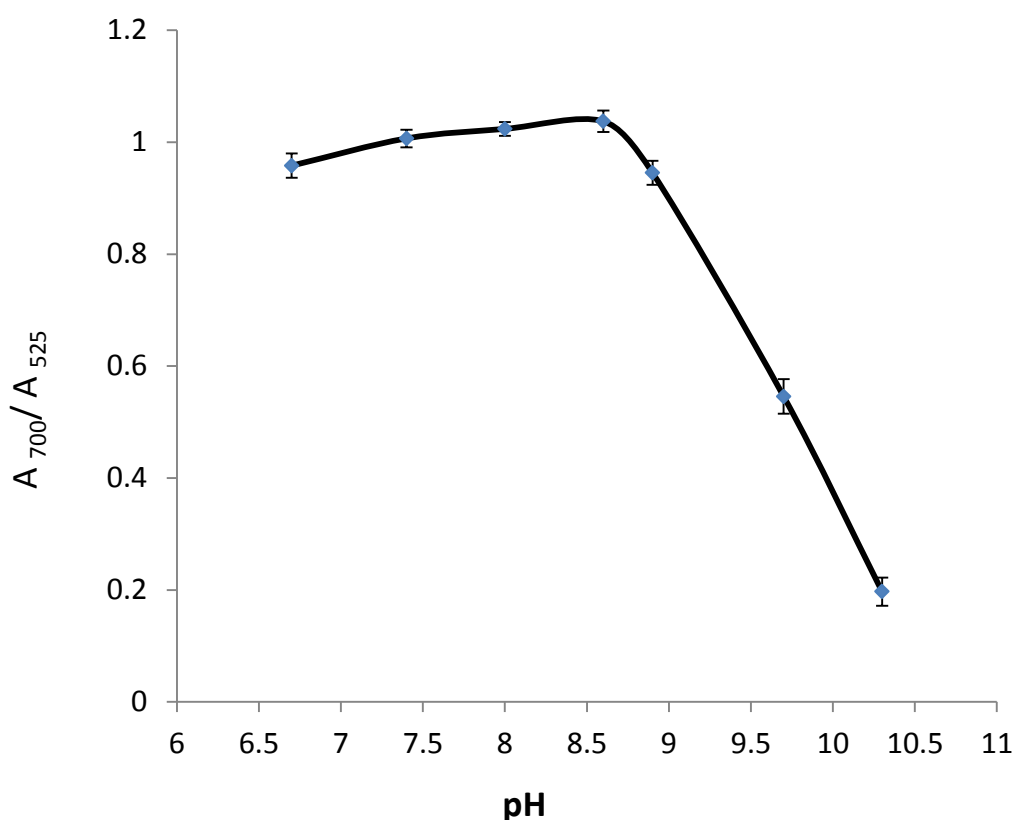


**Figure 4-9** Effect of pH changes on the VP-EN-DC capped Au NPs assay for the detection of DPP-IV enzyme.

All incubations were done in the presence of 50 mM Tris buffer at the indicated pH values at 37°C for 30 min. The activity is expressed as  $A_{700}/A_{525}$ . Error bars represent the standard deviation (n = 3).

#### 4.3.8 Application of the Colorimetric Assay using Modified Au NPs for Detection of DPP-IV Activity in Biological Samples

Normal serum human DPP-IV activity ranges between 17 and 52.6 U/L (Lambeir *et al.* 2003). The developed colorimetric VP-EN-DC functionalized Au NP assay would, therefore, be suitable for the qualitative and quantitative determination of DPP-IV activity in human serum samples since the range of detection of the optimal assay is 1.5 -40 U/L. Human serum samples were spiked with varying DPP-IV amounts to give activities of (5, 10, 15, 20 and 25 U/L) to investigate the recoveries of the colorimetric assay (Fig. 4-10). With the addition of different activities of DPP-IV/CD26, the absorption of the SPR band decreases while the absorption at longer wavelengths increases. When the activity of DPP-IV/CD26 is continuously increased, a new broad band appears at 745 nm, and grows corresponding as the activity of DPP-IV/CD26 increases. By plotting the  $A_{750}/A_{525}$  of P-Au NPs versus the DPP-IV/CD26 activity, it can be noticed that  $A_{750}/A_{525}$  increases corresponding to the DPP-IV/CD26 activity (Fig. 4-11).

The recoveries of the spiked samples were in the range 83.6 –114.9% (Table 4-1). The very good recoveries and precision values are an indication of the reliability of the proposed method for the detection of DPP-IV/CD26 in biological samples.

**Table 4-1** Recoveries of DPP-IV/CD26 activity in spiked human serum samples using the P-Au NPs

Added (U/L)	Found (U/L)*	Recovery (%)	RSD** (%)
5	5.04± 0.19	100.8	3.23
10	8.36± 0.23	83.6	2.37
15	15.89± 0.33	105.9	2.1
20	22.99± 0.91	114.9	4
25	26.77± 0.34	107	1.31

\* Mean of three sample determinations ± standard deviation.

\*\* RSD: Relative standard deviation.

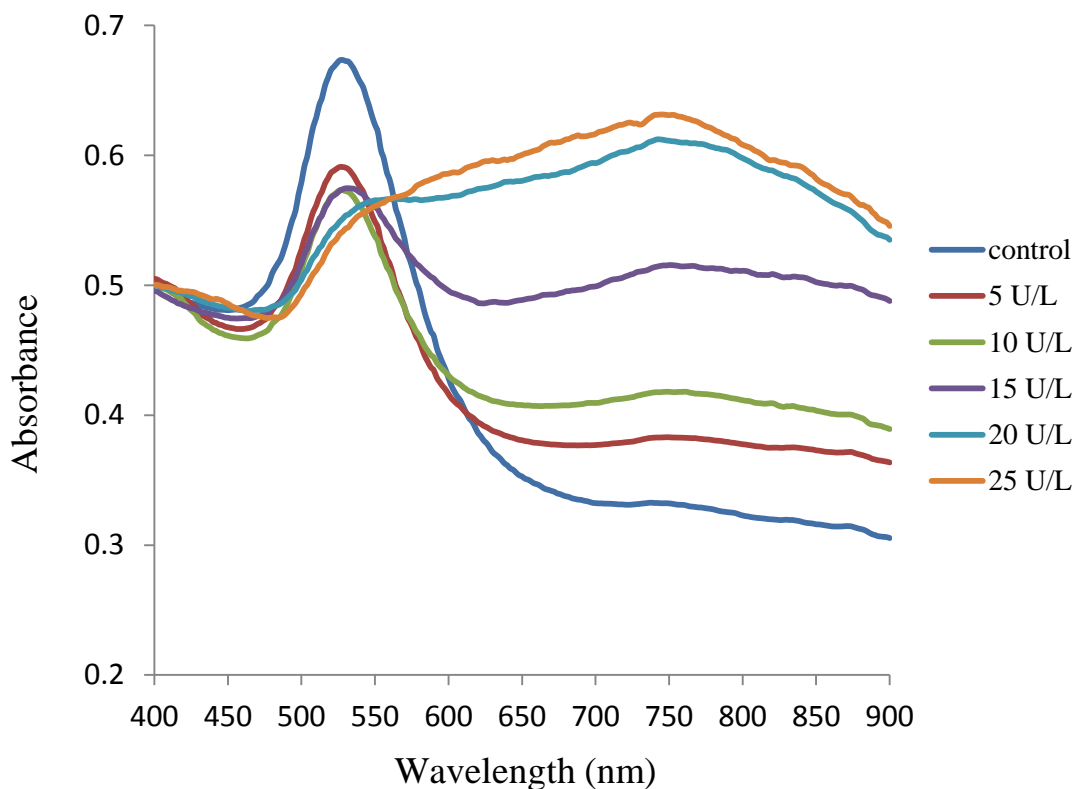


**Figure 4-10** UV-vis absorption spectra of the colorimetric assay using human serum samples spiked with DPP-IV standards (0, 5, 10, 15, 20 and 25 U/L DPP-IV/CD26).

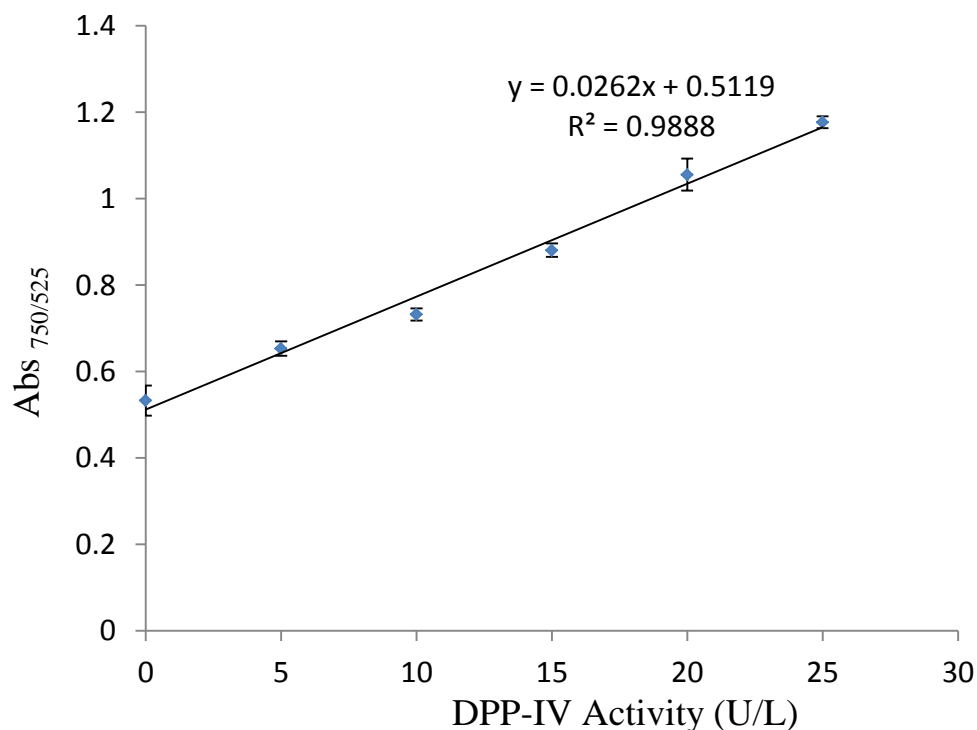


**Figure 4-11** Ratio plots of  $A_{750}/A_{525}$  versus DPP-IV/CD26 activity. Error bars represent the standard deviation ( $n = 3$ ). Ratio of absorbance for simulated (spiked) samples were chosen at 750 nm due to larger shift that was noticed in these samples.

### 4.3.9 Method Comparison

The developed VP-EN-DC Au NPs colorimetric assay was compared with the commonly used commercial Gly-Pro-pNA colorimetric assay (see section 1.9.1). The new method showed a good correlation with the standard assay when comparing the measured activity in human serum samples. This was demonstrated by linear regression analysis. Linear regression analysis of VP-EN-DC Au NPs compared with Gly-Pro-pNA showed a curve with the following equation: ( $y = 0.8484x + 0.1852$ ). Fig. 4-12 displays the results with the standard samples using both methods. Evaluation of these experimental data reveals a strong positive correlation between the two methods, with a correlation coefficient of 0.975, demonstrating that the results obtained from the developed novel method reported here correlated well with those from the commercial standard DPP-IV/CD26 assay. These results indicate that the Au NP-based colorimetric assay is reliable for detection of DPP-IV/CD26 activity in human serum samples.

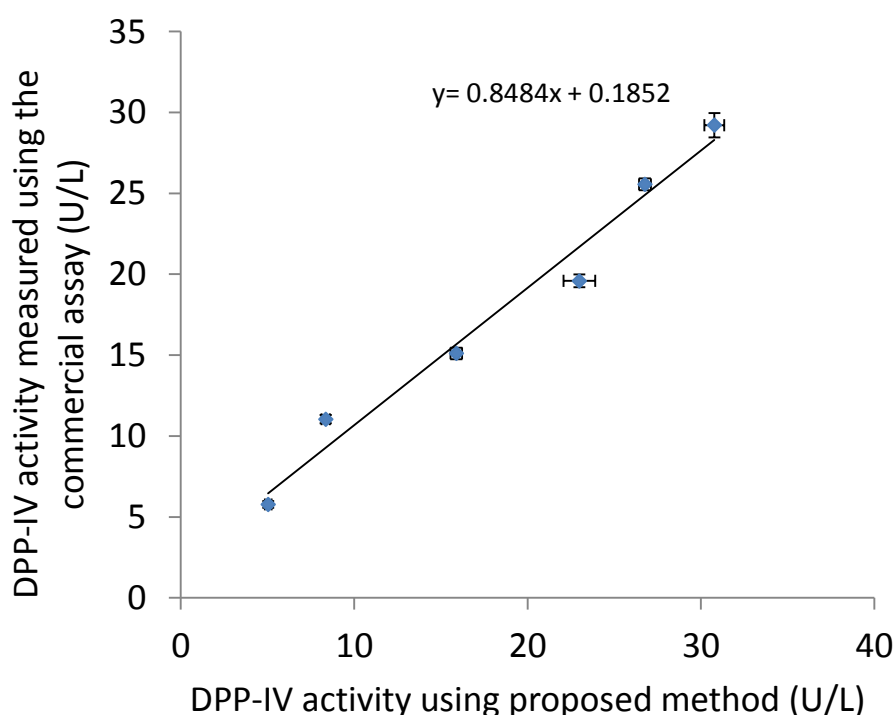


**Figure 4-12** Comparison of the assay results for DPP-IV/CD26 in human serum samples using the developed colorimetric assay and the Gly-Pro-pNA based commercial method, respectively. Error bars represent the standard deviation ( $n = 3$ ).

#### 4.3.10 Inhibition of the DPP-IV/CD26 Enzyme

DPP-IV/CD26 is sensitive to inhibition by many classes of serine protease inhibitors. DPP-IVi have been used for the management of type 2 diabetes because of their ability to raise the levels of active incretins, ultimately leading to increased insulin secretion and lower blood glucose levels (Green *et al.* 2006; Deacon 2011).

Experiments were conducted with 3-N-(((2S,3S)-2-Amino-3-methylpentanoyl)]-1,3-thiazolidine fumarate known as (P32/98) obtained from the DPP-IV/CD26 assay kit for biological samples (Enzo Life Science), which acts as a reversible competitive DPP-IV enzyme inhibitor. These experiments were unsuccessful as the purchased P32/98 inhibitor was dissolved in DMSO, which might have caused a general inhibition of DPP-IV activity.

Inhibition experiments were conducted using Vildagliptin, which belongs to the gliptin group of pharmaceuticals used as adjunctive medicines for type 2 diabetes. A stock solution of 100 mM Vildagliptin in deionized water was diluted in Tris buffer pH 8.3 at concentrations ranging from 10  $\mu$ M to 10 mM (final concentrations in the assay: 1  $\mu$ M–1mM). The resulting DPP-IV/CD26 activity was measured using the colorimetric Au NP assay (developed in this chapter) with slight modifications. A standard amount of DPP-IV/CD26 enzyme (20 U/L) was incubated with various concentrations of Vildagliptin in Tris buffer for 15 minutes at 37°C. The functionalized Au NPs were added to the enzyme plus inhibitor mixture and allowed to incubate for 15 minutes. UV-Visible spectroscopy was used to evaluate the residual DPP-IV activity quantitatively. As expected the inhibition increased with increasing concentration of Vildagliptin. The maximum inhibition of Vildagliptin was found to be 89.7% using 1 mM of the inhibitor. The IC<sub>50</sub> value, the inhibitor concentration required to reduce enzyme activity by 50%, was obtained from the plot of inhibitory ratio versus inhibitor concentration for 20 U/L DPP-IV was calculated to be 44.8  $\mu$ M (Fig 4-13).

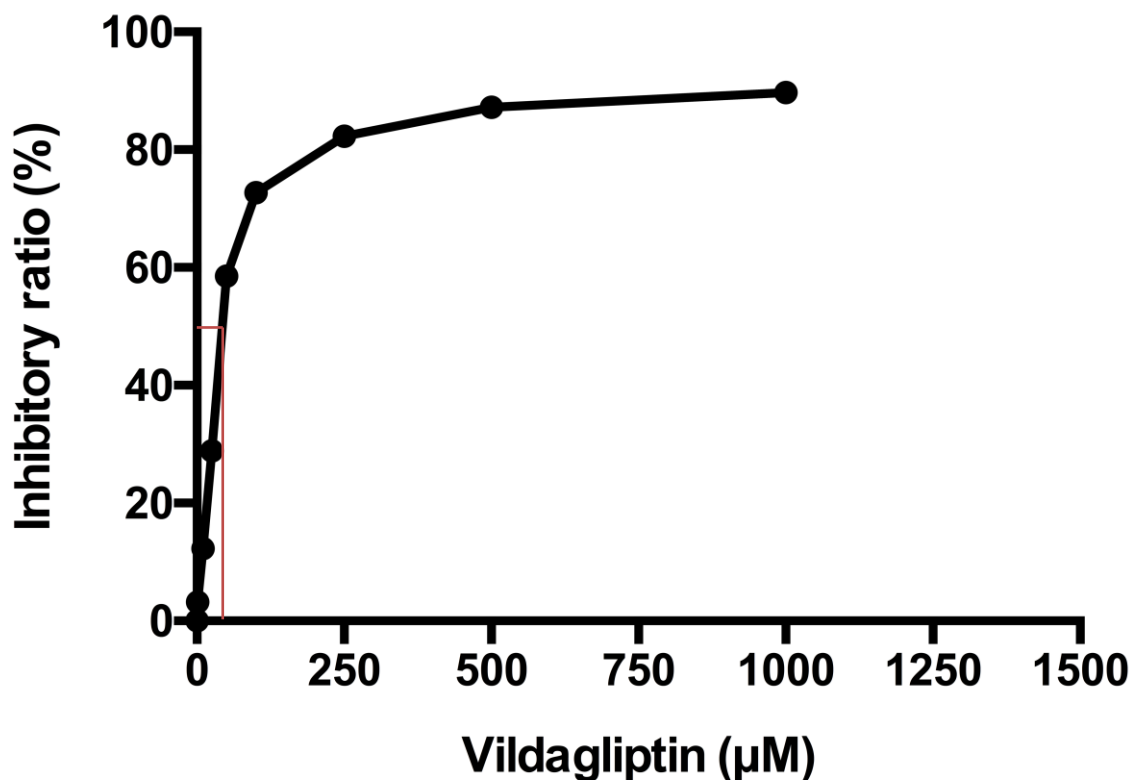


**Figure 4-13** Inhibitory ratio of different concentrations of Vildagliptin on DPP-IV/CD26 (20 U/L) activity.

Validation of an assay to determine its suitability for HTS was conducted by evaluating its performance based on the acceptable limits of Z factor and assay sensitivity (Inglese et al. 2007). The Z factor or value defines a characteristic parameter of the capability of the active compound identification for each given assay at the defined screening conditions (Table 4-2).

Table 4-2 Categories of screening assay quality by the value of the Z-factor.

<i>Z-factor value</i>	<i>Structure of assay</i>	<i>Related to screening</i>
1	SD = 0 (no variation), or the dynamic range $\rightarrow \infty$	An ideal assay
$1 > Z \geq 0.5$	Separation band is large	An excellent assay
$0.5 > Z > 0$	Separation band is small	A double assay
0	No separation band, the sample signal variation and control signal variation bands touch	A "yes/no" type assay
<0	No separation band, the sample signal variation and control signal variation bands overlap	Screening essentially impossible

The Z-factor is defined in terms of four parameters: the means and standard deviations of both the positive and negative controls. Given these values, the Z-factor is defined as:

$$Z = 1 - \frac{3SD \text{ of sample} + 3SD \text{ of control}}{|\text{mean of sample} - \text{mean of control}|} *$$

Given the data obtained in VP-ED-DC assay, the Z-score was determined to be 0.578 which is considered as an acceptable value for a screening assay (Zhang *et al.* 1999).

#### 4.4 Conclusions

In this study, a novel, simple, real-time and one-step colorimetric detection method for the measurement of DPP-IV/CD26 enzymatic activity, based on the aggregation of functionalized Au NPs in the presence of the enzyme, was developed. The relevance of this NP-based assay resides in the fact that visual detection or simple instrumentation can be used for this analysis.

In principle, aggregation of VP-EN-DC functionalized Au NPs can be used to measure the activity of DPP-IV/CD26 after hydrolysis of the peptide-functionalized Au NPs. The aggregation of the Au NPs induced a gradual colour change that was observed by the naked eye. Under the optimized conditions, a linear response range from 0 U/L to 40 U/L for DPP-IV/CD26 determination was obtained, and the calculated LOD was 1.5 U/L, making it suitable for the detection of DPP-IV/CD26 activity in serum (Lambeir *et al.* 2003).

The VP-EN-DC Au NP and GPDC Au NP (Chapter 3) assays to determine DPP-IV/CD26 activity both perform well, concerning qualitative and quantitative determination of DPP-IV/CD26 activity. Nonetheless, an enhancement in the linear detection range of DPP-IV/CD26 was achieved with the VP-EN-DC substrates by a factor of 3.5-4. This method have been validated in terms of screening assay quality and proved to be potential tool for identification of DPP-IV inhibitors.

This method displays selectivity for DPP-IV/CD26 over a selected number of serum proteins. More importantly, the selectivity and sensitivity of this method was used to

measure the DPP-IV/CD26 activity in human serum. The recovery of DPP-IV/CD26 levels in serum samples spiked with varying concentrations of DPP-IV/CD26 was determined to be in the range, 83.6 - 114.9% with a relative standard deviation of 1.31 - 4%. The proposed method could also be used for measurement of effectiveness of DPP-IV inhibitors. A deviation to higher wavelength (750 nm instead of 700 nm) in spiked serum samples might be due interference from non-analyte constituents in the sample.

A possible improvement to this system would be the addition of a self-cleavable spacer that could be spontaneously cleaved from the attached substrate ligand when DPP-IV/CD26 hydrolyses the first two amino acid residues as used by Diez - Torrubia *et al.* (2012). Cyclization self-cleavage spacers can be linked to the dipeptide through an amide bond (cleavable by DPP-IV/CD26) and coupled from the other end to the OH group of the ligand capped Au NP through a metabolically labile ester linkage, which will undergo spontaneous chemical hydrolysis after cleavage of the terminal amino acids. These results indicate that colloidal stability of NP conjugates must be an important consideration for solution-based NP detection assays, if they are to be used in a clinical setting. Also, that further work must be done in order to determine if other strategies can be investigated to enhance stability with minimum effect on assay sensitivity.

Compared to the traditional (fluorogenic and luminescent) commercial DPP-IV/CD26 assays, this system has the advantage of portability, simplicity for the end user application without the need for complex instrumentation. The developed method offers a new approach for developing simple, fast, reliable and sensitive sensors for DPP-IV detection that is an easy to access diagnostic and/or prognostic tool for different diseases.

## Chapter 5

---

### **Enhancing Gold Nanoparticle Stability for Colorimetric Detection of DPP-IV/CD26 Activity**

---

## 5.1 Introduction

To be suitable for use in biological assays, colloidal Au NP solutions must remain stable over a wide range of ionic strength particularly in biological environments such as serum, which has high ionic strength. Therefore, it is essential that attention is paid to the choice of the capping ligands as these surface bound ligands are responsible for NP stabilization against aggregation and provide the desired NP properties (e.g. hydrophilicity/hydrophobicity, surface charge, ligand arrangement, chemical reactivity, etc.) (Boisselier & Astruc 2009; Zhou *et al.* 2009; Balasubramanian *et al.* 2010). A general method of stabilizing Au NPs is the use of electrostatic repulsion between Au NPs, which are modified with charged ligands such as citrate (Martin *et al.* 2010) or triphenylphosphine (Ju-Nam *et al.* 2006). However, the stability of electrostatically stabilized Au NPs is affected by numerous factors in solution, including pH, ionic strength, and temperature (Wang *et al.* 2013).

In order to improve the stability of Au NPs under biological conditions, several methods have been developed. These methods generally involve the functionalization of Au NPs with ligands that provide either steric or electrostatic stabilization and hence impart further stability to Au NP formulation. One of the most commonly used approaches involves the modification of the Au NP surface by assembling a monolayer of peptide capping ligands (Lévy 2006). A combinatorial design approach enables the synthesis of very stable Au NPs with properties in aqueous media that are determined by the amino acid sequence of the appended cysteine-terminated pentapeptide (Wang *et al.* 2005).

The design strategy of these peptides takes into account the ability of certain amino acid residues to self-assemble into a dense layer that excludes water, and a hydrophilic terminus to ensure solubility and stability in water (Lévy *et al.* 2004). This type of NP-peptide probe has been utilized in the development of a colorimetric kinase activity assay (Wang *et al.* 2006) in which the kinase-substrate was detected by specific binding

of Au NPs to the phosphorylated product immobilized on a microarray (Sun *et al.* 2007). The method is based on labeling specific recognition or phosphorylation events on a microarray with Au NPs using avidin-biotin chemistry followed by silver enhancement and resonance light scattering detection. This format allows the production of highly stable Au NP platforms.

Another widely applied method is the incorporation of a thiol-containing polyethylene glycol (dithiol-PEG) moiety into the functional ligand, because of its good solubility, biocompatibility and anti-fouling properties, which render NPs resistant to non-specific protein adsorption (Eck *et al.* 2008; Manson *et al.* 2011). Number of workers have utilized functional PEGylated Au NPs in targeted drug delivery and as biosensors in complex media (Schiffelers *et al.* 2004; Dreaden *et al.* 2009; Free *et al.* 2009). Dougan and colleagues investigated the effect of using multiple thiol linker system on minimizing undesirable aggregation events caused by thiol desorption, resulting in the loss of function of the probe (Dougan *et al.* 2007).

Dithiols have also been used because of their higher coupling efficiency to Au NP surfaces, compared to monothiol and so enhance monolayer stability (Susumu *et al.* 2007; Hermanson 2013). A number of dithiols such as dihydrolipoic acid derivatives have been assessed for the functionalization of Au NPs (Abad *et al.* 2005; Garcia *et al.* 2005; Eck *et al.* 2008) and di- or polythiol PEGs (Wang *et al.* 2007; Kumar *et al.* 2008) in order to impart further stability.

In this chapter, the effect of incorporating stabilizer moieties into the assay format and their effect on DPP-IV detection by three distinct methods was assessed. Table 5-1 displays the complete sequence of the peptide constructs used in these experiments.

**Table 5-1** Peptide sequences trialled to enhance Au NP stability.

Name	Sequence	No of amino acids
C/G dipeptide	Cys-Ala-Leu-Asn-Asn & Gly-Pro-Asp-Cys	5 & 4
GPG-EN-PEG <sub>4</sub> -LA	Gly-Pro-Gly-ethylenediamine-PEG <sub>4</sub> -lipoamide	3
GPDCALNNC	Gly-Pro-Asp-Cys-Ala-Leu-Asn-Asn-Cys	9

These approaches were chosen because they are well established in their use in NP systems and also for their predictable stability properties (Zhu *et al.* 2012; Wang *et al.* 2013). The aim of this study is to enhance the stability of functionalized Au NPs by incorporating stabilizers and to evaluate their effect on DPP-IV detection (see Table 5-2).

The first trial involved a biofunctionalization (a biorecognition ligand and separate stabilizer ligand), while the second approach involved the modification of the functional ligand by incorporating a stabilizer in the sequence (PEGylation or penta peptide CALNN incorporation). The use of immobilized PEG coating on the gold surface *via* dithiol anchor groups on one end of the PEG chain and coupling of biological molecules *via* carboxy groups on the external side of the PEG ligand was investigated

GPDC was chosen as the functional ligand when using bifunctionalization as it provides a fast and simple approach for the detection of DPP-IV activity (discussed in Chapter 3), on the other hand CALNN was chosen as a stabilizing ligand with established high stability index (Lévy 2006).



## 5.2 Experimental

### 5.2.1 Materials and Methods

The enzyme, gold and citrate salts were all supplied and used as described in section 3.2.1. GPDC (~ 95% purity) and GPDCALNNC peptide (>90% purity) were purchased from Thermo Fisher Scientific GmbH (Germany). GPG-ethylenediamine-PEG<sub>4</sub>-lipoamide (95% pure) was purchased from Cambridge Research Biochemicals (UK). CALNN peptide (90% pure) was purchased from China peptide (China).

The citrate stabilized Au NPs were synthesized by using the Grabar method as described in section 3.2.2. All glassware and magnetic stirrer bars used in the syntheses were thoroughly cleaned in aqua regia (HCl/HNO<sub>3</sub> 3:1, v/v), rinsed in distilled water, and oven-dried prior to use.

### 5.2.2 Au NPs modified with capping ligands preparation:

#### 5.2.2.1 CALNN, GPDC bifunctionalized Au NPs (C/G Au NPs)

C/G Au NPs were prepared by addition of peptide mixture (CALNN and GPDC) in various ratios to the solution of Au NPs. GPDC is employed as a functional group which has been evaluated as substrate for DPP-IV (Chapter 3); CALNN is used as a stabilizer because pure GPDC modified Au NPs exhibit poor stability under physiological condition (ionic strength of 50–200 mM). The stability of C/G -Au NPs is increased by increasing the molar ratio of CALNN to GPDC in the peptide mixture. Bifunctionalized peptide Au NPs were prepared as in the reported procedure of (Wang *et al.* 2006) with slight modification. Different proportions of CALNN in the ligand shell were obtained by adjusting the ratio of CALNN to GPDC (1:4, 1:6, 1:8 and 1:10) in the peptide mixture. An aqueous solution of peptide mixture (CALNN and GPDC) for each concentration ratio was added to the solution of Au NPs.

### **5.2.2.2 Gly-Pro-Gly-ethylenediamine-PEG<sub>4</sub>-lipoamide (GPG-EN-PEG<sub>4</sub>-LA)**

In order to use (GPG-EN-PEG<sub>4</sub>-LA) the ring (1,2-dithiolane) has to be opened to form a bidentate thiol anchoring group. Ring opening was achieved by incubation of the ligand with 50 mM Tris (2-carboxyethyl) phosphine hydrochloride (TCEP) as a reducing agent in 10:1 (v/v) ratio for one hour at room temperature. Functionalized Au NPs were prepared by adding an aqueous solution of PEGylated ligand to the solution of 15 nm Au NPs.

### **5.2.2.3 GPDCALNNC peptide**

Au NPs functionalized with GPDCALNNC peptide were prepared by adding 1 mM peptide solution dissolved in sodium phosphate buffer (pH 7.4) to the solution of 15 nm Au NPs in a 1:10 (v/v) ratio.

### **5.2.3 Purification**

The gold conjugates were purified from excess protein and nanoparticles before using for any experiment or storing. After overnight incubation at room temperature, excess peptides were removed by two centrifugations (14,500 rpm) for 15 minutes using a 5415D Eppendorf centrifuge (Eppendorf, Germany). These speeds and times were optimised and determined experimentally. The final product was a loose red precipitate. The pellet was resuspended and stored in deionized water and stored at 4°C.

### **5.2.4 Instrumental Techniques**

All zeta potential analysis was carried out using the Malvern Zetasizer Nano ZS. The scattered light was detected at 135° angle, with Non-Invasive Backscatter (NIBS) technology. The refractive index of the particle (1.59) polystyrene standard, refractive index (1.33) and the viscosity (0.88) of ultrapure water were taken at 25°C for measurements. All the data analyses were performed in automatic mode. Measured size range was presented as the mean value of 4 runs. For zeta potential measurements,

universal dip cell with applied voltage less than 5 V was used and the Smoluchowski approximation was employed by the instrument's software to calculate zeta potential values for aqueous solutions of AuNPs (F(Ka) value = 1.5).

FTIR spectra were obtained using a PerkinElmer spectrum 100 Fourier Transform Infrared Spectrometer (PerkinElmer, USA). The KBr pellet technique has been most commonly adopted for recording the spectra. However, in this work, the purified samples were lyophilized and the powdered solid were characterized directly in their free-standing state.

The type of gel electrophoresis, used in this study, is agarose gel; TAE (Tris-acetate-EDTA) buffer was used for running the samples through the gel. An electrical current is placed across the gel to mobilise the Au NPs preparations. The voltage, the amount of time under current and the amount of agarose used in the gel all affect how far the Au NP will travel and must be optimised for good separation. The Au NP samples were loaded on 1.5% agarose gels, 1 × TAE buffer, and run for 75 minutes at 100 V.

#### **5.2.5 Assay of DPP-IV/CD26 activity**

To perform the colorimetric assays for DPP-IV/CD26, Aliquots of each modified Au NP preparation were incubated with the enzyme at varying activities in Tris buffer (50 mM, pH 8.3), in the wells of a transparent 96-well microtiter plate. The contents were gently mixed using a plate shaker at 300-400 rpm for 60 seconds; and then incubated at 37 °C for 15 minutes. The UV-vis absorption spectrum of the solution was recorded using an absorbance scan from 400-900nm.

## 5.3 Results and Discussion

### 5.3.1 Investigation of Peptide Coupling using UV-Visible Spectroscopy

UV-vis absorption spectroscopy allowed monitoring of the interaction of the various ligand substrates with Au NPs, since SPR is highly sensitive to the NP environment. The Au NP colloid was found by TEM to be mainly comprised of 14 nm gold spheres exhibiting an extinction maximum at 523-524 nm (Figure 5-1), following NP conjugation and coupling reaction with functional ligands (GPDCALNNC or GPG-EN-PEG<sub>4</sub>-LA) a slight shift in the absorption maximum was observed between 2.5 and 1.7 nm respectively while C/G modified Au NPs displayed an absorption band shift of 2.9 nm. This shift in  $\lambda$  max of Au NPs was due to the modification of the Au NPs with the various ligands. The coupling of the stabilizing ligands alters the level of the electromagnetic modelling of the optical function due to the asymmetric environment. The effect of ligand coupling on the LSPR shift of gold colloids can be accounted for by assuming the contribution of the dielectric of the organic shell (Ghosh *et al.* 2007).

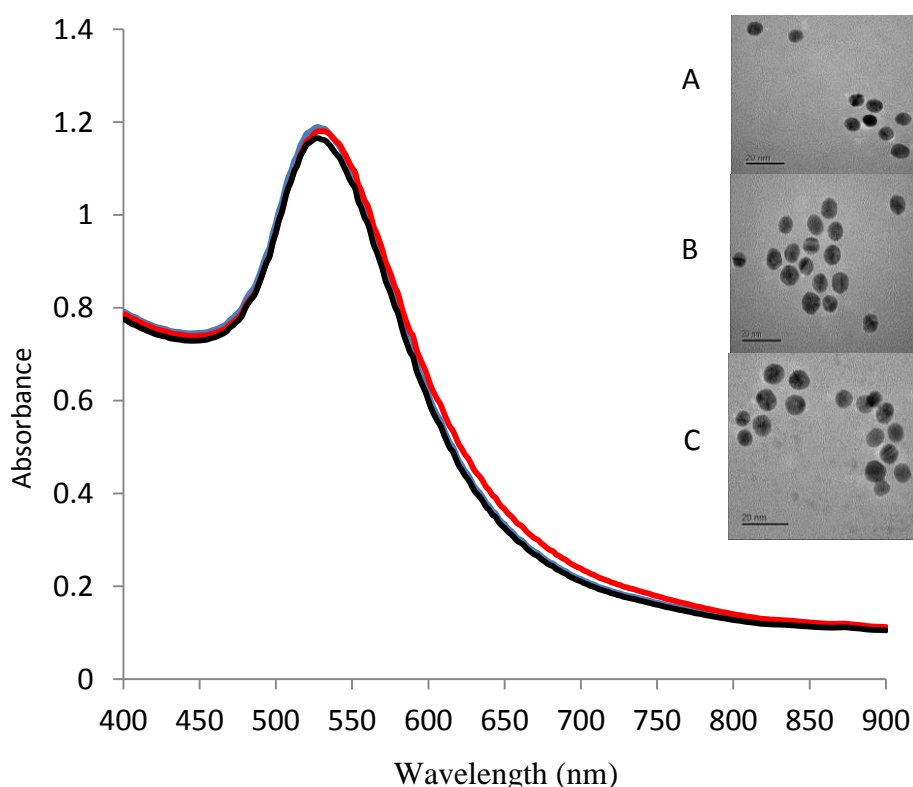


**Figure 5-1** UV-Vis absorption spectrum of modified Au NPs [black: GPDCALNNC (A), blue: GPG-EN-PEG<sub>4</sub>-LA (B) and red: C/G capped Au NPs (C)].

### 5.3.2 Evaluation of Ligand Coupling by Gel Electrophoresis

Nanoparticles were observed as a red band passing through the gel while running. Au NPs were not stained by Coomassie blue R-250. The coupling of the peptide to Au NPs can be observed by gel electrophoresis (Liu *et al.* 2007; Bartczak & Kanaras 2011; Zhao *et al.* 2012).

Proper gel shift and the difference between modified and unmodified Au NPs in the gel were noticed by comparing the band migration for modified NPs and citrate (unmodified) NPs as shown in Fig 5-2. The bands of the unmodified and peptide-capped Au NPs were directly visible by the red colour of the Au colloid. The C/G capped NPs and GPDC functionalized NPs had greater mobility than unmodified Au NPs due to change in the charge and/or size occurred as a result of the peptide coupling. Tailing was observed in the case of citrate Au NPs due to Aggregates of the Au NPs not penetrated the gel and small amounts of free gold gave background staining.

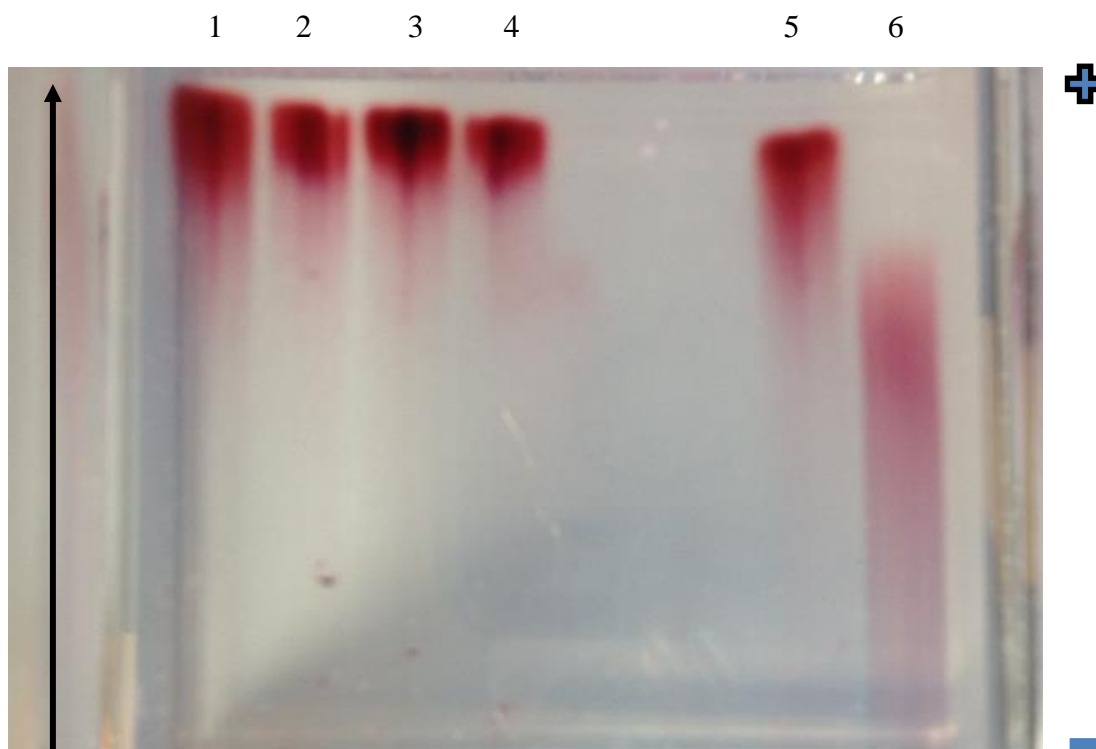


**Figure 5-2** Agarose gel electrophoresis of citrate and peptide capped Au NPs.

True colour photograph of a 1.5% agarose gel run for 75 min at 100 V. The six lanes contain, (lanes 1 to 4); C/G capped Au NPs prepared in different ratios (1:4, 1:6, 1:8 and 1:10), (lanes 5 and 6); GPDC capped Au NPs and citrate Au NPs.

### 5.3.3 Evaluation of Ligand Coupling to Gold Nanoparticle Surfaces by FTIR and Raman Spectroscopy

FTIR spectroscopy was employed to detect changes to the characteristic bands of thiol after Au NP coupling, as free thiol is expected to bind to the Au NP surface via thiolate bonds. Generally, amino acids exist as zwitterions and display spectra featuring both primary amine and carboxylate functional groups. The bands for  $\text{NH}_3^+$  stretch (very broad), NH bend (asymmetric/symmetric), and  $\text{COO}^-$  (carboxylate ion) stretch (asymmetric/symmetric) are typical for this type of compounds (Pavia *et al.* 2014). In the case of GPDCALNNC peptide composed of nine amino acids, the main focus was to look for changes in the thiol group in the cysteine. Fig. 5-3 shows the FTIR spectra of the GPDCALNNC before and after coupling to Au NPs. Bands seen in the spectra are identified as follows. The band in (spectra A) at 1652 and 1385  $\text{cm}^{-1}$  corresponds to the asymmetric and symmetric stretching of  $\text{COO}^-$ . A band at 1522  $\text{cm}^{-1}$  corresponds to N-H bend and the very broad band of  $\text{NH}_3^+$  stretch was observed in the 3000–3500  $\text{cm}^{-1}$  range. In addition, a weak band near 2550  $\text{cm}^{-1}$  confirms the presence of the SH group in the cysteine molecule. These values are in good agreement to those reported by Aryal *et al.* (2006b) for cysteine capped Au NPs.

These results are in good agreement with IR spectra of a peptide or amino acids, but characteristic SH band around 2500-2600  $\text{cm}^{-1}$  seems to be very weak because of the low amount of sulphur in the peptide. However, small changes in the absorption spectra were detected in the case of GPDCALNN capped Au NPs (spectra B). A shift in the position of  $\text{COO}^-$  and  $\text{NH}_3^+$  stretching is likely due to a change in their dipole moment, when cysteine binds on a metal surface with high electron density. Although significant band changes due to SH were not observed in the spectra of free and NP coupled peptide, other bands of  $\text{COO}^-$  and  $\text{NH}_3^+$  in spectra B encountered a displacement that may indicate the peptide coupling to Au NP surface.

Raman spectroscopy failed to demonstrate any changes in vibration when the peptide was bound to the Au NPs, which might be attributed to the concentration of Au NPs in the solution.

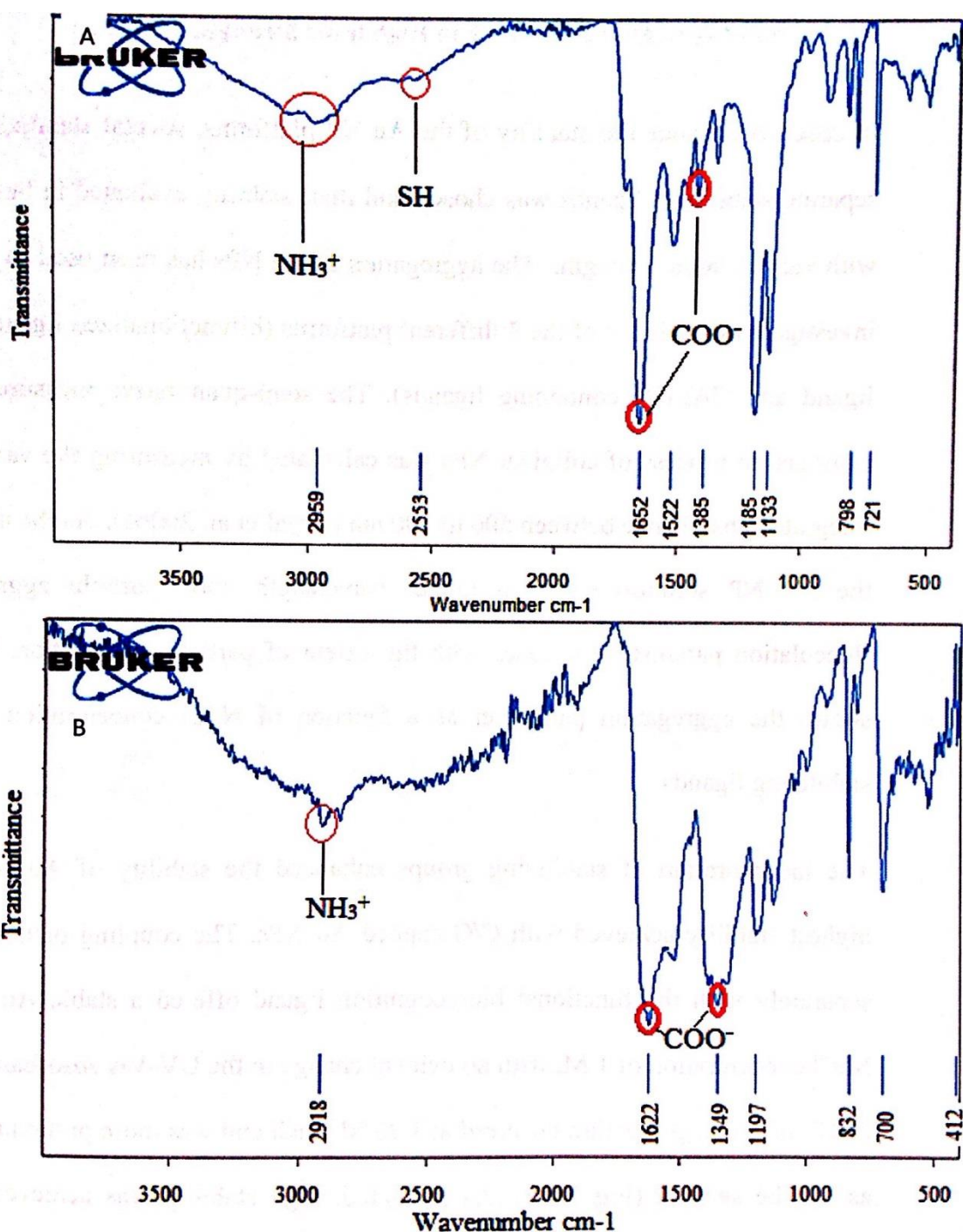


**Figure 5-3** Infrared spectra of stabilized ligand GPDCALNNC (A) and GPDCALNNC capped Au NPs (B). Functional ligands inside red circles represent the shift in the band position and disappearance of thiol band suggesting a formation of thiolate-gold bond.

### 5.3.4 Stability of Modified Au NPs in High Ionic Strength Solutions

In order to enhance the stability of the Au NP platforms, several stabilizing groups or separate stabilizing ligands were chosen and their stability evaluated in buffer solutions with varying ionic strength. The aggregation of Au NPs was used as a means of investigating the stability of the 3 different platforms (bifunctionalized ligand, PEGylated ligand and CALNN containing ligands). The semi-quantitative measurement of the aggregation process of colloidal NPs was calculated by measuring the variation of the integrated absorbance between 500 to 700 nm (Aryal *et al.* 2006a). As the absorbance of the Au NP solution shifts to longer wavelengths upon particle aggregation, the flocculation parameter increases with the extent of particle aggregation. Figure 5-4 shows the aggregation parameter as a function of NaCl concentration for different stabilizing ligands.

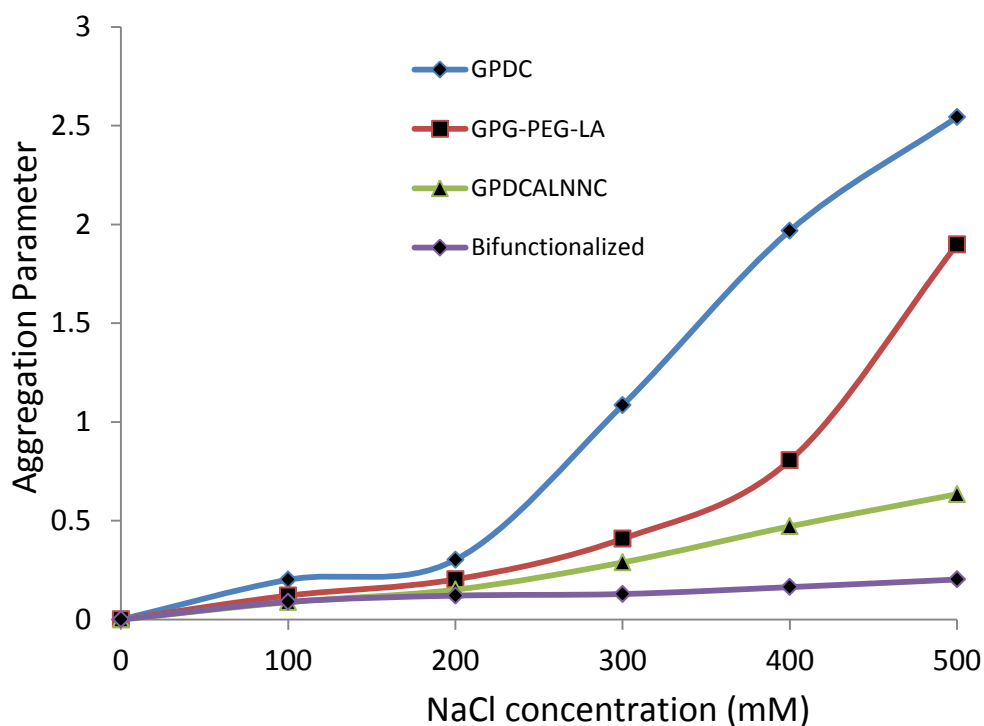


**Figure 5-4** Effect of introducing different stabilizing groups on the stability of Au NPs at different ionic strengths. The aggregation parameter is defined as follows:  $AP = (A - A_0)/A_0$ , where  $A$  is the integrated absorbance between 500 and 700 nm of the sample and  $A_0$  is the integrated absorbance between 500 and 700 nm of the initial, fully dispersed solution of NPs.

The incorporation of stabilizing groups enhanced the stability of Au NPs with the highest stability achieved with the C/G capped Au NPs. The coupling of CALNN ligand separately with the functional biorecognition ligand offered a stable Au NP up to a NaCl concentration of 1 M, with no evident change in the UV-Vis absorbance spectrum. NaCl-induced reversible aggregation (Yang et al. 2012) occurred at 1.25 M NaCl and was more pronounced at 1.5 M, as can be seen in (Fig 5-5). As predicted, high stability was achieved due to the formation of a compact self-assembled peptide layer (Lévy *et al.* 2004).

The other systems investigated were GPDCALNNC-capped NPs and PEGylated ligand tagged with biorecognition element GP, in which good stability was achieved, but to a lesser extent than that obtained by bifunctionalization of the ligand.

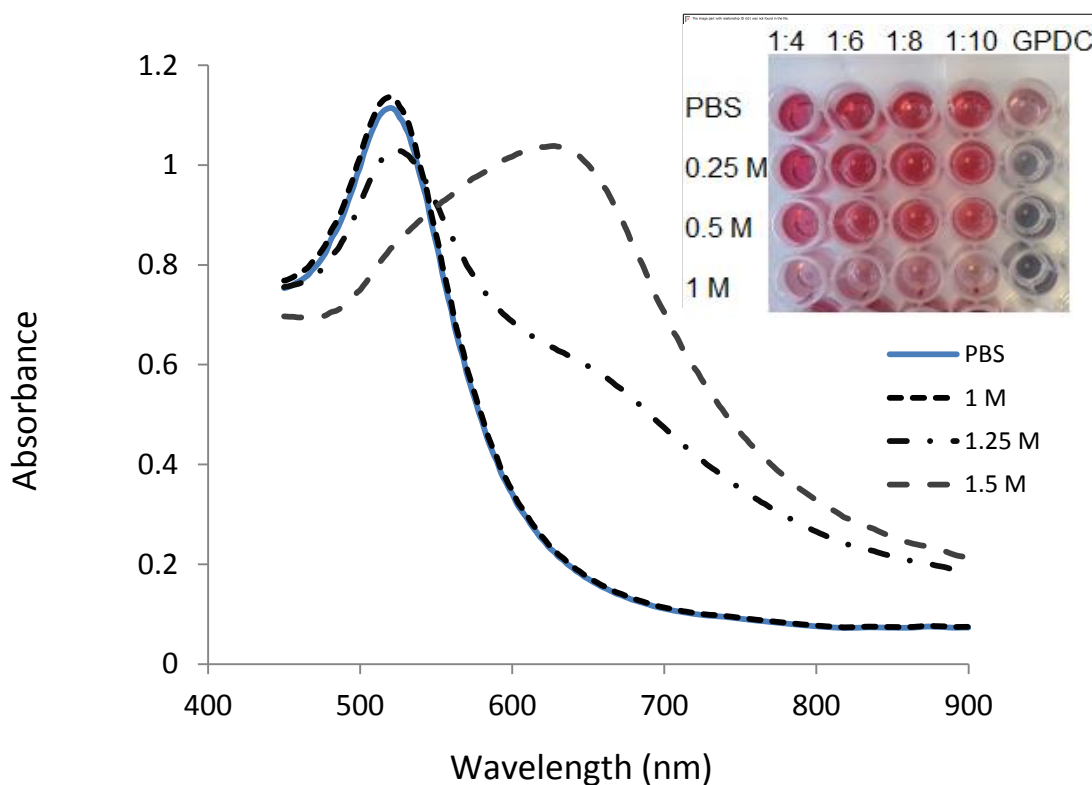


**Figure 5-5** UV-Vis study of C/G capped Au NP stability as a function of NaCl concentration (Inset: stability of C/G capped Au NPs (1:4, 1:6, 1:8 and 1:10) compared to GPDC capped Au NPs in NaCl solutions with various ionic strengths. As higher concentrations of the salt were added, a greater screening of charges stabilizing the modified Au NPs occur leading to the red shift of absorption band and band broadening.

### 5.3.5 Investigation of Zeta potential and Hydrodynamic Radius

To further assess the stability of the modified Au NP formulations, the zeta potential was measured to give further insight into understanding of the state of the NP surface and predicting the long-term stability of the NP solution. Table (5-3) summarizes the zeta potential values and hydrodynamic radii of the different functionalized Au NP preparations. The zeta potential values further confirm that highest stability is achieved with the bifunctionalized Au NP preparation.

**Table 5-3** Average zeta potential and hydrodynamic radius of different peptide stabilized Au NPs

Sample	Zeta potential (mV)	Average hydrodynamic radius (nm)
GPDC: CALNN 4:1	-46.1	22.88
GPDC: CALNN 6:1	-38.9	23.68
GPDC: CALNN 10:1	-39.0	35.42
GPDCALNNC	-35.9	39.5
GPG-PEG <sub>4</sub> -LA	-16.5	38.1

The stability of C/G capped Au NPs is improved by increasing the molar ratio of CALNN to GPDC in the peptide mixture as can be seen in Table 5-3. These data are in good agreement with the stability noticed in high ionic strength solutions. However, it should be noted that PEGylated ligand displays the lowest zeta potential, which does not coincide with the stability it demonstrates in saline solutions and this can be interpreted by steric repulsion imparted by coiled PEG whilst the zeta descriptor measures the electrostatic potential that exists between the shear plane of a NP and the solvent (Jokerst *et al.* 2011).

### 5.3.6 Detection of DPP-IV Activity using Functionalized Au NPs

The C/G capped Au NPs showed a typical SPR peak at 525 nm, i.e., a red shift of 3 nm with respect to the unmodified Au NPs, and good stability in phosphate buffer saline PBS. After carefully adjusting the molar ratio of CALNN to GPDC, the molar ratio of CALNN to GPDC at 1:10 in the reaction mixture was selected in order to evaluate the sensitivity of the method to DPP-IV/CD26, as this mixture found to be stable (as shown in Table (5-3) whilst simultaneously having the highest ratio of bound functional ligand. A perceptible colour change from red to faint purple was only obtained with 15 U/L of DPP-IV activity and it became more evident with increasing activity to 30 U/L (Figure 5-6). The ratio of absorption at 750 and 525 nm was used to evaluate the response of dipeptide capped Au NPs to DPP-IV/CD26 (Figure 5-6).

Similar conditions were applied to measure DPP-IV/CD26 activity using the PEGylated Au NP system or by GPDCALNNC Au NP system but neither caused colour changes nor significant UV-Visible spectral shift were observed, even with high activities DPP-IV (> 50 U/L). The total lack of response was attributed to steric hindrance caused by the compact structure of the remaining ligands (whether PEG or CALNN) bound to the NP consequently preventing NPs aggregation. Another potential reason for the lack of response to DPP-IV/CD26 in the case of GPDCALNNC is the presence of two cysteine residues in the sequence that may form disulphide bridges leading to a variable percentage of dimerized products (Chen *et al.* 2001).

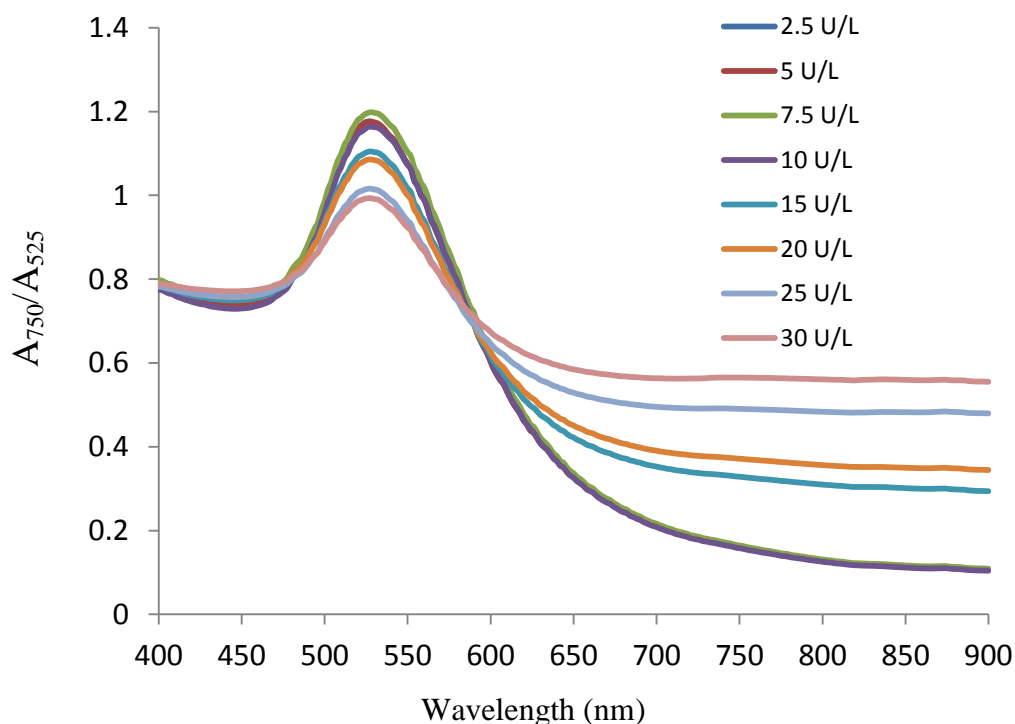


**Figure 5-6** UV–Visible absorption spectra of C/G capped Au NPs after incubation with different activities of DPP-IV/CD26. The DPP-IV/CD26 activity ranged from 10 to 30 U/L. Lower DPP-IV/CD26 activities did not induce spectral changes.

### 5.3.7 Quantitative Determination of DPP-IV/CD26 Activity

Results of the Au NP assay revealed that the colour change was directly proportional to the DPP-IV activity present. The assay provided quantitative estimation of total DPP-IV activity in the range of 10 - 30 U/L. The ratios of spectral absorbance  $A_{750}/A_{525}$  of the reacted Au NP solutions were plotted as a function of the corresponding standard activities of DPP-IV (U/ L). These two absorbance values,  $A_{750}$  and  $A_{525}$  were chosen to represent the relative amount of aggregated and dispersed Au NPs respectively. The increase in the absorbance at 750 nm indicates the formation of the Au NPs clusters/aggregates, while the peak at 525 nm represents the  $\lambda_{max}$  of suspended C/G Au NPs (Chen *et al.* 2014; He *et al.* 2017). Fig. 5-7 shows that the absorption ratio ( $A_{750}/A_{525}$ ) of C/G -Au NPs is increased by increasing the activity of DPP-IV/CD26 from 10 to 30 U/L.

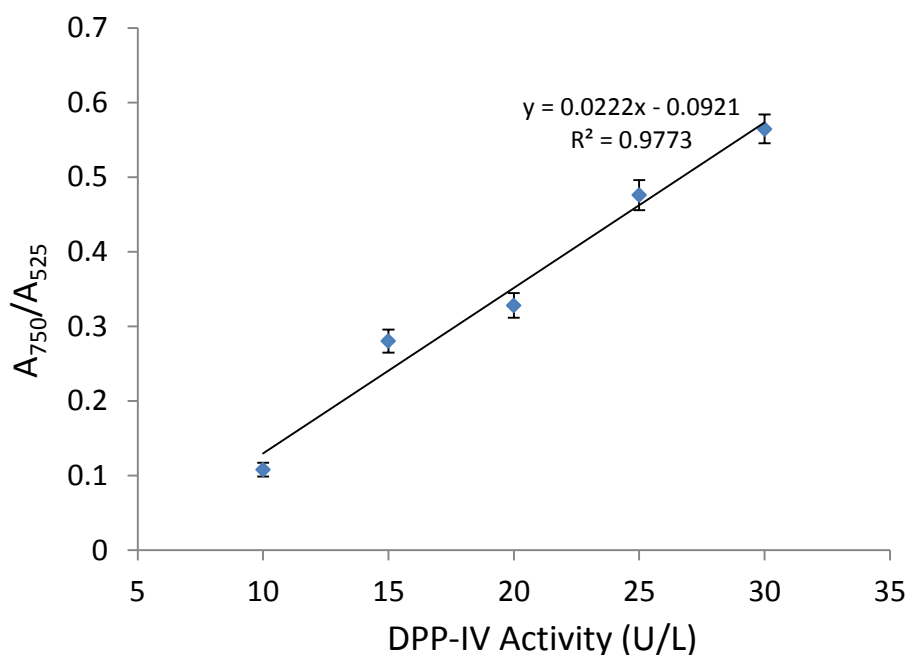


**Figure 5-7** Calibration curve of  $A_{750}/A_{525}$  versus the different activities DPP-IV incubated with C/G capped Au NPs. Error bars represent the standard deviation (n=3).

#### 5.4 Conclusion

Three approaches for enhancing modified Au NP system stability were developed and their performance evaluated. These approaches involved different strategies to enhance the stability of Au NP for colorimetric detection of DPP-IV in high ionic strength medium.

The first strategy used the incorporation of a PEGylated sequence with a dithiol anchor because the surface properties of these systems can be engineered through the introduction of functional ligands to create biorecognition ligands (Dixit *et al.* 2006; Eck *et al.* 2008).

The other two strategies used a peptide sequence (CALNN) designed by Lévy *et al.* (2004). This peptide was selected from 58 peptide sequences tested, for its high stability and resistance to electrolyte induced Au NP aggregation. In one strategy CALNN peptide was introduced separately as a stabilizer with the previously tested functional ligands, while the third approach involved decoration of CALNN peptide with the GPDC ligand.

The stability of these three systems were evaluated against high ionic strength solution and exhibited high resistance to aggregation in solutions with up to 0.5 M NaCl, with the highest stability achieved by C/G capped Au NP. Further stability studies were conducted by zeta potential measurements. C/G capped Au NPs displayed the highest zeta potential value which coincides with its highest stability in saline solution whilst the PEGylated ligand expressed low zeta potential value, which might be attributed to the low surface charge of the ligand.

Detection of DPP-IV/CD26 activity using the three approaches were conducted under optimal conditions and only C/G capped Au NPs showed a response with a colour change when incubated with DPP-IV/CD26. C/G capped Au NPs were less sensitive than the mono functionalized systems described in Chapters 3 and 4, with a dynamic range of 10-30 U/L but with very high stability in ionic solutions. This could be attributed to the presence of compact dense layers of CALNN which hampered effective Au NP aggregation and hence reduced analytical sensitivity.

In spite of these limitations, the developed bifunctionalized assay was successfully evaluated by gel electrophoresis, zeta potential and hydrodynamic radius measurements and tested for the assay of DPP-IV activity. These Au NP systems gave an insight into different stabilization systems and their effect on the aggregation process. There are a number of parameters to be considered when incorporating a stabilizer such as the length of the stabilizer residue, the compact density of the stabilizer and stabilizer to functional ligand ratio (Lin *et al.* 2005).

Other approaches that can be tried to produce Au NPs that withstand nonspecific aggregation include surface modification by polysaccharides, mixed charge self-assembly, or zwitterionic polymers (Yang *et al.* 2009, Nowinski *et al.* 2014, Ho *et al.* 2015). One of these approaches developed by Nowinski and colleagues was composed of a peptide-capped Au NP platform that resists aggregation in human serum at 37° C

for 24 h. This system was based on imitating natural proteins by designing a low fouling peptide composed of interchanging negatively charged glutamic acid and positively charged lysine residues on their surface. The EK sequence creates a strong hydration layer of zwitterionic materials imparting resistance to nonspecific protein adsorption. Furthermore, the EK sequence mimics the surfaces of human proteins which have adapted to avoid nonspecific adsorption and display stability in complex media (Fig. 5-8).

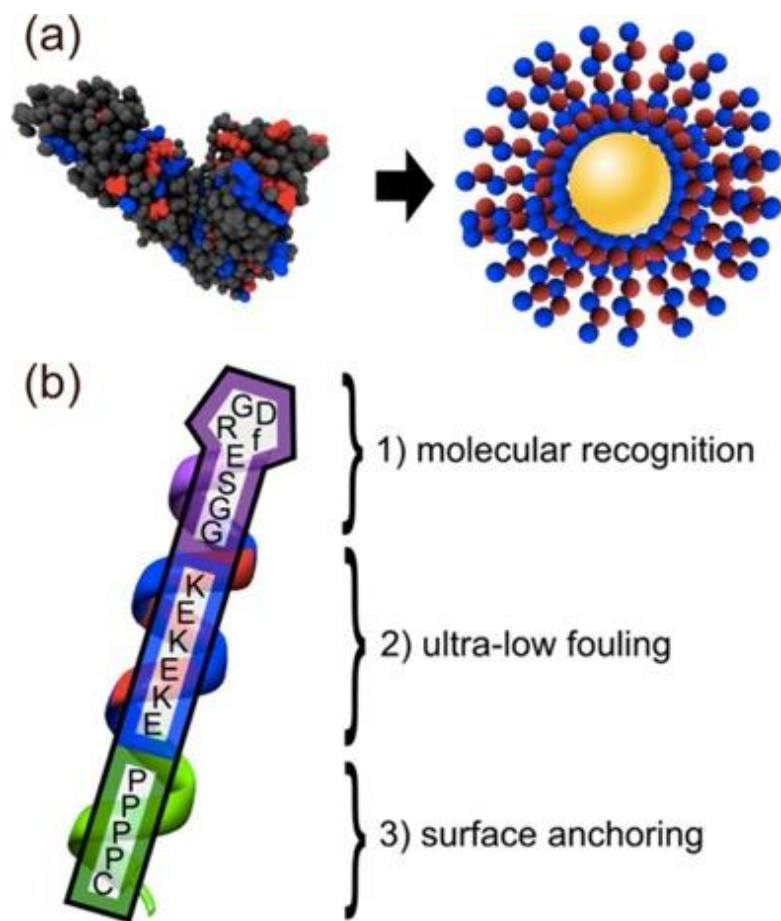


**Figure 5-8** (a) Schematic depicting the design of the stealth peptide sequence inspired by the analysis of human protein surfaces, which contain E and K as the most prevalent amino acids on the surface (indicated by red and blue spheres). (b) All-in-one natural peptide sequence with three distinct functions: (1) biomolecular recognition via cyclic RGD (purple); (2) ultralow fouling via EK (red and blue); and (3) surface anchoring via PPPPC (green). Reproduced with permission from (Nowinski et al. 2014).

## **Chapter 6**

---

### **Gold Nanorods as Potential Alternative for the Development of DPP-IV Colorimetric Sensors**

---

## 6.1 Introduction

Gold nanorods (Au NRs) are elongated NPs with unique optical properties, which depend on their their length-to-width ratio (Sau *et al.* 2010; Li *et al.* 2014). Au NRs hold great potential as the next-generation of sensor systems because of their elongated nanostructure, sharp/polarized near-infrared resonance and tunable plasmon resonance spectra (Chen *et al.* 2013; Park *et al.* 2014).

In particular, its localized surface plasmon resonance (LSPR) absorption is extremely sensitive to the size, composition, distance, and the surrounding media, based on which great progress in colorimetric sensors have been made. This allows the ability to tune the NR absorption as shown in Fig. 6-1 from 550nm to 1400nm through different manufacturing processes. This tuning results in the ability of Au NRs to scatter at wavelengths across the visible and near-IR regions (Tong *et al.* 2009).

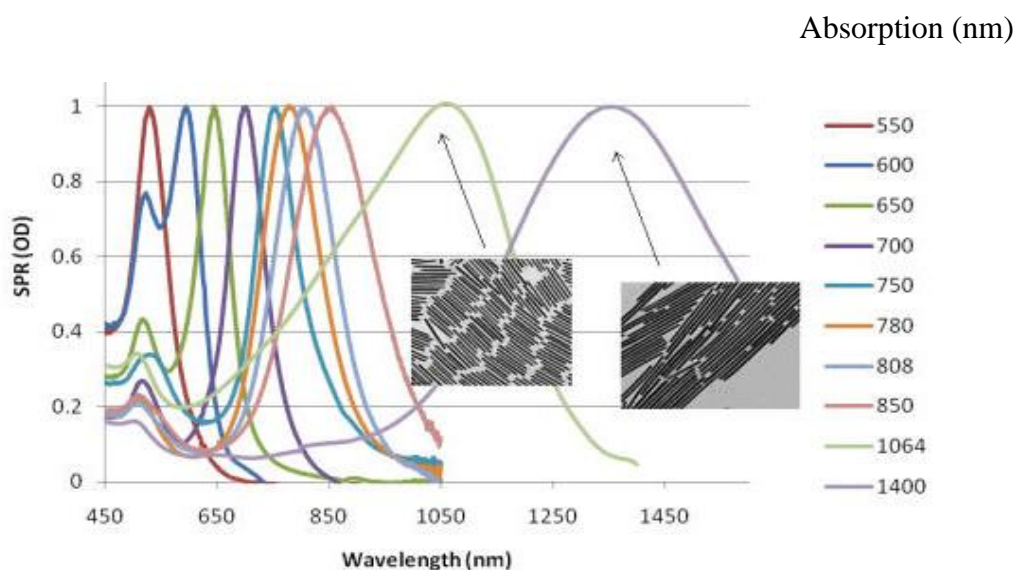


**Figure 6-1** Gold nanorod peak absorption and scattering (extinction) can be tuned across the visible and near IR spectra as shown on a plot of SPR to wavelength. Adapted from Sigma-Aldrich.

Au NRs have two principal plasmon absorption bands: a transverse LSPR band located in the visible region around 520 nm and a longitudinal LSPR band, located in a longer wavelength region usually between (800 - 900 nm) which can be modified by varying the aspect ratio (length/width) of the Au NRs from the visible to the near-IR region

(Truong *et al.* 2012; Alkilany *et al.* 2012). The difference in the absorption characteristics of Au NRs and Au NPs can be identified by UV-visible spectroscopy (Fig 6-2).

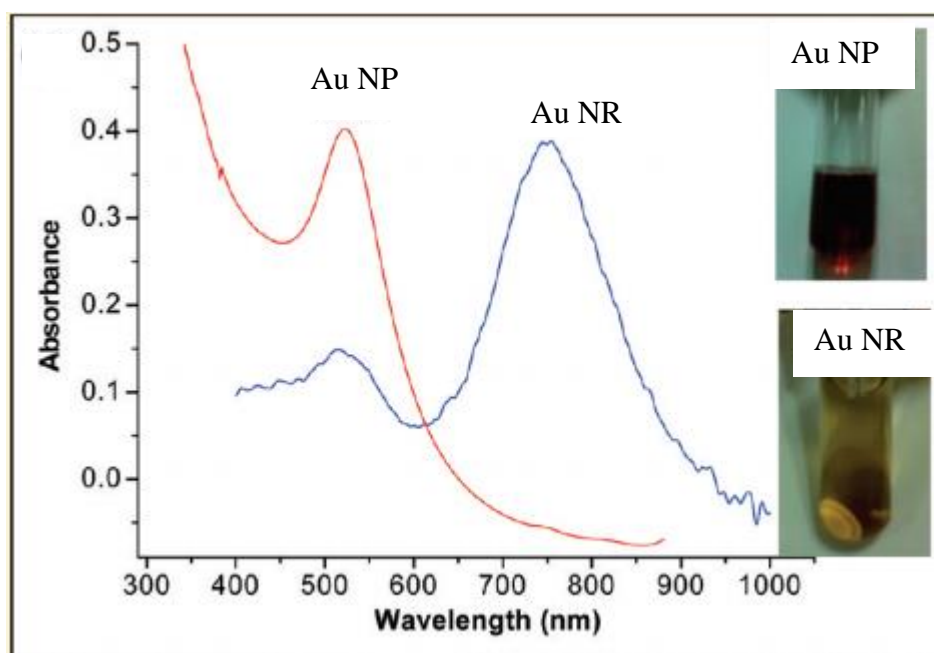


**Figure 6-2** Comparison of the UV-visible spectra of Au NPs and Au NRs. Reproduced with permission from (Chakraborty *et al.* 2011)

### 6.1.1 Au NR Synthesis

Au NRs synthesized by seed-mediated growth method have a strong capping of bilayer cetyl trimethyl ammonium bromide (CTAB) surfactant, which provides the surface of NRs with a cationic surface charge and this ensures their stability in aqueous solution via electrostatic repulsion. However, the CTAB-stabilized Au NRs aggregate rapidly in buffer or cell culture media because of the screen produced by high salt concentration, which can reduce the repulsive interactions between individual Au NRs (Gao *et al.* 2003).

### 6.1.2 Biomedical Applications of Au NRs

The unique properties of Au NRs find applications in the fields of imaging, therapy and sensing (Kim *et al.* 2017a; Sun *et al.* 2017; Aioub *et al.* 2017). Due to the strong light scattering in the NIR region, Au NRs can be used for bioimaging using dark field

scattering microscopy. By conjugating specific ligands to the Au NRs, they have been widely used for cancer imaging with dark field imaging. For example, Huang *et al.* (2006) used monoclonal anti-epidermal growth factor receptor (anti-EGFR) antibodies conjugated to Au NRs for distinguishing cancer cells from normal cells with a dark-field microscope due to EGFR over-expressed in many malignant epithelial tumour cells. In contrast to organic fluorophores and quantum dots, Au NRs have considerable advantages such as biocompatibility, no photobleaching or decomposition, and an enhanced absorption and scattering signal (Ma *et al.* 2013).

Au NRs are very attractive means for photothermal therapy due to their modifiable absorption in the NIR region and higher photothermal conversion efficiency than most other shapes of gold nanostructures, such as Au NPs and gold nanoshells. Tong *et al.* (2007) investigated the photothermal effects of folate-conjugated Au NRs to human malignant nasopharyngeal carcinoma cells and found that the photothermolysis of cancer cells with a high expression of folate receptors was much more effective than that of normal cells with fewer folate receptors.

Apart from photothermal therapy, Au NRs represent a good option for drug delivery and the photothermal effect can be used to actively release drugs. Alkilany *et al.* (2008) employed the hydrophobic region near the Au NR surface provided by CTAB bilayer to sequester a model drug-1-naphthol. Alper *et al.* (2009) studied the controlled release behaviour of fluorescence dye loaded Au NRs under laser irradiation.

In terms of the detection sensitivity of plasmon spectroscopy, Au NRs exhibit higher refractive index sensitivities, which is typically  $\sim 250$  nm per refractive index unit compared with  $\sim 60$  nm per refractive index unit for spherical nanostructures, which make the use of Au NRs the platform of choice when increased sensitivity is required (Chen *et al.* 2008; Guo *et al.* 2015).

## **6.2 Experimental**

### **6.2.1 Materials and Methods**

CTAB and Au NRs stabilized with CTAB aqueous solution were purchased from Sigma Aldrich, UK. The mean size of the NRs was  $45 \pm 5$  and  $10 \pm 1$  nm in longitudinal and transverse directions, respectively.

### **6.2.2 Preparation of NRs**

To remove the excess amount of CTAB included in the stock dispersion of the NRs, the dispersion was centrifuged (11, 000 rpm for 15 min at 37 °C). The supernatant was decanted and the precipitated NRs were dispersed in 10 mM HEPES (pH 7.2) with a final optical density of 0.2. Since the obtained NR dispersion was stable for 24 hours, the dispersion was used for the assay within 2 h after the preparation.

### **6.2.3 Functionalization of Au NRs with Peptide Ligands**

GPDC and VP-EN-DC peptides were evaluated for their coupling to Au NR and their potential in development of effective sensing system for DPP-IV/CD26 activity. The Au NRs, stabilized with CTAB, were further modified with GPDC peptide in the first trial and with VP-EN-DC in the second trial at room temperature to form the molecular probes for target detection. Each peptide was incubated with the Au NRs solution separately in a 1:10 (v/v) and the reaction mixture was set aside to react for 2 hours at room temperature. After incubation, the suspensions were centrifuged twice using 5000 rpm for 10 min using an Eppendorf centrifuge (Eppendorf, Germany), decanted and redispersed in deionized water.

### **6.2.4 Instrumental technique**

The same UV-Visible spectroscopy instrumentation methods were used as in section 3.2.3.

### 6.3 Results and Discussion

In general, Au NRs exhibit two SPR bands, namely, the transverse band and the longitudinal band, corresponding to the oscillation of electrons along the short and long axis Au NR respectively. In this study, the Au NRs showed a strong and broad longitudinal absorption band at 840 nm and the transverse absorption band at 510 nm (Fig. 6-3). Au NRs were further modified with peptide ligand to form molecular probes used for the target detection.

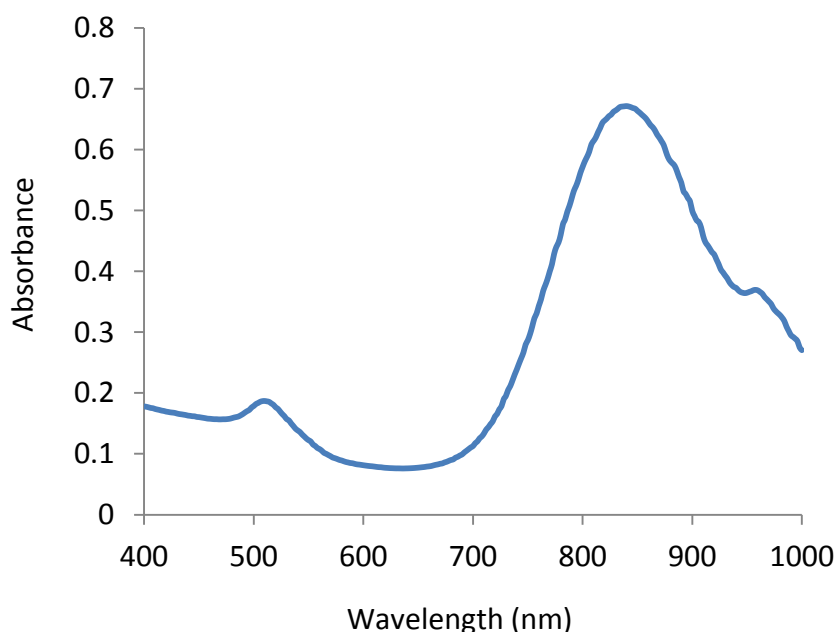


**Figure 6-3** UV–visible absorption spectrum of Au NRs (Sigma Aldrich 716839). The figure shows a transverse absorption band at 510 nm and a longitudinal absorption band at 840 nm corresponding to the oscillation of electrons along the short and long axis of Au NRs respectively.

Coupling of GPDC peptide to the Au NRs resulted in a formation of one large peak at 976 nm and (Fig. 6-4) and disappearance the small peak and fading of the brown coloration of the Au NR suspension suggesting that the coupling process led to aggregation of the Au NRs and that this may have taken place due to the cationic nature of Au NRs, derived from an adsorbed CTAB, used in this study. The NRs were aggregated by addition of anionic substrate peptide (GPDC) due to neutralization of the surface charge.

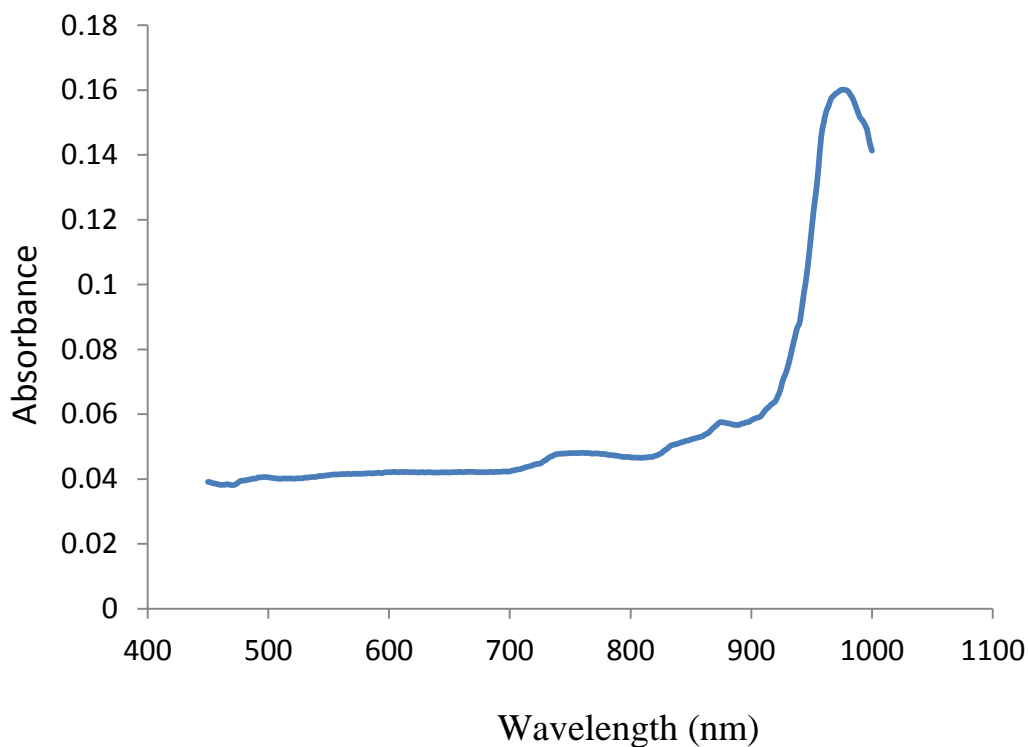


**Figure 6-4** UV-Vis absorption spectra of GPDC capped Au NRs

UV-visible spectra of Au NRs after conjugation with VP-EN-DC peptide ligands show that there was a slight red shift in both longitudinal and transverse absorption peaks after conjugation with capture probes (Fig. 6-5). This is due to the change in the refractive index of the medium upon the binding the VP-EN-DC peptide with the Au NRs. The slight broadening in the peaks has taken place due to the increase in size of the conjugates after interaction of the Au NRs with peptide ligand.

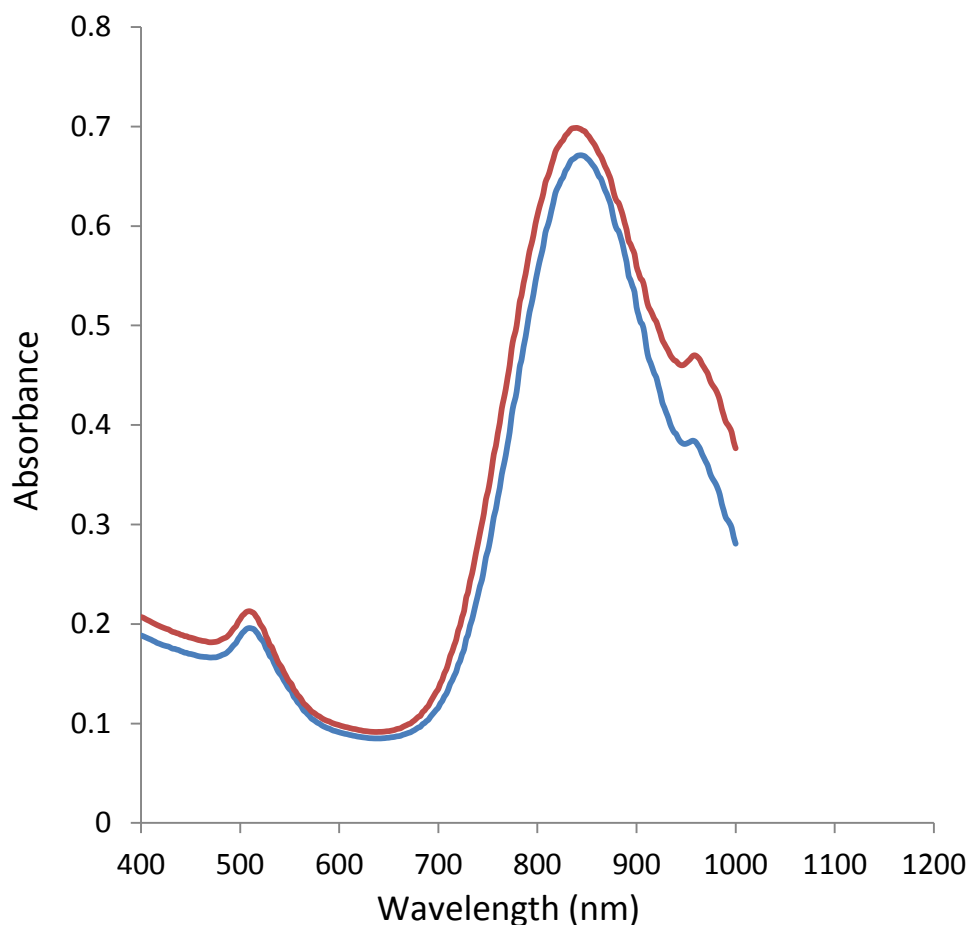


**Figure 6-5** UV-Visible absorption spectra of dispersed -Au NRs (blue) and VP-EN-DC capped Au NPs (red).

The addition of DPP-IV/CD26 to the VP-EN-DC functionalized Au NRs resulted in discoloration of the Au NRs and clear alteration of the absorption spectra, which may indicate the Au NR solution was not stable enough and to further support this claim, a buffer solution without enzyme was added to the Au NRs solution and caused a similar discoloration of the Au NR solution (Fig. 6-6).

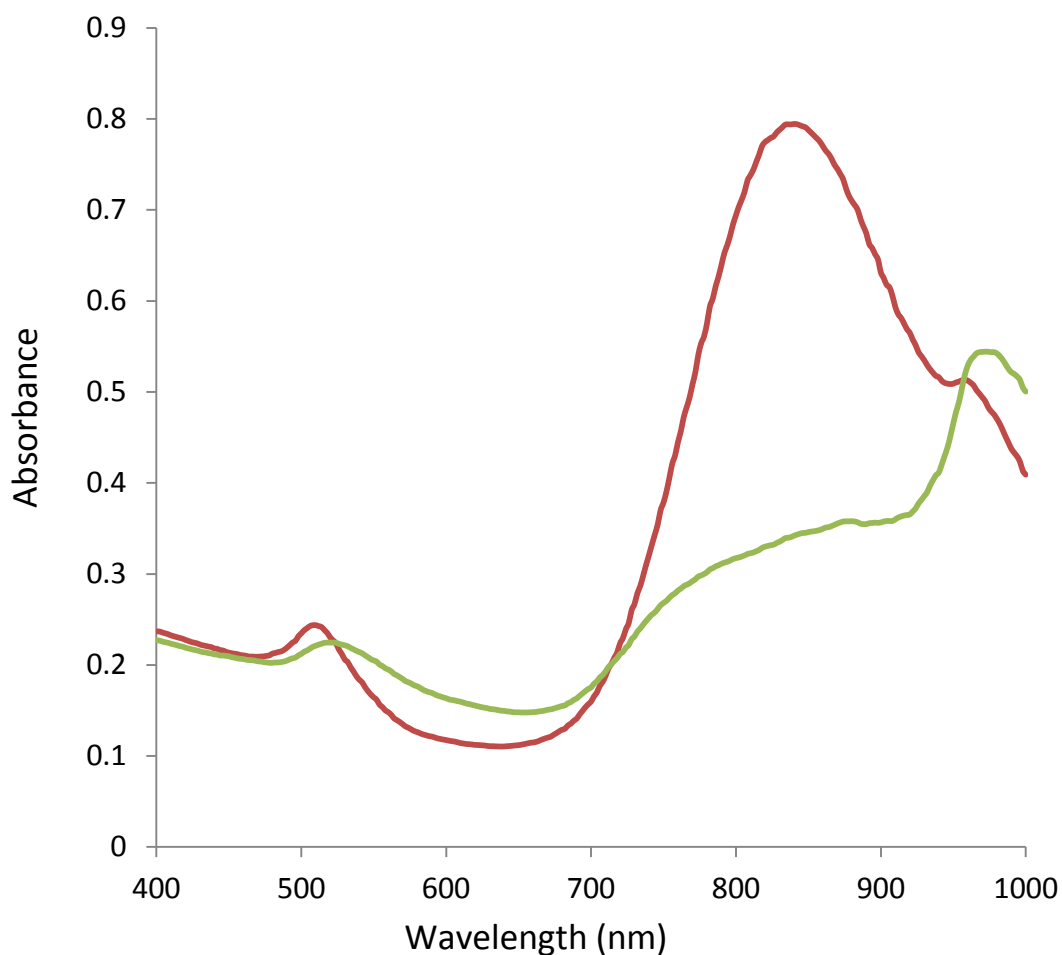


**Figure 6-6** DPP-IV/CD26 activity detection using a VP-EN-DC modified Au NR assay. Addition of DPP-IV/CD26 to the peptide modified Au NR (red) resulted in a shift and of the absorption band and discoloration of the solution (green).

#### 6.4 Conclusion

Spherical Au NPs have been used in various biomedical applications. However, they have not been optimized because spherical gold nanoparticles have limited peak absorptions (maximum ~580nm for 100nm diameter particles) which fall below the transmission window of 650 – 900nm for biological entities (skin, tissue and hemoglobin). Au NRs behave similarly to the gold nanoparticles, but are elongated to optimize their peak absorption and scattering characteristics. This allows the ability to tune the NR absorption from 550nm to 1400nm through different manufacturing processes

A preliminary study on development of Au NR colorimetric sensing assay for the detection of DPP-IV/CD26 activity was conducted. Although the assay still needs further optimization for detection of the target enzyme in terms of achieving an alternative and more powerful sensing methods, but it still provided a basis for further exploration and investigation.

The effect of ligand (peptide) net charge is one of important issue that need to be considered in the design of Au NR sensor as has been observed in this study. A possible explanation for the discoloration seen with the GPDC peptide is the electrostatic attraction of a negatively charged peptide with the positively charged CTAB capped Au NRs.

## **Chapter 7**

---

### **Conclusions and Future Work**

---

## Conclusions and Future Work

The design and use of nanomaterial platforms functionalized with peptide substrates in the development of a fast, robust and reproducible colorimetric tool for detection and quantitation of DPP-IV/CD26 activity is reported in this thesis. The enzyme has great potential to be used in the prognosis or diagnosis of diseases in which DPP-IV/CD26 are implied as well as for HTS of pharmaceutical targets for DPP-IV/CD26 activity. The research involved the design of potential DPP-IV peptide substrates and their use in the functionalization of Au NPs. The application of these functionalized Au NP systems in the assay of DPP-IV/CD26 activity was assessed both qualitatively and quantitatively. Various optimization and validation experiments were conducted to determine and validate the sensitivity, stability and enzyme kinetics.

In Chapters 3 and 4 the successful development of two individual approaches, both utilising Au NP-peptide conjugates, for the detection of the peptidase activity were presented (Table 7-1). The goal was to develop an accurate, sensitive and easily prepared assay for the detection of the peptidase activity. The design of the assay reflected these goals at each step of the process. The use of peptide substrates that can be hydrolysed by DPP-IV/CD26 enzyme relied on a thorough literature review about the mechanism of action of the enzyme besides investigating problems associated with the use of traditional substrates with the aim of providing stable Au NP colloidal solutions as well as serving as the bio recognition element for the enzyme. Comparing the level of enzyme activity that can be measured using the developed assays mentioned in table 7-1 with the enzyme activity in various pathological conditions (Table 1-4) it can be concluded that with the use of appropriate dilutions it possible to use these assays can as diagnostic and prognostic tool for many disease conditions.

**Table 7-1** Summary of the performance of developed assays

Assay	LOD U/L	Dynamic range
Gly-Pro-Asp-Cys Au NPs	1	2-12
Val-Pro-ED-Asp-Cys Au NPs	1.5	0-40

Conjugation of peptides and proteins to Au NPs mainly depends upon different mechanisms such as, dative binding between the gold conducting electrons and sulphur atoms which are present in cysteine residues (if present) in the protein and ionic attraction between the gold nanoparticles and the proteins (Bastús *et al.* 2009). In some proteins, the sulphhydryl functionality may be in the form of a disulphide group and in other proteins sulphhydryl sites may be buried within the protein structure, and therefore inaccessible to the Au NPs (Maus *et al.* 2010). The coupling process of peptides to the NP surface in this work relied on a ligand exchange process, in which thiolate or cysteine-capped peptide substituted citrate, as the former has stronger binding efficiency with the metal surface (Häkkinen 2012).

It was also observed that conjugation of peptides to NPs was higher with the concentrated peptide solution than diluted one. Peptide conjugation efficiencies were improved by gentle agitation of the mixture after addition of the peptide, since generating air bubbles by vigorous agitation may denature the peptide solution or promote oxidation of thiol groups catalysed by atmospheric oxygen (Hainfeld 1988). However, once the optimal conditions were identified, the coating process was usually reproducible and was easy to scale-up.

Factors, such as pH, ionic strength and the structure of the substrate, that influence the assay efficiency were investigated in order to optimize these parameters to provide a well-designed biosensing platform, that can function in complex biological samples. It was found that the assay is responsive over an acceptable range of pH (7-9), at lower pH it loses responsiveness gradually, whilst at pH > 9 colour changes were not observed,

which can be attributed to conformational changes in the enzyme itself and not the functionalized Au NPs.

Several analytical tools have been employed to investigate and confirm attachment of the different peptides or thiol containing molecules to the Au NP surface and these included direct and indirect methods. XPS was utilized to provide direct evidence of thiolate interaction with the metal surface, by studying changes in the binding energy of the involved elements. Moreover, further characterization was conducted using a range of techniques including UV-Visible spectrophotometry, hydrodynamic radius measurements by DLS, zeta potential, FTIR and gel electrophoresis, to investigate changes to the physical and chemical properties of the modified Au NPs. These techniques provided further information about size, charge and molecular weight changes after modification of the NP surface with various ligands.

Results showed that upon the addition of DPP-IV/CD26, the peptides were cleaved resulting in detectable optical changes due to the distance-dependent change between neighbouring molecules. The SPR based colour shift was due to the coupling of Au NPs mediated by the specific interaction of DPP-IV/CD26 and designed peptide molecules, demonstrated that the NPs can be potentially used as molecular labels for detection of DPP-IV/CD26 associated diseases.

As this colorimetric assay was based on aggregation of colloidal particles, it was critical to have a design that offers easy surface modification and a fast-colorimetric response and for this purpose, a non-crosslinking aggregation of Au NPs was chosen. In contrast to the DPP-IV/CD26 colorimetric Au NP assay recently developed by Xia and colleagues (2016), which relied on the formation of crosslinked aggregates, the design of a non-crosslinking aggregation method for detection of DPP-IV enzyme activity was considered to be more appropriate as it overcomes the limitation encountered with crosslinking aggregation as it offers more robust assay for use in biological fluids,

eliminates the need for designing target analytes with two or more binding sites and creates a hindrance free environment for the peptidase activity of the enzyme.

Herein, a new concept is demonstrated that overcomes this limitation by achieving enzyme-responsive nanoparticle systems that are not only sensitive and reliable, but also universal, simple, and economical in operation. The recognition sites of proteases are typically short, as shown in Chapter 4; our system was composed of two elements: functional Au NP probe and an appropriate diamine linker that can couple with both distal bio recognition site from one hand and with anchoring part from the other hand.

Quantification of the enzymatic hydrolysis of the peptide substrates and relating the value to the enzyme activity was developed using a UV- visible spectrophotometer that was able to show in real-time the increase in absorbance at higher wavelengths (650 nm or more) and decrease in absorbance at around (520 nm) with the addition of DPP-IV/CD26.

The first method developed for the assay of DPP-IV/CD26 (GPDC Au NPs) was able to quantify the detection of DPP-IV/CD26 activity ranging from 2 U/L to 12 U/L. In order to enhance the quantification capability of this assay, another ligand was designed, which incorporated a spacer molecule (ethylene diamine) as the spacer, which should increase the distance of the hydrolysable moiety from the NP surface and impart further stability on the Au NP system. This system (VP-EN-DC Au NPs) met these expectations by increasing the linear dynamic range of the assay by a factor of 3.5-4, so that changes in DPP-IV/CD26 activity over a broader range (0-40 U/L) thus providing a method that can be used to determine the levels of DPP-IV/CD26 in physiological fluids such as serum and plasma. This assay was also used to evaluate a DPP-IV inhibitor potency, which demonstrates its use as a HTS tool for pharmaceuticals.

In the development of colorimetric sensing assays for routine use in biological samples, it is important to take cognisance of the fact that the interferences caused by cellular

components and macromolecules can affect the analytical performance of the sensor. Nevertheless, some reports of measurement of enzyme activity via Au NPs in cell lysates have shown promising results (Oishi *et al.* 2007, Kang *et al.* 2010). In complex samples, such as serum, saliva or cerebrospinal fluid, Au NPs surfaces are exposed to biomolecules, cells, and tissues which can potentially impair the performance of the measurement. The occurrence of nonspecific binding and ligand exchange should be taken into account when developing biosensing applications. These interferences must be carefully studied during method validation. Potential interferences can occur when charge bearing ligands interact non-specifically with other charged biomolecules (Aldewachi *et al.* 2018).

Significantly, it is expected that this approach can be directed toward a wide variety of enzymes by simply changing the recognition sequence found beyond the diamine linker. Furthermore, this system enables assaying of DPP-IV activity and screen its inhibitors. The unique optical properties of Au NPs and the recognition sequence of the protease make this novel assay not only sensitive and reliable, but also universally applicable in its operation and easily adaptable to HTS. In addition, the assay presented here is simpler in format than that presented by Xia *et al.* (2016). It involves only a single step for detection of DPP-IV activity, which offers the advantages of simplicity and cost efficiency.

Validation experiments were conducted by comparing the performance of developed nano platform assay described in Chapter 4 with the standard Gly-Pro-pNA assay, which is still considered as the gold standard method for detection and evaluation of DPP-IV/CD26 activity. Linear regression analysis showed that results obtained from the VP-EN-DC capped Au NP assay correlated well with the standard commercial colorimetric assay.

The potential instability of Au NPs in high ionic strength solutions was of concern after the GPDC modified Au NPs experienced an electrolyte induced aggregation, reported in Chapter 5. Many approaches have been trialled to overcome this problem, which included the incorporation of stabilizer peptide sequence or PEGylated ligand molecules decorated with the biorecognition element or bifunctionalization of Au NPs by modifying the NPs surface with two different peptide sequences. Although much more stable Au NP systems were achieved by all of these three approaches, a colorimetric response was only achieved using the bifunctionalized Au NP assay. The major problem observed was that at times the colloidal solution was too stable because the hindrance effect caused by non-functional (stabilizer) ligand in the case of bifunctionalized Au NP was observed.

In Chapter 6 the work conducted on the development of an Au NR colorimetric detection assay for the DPP-IV/CD26 activity was reported. The assay sought to create a highly sensitive detection assay for protease detection. The Au NR experiments were unsuccessful in the detection of DPP-IV/CD26 activity due to limited trials and difference in the surface charge of Au NRs, which is governed by the surfactant coating of CTAB, but the knowledge that was gained of the peptide functionalisation could pave the way for further investigation of Au NRs to the development of highly sensitive and stable assay for detection of the protease activity.

Biological tests detecting the activity of target analytes have become faster, more sensitive and more flexible when nanoscale particles are used as sensors, with several benefits over more conventional methods, such as fluorescence and chemiluminescence technology (Baptista *et al.* 2008). The system developed here is portable and would permit on-site analysis of samples, reducing the need for laboratory testing. It is also sensitive and rapid and could be useful for a range of applications. Additional features of this assay include fast response time, less interference from non-analyte components,

and kinetic data is obtained with high resolution and real time monitoring of enzyme activity. The final result of this project was the development of a convenient colorimetric biosensor for the identification of disease-related DPP-IV/CD26 protease enzyme, which offers a real alternative approach from traditional assays, without the need for complex instrumentation.

The Integration of labelled Au NPs in microfluidics testing device is another important concern to pave the road to efficient strategies with enhanced performance and reduced complexity, e.g., Aptamers were tethered to Au NPs as part of a lateral flow assay-like dry-reagent assay strip to detect thrombin (Xu *et al.* 2008). Noble metal NPs are attractive for lateral flow POC diagnostics because they are visible without an external excitation source or emission sensor, and unlike small-molecule dyes, resist photobleaching. These sensing schemes have the potential to be involved in designing Au NP coupled microfluidic chips for POC biochemical assays. The logical next step in this research would be the continuation of experiments to transform this test into a lateral flow assay format that could offer an early detection tool for disease management in resource restrained parts of the world.

# References

---

- Abad, J. M., Mertens, S. F., Pita, M., Fernández, V. M. & Schiffrin, D. J.** 2005. Functionalization of thioctic acid-capped gold nanoparticles for specific immobilization of histidine-tagged proteins. *Journal of the American Chemical Society*, **127**, 5689-5694.
- Abbott, C. A., Yu, D. M., Woollatt, E., Sutherland, G. R., McCaughan, G. W. & Gorrell, M. D.** 2000. Cloning, expression and chromosomal localization of a novel human dipeptidyl peptidase (DPP) IV homolog, DPP8. *European Journal of Biochemistry*, **267**, 6140-6150.
- Agasti, S. S., Rana, S., Park, M., Kim, C. K., You, C. & Rotello, V. M.** 2010. Nanoparticles for detection and diagnosis. *Advanced Drug Delivery Reviews*, **62**, 316-328.
- Ahlbom, A., Bridges, J., De Jong, W., Jung, T., Mattsson, O., Pagès, J., Rydzynski, K., Stahl, D. & Thomsen, M.** 2009. Scientific Committee on Emerging and Newly Identified Health Risks SCENIHR Risk Assessment of Products of Nanotechnologies.
- Ahmed, R. H., Huri, H. Z., Al-Hamodi, Z., Salem, S. D. & Muniandy, S.** 2015. Serum levels of soluble CD26/dipeptidyl peptidase-IV in type 2 diabetes mellitus and its association with metabolic syndrome and therapy with antidiabetic agents in malaysian subjects. *PloS One*, **10**, e0140618.
- Ahmed, S. & Ikram, S.** 2016. Biosynthesis of gold nanoparticles: A green approach. *Journal of Photochemistry and Photobiology B: Biology*, **161**, 141-153.
- Aili, D., Selegård, R., Baltzer, L., Enander, K. & Liedberg, B.** 2009. Colorimetric protein sensing by controlled assembly of gold nanoparticles functionalized with synthetic receptors. *Small*, **5**, 2445-2452.
- Aioub, M., Panikkanvalappil, S. R. & El-Sayed, M. A.** 2017. Platinum-Coated Gold Nanorods: Efficient Reactive Oxygen Scavengers That Prevent Oxidative Damage Toward Healthy, Untreated Cells During Plasmonic Photothermal Therapy. *ACS nano*, **11**, 579-586.
- Aldewachi, H.S., Woodroffe, N., Turega, S. and Gardiner, P.H.,** 2017. Optimization of gold nanoparticle-based real-time colorimetric assay of dipeptidyl peptidase IV activity. *Talanta*, **169**, 13-19.
- Aldewachi, H.S., Chalati, T., Woodroffe, N., Bricklebank, N., Sharrack B. and Gardiner, P.H.,** 2018. Gold Nanoparticle-Based Colorimetric Biosensors. *Nanoscale*, In press.
- Ali-Löytty, H., Louie, M. W., Singh, M. R., Li, L., Sanchez Casalongue, H. G., Ogasawara, H., Crumlin, E. J., Liu, Z., Bell, A. T. & Nilsson, A.** 2016. Ambient-pressure XPS study of a Ni-Fe electrocatalyst for the oxygen evolution reaction. *The Journal of Physical Chemistry C*, **120**, 2247-2253.
- Alivisatos, A. P.** 1996. Perspectives on the physical chemistry of semiconductor nanocrystals. *The Journal of Physical Chemistry*, **100**, 13226-13239.

- Alivisatos, P.** 2004. The use of nanocrystals in biological detection. *Nature Biotechnology*, **22**, 47-52.
- Al-Johani, H., Abou-Hamad, E., Jedidi, A., Widdifield, C.M., Viger-Gravel, J., Sangaru, S.S., Gajan, D., Anjum, D.H., Ould-Chikh, S., Hedhili, M.N. and Gurinov, A.**, 2017. The structure and binding mode of citrate in the stabilization of gold nanoparticles. *Nature Chemistry*, **9**, 890.
- Alkilany, A.M., Abulateefeh, S.R., Mills, K.K., Bani Yaseen, A.I., Hamaly, M.A., Alkhatib, H.S., Aiedeh, K.M. and Stone, J.W.**, 2014. Colloidal stability of citrate and mercaptoacetic acid capped gold nanoparticles upon lyophilization: effect of capping ligand attachment and type of cryoprotectants. *Langmuir*, **30**, 13799-13808.
- Alkilany, A. M., Thompson, L. B., Boulos, S. P., Sisco, P. N. & Murphy, C. J.** 2012. Gold nanorods: their potential for photothermal therapeutics and drug delivery, tempered by the complexity of their biological interactions. *Advanced Drug Delivery Reviews*, **64**, 190-199.
- Amendola, V., Pilot, R., Frasconi, M., Maragò, O.M. and Iati, M.A.**, 2017. Surface plasmon resonance in gold nanoparticles: a review. *Journal of Physics: Condensed Matter*, **29**, 203002-203049.
- Angus, J. C., Morrow, D. L., Dunning, J. W. & French, M. J.** 1969. Motion Measurement by Laser Doppler Techniques. *Industrial & Engineering Chemistry*, **61**, 8-20.
- Anker, J. N., Hall, W. P., Lyandres, O., Shah, N. C., Zhao, J. & Van Duyne, R. P.** 2008. Biosensing with plasmonic nanosensors. *Nature Materials*, **7**, 442-453.
- Ansorge, S. & Langner, J.** 1997. *Cellular Peptidases in Immune Functions and Diseases*. : Springer Science & Business Media, New York. Google books. Web. 29 June 2013 <http://books.google.com>
- Aratake, Y., Umeki, K., Kiyoyama, K., Hinoura, Y., Sato, S., Ohno, A., Kuribayashi, T., Hirai, K., Nabeshima, K. & Kotani, T.** 2002. Diagnostic utility of galectin-3 and CD26/DPPIV as preoperative diagnostic markers for thyroid nodules. *Diagnostic Cytopathology*, **26**, 366-372.
- Aryal, S., KC, R. B., Bhattarai, N., Kim, C. K. & Kim, H. Y.** 2006a. Study of electrolyte induced aggregation of gold nanoparticles capped by amino acids. *Journal of Colloid and Interface Science*, **299**, 191-197.
- Aryal, S., Remant, B., Dharmaraj, N., Bhattarai, N., Kim, C. H. & Kim, H. Y.** 2006b. Spectroscopic identification of S Au interaction in cysteine capped gold nanoparticles. *Spectrochimica Acta Part A: Molecular and Biomolecular Spectroscopy*, **63**, 160-163.
- Atkins, P., Paula, J. d. & Peter Atkins, Julio de Paula.** 2010. *Atkins Physical Chemistry. Vol 1+ Vol 2+ Student Solutions Manual*. WH Freeman.
- Bain, C.D., Biebuyck, H.A. and Whitesides, G.M.**, 1989. Comparison of self-assembled monolayers on gold: coadsorption of thiols and disulfides. *Langmuir*, **5**, 723-727.
- Balasubramanian, S. K., Yang, L., Yung, L. L., Ong, C., Ong, W. & Liya, E. Y.** 2010. Characterization, purification, and stability of gold nanoparticles. *Biomaterials*, **31**, 9023-9030.

- Ban, Z., Bosques, C. J. & Sasisekharan, R.** 2008. A simple assay to probe disease-associated enzyme activity using glycosaminoglycan-assisted synthesized gold nanoparticles. *Organic & biomolecular chemistry*, **6**, 4290-4292.
- Baptista, P., Pereira, E., Eaton, P., Doria, G., Miranda, A., Gomes, I., Quaresma, P. & Franco, R.** 2008. Gold nanoparticles for the development of clinical diagnosis methods. *Analytical and Bioanalytical Chemistry*, **391**, 943-950.
- Baraton, M.** 2002. Surface analysis of semiconducting nanoparticles by FTIR spectroscopy. In: *Nanocrystalline Metals and Oxides* (Ed. by Anonymous ), 165-187. Springer.
- Bartczak, D. & Kanaras, A. G.** 2011. Preparation of peptide-functionalized gold nanoparticles using one pot EDC/sulfo-NHS coupling. *Langmuir*, **27**, 10119-10123.
- Bastús, N.G., Sánchez-Tilló, E., Pujals, S., Farrera, C., López, C., Giralt, E., Celada, A., Lloberas, J. and Puentes, V.,** 2009. Homogeneous conjugation of peptides onto gold nanoparticles enhances macrophage response. *ACS Nano*, **3**, 1335-1344.
- Basu, S., Ghosh, S. K., Kundu, S., Panigrahi, S., Praharaj, S., Pande, S., Jana, S. & Pal, T.** 2007. Biomolecule induced nanoparticle aggregation: effect of particle size on interparticle coupling. *Journal of Colloid and Interface Science*, **313**, 724-734.
- Baticic Pucar, L., Pernjak Pugel, E., Detel, D. & Varljen, J.** 2017. Involvement of DPP IV/CD26 in cutaneous wound healing process in mice. *Wound Repair and Regeneration*, **25**, 25-40.
- Becker, R. & Döring, W.** 1935. Kinetische behandlung der keimbildung in übersättigten dämpfen. *Annalen der Physik*, **416**, 719-752.
- Beerbom, M., Gargagliano, R. & Schlaf, R.** 2005. Determination of the electronic structure of self-assembled L-cysteine/Au interfaces using photoemission spectroscopy. *Langmuir*, **21**, 3551-3558.
- Bella, A. M., Erickson, R. H. & Kim, Y. S.** 1982. Rat intestinal brush border membrane dipeptidyl-aminopeptidase IV: kinetic properties and substrate specificities of the purified enzyme. *Archives of Biochemistry and Biophysics*, **218**, 156-162.
- Bercu, B. B. & Walker, R. F.** 2012. *Growth Hormone Secretagogues*. : Springer Science & Business Media.
- Bergamini, L., Voliani, V., Cappello, V., Nifosi, R. & Corni, S.** 2015. Non-linear optical response by functionalized gold nanospheres: identifying design principles to maximize the molecular photo-release. *Nanoscale*, **7**, 13345-13357.
- Berne, B. J. & Pecora, R.** 2013. *Dynamic Light Scattering: With Applications to Chemistry, Biology, and Physics*. : Courier Corporation.
- Bhattacharjee, R. R., Das, A. K., Haldar, D., Si, S., Banerjee, A. & Mandal, T. K.** 2005. Peptide-assisted synthesis of gold nanoparticles and their self-assembly. *Journal of Nanoscience and Nanotechnology*, **5**, 1141-1147.

- Bishnoi, S. W., Rozell, C. J., Levin, C. S., Gheith, M. K., Johnson, B. R., Johnson, D. H. & Halas, N. J.** 2006. All-optical nanoscale pH meter. *Nano letters*, **6**, 1687-1692.
- Blanco-Prieto, S., Vázquez-Iglesias, L., Rodríguez-Girondo, M., Barcia-Castro, L., Fernández-Villar, A., Botana-Rial, M. I., Rodríguez-Berrocal, F. J. & de la Cadena, María Páez.** 2015. Serum calprotectin, CD26 and EGF to establish a panel for the diagnosis of lung cancer. *PLoS One*, **10**, e0127318.
- Blatchford, C., Campbell, J. & Creighton, J.** 1982. Plasma resonance—enhanced raman scattering by absorbates on gold colloids: the effects of aggregation. *Surface Science*, **120**, 435-455.
- Boccardi, V., Marano, L., Rossetti, R. R. A., Rizzo, M. R., di Martino, N. & Paolisso, G.** 2015. Serum CD26 levels in patients with gastric cancer: a novel potential diagnostic marker. *BMC Cancer*, **15**, 703.
- Bohren, C. F. & Huffman, D. R.** 2008. *Absorption and Scattering of Light by Small Particles*. : John Wiley & Sons.
- Boinovich, L.** 2010. DLVO forces in thin liquid films beyond the conventional DLVO theory. *Current Opinion in Colloid & Interface Science*, **15**, 297-302.
- Boisselier, E. & Astruc, D.** 2009. Gold nanoparticles in nanomedicine: preparations, imaging, diagnostics, therapies and toxicity. *Chemical Society Reviews*, **38**, 1759-1782.
- Boisselier, E., Salmon, L., Ruiz, J. & Astruc, D.** 2008. How to very efficiently functionalize gold nanoparticles by “click” chemistry. *Chemical Communications*, , 5788-5790.
- Boonacker, E. & Van Noorden, C. J.** 2003. The multifunctional or moonlighting protein CD26/DPPIV. *European Journal of Cell Biology*, **82**, 53-73.
- Bovin, J. & Malm, J.** 1991. Atomic resolution electron microscopy of small metal clusters. *Zeitschrift für Physik D Atoms, Molecules and Clusters*, **19**, 293-298.
- Bourg, M.C., Badia, A. and Lennox, R.B.,** 2000. Gold– sulfur bonding in 2D and 3D self-assembled monolayers: XPS characterization. *The Journal of Physical Chemistry B*, **104**, 6562-6567.
- Bower, P., Louie, E., Long, J., Stayton, P. & Drobny, G.** 2005. Solid-state NMR structural studies of peptides immobilized on gold nanoparticles. *Langmuir*, **21**, 3002-3007.
- Brack, M.** 1993. The physics of simple metal clusters: self-consistent jellium model and semiclassical approaches. *Reviews of modern physics*, **65**, 677.
- Brogie, L. d.** 1924. XXXV. A tentative theory of light quanta. *Philosophical Magazine Series 6*, **47**, 446-458.
- Broxmeyer, H. E.** 2008. Chemokines in hematopoiesis. *Current Opinion in Hematology*, **15**, 49-58.

- Brust, M., Fink, J., Bethell, D., Schiffrin, D. & Kiely, C.** 1995. Synthesis and reactions of functionalised gold nanoparticles. *Journal of the Chemical Society, Chemical Communications*, , 1655-1656.
- Brust, M., Walker, M., Bethell, D., Schiffrin, D. J. & Whyman, R.** 1994. Synthesis of thiol-derivatised gold nanoparticles in a two-phase liquid–liquid system. *Journal of the Chemical Society, Chemical Communications*, **7**, 801-802.
- Buckley, S. J., Collins, P. J. & O'Connor, B. F.** 2004. The purification and characterisation of novel dipeptidyl peptidase IV-like activity from bovine serum. *The International Journal of Biochemistry & Cell Biology*, **36**, 1281-1296.
- Bürgi, T.** 2015. Properties of the gold–sulphur interface: from self-assembled monolayers to clusters. *Nanoscale*, **7**, 15553-15567.
- Bušek, P., Malík, R. & Šedo, A.** 2004. Dipeptidyl peptidase IV activity and/or structure homologues (DASH) and their substrates in cancer. *The International Journal of Biochemistry & Cell Biology*, **36**, 408-421.
- Cao, Y., Yu, J., Bo, B., Shu, Y. & Li, G.** 2013. A simple and general approach to assay protease activity with electrochemical technique. *Biosensors and Bioelectronics*, **45**, 1-5.
- Champness, P. E.** 2001. *Electron Diffraction in the Transmission Electron Microscope. RMS Microscopy Handbook no. 47.* : Oxford.: BIOS Scientific publishers Ltd.
- Chandrawati, R. & Stevens, M. M.** 2014. Controlled assembly of peptide-functionalized gold nanoparticles for label-free detection of blood coagulation Factor XIII activity. *Chemical Communications*, **50**, 5431-5434.
- Chen, C., Huang, C. & Chang, H.** 2010a. Label-free colorimetric detection of picomolar thrombin in blood plasma using a gold nanoparticle-based assay. *Biosensors and Bioelectronics*, **25**, 1922-1927.
- Chen, G., Xie, Y., Zhang, H., Wang, P., Cheung, H., Yang, M. & Sun, H.** 2014. A general colorimetric method for detecting protease activity based on peptide-induced gold nanoparticle aggregation. *RSC Advances*, **4**, 6560-6563.
- Chen, H., Shao, L., Li, Q. & Wang, J.** 2013. Gold nanorods and their plasmonic properties. *Chemical Society Reviews*, **42**, 2679-2724.
- Chen, H., Kou, X., Yang, Z., Ni, W. & Wang, J.** 2008. Shape-and size-dependent refractive index sensitivity of gold nanoparticles. *Langmuir*, **24**, 5233-5237.
- Chen, J., Wang, D., Xi, J., Au, L., Siekkinen, A., Warsen, A., Li, Z., Zhang, H., Xia, Y. & Li, X.** 2007. Immuno gold nanocages with tailored optical properties for targeted photothermal destruction of cancer cells. *Nano Letters*, **7**, 1318-1322.
- Chen, L., Annis, I. & Barany, G.** 2001. Disulfide bond formation in peptides. *Current Protocols in Protein Science*, , 18.6. 1-18.6. 19.

- Chen, R., Wu, J., Li, H., Cheng, G., Lu, Z. & Che, C.** 2010b. Fabrication of gold nanoparticles with different morphologies in HEPES buffer. *Rare Metals*, **29**, 180-186.
- Cheng, F., He, Y., Xing, X., Tan, D., Lin, Y., Pang, D. & Tang, H.** 2015. A gold nanoparticle-based label free colorimetric aptasensor for adenosine deaminase detection and inhibition assay. *Analyst*, **140**, 1572-1577.
- Cheng, J., Sun, Y., Zhou, L., Zhang, K., Wang, J., Wu, Z. & Pei, R.** 2014. Phosphorylation triggered poly-nanoparticle assembly for naked-eye distinguishable T4 polynucleotide kinase detection. *RSC Advances*, **4**, 56731-56735.
- Cheng, W., Dong, S. & Wang, E.** 2003. Synthesis and self-assembly of cetyltrimethylammonium bromide-capped gold nanoparticles. *Langmuir*, **19**, 9434-9439.
- Cheong, S., Watt, J. D. & Tilley, R. D.** 2010. Shape control of platinum and palladium nanoparticles for catalysis. *Nanoscale*, **2**, 2045-2053.
- Chow, M. & Zukoski, C.** 1994. Gold sol formation mechanisms: role of colloidal stability. *Journal of colloid and interface science*, **165**, 97-109.
- Chu, B.** 2008. Dynamic light scattering. In: *Soft Matter Characterization* (Ed. by Anonymous ), pp. 335-372. Springer.
- Chung, K., Cheng, J., Suen, C., Huang, C., Tsai, C., Huang, L., Chen, Y., Wang, A. H., Jiaang, W. & Hwang, M.** 2010. The dimeric transmembrane domain of prolyl dipeptidase DPP-IV contributes to its quaternary structure and enzymatic activities. *Protein Science*, **19**, 1627-1638.
- Chusuei, C. C. & Goodman, D. W.** 2002. X-ray photoelectron spectroscopy. *Encyclopedia of physical science and technology*, **17**, 921-938.
- Cobley, C. M., Chen, J., Cho, E. C., Wang, L. V. & Xia, Y.** 2011. Gold nanostructures: a class of multifunctional materials for biomedical applications. *Chemical Society Reviews*, **40**, 44-56.
- Coelho, S. C., Rangel, M., Pereira, M. C., Coelho, M. A. & Ivanova, G.** 2015. Structural characterization of functionalized gold nanoparticles for drug delivery in cancer therapy: a NMR based approach. *Physical Chemistry Chemical Physics*, **17**, 18971-18979.
- Cordero, O. J., Salgado, F. J. & Nogueira, M.** 2009. On the origin of serum CD26 and its altered concentration in cancer patients. *Cancer immunology, immunotherapy*, **58**, 1723-1747.
- Cordero, O. J., Varela-Calviño, R., López-González, T., Calviño-Sampedro, C., Viñuela, J. E., Mouriño, C., Hernández-Rodríguez, Í, Rodríguez-López, M., de la Iglesia, Bruno Aspe & Pego, J. M.** 2015. CD26 Expression on T Helper Populations and sCD26 Serum Levels in Patients with Rheumatoid Arthritis. *PloS one*, **10**, e0131992.
- Cordero, O. J., Ayude, D., Nogueira, M., Rodriguez-Berrocal, F. J. & de la Cadena, M. P.** 2000. Preoperative serum CD26 levels: diagnostic efficiency and predictive value for colorectal cancer. *British journal of cancer*, **83**, 1139-1146.
- Correa, S., Naranjo, A. & Herrera, A.** 2016. Biosynthesis and characterization of gold nanoparticles using extracts of tamarindus indica L leaves. **687**, 012082.

- Corrie, S., Coffey, J., Islam, J., Markey, K. & Kendall, M.** 2015. Blood, sweat, and tears: Developing clinically relevant protein biosensors for integrated body fluid analysis. *Analyst*, **140**, 4350-4364.
- Creighton, J. A. & Eadon, D. G.** 1991. Ultraviolet-visible absorption spectra of the colloidal metallic elements. *Journal of the Chemical Society, Faraday Transactions*, **87**, 3881-3891.
- Cunningham, D. F. & O'Connor, B.** 1997. Proline specific peptidases. *Biochimica et Biophysica Acta (BBA)-Protein Structure and Molecular Enzymology*, **1343**, 160-186.
- Dang, N. & Morimoto, C.** 2002. CD26: an expanding role in immune regulation and cancer. *Histology and Histopathology*, **17**, 1213-1226
- Daniel, M. & Astruc, D.** 2004. Gold nanoparticles: assembly, supramolecular chemistry, quantum-size-related properties, and applications toward biology, catalysis, and nanotechnology. *Chemical Reviews*, **104**, 293-346.
- Danks, A., Hall, S. & Schnepf, Z.** 2016. The evolution of 'sol-gel' chemistry as a technique for materials synthesis. *Materials Horizons*, **3**, 91-112.
- De Chiara, L., Rodríguez-Piñeiro, A. M., Cordero, O. J., Vázquez-Tuñas, L., Ayude, D., Rodríguez-Berrocal, F. J. & de la Cadena, María Páez.** 2014. Postoperative serum levels of sCD26 for surveillance in colorectal cancer patients. *PloS One*, **9**, e107470.
- De Gennes, P.** 1987. Polymers at an interface; a simplified view. *Advances in Colloid and Interface Science*, **27**, 189-209.
- de la Haba-Rodríguez, J., Macho, A., Calzado, M. A., Blázquez, M. V., Gomez, M. A., Muñoz, E. E. & Aranda, E.** 2002. Soluble dipeptidyl peptidase IV (CD-26) in serum of patients with colorectal carcinoma. *Neoplasma*, **49**, 307-311.
- De Vasconcelos, C., Pereira, M. & Fonseca, J.** 2005. Polyelectrolytes in solution and the stabilization of colloids. *Journal of Dispersion Science and Technology*, **26**, 59-70.
- Deacon, C. F.** 2011. Dipeptidyl peptidase-4 inhibitors in the treatment of type 2 diabetes: a comparative review. *Diabetes, Obesity and Metabolism*, **13**, 7-18.
- Delezuch, W., Marttinen, P., Kokki, H., Heikkinen, M., Vanamo, K., Pulkki, K. & Matinlauri, I.** 2012. Serum and CSF soluble CD26 and CD30 concentrations in healthy pediatric surgical outpatients. *Tissue Antigens*, **80**, 368-375.
- Demuth, H. & Heins, J.** 1995. Catalytic mechanism of dipeptidyl peptidase IV. *Dipeptidyl peptidase IV (CD26) in metabolism and the immune response*, ed. Fleischer, B. (R. G. Landes, Austin, TX), 1-35.
- Detel, D., Persic, M. & Varljen, J.** 2007. Serum and intestinal dipeptidyl peptidase IV (DPP IV/CD26) activity in children with celiac disease. *Journal of Pediatric Gastroenterology and Nutrition*, **45**, 65-70.

- Diez-Torrubia, A., Cabrera, S., De Meester, I., Camarasa, M., Balzarini, J. & Velázquez, S.** 2012. Dipeptidyl Peptidase IV-Activated Prodrugs of Anti-Varicella Zoster Virus Bicyclic Nucleoside Analogues Containing Different Self-Cleavage Spacer Systems. *ChemMedChem*, **7**, 1612-1622.
- Ding, X., Ge, D. & Yang, K.** 2014. Colorimetric protease assay by using gold nanoparticles and oligopeptides. *Sensors and Actuators B: Chemical*, **201**, 234-239.
- Dinkel, R., Braunschweig, B. & Peukert, W.** 2016. Fast and Slow Ligand Exchange at the Surface of Colloidal Gold Nanoparticles. *The Journal of Physical Chemistry C*, **120**, 1673-1682.
- Dixit, V., Van den Bossche, J., Sherman, D. M., Thompson, D. H. & Andres, R. P.** 2006. Synthesis and grafting of thioctic acid- PEG- folate conjugates onto Au nanoparticles for selective targeting of folate receptor-positive tumor cells. *Bioconjugate Chemistry*, **17**, 603-609.
- Dougan, J. A., Karlsson, C., Smith, W. E. & Graham, D.** 2007. Enhanced oligonucleotide-nanoparticle conjugate stability using thioctic acid modified oligonucleotides. *Nucleic Acids Research*, **35**, 3668-3675..
- Doyen, M., Bartik, K. & Bruylants, G.** 2013. UV-Vis and NMR study of the formation of gold nanoparticles by citrate reduction: Observation of gold-citrate aggregates. *Journal of Colloid and Interface Science*, **399**, 1-5.
- Dreaden, E. C., Alkilany, A. M., Huang, X., Murphy, C. J. & El-Sayed, M. A.** 2012. The golden age: gold nanoparticles for biomedicine. *Chemical Society Reviews*, **41**, 2740-2779.
- Dreaden, E. C., Mwakwari, S. C., Sodji, Q. H., Oyelere, A. K. & El-Sayed, M. A.** 2009. Tamoxifen-poly(ethylene glycol)-thiol gold nanoparticle conjugates: enhanced potency and selective delivery for breast cancer treatment. *Bioconjugate Chemistry*, **20**, 2247-2253.
- Duan, H., Wang, D. & Li, Y.** 2015. Green chemistry for nanoparticle synthesis. *Chemical Society Reviews*, **44**, 5778-5792.
- Durinx, C., Neels, H., Auwera, J. V. d., Naelaerts, K., Scharpé, S. & Meester, I. D.** 2001. Reference values for plasma dipeptidyl peptidase IV activity and their association with other laboratory parameters. *Clinical chemistry and laboratory medicine*, **39**, 155-159.
- Durinx, C., Lambeir, A., Bosmans, E., Falmagne, J., Berghmans, R., Haemers, A., Scharpé, S. & De Meester, I.** 2000. Molecular characterization of dipeptidyl peptidase activity in serum. *European Journal of Biochemistry*, **267**, 5608-5613.
- Durr, N. J., Larson, T., Smith, D. K., Korgel, B. A., Sokolov, K. & Ben-Yakar, A.** 2007. Two-photon luminescence imaging of cancer cells using molecularly targeted gold nanorods. *Nano Letters*, **7**, 941-945.
- Dykman, L., Lyakhov, A., Bogatyrev, V. & Shchyogolev, S. Y.** 1998. Synthesis of colloidal gold using high-molecular-weight reducing agents. *Colloid journal of the Russian Academy of Sciences*, **60**, 700-704.
- Dykman, L. & Khlebtsov, N.** 2012. Gold nanoparticles in biomedical applications: recent advances and perspectives. *Chemical Society Reviews*, **41**, 2256-2282.

**Eck, W., Craig, G., Sigdel, A., Ritter, G., Old, L. J., Tang, L., Brennan, M. F., Allen, P. J. & Mason, M. D.** 2008. PEGylated gold nanoparticles conjugated to monoclonal F19 antibodies as targeted labeling agents for human pancreatic carcinoma tissue. *ACS Nano*, **2**, 2263-2272.

**Egerton, R. F.** 2005. *Physical Principles of Electron Microscopy*. : Springer.

**Eisenthal, R. & Danson, M. J.** 2002. *Enzyme Assays: A Practical Approach*. : Oxford University Press, USA.

**Elghanian, R., Storhoff, J. J., Mucic, R. C., Letsinger, R. L. & Mirkin, C. A.** 1997. Selective colorimetric detection of polynucleotides based on the distance-dependent optical properties of gold nanoparticles. *Science (New York, N.Y.)*, **277**, 1078-1081.

**El-Sayed, I. H., Huang, X. & El-Sayed, M. A.** 2005. Surface plasmon resonance scattering and absorption of anti-EGFR antibody conjugated gold nanoparticles in cancer diagnostics: applications in oral cancer. *Nano Letters*, **5**, 829-834.

**El-Sayed, M. A.** 2001. Some interesting properties of metals confined in time and nanometer space of different shapes. *Accounts of Chemical Research*, **34**, 257-264.

**Emwas, A. M.** 2015. The strengths and weaknesses of NMR spectroscopy and mass spectrometry with particular focus on metabolomics research. *Metabolomics: Methods and Protocols*, , 161-193.

**Enustun, B. & Turkevich, J.** 1963. Coagulation of colloidal gold. *Journal of the American Chemical Society*, **85**, 3317-3328.

**Fadini, G. P. & Avogaro, A.** 2011. Cardiovascular effects of DPP-4 inhibition: beyond GLP-1. *Vascular Pharmacology*, **55**, 10-16.

**Faraday, M.** 1857. The Bakerian lecture: experimental relations of gold (and other metals) to light. *Philosophical Transactions of the Royal Society of London*, **147**, 145-181.

**Faulk, W. P. & Taylor, G. M.** 1971. Communication to the editors: an immunocolloid method for the electron microscope. *Immunochemistry*, **8**, 1081-1083.

**Fendler, J. H.** 1996. The colloidal domain: Where physics, chemistry, biology, and technology meet. By D.Fennell Evans and Hakån Wennerström. VCH Publishers, New York 1994, XXXII, 515

**Feynman, R. P.** 1960. There's plenty of room at the bottom. *Engineering and Science*, **23**, 22-36.

**Finney, E. E. & Finke, R. G.** 2008. Nanocluster nucleation and growth kinetic and mechanistic studies: A review emphasizing transition-metal nanoclusters. *Journal of Colloid and Interface Science*, **317**, 351-374.

**Firneisz, G., Lakatos, P. L. & Szalay, F.** 2001. Serum dipeptidyl peptidase IV (DPP IV, CD26) activity in chronic hepatitis C. *Scandinavian Journal of Gastroenterology*, **36**, 877-880.

**Fisker, R., Carstensen, J. M., Hansen, M. F., Bødker, F. & Mørup, S.** 2000. Estimation of nanoparticle size distributions by image analysis. *Journal of Nanoparticle Research*, **2**, 267-277.

- Franco, R., Valenzuela, A., Lluís, C. & Blanco, J.** 1998. Enzymatic and extraenzymatic role of ecto-adenosine deaminase in lymphocytes. *Immunological Reviews*, **161**, 27-42.
- Free, P., Shaw, C. P. & Lévy, R.** 2009. PEGylation modulates the interfacial kinetics of proteases on peptide-capped gold nanoparticles. *Chemical Communications*, , 5009-5011.
- Freestone, I., Meeks, N., Sax, M. & Higgitt, C.** 2007. The Lycurgus cup—a roman nanotechnology. *Gold Bulletin*, **40**, 270-277.
- Frens, G.** 1973. Controlled nucleation for the regulation of the particle size in monodisperse gold suspensions. *Nature*, **241**, 20-22.
- Garcia, B., Salomé, M., Lemelle, L., Bridot, J., Gillet, P., Perriat, P., Roux, S. & Tillement, O.** 2005. Sulphur K-edge XANES study of dihydrolipoic acid capped gold nanoparticles: dihydrolipoic acid is bound by both sulphur ends. *Chemical communications*, , 369-371.
- Ghosh, S.K. and Pal, T.,** 2007. Interparticle coupling effect on the surface plasmon resonance of gold nanoparticles: from theory to applications. *Chem. Rev*, **107**, 4797-4862.
- Gittins, D. I. & Caruso, F.** 2001. Spontaneous phase transfer of nanoparticulate metals from organic to aqueous media. *Angewandte Chemie International Edition*, **40**, 3001-3004.
- Glomm, W. R.** 2005. Functionalized gold nanoparticles for applications in bionanotechnology. *Journal of Dispersion Science and Technology*, **26**, 389-414.
- Goddard, J. & Reymond, J.** 2004. Enzyme assays for high-throughput screening. *Current Opinion in Biotechnology*, **15**, 314-322.
- Gonella, G., Terreni, S., Cvetko, D., Cossaro, A., Mattera, L., Cavalleri, O., Rolandi, R., Morgante, A., Floreano, L. & Canepa, M.** 2005. Ultrahigh vacuum deposition of L-cysteine on Au (110) studied by high-resolution X-ray photoemission: from early stages of adsorption to molecular organization. *The Journal of Physical Chemistry B*, **109**, 18003-18009.
- Gonzalez-Gronow, M., Misra, U. K., Gawdi, G. & Pizzo, S. V.** 2005. Association of plasminogen with dipeptidyl peptidase IV and Na<sup>+</sup>/H<sup>+</sup> exchanger isoform NHE3 regulates invasion of human 1-LN prostate tumor cells. *The Journal of Biological Chemistry*, **280**, 27173-27178.
- Goodwin, S.R., Reeds, D.N., Royal, M., Struthers, H., Laciny, E. and Yarasheski, K.E.,** 2013. Dipeptidyl peptidase IV inhibition does not adversely affect immune or virological status in HIV infected men and women: a pilot safety study. *The Journal of Clinical Endocrinology & Metabolism*, **98**, 743-751.
- Grabar, K. C., Freeman, R. G., Hommer, M. B. & Natan, M. J.** 1995. Preparation and characterization of Au colloid monolayers. *Analytical Chemistry*, **67**, 735-743.
- Green, B. D., Flatt, P. R. & Bailey, C. J.** 2006. Dipeptidyl peptidase IV (DPP IV) inhibitors: A newly emerging drug class for the treatment of type 2 diabetes. *Diabetes & Vascular Disease Research*, **3**, 159-165.
- Green, F.** 1925. The Colloidal Gold Reaction of the Cerebrospinal Fluid. *Canadian Medical Association Journal*, **15**, 1139-1143.

- Griffiths, P. R. & De Haseth, J. A.** 2007. *Fourier Transform Infrared Spectrometry*. : John Wiley & Sons.
- Gul, S., Sreedharan, S. & Brocklehurst, K.** 1998. *Enzyme Assays: Essential Data*. : John Wiley & Son Limited.
- Guo, L., Jackman, J. A., Yang, H., Chen, P., Cho, N. & Kim, D.** 2015. Strategies for enhancing the sensitivity of plasmonic nanosensors. *Nano Today*, **10**, 213-239.
- Gupta, R., Walunj, S. S., Tokala, R. K., Parsa, K. V., Singh, S. K. & Pal, M.** 2009. Emerging drug candidates of dipeptidyl peptidase IV (DPP IV) inhibitor class for the treatment of type 2 diabetes. *Current Drug Targets*, **10**, 71-87.
- Habashi, F.** 2016. Purple of Cassius. *European Chemistry Bulletin*, **5**, 416-419.
- Hadjipanayis, G. C. & Siegel, R. W.** 2012. *Nanophase Materials: Synthesis-Properties-Applications*. : Springer Science & Business Media.
- Hahn, M. A., Singh, A. K., Sharma, P., Brown, S. C. & Moudgil, B. M.** 2011. Nanoparticles as contrast agents for in-vivo bioimaging: current status and future perspectives. *Analytical and Bioanalytical Chemistry*, **399**, 3-27.
- Häkkinen, H.**, 2012. The gold-sulfur interface at the nanoscale. *Nature Chemistry*, **4**, 443-455.
- Halperin, W.** 1986. Quantum size effects in metal particles. *Reviews of Modern Physics*, **58**, 533.
- Hanaor, D., Michelazzi, M., Leonelli, C. and Sorrell, C.C.**, 2012. The effects of carboxylic acids on the aqueous dispersion and electrophoretic deposition of ZrO<sub>2</sub>. *Journal of the European Ceramic Society*, **32**, 235-244.
- Hanauer, M., Pierrat, S., Zins, I., Lotz, A. & Sönnichsen, C.** 2007. Separation of nanoparticles by gel electrophoresis according to size and shape. *Nano Letters*, **7**, 2881-2885.
- Hauser, E. A.** 1955. The history of colloid science: In memory of Wolfgang Ostwald. *J.Chem.Educ*, **32**, 2.
- Havre, P. A., Abe, M., Urasaki, Y., Ohnuma, K., Morimoto, C. & Dang, N. H.** 2008. The role of CD26/dipeptidyl peptidase IV in cancer. *Frontiers Bioscience*, **13**, 1634-1645.
- Hayat, M. A.** 2012. *Colloidal Gold: Principles, Methods, and Applications*. : Elsevier.
- He, Y., Cheng, F., Pang, D. & Tang, H.** 2017. Colorimetric and visual determination of DNase I activity using gold nanoparticles as an indicator. *Microchimica Acta*, **184**, 101-106.
- Hegen, M., Niedobitek, G., Klein, C. E., Stein, H. & Fleischer, B.** 1990. The T cell triggering molecule Tp103 is associated with dipeptidyl aminopeptidase IV activity. *Journal of Immunology (Baltimore, Md.: 1950)*, **144**, 2908-2914.
- Helfrich, A. & Bettmer, J.** 2011. Analysis of gold nanoparticles using ICP-MS-based hyphenated and complementary ESI-MS techniques. *International Journal of Mass Spectrometry*, **307**, 92-98.

- Hermanson, G. T.** 2013. *Bioconjugate Techniques*. : Academic press.
- Hertlein, C., Helden, L., Gambassi, A., Dietrich, S. & Bechinger, C.** 2008. Direct measurement of critical Casimir forces. *Nature*, **451**, 172-175.
- Hetmańczyk, K., Bednarska-Makaruk, M., Kierus, K., Murawska-Izdebska, S., Piekutowska-Abramczuk, D., Pilch, B., Tylki-Szymańska, A. & Ługowska, A.** 2016. Monitoring of dipeptidyl peptidase-IV (DPP-IV) activity in patients with mucopolysaccharidoses types I and II on enzyme replacement therapy—Results of a pilot study. *Clinical Biochemistry*, **49**, 458-462.
- Hildebrandt, M., Rose, M., Rüter, J., Salama, A., Mönnikes, H. & Klapp, B.** 2001. Dipeptidyl peptidase IV (DP IV, CD26) in patients with inflammatory bowel disease. *Scandinavian Journal of Gastroenterology*, **36**, 1067-1072.
- Hildebrandt, M., Klapp, B., Hoffmann, T. & Demuth, H.** 2003. *Dipeptidyl Aminopeptidases in Health and Disease*. : Springer Science & Business Media.
- Hino, M., Nagatsu, T., Kakumu, S., Okuyama, S., Yoshii, Y. & Nagatsu, I.** 1975. Glycylprolyl  $\beta$ -naphthylamidase activity in human serum. *Clinica Chimica Acta*, **62**, 5-11.
- Hinterwirth, H., Kappel, S., Waitz, T., Prohaska, T., Lindner, W. & Lämmerhofer, M.** 2013. Quantifying thiol ligand density of self-assembled monolayers on gold nanoparticles by inductively coupled plasma–mass spectrometry. *ACS Nano*, **7**, 1129-1136.
- Hoffmann, T., Faust, J., Neubert, K. & Ansorge, S.** 1993. Dipeptidyl peptidase IV (CD 26) and aminopeptidase N (CD 13) catalyzed hydrolysis of cytokines and peptides with N-terminal cytokine sequences. *FEBS letters*, **336**, 61-64.
- Hong, S.** 2013. Optimization, Modification and Application of Gold Nanoparticles as the Substrates of Surface Enhanced Raman Spectroscopy. University of South Florida.
- Hopsu-Havu, V. K. & Glenner, G. G.** 1966. A new dipeptide naphthylamidase hydrolyzing glycyl-prolyl- $\beta$ -naphthylamide. *Histochemistry and Cell Biology*, **7**, 197-201.
- Hostetler, M. J., Templeton, A. C. & Murray, R. W.** 1999. Dynamics of place-exchange reactions on monolayer-protected gold cluster molecules. *Langmuir*, **15**, 3782-3789.
- Howie, A., Marks, L. & Pennycook, S.** 1982. New imaging methods for catalyst particles. *Ultramicroscopy*, **8**, 163-174.
- Hu, J., Ni, P., Dai, H., Sun, Y., Wang, Y., Jiang, S. & Li, Z.** 2015. Aptamer-based colorimetric biosensing of abrin using catalytic gold nanoparticles. *Analyst*, **140**, 3581-3586.
- Hu, M., Novo, C., Funston, A., Wang, H., Staleva, H., Zou, S., Mulvaney, P., Xia, Y. & Hartland, G. V.** 2008. Dark-field microscopy studies of single metal nanoparticles: understanding the factors that influence the linewidth of the localized surface plasmon resonance. *Journal of Materials Chemistry*, **18**, 1949-1960.
- Hu, X., Guo, T., Fu, X. & Hu, X.** 2003. Nanoscale oxide structures induced by dynamic electric field on Si with AFM. *Applied Surface Science*, **217**, 34-38.

- Huang X H, El-Sayed I H, Qian W, et al.** 2006. Cancer cell imaging and photothermal therapy in the near-infrared region by using gold nanorods. *Journal of American Chemical Society*, **128**: 2115–2120
- Huang, H., Zhang, Q., Luo, J. & Zhao, Y.** 2012. Sensitive colorimetric detection of lysozyme in human serum using peptide-capped gold nanoparticles. *Analytical Methods*, **4**, 3874-3878.
- Huang, X., Jain, P. K., El-Sayed, I. H. & El-Sayed, M. A.** 2008. Plasmonic photothermal therapy (PPTT) using gold nanoparticles. *Lasers in Medical Science*, **23**, 217-228.
- Hunt, L.** 1976. The true story of Purple of Cassius. *Gold Bulletin*, **9**, 134-139.
- Hunter, R. J.** 2013. *Zeta potential in Colloid Science: Principles and Applications*.: Academic press.
- Inglese, J., Johnson, R.L., Simeonov, A., Xia, M., Zheng, W., Austin, C.P. and Auld, D.S.,** 2007. High-throughput screening assays for the identification of chemical probes. *Nature Chemical Biology*, **3**, 466-479.
- Israelachvili, J. N.** 2011. *Intermolecular and Surface Forces*. : Academic press.
- Iwaki-Egawa, S., Watanabe, Y., Kikuya, Y. & Fujimoto, Y.** 1998. Dipeptidyl peptidase IV from human serum: purification, characterization, and N-terminal amino acid sequence. *Journal of Biochemistry*, **124**, 428-433.
- Jana, N. R., Gearheart, L. & Murphy, C. J.** 2001. Evidence for seed-mediated nucleation in the chemical reduction of gold salts to gold nanoparticles. *Chemistry of Materials*, **13**, 2313-2322.
- Jans, H., Liu, X., Austin, L., Maes, G. & Huo, Q.** 2009. Dynamic light scattering as a powerful tool for gold nanoparticle bioconjugation and biomolecular binding studies. *Analytical Chemistry*, **81**, 9425-9432.
- Ji, X., Song, X., Li, J., Bai, Y., Yang, W. & Peng, X.** 2007. Size control of gold nanocrystals in citrate reduction: the third role of citrate. *Journal of the American Chemical Society*, **129**, 13939-13948.
- John, S.** 1987. Strong localization of photons in certain disordered dielectric superlattices. *Physical Review Letters*, **58**, 2486.
- Jokerst, J.V., Lobovkina, T., Zare, R.N. and Gambhir, S.S.,** 2011. Nanoparticle PEGylation for imaging and therapy. *Nanomedicine*, **6**, 715-728.
- Jones, D., Dang, N. H., Duvic, M., Washington, L. T. & Huh, Y. O.** 2001. Absence of CD26 expression is a useful marker for diagnosis of T-cell lymphoma in peripheral blood. *American Journal of Clinical Pathology*, **115**, 885-892.
- Ju-Nam, Y., Bricklebank, N., Allen, D. W., Gardiner, P. H., Light, M. E. & Hursthouse, M. B.** 2006. Phosphonioalkylthiosulfate zwitterions—new masked thiol ligands for the formation of cationic functionalised gold nanoparticles. *Organic & Biomolecular Chemistry*, **4**, 4345-4351.
- Jungraithmayr, W., De Meester, I., Matheussen, V., Baerts, L., Arni, S. & Weder, W.** 2012. CD26/DPP-4 inhibition recruits regenerative stem cells via stromal cell-derived factor-1 and

beneficially influences ischaemia-reperfusion injury in mouse lung transplantation. *European journal of cardio-thoracic surgery : official journal of the European Association for Cardio-thoracic Surgery*, **41**, 1166-1173.

**Kadlubar, F. F., Miller, J. A. & Miller, E. C.** 1978. Guanyl O6-arylation and O6-arylation of DNA by the carcinogen N-hydroxy-1-naphthylamine. *Cancer research*, **38**, 3628-3638.

**Kang, D., Zuo, X., Yang, R., Xia, F., Plaxco, K. W. & White, R. J.** 2009. Comparing the properties of electrochemical-based DNA sensors employing different redox tags. *Analytical Chemistry*, **81**, 9109-9113.

**Kaspari, A., Diefenthal, T., Grosche, G., Schierhorn, A. & Demuth, H.** 1996. Substrates containing phosphorylated residues adjacent to proline decrease the cleavage by proline-specific peptidases. *Biochimica et Biophysica Acta (BBA)-Protein Structure and Molecular Enzymology*, **1293**, 147-153.

**Kato, T., Nagatsu, T., Kimura, T. & Sakakibara, S.** 1978. Fluorescence assay of X-prolyl dipeptidyl-aminopeptidase activity with a new fluorogenic substrate. *Biochemical medicine*, **19**, 351-359.

**Katz, E. & Willner, I.** 2004. Integrated nanoparticle–biomolecule hybrid systems: synthesis, properties, and applications. *Angewandte Chemie International Edition*, **43**, 6042-6108.

**Keating, C.D., Kovaleski, K.M. and Natan, M.J.,** 1998. Protein: colloid conjugates for surface enhanced Raman scattering: stability and control of protein orientation. *The Journal of Physical Chemistry B*, **102**, 9404-9413.

**Kerker, M.** 2013. *The Scattering of Light and Other Electromagnetic Radiation: Physical Chemistry: A Series of Monographs*. Academic press.

**Khlebtsov, B. & Khlebtsov, N.** 2011. On the measurement of gold nanoparticle sizes by the dynamic light scattering method. *Colloid Journal*, **73**, 118-127.

**Kim, E. J., Kim, E. B., Lee, S. W., Cheon, S. A., Kim, H., Lee, J., Lee, M., Ko, S. & Park, T. J.** 2017a. An easy and sensitive sandwich assay for detection of Mycobacterium tuberculosis Ag85B antigen using quantum dots and gold nanorods. *Biosensors and Bioelectronics*, **87**, 150-156.

**Kim, G. B., Lee, J. O. & Kim, Y.** 2017b. Graying the self-assembly of gold nanoparticles for improved enzyme activity assays. *Sensors and Actuators B: Chemical*, **246**, 271-277.

**Kim, T., Lee, C., Joo, S. & Lee, K.** 2008. Kinetics of gold nanoparticle aggregation: experiments and modeling. *Journal of Colloid and Interface Science*, **318**, 238-243.

**Kim, Y. B., Kopcho, L. M., Kirby, M. S., Hamann, L. G., Weigelt, C. A., Metzler, W. J. & Marcinkeviciene, J.** 2006. Mechanism of Gly-Pro-pNA cleavage catalyzed by dipeptidyl peptidase-IV and its inhibition by saxagliptin (BMS-477118). *Archives of Biochemistry and Biophysics*, **445**, 9-18.

**Kim, N. H., Yu, T. & Lee, D. H.** 2014. The nonglycemic actions of dipeptidyl peptidase-4 inhibitors. *BioMed Research International*, **2014**, 368703.

- Kim, S. C., Schneeweiss, S., Glynn, R. J., Doherty, M., Goldfine, A. B. & Solomon, D. H.** 2015. Dipeptidyl peptidase-4 inhibitors in type 2 diabetes may reduce the risk of autoimmune diseases: a population-based cohort study. *Annals of the Rheumatic Diseases*, **74**, 1968-1975.
- Klajn, R., Stoddart, J. F. & Grzybowski, B. A.** 2010. Nanoparticles functionalised with reversible molecular and supramolecular switches. *Chemical Society Reviews*, **39**, 2203-2237.
- Klar, T., Perner, M., Grosse, S., von Plessen, G., Spirki, W. & Feldmann, J.** 1998. Near-field optical studies of surface plasmons in single metal nanoparticles. In *Quantum Electronics Conference, 1998. IQEC 98. Technical Digest. Summaries of papers presented at the International* (p. 93). IEEE
- Komiya, E., Hatano, R., Otsuka, H., Itoh, T., Yamazaki, H., Yamada, T., Dang, N.H., Tominaga, M., Suga, Y., Kimura, U. and Takamori, K.,** 2017. A possible role for CD26/DPPIV enzyme activity in the regulation of psoriatic pruritus. *Journal of Dermatological Science*, **86**, 212-221.
- Koo, H. C., Park, Y. H., Ahn, J., Waters, W. R., Palmer, M. V., Hamilton, M. J., Barrington, G., Mosaad, A. A., Park, K. T., Jung, W. K., Hwang, I. Y., Cho, S. N., Shin, S. J. & Davis, W. C.** 2005. Use of rMPB70 protein and ESAT-6 peptide as antigens for comparison of the enzyme-linked immunosorbent, immunochromatographic, and latex bead agglutination assays for serodiagnosis of bovine tuberculosis. *Journal of Clinical Microbiology*, **43**, 4498-4506.
- Kreibig, U. & Genzel, L.** 1985. Optical absorption of small metallic particles. *Surface Science*, **156**, 678-700.
- Kreibig, U. & Fragstein, C. v.** 1969. The limitation of electron mean free path in small silver particles. *Zeitschrift für Physik*, **224**, 307-323.
- Krpetic, Z., Nativo, P., Porta, F. & Brust, M.** 2009. A multidentate peptide for stabilization and facile bioconjugation of gold nanoparticles. *Bioconjugate Chemistry*, **20**, 619-624.
- Kubo, R.** 1962. Electronic properties of metallic fine particles. I. *Journal of the Physical Society of Japan*, **17**, 975-986.
- Kumar, S., Aaron, J. & Sokolov, K.** 2008. Directional conjugation of antibodies to nanoparticles for synthesis of multiplexed optical contrast agents with both delivery and targeting moieties. *Nature Protocols*, **3**, 314-320.
- Kumar, S., Gandhi, K. & Kumar, R.** 2007. Modeling of formation of gold nanoparticles by citrate method. *Industrial & Engineering Chemistry Research*, **46**, 3128-3136.
- Lafferty, J.** 1951. Boride cathodes. *Journal of Applied Physics*, **22**, 299-309.
- Lai, K. S., Ho, N., Cheng, J. D. & Tung, C.** 2007. Selective Fluorescence Probes for Dipeptidyl Peptidase Activity Fibroblast Activation Protein and Dipeptidyl Peptidase IV. *Bioconjugate Chemistry*, **18**, 1246-1250.
- Lambeir, A., Scharpe, S. & De Meester, I.** 2008. DPP4 inhibitors for diabetes—what next? *Biochemical Pharmacology*, **76**, 1637-1643.

- Lambeir, A., Durinx, C., Scharpé, S. & De Meester, I.** 2003. Dipeptidyl-peptidase IV from bench to bedside: an update on structural properties, functions, and clinical aspects of the enzyme DPP IV. *Critical Reviews in Clinical Laboratory Sciences*, **40**, 209-294.
- LaMer, V. K. & Dinegar, R. H.** 1950. Theory, production and mechanism of formation of monodispersed hydrosols. *Journal of the American Chemical Society*, **72**, 4847-4854.
- Lamers, D., Famulla, S., Wronkowitz, N., Hartwig, S., Lehr, S., Ouwens, D. M., Eckardt, K., Kaufman, J. M., Ryden, M., Muller, S., Hanisch, F. G., Ruige, J., Arner, P., Sell, H. & Eckel, J.** 2011. Dipeptidyl peptidase 4 is a novel adipokine potentially linking obesity to the metabolic syndrome. *Diabetes*, **60**, 1917-1925.
- Laromaine, A., Koh, L., Murugesan, M., Ulijn, R. V. & Stevens, M. M.** 2007. Protease-triggered dispersion of nanoparticle assemblies. *Journal of the American Chemical Society*, **129**, 4156-4157.
- Lemire, C., Meyer, R., Shaikhutdinov, S. & Freund, H.** 2004. Do quantum size effects control CO adsorption on gold nanoparticles? *Angewandte Chemie International Edition*, **43**, 118-121.
- Lévy, R.** 2006. Peptide-Capped Gold Nanoparticles: Towards Artificial Proteins. *ChemBioChem*, **7**, 1141-1145.
- Lévy, R., Thanh, N. T., Doty, R. C., Hussain, I., Nichols, R. J., Schiffrin, D. J., Brust, M. & Fernig, D. G.** 2004. Rational and combinatorial design of peptide capping ligands for gold nanoparticles. *Journal of the American Chemical Society*, **126**, 10076-10084.
- Li, C. M., Zhen, S. J., Wang, J., Li, Y. F. & Huang, C. Z.** 2013. A gold nanoparticles-based colorimetric assay for alkaline phosphatase detection with tunable dynamic range. *Biosensors and Bioelectronics*, **43**, 366-371.
- Li, C., Li, D., Wan, G., Xu, J. & Hou, W.** 2011. Facile synthesis of concentrated gold nanoparticles with low size-distribution in water: temperature and pH controls. *Nanoscale Research Letters*, **6**, 1.
- Li, G., Wang, T., Bhosale, S., Zhang, Y. & Fuhrhop, J.** 2003. Completely reversible aggregation of nanoparticles by varying the pH. *Colloid and Polymer Science*, **281**, 1099-1103.
- Li, H. & Rothberg, L. J.** 2004. DNA sequence detection using selective fluorescence quenching of tagged oligonucleotide probes by gold nanoparticles. *Analytical Chemistry*, **76**, 5414-5417.
- Li, N., Zhao, P. & Astruc, D.** 2014. Anisotropic gold nanoparticles: synthesis, properties, applications, and toxicity. *Angewandte Chemie International Edition*, **53**, 1756-1789.
- Li, X. Q., Sun, X. H., Cai, S., Ying, X. X. & Li, F. M.** 2009. Investigation on the chemical constituents and variation of the flower buds of *Lonicera* species by UPLC-ESI-MS/MS and principle component analysis. *Yao xue xue bao = Acta Pharmaceutica Sinica*, **44**, 895-904.
- Liang, Z., Liu, Y., Ng, S. S., Li, X., Lai, L., Luo, S. & Liu, S.** 2011. The effect of pH value on the formation of gold nanoshells. *Journal of Nanoparticle Research*, **13**, 3301-3311.

- Lim, T.** 2016. *Nanosensors: Theory and Applications in Industry, Healthcare and Defense*. : CRC Press.
- Lin, S., Chen, C., Lin, M. & Hsu, H.** 2005. A cooperative effect of bifunctionalized nanoparticles on recognition: sensing alkali ions by crown and carboxylate moieties in aqueous media. *Analytical Chemistry*, **77**, 4821-4828.
- Link, S. & El-Sayed, M. A.** 2000. Shape and size dependence of radiative, non-radiative and photothermal properties of gold nanocrystals. *International Reviews in Physical Chemistry*, **19**, 409-453.
- Link, S. & El-Sayed, M. A.** 1999. Size and temperature dependence of the plasmon absorption of colloidal gold nanoparticles. *The Journal of Physical Chemistry B*, **103**, 4212-4217.
- Liu, D., Yang, J., Wang, H., Wang, Z., Huang, X., Wang, Z., Niu, G., Hight Walker, A. & Chen, X.** 2014. Glucose oxidase-catalyzed growth of gold nanoparticles enables quantitative detection of attomolar cancer biomarkers. *Analytical Chemistry*, **86**, 5800-5806.
- Liu, T., Zhao, J., Zhang, D. & Li, G.** 2009. Novel method to detect DNA methylation using gold nanoparticles coupled with enzyme-linkage reactions. *Analytical Chemistry*, **82**, 229-233.
- Liu, Y., Shipton, M. K., Ryan, J., Kaufman, E. D., Franzen, S. & Feldheim, D. L.** 2007. Synthesis, stability, and cellular internalization of gold nanoparticles containing mixed peptide- poly (ethylene glycol) monolayers. *Analytical Chemistry*, **79**, 2221-2229.
- Liu, Y., Zhang, L., Wei, W., Zhao, H., Zhou, Z., Zhang, Y. & Liu, S.** 2015a. Colorimetric detection of influenza A virus using antibody-functionalized gold nanoparticles. *Analyst*, **140**, 3989-3995.
- Liu, Z., Xia, X., Yang, C. & Wang, L.** 2015b. Visual detection of Maize chlorotic mottle virus using unmodified gold nanoparticles. *RSC Advances*, **5**, 100891-100897.
- Liz-Marzán, L. M.** 2006. Tailoring surface plasmons through the morphology and assembly of metal nanoparticles. *Langmuir*, **22**, 32-41.
- Lou, X., Xiao, Y., Wang, Y., Mao, H. & Zhao, J.** 2009. Label-Free Colorimetric Screening of Nuclease Activity and Substrates by Using Unmodified Gold Nanoparticles. *ChemBioChem*, **10**, 1973-1977.
- Lourenco, C., Teixeira, M., Simões, S. & Gaspar, R.** 1996. Steric stabilization of nanoparticles: size and surface properties. *International Journal of Pharmaceutics*, **138**, 1-12.
- Lu, Y., Wang, L., Chen, D. & Wang, G.** 2012. Determination of the concentration and the average number of gold atoms in a gold nanoparticle by osmotic pressure. *Langmuir*, **28**, 9282-9287.
- Lyklema, H.** 2000. Preface to volume III: Liquid-fluid interfaces. *Fundamentals of Interface and Colloid Science*, **3**, 3-5.
- Lyklema, J.** 2005. *Fundamentals of Interface and Colloid Science: Soft Colloids*. : Academic press.

- Maes, M., Scharpé, S., Desnyder, R., Ranjan, R. & Meltzer, H.** 1996. Alterations in plasma dipeptidyl peptidase IV enzyme activity in depression and schizophrenia: effects of antidepressants and antipsychotic drugs. *Acta Psychiatrica Scandinavica*, **93**, 1-8.
- Maes, M., De Meester, I., Vanhoof, G., Scharpe, S., Bosmans, E., Vandervorst, C., Verkerk, R., Minner, B., Suy, E. & Raus, J.** 1991. Decreased serum dipeptidyl peptidase IV activity in major depression. *Biological Psychiatry*, **30**, 577-586.
- Maes, M., Lin, A., Bonaccorso, S., Vandoolaeghe, E., Song, C., Goossens, F., De Meester, I., Degroote, J., Neels, H. & Scharpé, S.** 1999. Lower activity of serum peptidases in abstinent alcohol-dependent patients. *Alcohol*, **17**, 1-6.
- Maiorano, G., Sabella, S., Sorce, B., Brunetti, V., Malvindi, M. A., Cingolani, R. & Pompa, P. P.** 2010. Effects of cell culture media on the dynamic formation of protein–nanoparticle complexes and influence on the cellular response. *ACS Nano*, **4**, 7481-7491.
- Manea, F., Bindoli, C., Polizzi, S., Lay, L. & Scrimin, P.** 2008. Expedient synthesis of water-soluble, monolayer-protected gold nanoparticles of controlled size and monolayer composition. *Langmuir*, **24**, 4120-4124.
- Manson, J., Kumar, D., Meenan, B. J. & Dixon, D.** 2011. Polyethylene glycol functionalized gold nanoparticles: the influence of capping density on stability in various media. *Gold bulletin*, **44**, 99-105.
- Martin, M. N., Basham, J. I., Chando, P. & Eah, S.** 2010. Charged gold nanoparticles in non-polar solvents: 10-min synthesis and 2D self-assembly. *Langmuir*, **26**, 7410-7417.
- Matić, I. Z., Đorđić, M., Grozdanić, N., Damjanović, A., Kolundžija, B., Erić-Nikolić, A., Džodić, R., Šašić, M., Nikolić, S. & Dobrosavljević, D.** 2012. Serum activity of DPP-IV and its expression on lymphocytes in patients with melanoma and in people with vitiligo. *BMC Immunology*, **13**, 48-54.
- Maus, L., Dick, O., Bading, H., Spatz, J.P. and Fiammengo, R.,** 2010. Conjugation of peptides to the passivation shell of gold nanoparticles for targeting of cell-surface receptors. *ACS Nano*, **4**, 6617-6628.
- McDonagh, B. H., Singh, G., Bandyopadhyay, S., Lystvet, S. M., Ryan, J. A., Volden, S., Kim, E., Sandvig, I., Sandvig, A. & Glomm, W. R.** 2015. Controlling the self-assembly and optical properties of gold nanoclusters and gold nanoparticles biomineralized with bovine serum albumin. *RSC Advances*, **5**, 101101-101109.
- Mentlein, R.** 1999. Dipeptidyl-peptidase IV (CD26)-role in the inactivation of regulatory peptides. *Regulatory Peptides*, **85**, 9-24.
- Mentlein, R.** 1988. Proline residues in the maturation and degradation of peptide hormones and neuropeptides. *FEBS Letters*, **234**, 251-256.
- Mentlein, R., GALLWITZ, B. & SCHMIDT, W. E.** 1993. Dipeptidyl-peptidase IV hydrolyses gastric inhibitory polypeptide, glucagon-like peptide-1 (7–36) amide, peptide histidine methionine and is responsible for their degradation in human serum. *European Journal of Biochemistry*, **214**, 829-835.

- Mikhlin, Y., Karacharov, A., Likhatski, M., Podlipskaya, T., Zubavichus, Y., Veligzhanin, A. & Zaikovski, V.** 2011. Submicrometer intermediates in the citrate synthesis of gold nanoparticles: New insights into the nucleation and crystal growth mechanisms. *Journal of Colloid and Interface Science*, **362**, 330-336.
- Miller, C. C.** 1924. The Stokes-Einstein Law for diffusion in solution. *Proceedings of the Royal Society of London. Series A, Containing Papers of a Mathematical and Physical Character*, **106**, 724-749.
- Mocanu, A., Cernica, I., Tomoaia, G., Bobos, L., Horovitz, O. & Tomoaia-Cotisel, M.** 2009. Self-assembly characteristics of gold nanoparticles in the presence of cysteine. *Colloids and Surfaces A: Physicochemical and Engineering Aspects*, **338**, 93-101.
- Morimoto, C. & Schlossman, S. F.** 1998. The structure and function of CD26 in the T-cell immune response. *Immunological Reviews*, **161**, 55-70.
- Mortier, A., Gouwy, M., Van Damme, J., Proost, P. & Struyf, S.** 2016. CD26/dipeptidylpeptidase IV-chemokine interactions: double-edged regulation of inflammation and tumor biology. *Journal of Leukocyte Biology*, **99**, 955-969.
- Moskovits, M.** 1985. Surface-enhanced spectroscopy. *Reviews of Modern Physics*, **57**, 783.
- Mulvaney, P.** 1996. Surface plasmon spectroscopy of nanosized metal particles. *Langmuir*, **12**, 788-800.
- Murphy, C.J., Gole, A.M., Hunyadi, S.E., Stone, J.W., Sisco, P.N., Alkilany, A., Kinard, B.E. and Hankins, P.,** 2008. Chemical sensing and imaging with metallic nanorods. *Chemical Communications*, **5**, 544-557
- Murphy, C. J., Sau, T. K., Gole, A. M., Orendorff, C. J., Gao, J., Gou, L., Hunyadi, S. E. & Li, T.** 2005. Anisotropic metal nanoparticles: synthesis, assembly, and optical applications. *The Journal of Physical Chemistry B*, **109**, 13857-13870.
- Myers, J. A., Curtis, B. S. & Curtis, W. R.** 2013. Improving accuracy of cell and chromophore concentration measurements using optical density. *BMC biophysics*, **6**, 4-19.
- Nagatsu, T., Hino, M., Fuyamada, H., Hayakawa, T., Sakakibara, S., Nakagawa, Y. & Takemoto, T.** 1976. New chromogenic substrates for X-prolyl dipeptidyl-aminopeptidase. *Analytical Biochemistry*, **74**, 466-476.
- Napper, D. H.** 1977. Steric stabilization. *Journal of colloid and interface science*, **58**, 390-407.
- Nash, M. A., Waitumbi, J. N., Hoffman, A. S., Yager, P. & Stayton, P. S.** 2012. Multiplexed enrichment and detection of malarial biomarkers using a stimuli-responsive iron oxide and gold nanoparticle reagent system. *ACS Nano*, **6**, 6776-6785.
- Nazarian, A., Lawlor, K., Philip, J., Ghosh, M., Yaneva, M., Villanueva, J., Saghatelian, A., Assel, M., Vickers, A. J. & Eastham, J. A.** 2014. Inhibition of circulating dipeptidyl peptidase 4 activity in patients with metastatic prostate cancer. *Molecular & Cellular Proteomics*, **13**, 3082-3096.

- Ni, R. Z., Huang, J. F., Xiao, M. B., Li, M. & Meng, X. Y.** 2003. Glycylproline dipeptidyl aminopeptidase isoenzyme in diagnosis of primary hepatocellular carcinoma. *World Journal of Gastroenterology*, **9**, 710-713.
- Niemeyer, C. M.** 2001. Nanoparticles, proteins, and nucleic acids: biotechnology meets materials science. *Angewandte Chemie International Edition*, **40**, 4128-4158.
- Nossier, A. I., Mohammed, O. S., El-deen, R. R. F., Zaghloul, A. S. & Eissa, S.** 2016. Gelatin-modified gold nanoparticles for direct detection of urinary total gelatinase activity: Diagnostic value in bladder cancer. *Talanta*, **161**, 511-519.
- Nowinski, A.K., White, A.D., Keefe, A.J. and Jiang, S.,** 2014. Biologically inspired stealth peptide-capped gold nanoparticles. *Langmuir*, **30**, 1864-1870.
- O'Brien, M.** 2006. DPP IV-Glo protease assay: a more sensitive method for measuring Gly-Pro cleaving activity in serum. *Promega Corporation Cell Notes*, **16**, 9-11.
- O'Brien, M., Daily, B., Schurria, M. & Riss, T.** 2006. Assay for DPPIV Activity Using A Homogenous, Luminiscent Method. *Handbook of Assay Development in Drug Discovery*, 125.
- O'Brien, R.W., Midmore B. R., Lamb A. Hunter R. J.,** 1990, Electroacoustic studies of moderately concentrated colloidal suspensions *Faraday Discuss. Chem. Soc.*, **90**, 301–312.
- Ogata, S., Misumi, Y. & Ikehara, Y.** 1989. Primary structure of rat liver dipeptidyl peptidase IV deduced from its cDNA and identification of the NH<sub>2</sub>-terminal signal sequence as the membrane-anchoring domain. *The Journal of biological chemistry*, **264**, 3596-3601.
- Ogawa, K. & Nagatsu, T.** 1979. Glycyl-prolyl-p-nitroanilidase (GPNAase) Activity in Cardiovascular Diseases. *Japanese Heart Journal*, **20**, 469-475.
- Ohnuma, K., Yamochi, T., Hosono, O. & Morimoto, C.** 2005. CD26 T cells in the pathogenesis of asthma. *Clinical & Experimental Immunology*, **139**, 13-16.
- Ojea-Jiménez, I., Bastús, N. G. & Puentes, V.** 2011. Influence of the sequence of the reagents addition in the citrate-mediated synthesis of gold nanoparticles. *The Journal of Physical Chemistry C*, **115**, 15752-15757.
- Oliveira, E., Núñez, C., Santos, H. M., Fernández-Lodeiro, J., Fernández-Lodeiro, A., Capelo, J. L. & Lodeiro, C.** 2015. Revisiting the use of gold and silver functionalised nanoparticles as colorimetric and fluorometric chemosensors for metal ions. *Sensors and Actuators B: Chemical*, **212**, 297-328.
- Omar, B. A., Liehua, L., Yamada, Y., Seino, Y., Marchetti, P. & Ahrén, B.** 2014. Dipeptidyl peptidase 4 (DPP-4) is expressed in mouse and human islets and its activity is decreased in human islets from individuals with type 2 diabetes. *Diabetologia*, **57**, 1876-1883.
- Oravec, T., Pall, M., Roderiquez, G., Gorrell, M. D., Ditto, M., Nguyen, N. Y., Boykins, R., Unsworth, E. & Norcross, M. A.** 1997. Regulation of the receptor specificity and function of the chemokine RANTES (regulated on activation, normal T cell expressed and secreted) by

dipeptidyl peptidase IV (CD26)-mediated cleavage. *The Journal of Experimental Medicine*, **186**, 1865-1872.

**Ostwald, C. W. W.** 1927. *Die Welt Der Vernachlässigten Dimensionen: Eine Einführung in Die Moderne Kolloidchemie Mit Besonderer Berücksichtigung Ihrer Anwendungen*. Theodor Steinkopff.

**Öya, H., Nagatsu, I. & Nagatsu, T.** 1972. Purification and properties of glycylprolyl  $\beta$ -naphthylamidase in human submaxillary gland. *Biochimica et Biophysica Acta (BBA)-Enzymology*, **258**, 591-599.

**Pan, Y., Guo, M., Nie, Z., Huang, Y., Peng, Y., Liu, A., Qing, M. & Yao, S.** 2012. Colorimetric detection of apoptosis based on caspase-3 activity assay using unmodified gold nanoparticles. *Chemical Communications*, **48**, 997-999.

**Papagianni, M. & Tziomalos, K.** 2015. Cardiovascular effects of dipeptidyl peptidase-4 inhibitors. *Hippokratia*, **19**, 195-199.

**Papavassiliou, G. C.** 1979. Optical properties of small inorganic and organic metal particles. *Progress in Solid State Chemistry*, **12**, 185-271.

**Park, J., Estrada, A., Sharp, K., Sang, K., Schwartz, J. A., Smith, D. K., Coleman, C., Payne, J. D., Korgel, B. A. & Dunn, A. K.** 2008. Two-photon-induced photoluminescence imaging of tumors using near-infrared excited gold nanoshells. *Optics Express*, **16**, 1590-1599.

**Park, K., Biswas, S., Kanel, S., Nepal, D. & Vaia, R. A.** 2014. Engineering the optical properties of gold nanorods: independent tuning of surface plasmon energy, extinction coefficient, and scattering cross section. *The Journal of Physical Chemistry C*, **118**, 5918-5926.

**Paterson, S. & De La Rica, R.** 2015. Solution-based nanosensors for in-field detection with the naked eye. *Analyst*, **140**, 3308-3317.

**Patungwasa, W. & Hodak, J. H.** 2008. pH tunable morphology of the gold nanoparticles produced by citrate reduction. *Materials Chemistry and Physics*, **108**, 45-54.

**Pavia, D. L., Lampman, G. M., Kriz, G. S. & Vyvyan, J. A.** 2014. *Introduction to Spectroscopy*. : Cengage Learning.

**Pavlov, V., Xiao, Y., Shlyahovsky, B. & Willner, I.** 2004. Aptamer-functionalized Au nanoparticles for the amplified optical detection of thrombin. *Journal of the American Chemical Society*, **126**, 11768-11769.

**Pease, L. F., Tsai, D., Zangmeister, R. A., Zachariah, M. R. & Tarlov, M. J.** 2007. Quantifying the surface coverage of conjugate molecules on functionalized nanoparticles. *The Journal of Physical Chemistry C*, **111**, 17155-17157.

**Peer, D., Karp, J. M., Hong, S., Farokhzad, O. C., Margalit, R. & Langer, R.** 2007. Nanocarriers as an emerging platform for cancer therapy. *Nature nanotechnology*, **2**, 751-760.

**Pellegrino, T., Sperling, R. A., Alivisatos, A. P. & Parak, W. J.** 2007. Gel electrophoresis of gold-DNA nanoconjugates. *Journal of Biomedicine & Biotechnology*, **2007**, 26796.

- Pengo, P., Polizzi, S., Battagliarin, M., Pasquato, L. & Scrimin, P.** 2003. Synthesis, characterization and properties of water-soluble gold nanoparticles with tunable core size. *Journal of Materials Chemistry*, **13**, 2471-2478.
- Penn, S. G., He, L. & Natan, M. J.** 2003. Nanoparticles for bioanalysis. *Current Opinion in Chemical Biology*, **7**, 609-615.
- Perenboom, J., Wyder, P. & Meier, F.** 1981. Electronic properties of small metallic particles. *Physics Reports*, **78**, 173-292.
- Perner, F., Gyuris, T., Rákóczy, G., Sárváry, E., Görög, D., Szalay, F., Kunos, I., Szönyi, L., Péterfy, M. & Takács, L.** 1999. Dipeptidyl peptidase activity of CD26 in serum and urine as a marker of cholestasis: experimental and clinical evidence. *Journal of Laboratory and Clinical Medicine*, **134**, 56-67.
- Pesika, N. S., Stebe, K. J. & Searson, P. C.** 2003. Relationship between absorbance spectra and particle size distributions for quantum-sized nanocrystals. *The Journal of Physical Chemistry B*, **107**, 10412-10415.
- Petryayeva, E. & Krull, U. J.** 2011. Localized surface plasmon resonance: nanostructures, bioassays and biosensing—a review. *Analytica Chimica Acta*, **706**, 8-24.
- Piao, J. Y. & Chung, D. S.** 2012. Novel colorimetric assay of LSD1 activity using gold nanoparticles. *Analyst*, **137**, 2669-2673.
- Pinchuk, A. O., Kalsin, A. M., Kowalczyk, B., Schatz, G. C. & Grzybowski, B. A.** 2007. Modeling of electrodynamic interactions between metal nanoparticles aggregated by electrostatic interactions into closely-packed clusters. *The Journal of Physical Chemistry C*, **111**, 11816-11822.
- Plissonneau, M., Pansieri, J., Heinrich-Balard, L., Morfin, J., Stransky-Heilkron, N., Rivory, P., Mowat, P., Dumoulin, M., Cohen, R. & Allémann, É.** 2016. Gd-nanoparticles functionalization with specific peptides for  $\beta$ -amyloid plaques targeting. *Journal of Nanobiotechnology*, **14**, 60.
- Polte, J.** 2015. Fundamental growth principles of colloidal metal nanoparticles—a new perspective. *CrystEngComm*, **17**, 6809-6830.
- Polte, J., Ahner, T. T., Delissen, F., Sokolov, S., Emmerling, F., Thünemann, A. F. & Kraehnert, R.** 2010. Mechanism of gold nanoparticle formation in the classical citrate synthesis method derived from coupled in situ XANES and SAXS evaluation. *Journal of the American Chemical Society*, **132**, 1296-1301.
- Pong, B., Elim, H. I., Chong, J., Ji, W., Trout, B. L. & Lee, J.** 2007. New insights on the nanoparticle growth mechanism in the citrate reduction of gold (III) salt: formation of the Au nanowire intermediate and its nonlinear optical properties. *The Journal of Physical Chemistry C*, **111**, 6281-6287.
- Pro, B. & Dang, N.** 2004. CD26 dipeptidyl peptidase IV and its role in cancer. *Histology and Histopathology*, **19**, 1345-1351

- Pujols-Ayala, I., Sacksteder, C. A. & Barry, B. A.** 2003. Redox-active tyrosine residues: Role for the peptide bond in electron transfer. *Journal of the American Chemical Society*, **125**, 7536-7538.
- Pyrz, W. D. & Buttrey, D. J.** 2008. Particle size determination using TEM: a discussion of image acquisition and analysis for the novice microscopist. *Langmuir*, **24**, 11350-11360.
- Quintela, I. A., Benildo, G., Lin, C. & Wu, V. C.** 2015. Simultaneous direct detection of Shiga-toxin producing *Escherichia coli* (STEC) strains by optical biosensing with oligonucleotide-functionalized gold nanoparticles. *Nanoscale*, **7**, 2417-2426.
- Rajput, N.** 2015. Methods of Preparation of Nanoparticles-A review. *International Journal of Advances in Engineering & Technology*, **7**, 1806.
- Ramezani, F., Habibi, M., Rafii-Tabar, H. & Amanlou, M.** 2015. Effect of peptide length on the conjugation to the gold nanoparticle surface: a molecular dynamic study. *DARU Journal of Pharmaceutical Sciences*, **23**, 9.
- Rasooly, A. & Herold, K. E.** 2009. *Biosensors and Biodetection*. Humana Press.
- Rawat, K. A., Basu, H., Singhal, R. K. & Kailasa, S. K.** 2015. Simultaneous colorimetric detection of four drugs in their pharmaceutical formulations using unmodified gold nanoparticles as a probe. *RSC Advances*, **5**, 19924-19932.
- Rawlings, N. D. & Barrett, A. J.** 1993. Evolutionary families of peptidases. *The Biochemical Journal*, **290**, 205-218.
- Reimer, L.** 2013. *Transmission Electron Microscopy: Physics of Image Formation and Microanalysis*. : Springer.
- Reiss, H.** 1951. The growth of uniform colloidal dispersions. *The Journal of Chemical Physics*, **19**, 482-487.
- Ren, Q., Bai, L., Zhang, X., Ma, Z., Liu, B., Zhao, Y. & Cao, Y.** 2015. Preparation, Modification, and Application of Hollow Gold Nanospheres. *Journal of Nanomaterials*, **2015**, 1-7.
- Richard, E., Arredondo-Vega, F. X., Santisteban, I., Kelly, S. J., Patel, D. D. & Hershfield, M. S.** 2000. The binding site of human adenosine deaminase for CD26/Dipeptidyl peptidase IV: the Arg142Gln mutation impairs binding to cd26 but does not cause immune deficiency. *The Journal of Experimental Medicine*, **192**, 1223-1236.
- Rojanathanes, R., Sereemasapun, A., Pimpha, N., Buasorn, V., Ekawong, P. & Wiwanitkit, V.** 2008. Gold nanoparticle as an alternative tool for a urine pregnancy test. *Taiwanese Journal of Obstetrics and Gynecology*, **47**, 296-299.
- Rosi, N. L. & Mirkin, C. A.** 2005. Nanostructures in biodiagnostics. *Chemical Reviews*, **105**, 1547-1562.
- Royal Academy of Engineering & Royal Society.** 2004. Nanoscience and nanotechnologies: opportunities and uncertainties.

- Sapsford, K. E., Algar, W. R., Berti, L., Gemmill, K. B., Casey, B. J., Oh, E., Stewart, M. H. & Medintz, I. L.** 2013. Functionalizing nanoparticles with biological molecules: developing chemistries that facilitate nanotechnology. *Chemical Reviews*, **113**, 1904-2074.
- Sardar, R., Funston, A. M., Mulvaney, P. & Murray, R. W.** 2009. Gold nanoparticles: past, present, and future. *Langmuir*, **25**, 13840-13851.
- Sato, K., Hosokawa, K. & Maeda, M.** 2003. Rapid aggregation of gold nanoparticles induced by non-cross-linking DNA hybridization. *Journal of the American Chemical Society*, **125**, 8102-8103.
- Sau, T. K., Rogach, A. L., Jäckel, F., Klar, T. A. & Feldmann, J.** 2010. Properties and applications of colloidal nonspherical noble metal nanoparticles. *Advanced Materials*, **22**, 1805-1825.
- Scanlan, M. J., Raj, B. K., Calvo, B., Garin-Chesa, P., Sanz-Moncasi, M. P., Healey, J. H., Old, L. J. & Rettig, W. J.** 1994. Molecular cloning of fibroblast activation protein alpha, a member of the serine protease family selectively expressed in stromal fibroblasts of epithelial cancers. *Proceedings of the National Academy of Sciences of the United States of America*, **91**, 5657-5661.
- Schiffelers, R. M., Ansari, A., Xu, J., Zhou, Q., Tang, Q., Storm, G., Molema, G., Lu, P. Y., Scaria, P. V. & Woodle, M. C.** 2004. Cancer siRNA therapy by tumor selective delivery with ligand-targeted sterically stabilized nanoparticle. *Nucleic Acids Research*, **32**, e149.
- Schmid, G.** 1992. Large clusters and colloids. Metals in the embryonic state. *Chemical Reviews*, **92**, 1709-1727.
- Schmid, G.** 2011. *Nanoparticles: From Theory to Application*. John Wiley & Sons.
- Schmiedl, A., Krainski, J., Schwichtenhövel, F., Schade, J., Klemann, C., Raber, K., Zscheppang, K., Beekmann, T., Acevedo, C. & Glaab, T.** 2010. Reduced airway inflammation in CD26/DPP4-deficient F344 rats is associated with altered recruitment patterns of regulatory T cells and expression of pulmonary surfactant proteins. *Clinical & Experimental Allergy*, **40**, 1794-1808.
- Sellers, H., Ulman, A., Shnidman, Y. & Eilers, J. E.** 1993. Structure and binding of alkanethiolates on gold and silver surfaces: implications for self-assembled monolayers. *Journal of the American Chemical Society*, **115**, 9389-9401.
- Shafirovich, E., Diakov, V. & Varma, A.** 2007. Combustion-assisted hydrolysis of sodium borohydride for hydrogen generation. *International Journal of Hydrogen Energy*, **32**, 207-211.
- Shah, N., Sattar, A., Benanti, M., Hollander, S. & Cheuck, L.** 2006. Magnetic resonance spectroscopy as an imaging tool for cancer: a review of the literature. *The Journal of the American Osteopathic Association*, **106**, 23-27.
- Shankar, S. S., Rai, A., Ahmad, A. & Sastry, M.** 2004. Rapid synthesis of Au, Ag, and bimetallic Au core–Ag shell nanoparticles using Neem (*Azadirachta indica*) leaf broth. *Journal of Colloid and Interface Science*, **275**, 496-502.

**Shim, J. & Gupta, V. K.** 2007. Reversible aggregation of gold nanoparticles induced by pH dependent conformational transitions of a self-assembled polypeptide. *Journal of Colloid and Interface Science*, **316**, 977-983.

**Sierra, J.A., Vanoni, C.R., Tumelero, M.A., Cid, C.C.P., Faccio, R., Franceschini, D.F., Creczynski-Pasa, T.B. and Pasa, A.A.,** 2016. Biogenic approaches using citrus extracts for the synthesis of metal nanoparticles: the role of flavonoids in gold reduction and stabilization. *New Journal of Chemistry*, **40**, 1420-1429.

**Sivaraman, S. K., Kumar, S. & Santhanam, V.** 2011. Monodisperse sub-10nm gold nanoparticles by reversing the order of addition in Turkevich method—The role of chloroauric acid. *Journal of Colloid and Interface Science*, **361**, 543-547.

**Smith, A. M., Marbella, L. E., Johnston, K. A., Hartmann, M. J., Crawford, S. E., Kozycz, L. M., Seferos, D. S. & Millstone, J. E.** 2015. Quantitative Analysis of Thiolated Ligand Exchange on Gold Nanoparticles Monitored by <sup>1</sup>H NMR Spectroscopy. *Analytical Chemistry*, **87**, 2771-2778.

**Smith, W.** 2008. Practical understanding and use of surface enhanced Raman scattering/surface enhanced resonance Raman scattering in chemical and biological analysis. *Chemical Society Reviews*, **37**, 955-964.

**Smitham, J. B., Evans, R. & Napper, D. H.** 1975. Analytical theories of the steric stabilization of colloidal dispersions. *Journal of the Chemical Society, Faraday Transactions 1: Physical Chemistry in Condensed Phases*, **71**, 285-297.

**Snoswell, D. R., Duan, J., Fornasiero, D. & Ralston, J.** 2005. Colloid stability of synthetic titania and the influence of surface roughness. *Journal of Colloid and Interface Science*, **286**, 526-535.

**Somborac-Baćura, A., Buljević, S., Rumora, L., Čulić, O., Detel, D., Pancirov, D., Popović-Grle, S., Varljen, J., Čepelak, I. & Žanić-Grubišić, T.** 2012. Decreased soluble dipeptidyl peptidase IV activity as a potential serum biomarker for COPD. *Clinical Biochemistry*, **45**, 1245-1250.

**Song, C. W.** 1984. Effect of local hyperthermia on blood flow and microenvironment: a review. *Cancer Research*, **44**, 4721s-4730s.

**Sönnichsen, C., Reinhard, B. M., Liphardt, J. & Alivisatos, A. P.** 2005. A molecular ruler based on plasmon coupling of single gold and silver nanoparticles. *Nature Biotechnology*, **23**, 741-745.

**Spampinato, V., Parracino, M. A., La Spina, R., Rossi, F. & Ceccone, G.** 2016. Surface Analysis of Gold Nanoparticles Functionalized with Thiol-Modified Glucose SAMs for Biosensor Applications. *Frontiers in Chemistry*, **4**, 1-12.

**Sperling, R. A., Gil, P. R., Zhang, F., Zanella, M. & Parak, W. J.** 2008. Biological applications of gold nanoparticles. *Chemical Society Reviews*, **37**, 1896-1908.

**Stankovic, M., Vlahovic, P., Avramovic, V. & Todorovic, M.** 2008. Distribution of dipeptidyl peptidase IV in patients with chronic tonsillitis. *Clinical and vaccine immunology : CVI*, **15**, 794-798.

**Storhoff, J. J. & Mirkin, C. A.** 1999. Programmed materials synthesis with DNA. *Chemical Reviews*, **99**, 1849-1862.

- Su, C., Wu, P. & Yeh, C.** 2003. Sonochemical synthesis of well-dispersed gold nanoparticles at the ice temperature. *The Journal of Physical Chemistry B*, **107**, 14240-14243.
- Sugimoto, T.** 1987. Preparation of monodispersed colloidal particles. *Advances in Colloid and Interface Science*, **28**, 65-108.
- Sugimoto, T., Shiba, F., Sekiguchi, T. & Itoh, H.** 2000. Spontaneous nucleation of monodisperse silver halide particles from homogeneous gelatin solution I: silver chloride. *Colloids and Surfaces A: Physicochemical and Engineering Aspects*, **164**, 183-203.
- Sun, B., Wu, J., Cui, S., Zhu, H., An, W., Fu, Q., Shao, C., Yao, A., Chen, B. & Shi, D.** 2017. In situ synthesis of graphene oxide/gold nanorods theranostic hybrids for efficient tumor computed tomography imaging and photothermal therapy. *Nano Research*, **10**, 37-48.
- Sun, L., Liu, D. & Wang, Z.** 2007. Microarray-based kinase inhibition assay by gold nanoparticle probes. *Analytical Chemistry*, **79**, 773-777.
- Sun, A. L., Deng, J. T., Guan, G. J., Chen, S. H., Liu, Y. T., Cheng, J., Li, Z. W., Zhuang, X. H., Sun, F. D. & Deng, H. P.** 2012. Dipeptidyl peptidase-IV is a potential molecular biomarker in diabetic kidney disease. *Diabetes & vascular disease research*, **9**, 301-308.
- Susumu, K., Uyeda, H. T., Medintz, I. L., Pons, T., Delehanty, J. B. & Mattoussi, H.** 2007. Enhancing the stability and biological functionalities of quantum dots via compact multifunctional ligands. *Journal of the American Chemical Society*, **129**, 13987-13996.
- Svedberg, T.** 1909. *Die Methoden Zur Herstellung Kolloider Lösungen Anorganischer Stoffe: Ein Hand-Und Hilfsbuch Für Die Chemie Und Industrie Der Kolloide.*
- Szczech, J. R. & Jin, S.** 2011. Nanostructured silicon for high capacity lithium battery anodes. *Energy & Environmental Science*, **4**, 56-72.
- Tanaka, T., Umeki, K., Yamamoto, I., Sakamoto, F., Noguchi, S. & Ohtaki, S.** 1995. CD26 (dipeptidyl peptidase IV/DPP IV) as a novel molecular marker for differentiated thyroid carcinoma. *International Journal of Cancer*, **64**, 326-331.
- Tanaka, T., Duke-Cohan, J. S., Kameoka, J., Yaron, A., Lee, I., Schlossman, S. F. & Morimoto, C.** 1994. Enhancement of antigen-induced T-cell proliferation by soluble CD26/dipeptidyl peptidase IV. *Proceedings of the National Academy of Sciences of the United States of America*, **91**, 3082-3086.
- Tasic, T., Bäumer, W., Schmiedl, A., Schwichtenhövel, F., Pabst, R., Raap, U., von Hörsten, S. & Stephan, M.** 2011. Dipeptidyl peptidase IV (DPP4) deficiency increases Th1-driven allergic contact dermatitis. *Clinical & Experimental Allergy*, **41**, 1098-1107.
- Tataurova, Y. N.** 2014. Proton NMR studies of functionalized nanoparticles in aqueous environments. PhD (Doctor of Philosophy), University of Iowa, Iowa City, USA.
- Templeton, A. C., Wuelfing, W. P. & Murray, R. W.** 2000. Monolayer-protected cluster molecules. *Accounts of Chemical Research*, **33**, 27-36.

- Templeton, A. C., Cliffel, D. E. & Murray, R. W.** 1999. Redox and fluorophore functionalization of water-soluble, tiopronin-protected gold clusters. *Journal of the American Chemical Society*, **121**, 7081-7089.
- Thanh, N. T., Maclean, N. & Mahiddine, S.** 2014. Mechanisms of nucleation and growth of nanoparticles in solution. *Chemical Reviews*, **114**, 7610-7630.
- Tiwari, N. R., Rathore, A., Prabhune, A. & Kulkarni, S. K.** 2010. Gold nanoparticles for colorimetric detection of hydrolysis of antibiotics by penicillin G acylase. *Advances in Bioscience and Biotechnology*, **1**, 322-329.
- Toma, H. E., Zamarion, V. M., Toma, S. H. & Araki, K.** 2010. The coordination chemistry at gold nanoparticles. *Journal of the Brazilian Chemical Society*, **21**, 1158-1176.
- Tomaszewska, E., Soliwoda, K., Kadziola, K., Tkacz-Szczesna, B., Celichowski, G., Cichomski, M., Szmaja, W. & Grobelny, J.** 2013. Detection limits of DLS and UV-Vis spectroscopy in characterization of polydisperse nanoparticles colloids. *Journal of Nanomaterials*, **2013**, 60, 1-10.
- Tong L, Zhao Y, Huff T B, et al.** 2007 Gold nanorods mediate tumor cell death by compromising membrane integrity. *Adv Mater*, **19**, 3136–3141.
- Tracy, J. B., Crowe, M. C., Parker, J. F., Hampe, O., Fields-Zinna, C. A., Dass, A. & Murray, R. W.** 2007. Electrospray ionization mass spectrometry of uniform and mixed monolayer nanoparticles: Au<sub>25</sub> [S (CH<sub>2</sub>)<sub>2</sub>Ph]<sub>18</sub> and Au<sub>25</sub> [S (CH<sub>2</sub>)<sub>2</sub>Ph]<sub>18-x</sub> (SR)<sub>x</sub>. *Journal of the American Chemical Society*, **129**, 16209-16215.
- Tran, N. & Webster, T. J.** 2010. Magnetic nanoparticles: biomedical applications and challenges. *Journal of Materials Chemistry*, **20**, 8760-8767.
- Truong, P. L., Kim, B. W. & Sim, S. J.** 2012. Rational aspect ratio and suitable antibody coverage of gold nanorod for ultra-sensitive detection of a cancer biomarker. *Lab on a Chip*, **12**, 1102-1109.
- Tsai, D., Davila-Morris, M., DelRio, F. W., Guha, S., Zachariah, M. R. & Hackley, V. A.** 2011. Quantitative determination of competitive molecular adsorption on gold nanoparticles using attenuated total reflectance–Fourier transform infrared spectroscopy. *Langmuir*, **27**, 9302-9313.
- Tscharnutter, W.** 2006. Photon Correlation Spectroscopy in Particle Sizing, *Encyclopedia of Analytical Chemistry*.
- Turkevich, J., Stevenson, P. C. & Hillier, J.** 1951. A study of the nucleation and growth processes in the synthesis of colloidal gold. *Discussions of the Faraday Society*, **11**, 55-75.
- Underwood, S. & Mulvaney, P.** 1994. Effect of the solution refractive index on the color of gold colloids. *Langmuir*, **10**, 3427-3430.
- van West, D., Monteleone, P., Di Lieto, A., De Meester, I., Durinx, C., Scharpe, S., Lin, A., Maj, M. & Maes, M.** 2000. Lowered serum dipeptidyl peptidase IV activity in patients with anorexia and bulimia nervosa. *European Archives of Psychiatry and Clinical Neuroscience*, **250**, 86-92.

- Varona, A., Blanco, L., Perez, I., Gil, J., Irazusta, J., López, J. I., Cadenas, M. L., Pinto, F. M. & Larrinaga, G.** 2010. Expression and activity profiles of DPP IV/CD26 and NEP/CD10 glycoproteins in the human renal cancer are tumor-type dependent. *BMC Cancer*, **10**, 193.
- Wagner, L., Klemann, C., Stephan, M. and von Hörsten, S.,** 2016. Unravelling the immunological roles of dipeptidyl peptidase 4 (DPP4) activity and/or structure homologue (DASH) proteins. *Clinical & Experimental Immunology*, **184**, 265-283.
- Wang, J., Wu, L., Ren, J. & Qu, X.** 2014a. Visual detection of telomerase activity with a tunable dynamic range by using a gold nanoparticle probe-based hybridization protection strategy. *Nanoscale*, **6**, 1661-1666.
- Wang, J., Duan, T., Sun, L., Liu, D. & Wang, Z.** 2009. Functional gold nanoparticles for studying the interaction of lectin with glycosyl complex on living cellular surfaces. *Analytical Biochemistry*, **392**, 77-82.
- Wang, L., Wang, L., Shi, X., Kariuki, N. N., Schadt, M., Wang, G. R., Rendeng, Q., Choi, J., Luo, J. & Lu, S.** 2007. Array of molecularly mediated thin film assemblies of nanoparticles: correlation of vapor sensing with interparticle spatial properties. *Journal of the American Chemical Society*, **129**, 2161-2170.
- Wang, Q., Li, R., Yin, B. & Ye, B.** 2015. Colorimetric detection of sequence-specific microRNA based on duplex-specific nuclease-assisted nanoparticle amplification. *Analyt*, **140**, 6306-6312.
- Wang, W., Wei, Q., Wang, J., Wang, B., Zhang, S. & Yuan, Z.** 2013. Role of thiol-containing polyethylene glycol (thiol-PEG) in the modification process of gold nanoparticles (AuNPs): Stabilizer or coagulant?. *Journal of Colloid and Interface Science*, **404**, 223-229.
- Wang, Y., Zhang, D., Liu, W., Zhang, X., Yu, S., Liu, T., Zhang, W., Zhu, W. & Wang, J.** 2014b. Facile colorimetric method for simple and rapid detection of endotoxin based on counterion-mediated gold nanorods aggregation. *Biosensors and Bioelectronics*, **55**, 242-248.
- Wang, Z., Grigo, C., Steinbeck, J., von Hörsten, S., Amann, K. & Daniel, C.** 2014c. Soluble DPP4 originates in part from bone marrow cells and not from the kidney. *Peptides*, **57**, 109-117.
- Wang, Z., Lévy, R., Fernig, D. G. & Brust, M.** 2006. Kinase-catalyzed modification of gold nanoparticles: a new approach to colorimetric kinase activity screening. *Journal of the American Chemical Society*, **128**, 2214-2215.
- Wang, Z., Lévy, R., Fernig, D. G. & Brust, M.** 2005. The peptide route to multifunctional gold nanoparticles. *Bioconjugate Chemistry*, **16**, 497-500.
- Watzky, M. A. & Finke, R. G.** 1997. Nanocluster size-control and "Magic Number" investigations. experimental tests of the "Living-metal polymer" concept and of mechanism-based size-control predictions leading to the syntheses of iridium (0) nanoclusters centering about four sequential magic numbers. *Chemistry of Materials*, **9**, 3083-3095.
- Wei, H., Li, B., Li, J., Wang, E. & Dong, S.** 2007. Simple and sensitive aptamer-based colorimetric sensing of protein using unmodified gold nanoparticle probes. *Chemical Communications*, **36**, 3735-3737.

- Weller, H.** 1993. Colloidal semiconductor Q-particles: chemistry in the transition region between solid state and molecules. *Angewandte Chemie International Edition in English*, **32**, 41-53.
- Wesley, U. V., Tiwari, S. & Houghton, A. N.** 2004. Role for dipeptidyl peptidase IV in tumor suppression of human non small cell lung carcinoma cells. *International Journal of Cancer*, **109**, 855-866.
- Wesley, U. V., McGroarty, M. & Homoyouni, A.** 2005. Dipeptidyl peptidase inhibits malignant phenotype of prostate cancer cells by blocking basic fibroblast growth factor signaling pathway. *Cancer Research*, **65**, 1325-1334..
- West, J. L. & Halas, N. J.** 2003. Engineered nanomaterials for biophotonics applications: improving sensing, imaging, and therapeutics. *Annual Review of Biomedical Engineering*, **5**, 285-292.
- Westley, C., Fisk, H., Xu, Y., Hollywood, K.A., Carnell, A.J., Micklefield, J., Turner, N.J. and Goodacre, R.,** 2017. Real-Time Monitoring of Enzyme-Catalysed Reactions using Deep UV Resonance Raman Spectroscopy. *Chemistry-A European Journal*, **23**, 6983-6987
- Whitesides, G. M.** 2003. The 'right' size in nanobiotechnology. *Nature Biotechnology*, **21**, 1161-1165.
- Williams, D. B. & Carter, C. B.** 2009. The transmission electron microscope. In: *Transmission Electron Microscopy* (Ed. by Anonymous ), 3-22. Springer.
- Wilson, M. J., Ruhland, A., Quast, B. J., Reddy, P. K., Ewing, S. L. & Sinha, A. A.** 2000. Dipeptidylpeptidase IV activities are elevated in prostate cancers and adjacent benign hyperplastic glands. *Journal of Andrology*, **21**, 220-226.
- Wu, B., Zou, F., Wang, X., Koh, K., Wang, K. & Chen, H.** 2017. The colorimetric assay of diamine oxidase activity with high sensitivity based on calixarene derivative-capped gold nanoparticles. *Analytical Methods*, **9**, 2153-2158.
- Wulandari, P., Li, X., Tamada, K. & Hara, M.** 2008. Conformational study of citrates adsorbed on gold nanoparticles using Fourier transform infrared spectroscopy. *Journal of Nonlinear Optical Physics & Materials*, **17**, 185-192.
- Xia, N., Wang, X., Wang, X. & Zhou, B.** 2016. Gold nanoparticle-based colorimetric and electrochemical methods for dipeptidyl peptidase-IV activity assay and inhibitor screening. *Materials*, **9**, 857-868.
- Xia, F., Zuo, X., Yang, R., Xiao, Y., Kang, D., Vallee-Belisle, A., Gong, X., Yuen, J. D., Hsu, B. B., Heeger, A. J. & Plaxco, K. W.** 2010. Colorimetric detection of DNA, small molecules, proteins, and ions using unmodified gold nanoparticles and conjugated polyelectrolytes. *Proceedings of the National Academy of Sciences of the United States of America*, **107**, 10837-10841.
- Xu, H., Mao, X., Zeng, Q., Wang, S., Kawde, A.N. and Liu, G.,** 2008. Aptamer-functionalized gold nanoparticles as probes in a dry-reagent strip biosensor for protein analysis. *Analytical Chemistry*, **81**, 669-675.

**Yang, C., Uertz, J., Yohan, D. & Chithrani, B.** 2014. Peptide modified gold nanoparticles for improved cellular uptake, nuclear transport, and intracellular retention. *Nanoscale*, **6**, 12026-12033.

**Yang, H., Heng, X., Wang, W., Hu, J. and Xu, W.,** 2012. Salt-induced size-selective separation, concentration, and preservation of zwitterion-modified gold nanoparticles. *RSC Advances*, **2**, 2671-2674.

**Yarbakht, M. & Nikkhah, M.** 2016. Unmodified gold nanoparticles as a colorimetric probe for visual methamphetamine detection. *Journal of Experimental Nanoscience*, **11**, 593-601.

**Yaron, A., Naider, F. & Scharpe, S.** 1993. Proline-dependent structural and biological properties of peptides and proteins. *Critical Reviews in Biochemistry and Molecular Biology*, **28**, 31-81.

**Yavuz, M. S., Cheng, Y., Chen, J., Cobley, C. M., Zhang, Q., Rycenga, M., Xie, J., Kim, C., Song, K. H. & Schwartz, A. G.** 2009. Gold nanocages covered by smart polymers for controlled release with near-infrared light. *Nature Materials*, **8**, 935-939.

**Yee, C.K., Ulman, A., Ruiz, J.D., Parikh, A., White, H. and Rafailovich, M.,** 2003. Alkyl selenide- and alkyl thiolate-functionalized gold nanoparticles: Chain packing and bond nature. *Langmuir*, **19**, 9450-9458.

**Yoo, D., Jeong, H., Noh, S., Lee, J. & Cheon, J.** 2013. Magnetically Triggered Dual Functional Nanoparticles for Resistance-Free Apoptotic Hyperthermia. *Angewandte Chemie International Edition*, **52**, 13047-13051.

**Yu, X., Lei, D. Y., Amin, F., Hartmann, R., Acuna, G. P., Guerrero-Martínez, A., Maier, S. A., Tinnefeld, P., Carregal-Romero, S. & Parak, W. J.** 2013. Distance control in-between plasmonic nanoparticles via biological and polymeric spacers. *Nano Today*, **8**, 480-493.

**Zabetakis, K., Ghann, W. E., Kumar, S. & Daniel, M.** 2012. Effect of high gold salt concentrations on the size and polydispersity of gold nanoparticles prepared by an extended Turkevich–Frens method. *Gold Bulletin*, **45**, 203-211.

**Zeng, Z., Mizukami, S. & Kikuchi, K.** 2012. Simple and real-time colorimetric assay for glycosidases activity using functionalized gold nanoparticles and its application for inhibitor screening. *Analytical Chemistry*, **84**, 9089-9095.

**Zhang, J.H., Chung, T.D. and Oldenburg, K.R.,** 1999. A simple statistical parameter for use in evaluation and validation of high throughput screening assays. *Journal of biomolecular screening*, **4**, 67-73.

**Zhang, J., Liu, Y., Lv, J., Cao, Y. & Li, G.** 2015. Dipeptidyl peptidase-IV activity assay and inhibitor screening using a gold nanoparticle-modified gold electrode with an immobilized enzyme substrate. *Microchimica Acta*, **182**, 281-288.

**Zhang, W., Tang, Y., Liu, J., Jiang, L., Huang, W., Huo, F. & Tian, D.** 2014. Colorimetric Assay for Heterogeneous-Catalyzed Lipase Activity: Enzyme-Regulated Gold Nanoparticle Aggregation. *Journal of Agricultural and Food Chemistry*, **63**, 39-42.

**Zhang, Y. & Ying, J. Y.** 2015. Homogeneous Immunochemical Assay on the Lateral Flow Strip for Measurement of DNase I Activity. *Analytical Chemistry*, **87**, 10193-10198.

- Zhao, P., Li, N. & Astruc, D.** 2013. State of the art in gold nanoparticle synthesis. *Coordination Chemistry Reviews*, **257**, 638-665.
- Zhao, W., Brook, M. A. & Li, Y.** 2008. Design of gold nanoparticle-based colorimetric biosensing assays. *ChemBioChem*, **9**, 2363-2371.
- Zhao, W., Chiuman, W., Lam, J. C., Brook, M. A. & Li, Y.** 2007. Simple and rapid colorimetric enzyme sensing assays using non-crosslinking gold nanoparticle aggregation. *Chemical Communications*, **0**, 3729-3731.
- Zhao, W., Yao, C., Luo, X., Lin, L. & Hsing, I.** 2012. Staining-free gel electrophoresis-based multiplex enzyme assay using DNA and peptide dual-functionalized gold nanoparticles. *Electrophoresis*, **33**, 1288-1291.
- Zheng, Y., Hong, Y., Wu, W., Sun, D., Wang, Y., Huang, J. & Li, Q.** 2015. Separation of different shape biosynthesized gold nanoparticles via agarose gel electrophoresis. *Separation and Purification Technology*, **151**, 332-337.
- Zhong, J., Rao, X. & Rajagopalan, S.** 2013. An emerging role of dipeptidyl peptidase 4 (DPP4) beyond glucose control: potential implications in cardiovascular disease. *Atherosclerosis*, **226**, 305-314.
- Zhou, B., Shen, M., Bányai, I. & Shi, X.** 2016. Structural characterization of PEGylated polyethylenimine-entrapped gold nanoparticles: an NMR study. *Analyst*, **141**, 5390-5397.
- Zhou, J., Ralston, J., Sedev, R. & Beattie, D. A.** 2009. Functionalized gold nanoparticles: synthesis, structure and colloid stability. *Journal of Colloid and Interface Science*, **331**, 251-262.
- Zhu, D., Li, X., Liu, X., Wang, J. & Wang, Z.** 2012. Designing bifunctionalized gold nanoparticle for colorimetric detection of Pb<sup>2+</sup> under physiological condition. *Biosensors and Bioelectronics*, **31**, 505-509.
- Zong, J., Cobb, S. L. & Cameron, N. R.** 2017. Peptide-functionalized gold nanoparticles: versatile biomaterials for diagnostic and therapeutic applications. *Biomaterials Science*, **5**, 872-886.